



HAL
open science

Development of Tools for Accurate Study of Supraharmonic Emissions in Smart Grids

Deepak Amaripadath

► **To cite this version:**

Deepak Amaripadath. Development of Tools for Accurate Study of Supraharmonic Emissions in Smart Grids. Other. Université Bourgogne Franche-Comté, 2019. English. NNT : 2019UBFCA016 . tel-02498270

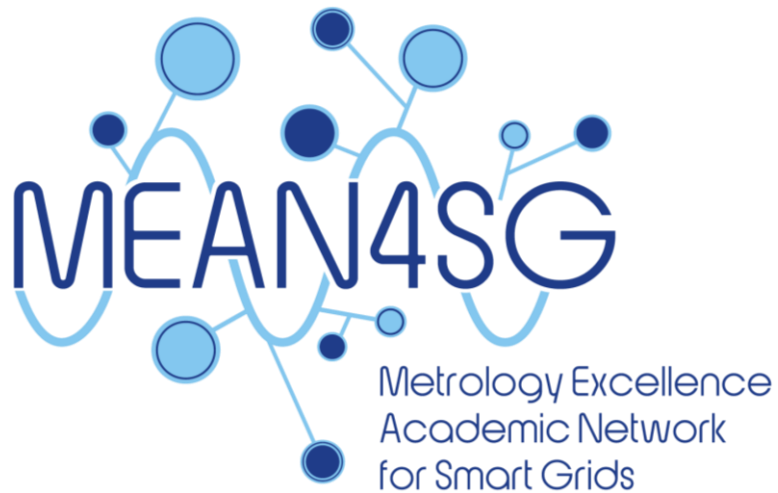
HAL Id: tel-02498270

<https://theses.hal.science/tel-02498270>

Submitted on 4 Mar 2020

HAL is a multi-disciplinary open access archive for the deposit and dissemination of scientific research documents, whether they are published or not. The documents may come from teaching and research institutions in France or abroad, or from public or private research centers.

L'archive ouverte pluridisciplinaire **HAL**, est destinée au dépôt et à la diffusion de documents scientifiques de niveau recherche, publiés ou non, émanant des établissements d'enseignement et de recherche français ou étrangers, des laboratoires publics ou privés.



Doctoral Thesis

Development of Tools for Accurate Study of Supraharmonic Emissions in Smart Grids

Deepak AMARIPADATH

Université Bourgogne Franche-Comté, France

Host Institution



Doctoral School



Academic Partner



Industrial Partner



NMI Partner



This project has received funding from the European Union's Horizon 2020 research and innovation programme under Grant Agreement no. 676042.



Doctoral Thesis of Université Bourgogne Franche-Comté (UBFC)
Prepared at Laboratoire National de Métrologie et d'Essais (LNE) and
Franche-Comté Electronique Mécanique Thermique et Optique - Sciences et Technologies
(FEMTO-ST)

Doctoral School no. 37
Sciences Pour l'Ingénieur et Microtechniques (SPIM)

Development of Tools for Accurate Study of Supraharmonic Emissions in Smart Grids

by

Deepak AMARIPADATH

A thesis submitted in partial fulfilment of the requirements for the degree of
Doctor of Philosophy in Electrical Engineering

Thesis submitted and defended in Trappes, France, on November 22, 2019.

Members of the Jury:

Prof. Marc PETIT	Professor, CentraleSupélec - Université Paris-Saclay, France	President
Prof. Mihaela ALBU	Professor, Universitatea Politehnica din București, Romania	Reviewer
Prof. Serhiy BOZHKO	Professor, University of Nottingham, United Kingdom	Reviewer
Dr. Daniela ISTRATE	Research Engineer, Laboratoire National de Métrologie et d'Essais, France	Examiner
Prof. Fei GAO	Professor, Université Bourgogne Franche-Comté, France	Director
Dr. Robin ROCHE	Associate Professor, Université Bourgogne Franche-Comté, France	Co-director

ABSTRACT

ABSTRACT

As the worldwide concern for the climate change and its effects are growing, the governments are forced to make strong decisions in favor of the implementation of the smart electrical grids. However, the success of these actions strongly depends on meeting the certain requirements of the electricity system raised by the quality of the energy supplied and the means to assess it. The smart electrical networks must tackle the challenges raised by the increasing uptake of the renewable energy sources, such as the photovoltaic (PV), wind, etc. and the equipment, such as photovoltaic inverters (PVI), electric vehicle chargers (EVC), etc. This introduces a complex dynamic operating environment for the distribution system. The distortions coming from the new generation and load equipment are generally larger and less regular than those due to the traditional generation and load equipment, making the power and energy measurements difficult to perform.

In this context, the thesis aims to quantify and reproduce the supraharmmonic emissions in the frequency range of 2 to 150 kHz. Therefore, the existing literature on the supraharmmonic emissions in the frequency range of 2 to 150 kHz is studied. The 4-channel measurement system is designed and implemented for the measurement of the fundamental and supraharmmonic components of the voltage and current waveforms in the frequency range of 2 to 150 kHz in the electrical network. The measurements are carried out in the Concept Grid platform. The individual equipment characterization and electrical network tests are carried out here. The waveforms acquired during the measurement campaigns are processed mathematically using the fast Fourier transform (FFT) algorithm and statistically using the analysis of variance (ANOVA) algorithm. The mathematical and statistical processing of the acquired waveforms helps to determine the individual effects and interactions of the different parameters in the generation of the supraharmmonic emissions in the electrical network. The various parameters, such as the primary and secondary emissions, effects of the cable length, effects of the sudden addition and removal of the load equipment are also studied.

The thesis describes the design of the complex waveform platform, which can be used for the laboratory testing and the characterization of the power quality analyzers (PQA) in the frequency range of 2 to 150 kHz. In the electrical networks, the waveform platform can be used to measure the supraharmmonic emissions in the frequency range of 2 to 150 kHz. The software architecture of the waveform platform is described here. In addition, the paper explains the hardware design of the waveform platform. It also includes the laboratory and electrical network applications of the waveform platform. The laboratory setup for the characterization of the PQA and the measurement schema for the electrical network waveforms are also depicted here. The uncertainty budget for the waveform platform is calculated considering the various factors, such as the cable length, noise, etc. are discussed in the thesis. Finally, the PQA is characterized in the frequency range of 2 to 150 kHz with respect to the waveform platform for varying emission amplitudes.

Keywords: Power quality, renewable energy sources, smart grids, supraharmmonic emissions, waveform platform.

ACKNOWLEDGEMENTS

ACKNOWLEDGEMENTS

This work would not have been possible without the support and help of many researchers, colleagues, and friends. I would like to thank, firstly, Prof. Mihaela ALBU and Prof. Serhiy BOZHKO for accepting to review this thesis, despite their active working schedules, and for their helpful comments. I would also like to address special thanks to Prof. Marc PETIT for accepting to be the president of the jury. I would like to express my sincere appreciation to the director of my thesis, Prof. Fei GAO for giving me the opportunity to accomplish this thesis. Then, I would like to thank my co-supervisors Dr. Robin ROCHE and Dr. Daniela ISTRATE for their guidance and support throughout the years of my doctoral thesis. I would especially like to thank and present my deepest gratitude to Dr. Robin Roche, for his encouragement, understanding, and valuable advices.

I appreciate the financial support of the European Union framework programme for research and innovation, Marie Skłodowska-Curie Actions for funding me during my doctoral research, and the Department of Low Frequency Electrical Metrology, LNE, France, for hiring me as an employee during the project. I address my special thanks to Mr. Loïc JOSEPH-AUGUSTE for inviting me to the Concept Grid, EDF, France, and giving me the opportunity to work with him and the members of the Concept Grid. I owe enormous gratitude to the entire team for providing me with their complementary and invaluable expertise, along with the warm welcome at the Concept Grid. I would also address my special thanks to Mr. Jean-Pierre BRAUN for inviting me to the Electrical Power and Energy Laboratory, METAS, Switzerland, and giving me the great opportunity to work with him and the members of the laboratory. It has been a fantastic experience where I learnt a lot and helped me achieve my goals. I also thank Mr. Dominique FORTUNÉ for his valuable contributions and suggestions to my doctoral thesis.

In addition, I would like to express my sincere thanks to the supervisory board members of the project MEAN4SG, who organized various training programmes, which helped me to grow as a professional in my career. During the three years of my doctoral studies, many researchers I met and worked with generously shared their expertise and friendship with me. I thank them all, and all the engineers, technicians, I have worked with during my doctoral thesis. My warmest regards should also be expressed to my family and friends for being supportive and standing by me through all these years. I owe an enormous amount to my parents for their constant encouragement to push onwards and to give the best of myself. I may certainly not have continued this far on my studies without their endless motivation.

TABLE OF CONTENTS

TABLE OF CONTENTS

Abstract	vi
Acknowledgements	viii
Table of Contents	x
Acronyms	xiv
List of Figures	xvii
List of Tables.....	xxii
Foreword	xxv
1 Introduction	2
1.1 Sustainable Development	2
1.2 Smart Grids.....	3
1.3 Distributed Generation	4
1.4 Intermittency in Smart Grids	5
1.5 Power Quality Issues	5
1.6 Motivation	8
1.7 Thesis Approach.....	8
1.8 Thesis Objectives	9
1.9 Manuscript Outline.....	10
2 Supraharmonic Emissions	12
2.1 Sources	12
2.2 Propagation of Supraharmonic Emissions.....	13
2.2.1 Primary and Secondary Emissions	13
2.2.2 Propagation between Equipment.....	14
2.2.3 Resonances	15
2.3 Interferences and Effects	16
2.4 Mitigation Techniques.....	17
2.5 Existing Standards.....	18
2.6 Measurement and Analysis Approaches	19
2.7 Research Challenges.....	21
3 Measurement Systems	23
3.1 Measurement System Version 1.....	23
3.1.1 Design.....	23
3.1.2 Characterization.....	25
3.2 Measurement System Version 2.....	38
3.2.1 Design.....	38
3.2.2 Characterization.....	40
3.3 Summary	50
4 Measurement Campaigns	53
Table of Contents	x

4.1	Concept Grid	53
4.2	Measurement Campaign 1	54
4.2.1	Commissioning Tests	55
4.2.2	Individual Equipment Tests.....	56
4.2.3	Electrical Network Tests	58
4.3	Measurement Campaign 2.....	62
4.3.1	Individual Equipment Tests.....	62
4.3.2	Multiple Equipment Tests	62
4.3.3	Electrical Network Tests	63
4.4	Summary	65
5	Mathematical and Statistical Analysis.....	67
5.1	Mathematical Analysis	67
5.2	Statistical Analysis	68
5.3	Measurement Campaign 1 Results.....	70
5.3.1	Commissioning Tests	70
5.3.2	Individual Equipment Tests.....	71
5.3.3	Electrical Network Tests	73
5.4	Measurement Campaign 2 Results.....	81
5.4.1	Individual Equipment Tests.....	81
5.4.2	Multiple Equipment Tests	83
5.4.3	Electrical Network Tests	85
5.4.4	Summary	89
6	Complex Waveform Platform	91
6.1	Objectives.....	91
6.2	Software Architecture.....	91
6.3	Hardware Architecture	94
6.4	Waveform Platform Schema	96
6.5	Waveform Platform Characterization.....	97
6.5.1	Waveform Generator	97
6.5.2	Data Acquisition Card.....	99
6.5.3	Waveform Uncertainty Budget.....	101
6.5.4	Power Quality Analyzer Characterization.....	109
6.6	Summary	113
7	Conclusions	116
7.1	Summary	116
7.2	Contributions.....	117
7.3	Future Work	118
8	References.....	120

Appendix A 128
Appendix B 145
Appendix C 166
Appendix D 183
Appendix E..... 199

ACRONYMS

ACRONYMS

ANOVA	Analysis of Variance
BPF	Band Pass Filter
CISPR	Comité International Spécial des Perturbations Radioélectriques
CFL	Compact Fluorescent Lamps
CO ₂	Carbon Dioxide
DAQ	Data Acquisition Card
DC	Direct Current
DFT	Discrete Fourier Transform
DSP	Digital Signal Processing
EC	European Commission
EDF	Electricité de France
EMC	Electromagnetic Compatibility
EMI	Electromagnetic Interference
ESR	Early Stage Researcher
ESS	Energy Storage Systems
ETP	European Technology Platform
EURAMET	European Association of National Metrology Institutes
EuT	Equipment under Test
EV	Electric Vehicles
EVC	Electric Vehicle Charger
FEMTO - ST	Franche-Comté Electronique Mécanique Thermique et Optique - Sciences et Technologies
FFT	Fast Fourier Transform
GHG	Green House Gases
GFCI	Ground Fault Circuit Interrupter
HF	High Frequency
HPF	High Pass Filter
ICT	Information and Communication Technology
IEC	International Electrotechnical Commission
ITN	Innovative Training Network
LabVIEW	Laboratory Virtual Instrument Engineering Workbench
LED	Light Emitting Diode
LF	Low Frequency
LISN	Line Impedance Stabilization Network
LNE	Laboratoire National de Métrologie et d'Essais
LPF	Low Pass Filter
LV	Low Voltage
MCbc	Maison Connecté bas carbone
MEAN4SG	Metrology Excellence Academic Network for Smart Grids
METAS	Federal Institute of Metrology
MP	Measurement Point

NI	National Instruments
PLC	Power Line Communication
PMU	Phasor Measurement Units
PoC	Point of Contact
PQ	Power Quality
PQA	Power Quality Analyzer
PV	Photovoltaic
PVI	Photovoltaic Inverter
PVI _I	Industrial PV Inverter
PVI _R	Residential PV Inverter
PWM	Pulse Width Modulation
PXI	Peripheral Component Interconnect eXtensions for Instrumentation
RES	Renewable Energy Systems
RMS	Root Mean Square
R&D	Research and Development
STFT	Short Time Fourier Transform
UN	United Nations
UTBM	Université de Technologie de Belfort-Montbéliard
UBFC	Université Bourgogne Franche-Comté
VSU	Voltage Sensor Unit
VT	Voltage Transformer

LIST OF FIGURES

LIST OF FIGURES

Fig. 1. MEAN4SG beneficiaries and partner organizations.....	xxv
Fig. 2. UN 2030 agenda for sustainable development objectives	2
Fig. 3. Electric power generated by different sources	3
Fig. 4. Greenhouse gas emissions from different energy sources	3
Fig. 5. Distributed generation network.....	4
Fig. 6. Thesis approach.....	9
Fig. 7. Voltage measurements from PVI in time and frequency	12
Fig. 8. Current measurements from PVI in time and frequency.....	13
Fig. 9. Equipment connection to the electrical network.....	14
Fig. 10. Primary and secondary emissions	14
Fig. 11. Simplified model for equipment to grid connection	15
Fig. 12. Capacitor burned due to supraharmonic emissions.....	17
Fig. 13. Multi-level controller topology	17
Fig. 14. PQube 3 output for voltage supraharmonic emission at 23 kHz.....	18
Fig. 15. Laboratory setup for PVI testing [45]	19
Fig. 16. Measured waveform from a LED lamp	20
Fig. 17. DFT analysis outcome of current emissions from a LED lamp.....	20
Fig. 18. STFT analysis outcome of current emissions from a LED lamp	21
Fig. 19. Measurement system version 1 electrical schema.....	24
Fig. 20. VT and VSU used in channel 1 and 2	24
Fig. 21. LFR 06/6 and CWT015 used in channels 3 and 4	25
Fig. 22. Lecroy Waverunner oscilloscope.....	25
Fig. 23. Characterization schema for VT	26
Fig. 24. Frequency characterization curve for VT at reference voltage of 7V.....	27
Fig. 25. Amplitude characterization curve for VT at reference frequency of 50 Hz.....	27
Fig. 26. Characterization schema for HPF	28
Fig. 27. Frequency characterization curve for HPF at reference voltage of 3.50 V.....	29
Fig. 28. Amplitude characterization curve for HPF at reference frequency of 50 Hz.....	29
Fig. 29. Characterization schema for VSU.....	30
Fig. 30. Frequency characterization curve for VSU at reference voltage of 2.80 V	31
Fig. 31. Amplitude characterization curve for VSU at reference frequency of 50 kHz	31
Fig. 32. Frequency characterization schema for LFR 06/6 up to 10 kHz.....	32
Fig. 33. Frequency characterization schema for LFR 06/6 from 10 to 150 kHz.....	32
Fig. 34. Amplitude characterization schema for LFR 06/6.....	33
Fig. 35. Frequency characterization curve for LFR 06/6 at reference current of 1 A	34
Fig. 36. Amplitude characterization curve for LFR 06/6 at reference frequency of 50 Hz.....	35
Fig. 37. Frequency characterization schema for CWT015 with HPF up to 10 kHz.....	36
Fig. 38. Frequency characterization schema for CWT015 with HPF from 10 to 150 kHz.	36
Fig. 39. Frequency characterization curve for CWT015 with HPF at reference current of 1 A	37
Fig. 40. Amplitude characterization curve for CWT015 with HPF at reference frequency of 5 kHz... 38	

Fig. 41. Measurement system version 2 electrical schema.....	39
Fig. 42. VT used in channel 1	39
Fig. 43. Optoisolator used in channel 2.....	39
Fig. 44. LFR 03/3 used in channel 4	40
Fig. 45. Characterization schema for VT with divider.....	41
Fig. 46. Frequency characterization curve for VT with divider at reference voltage of 6 V.....	41
Fig. 47. Amplitude characterization curve for VT with divider at reference frequency of 50 Hz	42
Fig. 48. Characterization schema for optoisolator.....	43
Fig. 49. Frequency characterization curve for optoisolator at reference voltage of 3.50 V	44
Fig. 50. Amplitude characterization curve for optoisolator at reference frequency of 20 kHz.....	44
Fig. 51. Characterization schema for HPF with optoisolator	45
Fig. 52. Frequency characterization curve for HPF with optoisolator at reference voltage of 3.50 V..	46
Fig. 53. Amplitude characterization curve for HPF with optoisolator at reference frequency of 20 kHz	47
Fig. 54. Frequency characterization schema for LFR 03/3 with HPF up to 10 kHz	48
Fig. 55. Frequency characterization schema for LFR 03/3 with HPF from 10 to 150 kHz	48
Fig. 56. Frequency characterization curve for LFR 03/3 with HPF at reference current of 1 A.....	49
Fig. 57. Amplitude characterization curve for LFR 03/3 with HPF at reference frequency of 5 kHz ..	50
Fig. 58. Concept Grid platform	53
Fig. 59. Concept Grid platform measurement points	54
Fig. 60. Configuration 1 for commissioning tests of measurement system version 1.....	55
Fig. 61. Configuration 2 for commissioning tests of measurement system version 1.....	56
Fig. 62. Individual equipment test schema for PVI _s	58
Fig. 63. Individual equipment test schema.....	58
Fig. 64. Electrical network test schema.....	60
Fig. 65. Electrical network to measurement system connection	61
Fig. 66. Multiple equipment test schema for PVI and fast charging EVC.....	63
Fig. 67. Electrical network to measurement system connection	64
Fig. 68. Current supraharmonic emissions from heat pump in time during campaign 1	67
Fig. 69. Current supraharmonic emissions from heat pump in frequency during campaign 1.....	67
Fig. 70. Current supraharmonic emissions from fast charging EVC in time during campaign 2	68
Fig. 71. Current supraharmonic emissions from fast charging EVC in frequency during campaign 2.	68
Fig. 72. Interpretation of interaction effects.....	69
Fig. 73. Voltage supraharmonic emissions from PVI ₁ in time during campaign 1	71
Fig. 74. Voltage supraharmonic emissions from PVI ₁ in frequency during campaign 1.....	71
Fig. 75. Current supraharmonic emissions from PVI ₁ in time during campaign 1	72
Fig. 76. Current supraharmonic emissions from PVI ₁ in frequency during campaign 1.	72
Fig. 77. Voltage supraharmonic emissions from fast charging EVC in time during campaign 1	72
Fig. 78. Voltage supraharmonic emissions from fast charging EVC in frequency during campaign 1	72
Fig. 79. Current supraharmonic emissions from fast charging EVC in time during campaign 1	73
Fig. 80. Current supraharmonic emissions fast charging from EVC in frequency during campaign 1.	73
Fig. 81. Voltage supraharmonic emissions from C ₉ in time during campaign 1.....	73
Fig. 82. Voltage supraharmonic emissions from C ₉ in frequency during campaign 1	74

Fig. 83. Current supraharmonic emissions from C_9 in time domain campaign 1.....	74
Fig. 84. Current supraharmonic emissions from C_9 in frequency during campaign 1	74
Fig. 85. Voltage supraharmonic emissions from electrical network tests	75
Fig. 86. Current supraharmonic emissions from electrical network tests	75
Fig. 87. Individual effects of PVI_I on voltage emissions from 4 to 6 kHz	78
Fig. 88. Interactions between PVI_R and PVI_I on voltage emissions from 4 to 6 kHz	78
Fig. 89. Voltage supraharmonic emissions from PVI_R in time during campaign 1.....	80
Fig. 90. Voltage supraharmonic emissions from PVI_R in frequency during campaign 1.....	80
Fig. 91. Current supraharmonic emissions from PVI_R in time during campaign 1	80
Fig. 92. Current supraharmonic emissions from PVI_R in frequency during campaign 1	81
Fig. 93. Voltage supraharmonic emissions from PVI_I at terminal in time during campaign 2	81
Fig. 94. Voltage supraharmonic emissions from PVI_I at terminal in frequency during campaign 2	82
Fig. 95. Current supraharmonic emissions from PVI_I at terminal in time during campaign 2.....	82
Fig. 96. Current supraharmonic emissions from PVI_I at terminal in frequency during campaign 2.....	82
Fig. 97. Voltage supraharmonic emissions from PVI_I at 300 m in time during campaign 2	82
Fig. 98. Voltage supraharmonic emissions from PVI_I at 300 m in frequency during campaign 2.....	83
Fig. 99. Current supraharmonic emissions from PVI_I at 300 m in time during campaign 2.....	83
Fig. 100. Current supraharmonic emissions from PVI_I at 300 m in frequency during campaign 2	83
Fig. 101. Voltage supraharmonic emissions from PVI_I with EVC in time during campaign 2	84
Fig. 102. Voltage supraharmonic emissions from PVI_I with EVC in frequency during campaign 2....	84
Fig. 103. Current supraharmonic emissions from PVI_I with EVC in time during campaign 2.....	84
Fig. 104. Current supraharmonic emissions from PVI_I with EVC in frequency during campaign 2	85
Fig. 105. Voltage supraharmonic emissions from C_7 in time during campaign 2.....	86
Fig. 106. Voltage supraharmonic emissions from C_7 in frequency during campaign 2.....	86
Fig. 107. Current supraharmonic emissions from C_7 in time during campaign 2	86
Fig. 108. Current supraharmonic emissions from C_7 in frequency during campaign 2	86
Fig. 109. Voltage supraharmonic emissions from electrical network tests	87
Fig. 110. Current supraharmonic emissions from electrical network tests	88
Fig. 111. Waveform platform software architecture	91
Fig. 112. Standard waveforms.....	92
Fig. 113. Complex waveform.....	92
Fig. 114. Current sensor output in voltage from PVI_I	93
Fig. 115. Modulated waveform	93
Fig. 116. Waveform platform front panel	93
Fig. 117. Waveform platform.....	94
Fig. 118. NI TB-2706 terminal block.....	95
Fig. 119. NI TB-2706 pin layout.....	96
Fig. 120. Waveform platform laboratory schema	96
Fig. 121. Waveform platform electrical network schema	97
Fig. 122. Characterization schema of waveform generator.....	98
Fig. 123. Characterization curve of waveform generator Ch_0	98
Fig. 124. Characterization curve of waveform generator Ch_1	99

Fig. 125. Characterization schema of DAQ	100
Fig. 126. Characterization curve of DAQ for 20 mV	100
Fig. 127. Characterization curve of DAQ for 6 V	101
Fig. 128. Effects of noise on the waveform platform.....	105
Fig. 129. Electrical schema for waveform generator characterization	109
Fig. 130. Laboratory setup for waveform generator characterization	110
Fig. 131. PQube 3.....	110
Fig. 132. Frequency characterization of PQube 3 at fundamental frequency	111
Fig. 133. Frequency characterization of PQube 3 at supraharmonic frequency.....	112
Fig. 134. Amplitude characterization of PQube 3 at fundamental frequency	112
Fig. 135. Amplitude characterization of PQube 3 at supraharmonic frequency	113

LIST OF TABLES

LIST OF TABLES

Table 1. Graphical representation of PQ issues.....	7
Table 2. Performance characteristics of the Rogowski coils.....	25
Table 3. Equipment used for characterization of VT	25
Table 4. Equipment used for characterization of HPF	28
Table 5. Equipment used for characterization of VSU.....	30
Table 6. Equipment used for characterization of LFR 06/6	32
Table 7. Equipment used for characterization of CWT015 with HPF	35
Table 8. Performance characteristics of LFR 03/3.....	40
Table 9. Equipment used for characterization of transformer with divider.....	40
Table 10. Equipment used for characterization of optoisolator.....	42
Table 11. Equipment used for characterization of HPF with optoisolator	45
Table 12. Equipment used for characterization of LFR 03/3 with HPF.....	47
Table 13. Individual equipment list.....	57
Table 14. Test network parameters	59
Table 15. Electrical network test campaign 1 configurations	60
Table 16. Electrical network test campaign 2 configurations	64
Table 17. ANOVA table.....	70
Table 18. Measurement data from configuration 1	70
Table 19. Measurement data from configuration 2	71
Table 20. ANOVA Table for voltage emissions from 4 to 6 kHz.....	76
Table 21. Effects and interactions of electrical network parameters 1.....	79
Table 22. Effects and interactions of electrical network parameters 2.....	88
Table 23. Waveform platform specifications	94
Table 24. NI chassis specifications	95
Table 25. NI remote control specifications	95
Table 26. NI waveform generator specifications	95
Table 27. NI DAQ specifications	95
Table 28. Equipment used for characterization of waveform generator	97
Table 29. Equipment used for characterization of DAQ.....	99
Table 30. Equipment used for characterization of waveform generator	102
Table 31. Parameters of waveform platform uncertainty	103
Table 32. Waveform platform uncertainties from FFT windows.....	103
Table 33. Waveform platform uncertainty from cable length.....	105
Table 34. Waveform Generator + DAQ performance.....	106
Table 35. Waveform Generator + VT + Divider + DAQ performance.....	106
Table 36. Waveform Generator + HPF + DAQ performance	106
Table 37. Waveform Generator + Optoisolator + DAQ performance.....	106
Table 38. Rogowski Coil LFR 06/6 performance with the conductor positioning	106
Table 39. Rogowski Coil CWT015 performance.....	107
Table 40. Waveform platform uncertainty budget	108

Table 41. Equipment used for characterization of waveform generator	109
Table 42. PQube 3 measurement parameters	109

FOREWORD

FOREWORD

The work done in this thesis was funded in the framework of the project ‘Metrology Excellence Academic Network for Smart Grids - MEAN4SG’ (Grant Agreement No. 676042) under the Horizon 2020 Marie Skłodowska-Curie Innovative Training Network (ITN). The MEAN4SG network aims to educate 11 Early Stage Researchers (ESR) in the smart grids metrology field. The main actors in the field of smart grids metrology have worked together, along with the European Association of National Metrology Institutes (EURAMET), and relying on the support of the International Electrotechnical Commission (IEC), in order to design a training program coping with the principal Research and Development (R&D) challenges related to the smart grid metrology, while tackling the shortage of the highly-skilled professionals in this research area, which has been foreseen by the European Commission (EC).

The beneficiaries and partner organizations involved in the project, which includes the early stage researchers (ESR), are shown in Fig. 1. The main research challenges in the smart grid metrology field, which are identified by the European R&D community, and addressed by MEAN4SG are [1]:

- Power Quality (PQ) analysis;
- Smart grid modelling and management;
- Phasor Measurement Unit (PMU) applications;
- Smart cable diagnosis.

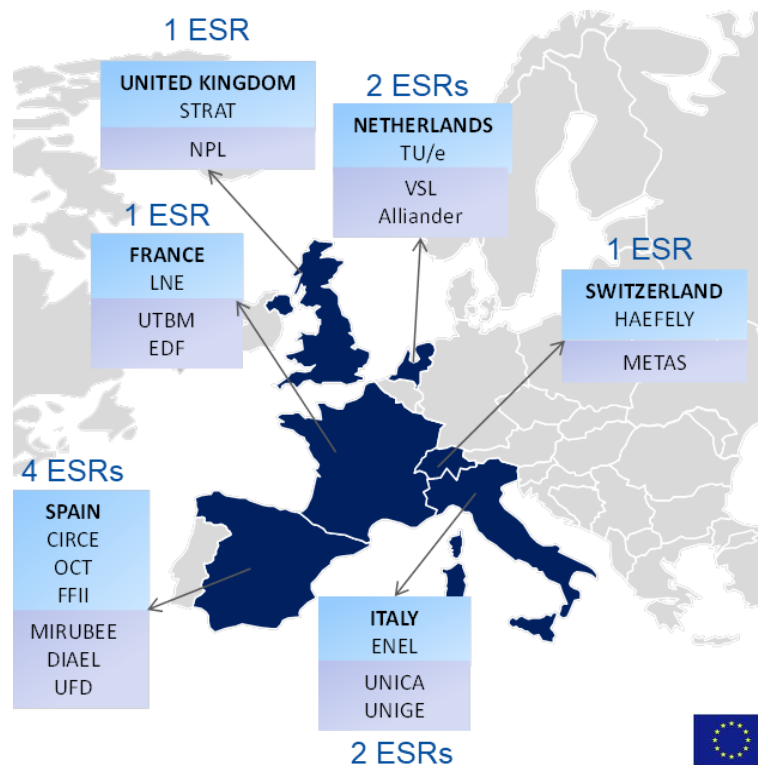


Fig. 1. MEAN4SG beneficiaries and partner organizations [1].

The thesis focuses on the first research challenge addressed by project MEAN4SG, which is PQ analysis in smart grids. The Laboratoire National de Métrologie et d’Essais (LNE), France, was the host institution for 36 months [1]. During the thesis, the secondments were hosted by 3 partners:

- Concept Grid, Electricité de France (EDF), France, for 2 months, where the real grid measurements are performed;

- Franche-Comté Electronique Mécanique Thermique et Optique - Sciences et Technologies (FEMTO-ST), Université de Technologie de Belfort-Montbéliard (UTBM) / Université Bourgogne Franche-Comté (UBFC), France, for 2 months, where the mathematical processing of measured waveforms is realized;
- Electrical Power and Energy Laboratory, Federal Institute of Metrology (METAS), Switzerland, for 3 months, where the supraharmonic waveform platform is implemented.

Therefore, the project offers an opportunity to work in industrial, academic, and metrological environments.

CHAPTER 1
INTRODUCTION

1 INTRODUCTION

With increasing awareness against the global warming and environmental degradation, the power and energy industry has been moving forward towards the smarter grid in the journey towards a more sustainable planet. The smart grid plays an important role in the sustainable development as it enables the integration of renewable energy systems (RES) like solar, wind, etc. using improved information and communication technology (ICT) like the smart metering to the existing electrical networks. The conversion of the traditional electric grid into smart grid increases the service value of the electric services through the notions of sustainability, conservation, and efficiency. The smart grid architecture enables the integration of new technologies, such as the electric vehicle (EV), smart metering, demand response, and energy storage etc. which are aimed to promote better energy savings, reduction in maintenance, disruption, and operational costs of the system [2].

1.1 Sustainable Development

Sustainable development is defined as, “the development that meets the needs of the present without compromising the ability of future generations to meet their own needs,” [3]. In 2015, the United Nations (UN) member states, adopted the 2030 agenda for sustainable development, which has 17 objectives for peace of the people and planet, for now and to the future. The UN 2030 agenda for sustainable development objectives are shown in Fig. 2. Out of the seventeen objectives, smart grids are directly related to the affordable and clean energy, and climate action [4].



Fig. 2. UN 2030 agenda for sustainable development objectives [4].

The UN aims to provide universal access to affordable and clean energy by the year 2030. This objective can be achieved through the integration of RES, such as solar, wind, etc. Expanding and updating the existing networks plays a crucial role in achieving this objective [4]. Therefore, studies concerning how the integration of these new technologies can impact the existing infrastructure are of great significance. Even though the rate of RES has been increasing in recent year, the capacity to meet an ever-growing energy demand is still limited. The percentage of power generated using different sources in 2017 is shown in Fig. 3. In 2017, a total of 25,570 TWh was generated across the globe [5]. Coal is still one of the major sources of power generation and contributes to 38% of the total power generated. Renewable sources account for 25% of power generation. Nuclear energy is used to generate 10% of global power. The remaining power is generated using oil and natural gas.

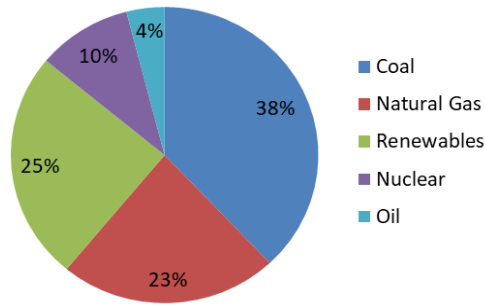


Fig. 3. Electric power generated by different sources [5].

With increased rate of industrialization, the world has been experiencing an escalation in the global temperature, surge in sea levels, and extreme weather conditions [4]. The increased level of greenhouse gases, such as the Carbon Dioxide (CO₂) is one of the primary reasons for these effects. The higher energy demand has resulted in the increase of CO₂ emissions to an historic high of 33.10 Gt in the year 2018, growing 1.70% compared to the previous year. CO₂ is one of the main greenhouse gases (GHG), which is the main contributor to the global warming. Two-thirds of these emissions were contributed from the power sector. The coal power plants were the largest single contributor to the rise in CO₂ emissions in 2018. In 2018, it reached to an overall rate of 10.10 Gt [5]. The greenhouse gas emissions from different energy sources are shown in Fig. 4.

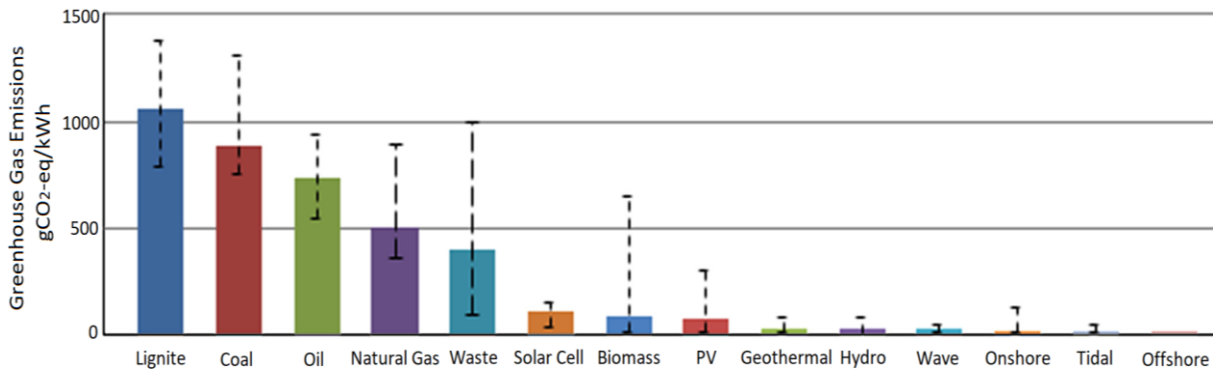


Fig. 4. Greenhouse gas emissions from different energy sources [6].

From Fig. 4, the non-renewable energy sources, such as the lignite, coal, oil, and natural gas etc. produce the largest greenhouse gas emissions ranging from 499 to 1054 gCO₂-eq/kWh, whereas the RES, such as the solar thermal cells, PV, geothermal, hydro, onshore, and offshore wind etc. produce only a fraction of this greenhouse gas emissions ranging around a value 100 gCO₂-eq/kWh. These values indicate the entire life-cycle emissions, which includes the mining, transportation of raw materials, construction, operation, and waste management [6]. Different regions in the world rely on different energy generation techniques ranging from the thermal power plants to the nuclear power plants. All these resources have different CO₂ emission rates, but the nature and impact of the smart grids will lead to cutting down of these emissions through the integration of RES [7]. The distributed generation through the integration of RES into the electrical networks is explained below.

1.2 Smart Grids

The European Technology Platform (ETP) for Electricity Networks of the Future, also known as ETP Smart Grids defines smart grids as an electricity network that can integrate the actions, such as generation, consumption, and storage in the electrical network in order to efficiently deliver the power

supplies [8]. The smart grid integrates the innovative products and services along with intelligent monitoring, control, communication, and self-healing technologies. The implementation of smart grids [8]-[11] aims to:

- facilitate better connections and operations between the generators of different capacities;
- provide the customers a better role in the system operation and optimization;
- improve the existing services effectively;
- give more information and choices to the customers;
- reduce the ramifications of existing systems on the environment;
- improve the existing level of security, reliability, and quality of the power supply;
- create and foster an integrated European market.

Some of the relevant aspects of smart grids, distributed generation, and challenges are detailed below.

1.3 Distributed Generation

The distributed generation technology is an approach which facilitates the production of the electric energy through the RES, such as the solar and wind, closer to the end users [12]. The distributed generation network consists of the RES, which is often coupled with the energy storage systems (ESS), such as the Lithium ion batteries, fuel cells, etc. [13]. This provides many potential benefits, such as cleaner, economic, safer, and unlimited source of the electric power [14]. A typical distributed generation network with the RES, such as the PV power plant, wind power plant, biopower plant, and microturbine, is shown in the Fig. 5. Other aspects of the distributed generation, which include the ESS, such as the Lithium ion batteries, fuel cells, and EV, etc. are also shown in Fig. 5.

The distributed generation technology often implements the intentional islanding from the electrical network during the power disturbances and outages to minimize the adverse effects, such as the production losses [15]. This ensures the continuous power supply in other locations of the network. The intentional Islanding technology contributes to the better efficiency and reliability in the distributed generation networks compared to the traditional electrical networks. This adds to the overall service value of the distributed generation network [15]-[17].

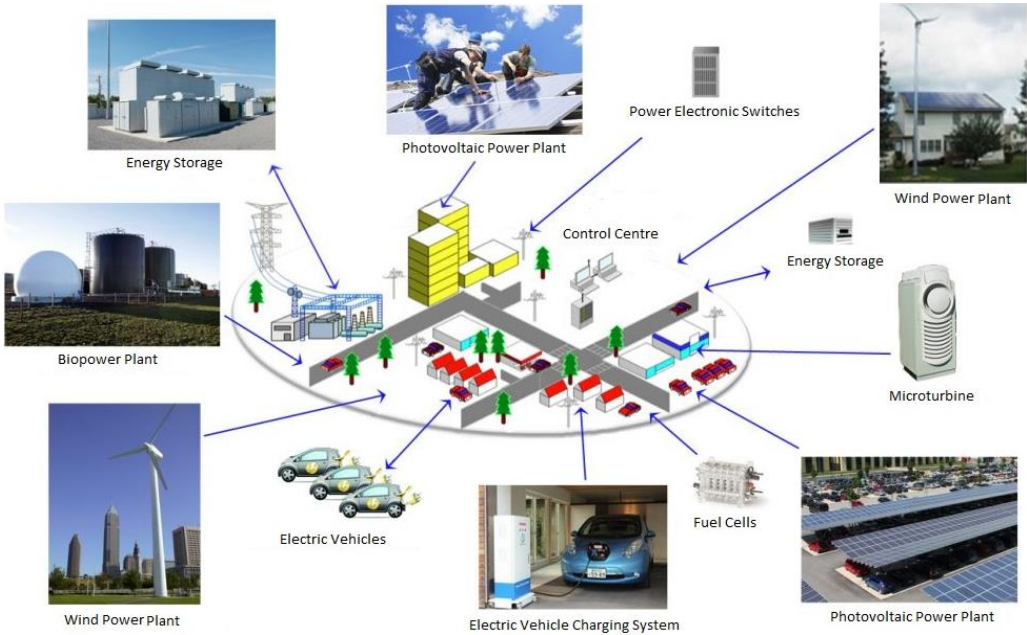


Fig. 5. Distributed generation network [13].

1.4 Intermittency in Smart Grids

The perception of the future electricity systems varies differently from the idea of one super grid to a large number of microgrids. Since both these visions are technologically feasible, the factors which would influence them are economic, institutional, and cultural [18]. The increased integration of the electrical networks with the RES and ESS are beneficial in many ways, but at the same time increases the interdependence on the infrastructure [19]. The increased interdependence adds to the additional vulnerabilities, such as the intermittency in the electrical network infrastructure.

The intermittency of the wind and PV systems can cause power fluctuations in the RES and makes the daily operation of the power grid more complex. In this case, day ahead, hour to hour, and real time planning and procedures are required, e.g., energy production is only possible during the day in the PV systems [20]. The nature of the solar and wind energy systems is not easily predictable, controllable, or dispatchable as in the case of the thermal or diesel energy systems. The RES are prone to the environmental factors, such as the humidity, snow fall, cloudiness etc. and the variability in the production due to these environmental factors makes the energy prediction difficult. Therefore, the power generation for a prolonged period of time is not ensured in most of these cases [21].

Integrating a larger number of RES with the grid is a solution to the intermittency. This seems contrary to the popular belief but increasing the number of the RES makes it more predictable due to the geographic diversity in most of the cases. The law of large numbers, which is a probability theory, states that, “the aggregate result of a large number of uncertain processes becomes more predictable as the total number of processes increases” [20]. Increasing the number of the small generators in a single location, rather than using a single large generator reduces the intermittency of RES.

In addition, the efficient modeling of the algorithms that can predict the wind and solar availability at specific location and time in advance is also an effective way to tackle the intermittency in the smart grids. Incentivizing the energy production at the right time and place is also an effective method against the intermittency, e.g., the production from the PV power plants tends to be higher during the day, and from the wind power plants are higher during the night [20]. Therefore, it is important to effectively integrate the RES to produce the required power, thereby maximizing the grid efficiency.

1.5 Power Quality Issues

PQ in an electrical network is considered to be perfect when the voltage waveform is sinusoidal, with constant frequency and amplitude [22]. In reality, this is however never the case. In addition to the traditional sources of PQ issues, such as electric motors, transformers, etc. the PQ in smart grids is mainly affected by the generation of emissions in the electrical networks by the power electronic converters interfaced with PV panels, EVCs, and batteries [23]. Some of the harmful effects of PQ issues are overheating of cables, compensation capacitors, transformers, and generators. PQ issues also result in the malfunctioning of safety devices [24]. Some of the PQ issues present in electrical networks are:

- voltage sags are the reduction of 10% or above of the recommended root mean square (RMS) voltage amplitude in the network, during a minute or less. They are commonly caused by the short circuits, starting of heavy loads, or overloading in the network. The fluctuating outputs from the RES may also cause voltage sags in the electrical network [25],[26];
- undervoltages are sags, which usually lasts for more than a minute. They are caused by the overloading in the transformers, or imperfections in the conductors [25];

- voltage swells are opposite to voltage sags and are the surge of 10% or above of the recommended RMS voltage amplitude in the network, and usually last a minute or less. They are usually caused by the sudden disconnection of the heavy loads in the network [25];
- overvoltages are swells, which usually lasts for more than a minute. They are caused by the lightning strikes, electrical switching of heavy loads, such as welding arch, or improper tap settings of the transformers [25];
- transients, which are short bursts of voltage ranging from a few volts to several thousand volts and last for just microseconds or milliseconds. They are caused by the lightning strikes, unfiltered electrical equipment, or instantaneous connection and disconnection of generators in the network [25],[27];
- flicker corresponds to the voltage fluctuations and can cause unsteadiness in the light stimulus with time. They are caused largely by the large fluctuating loads, such as the arc furnaces, rolling mill drives, etc. In addition, these fluctuations are caused by smaller loads, such as induction motors, elevators, etc. The intermittent behavior of RES, such as wind turbines, can also cause flicker in the electrical network [28];
- voltage unbalances are the measure of the voltage differences between the different phases of a multiphase system. Similarly, current unbalances are the measure of the current differences between the different phases of a multiphase system. In a balanced system, all the phase voltages and currents should be equal or close to equal. An unbalanced system is caused by overloading of one phase compared to the other phases in a multiphase system [29],[30].
- harmonics are the voltage and current emissions with frequencies up to 2 kHz and are integer multiples of the fundamental frequency. They are caused by the non-linear loads in the electrical network that draw current in distorted pulses rather than in a smooth sinusoidal manner [27],[31];
- supraharmonics are the voltage and current emissions from grid equipment in the frequency range of 2 to 150 kHz. They are caused by the increasing addition of the power electronic converters, such as PV panels and batteries, in the electrical network [23],[32],[33];
- interharmonics are the voltage and current emissions in the frequencies up to 2 kHz but are not the integer multiples of the fundamental frequency. The emissions with the frequencies lower than the fundamental frequency are known as subharmonics. They are caused by the random load changes in the equipment [34].

The economic impacts of PQ issues can be divided into the following categories [35]:

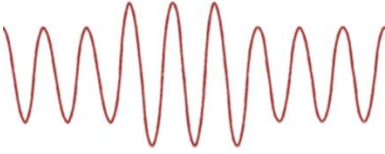
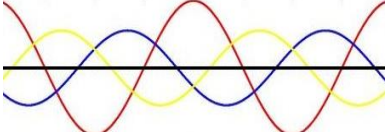
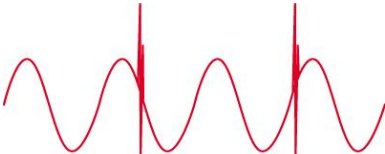
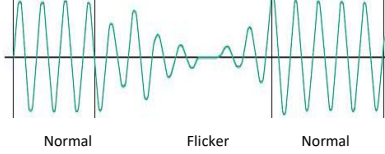
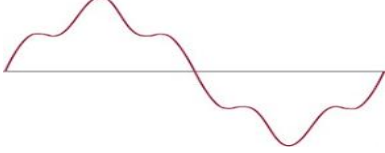
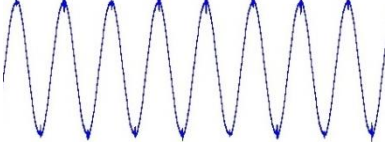
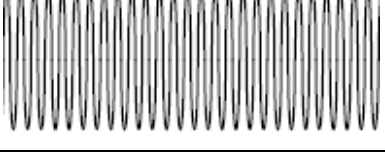
- partial or total loss of one or more processes, e.g., loss of process control due to voltage sags and swells;
- reduced long term productivity and quality, e.g., health issues among the employees due to flicker;
- increased maintenance costs due to the equipment failure, e.g., overheating of the transformers due to harmonics.

In addition, these economic impacts can be classified as follows [36],[37]:

- direct economic impacts, e.g., loss of production, equipment failures, and utility costs, etc.;
- indirect economic impacts, e.g., costs of income postponement, loss of market share, and restoration cost of brand equity, etc.;
- social economic impacts, e.g., personal injury, uncomfortable work environment, and failure of industrial safety, etc.

The graphical representation of these PQ issues is shown in Table 1.

Table 1. Graphical representation of PQ issues [38]-[42].

No.	Disturbance	Illustration
1	Voltage Sag	
2	Voltage Swell	
3	Voltage Unbalance	
4	Transients	
5	Flicker	
6	Harmonics	
7	Supraharmonics	
8	Interharmonics	

PQ issues have a strong economic impact on both utility and customers. It adds to the production and monetary losses in the industrial sectors. PQ is one of the influential factors for the customer satisfaction. Therefore, it is important to develop efficient, accurate, and feasible techniques to assure the PQ in smart grids.

1.6 Motivation

Despite all the benefits of implementing smart grid technology, there are still few areas of concern. The need to anticipate and address these possible downsides with smart grids, such as PQ issues, is of high significance. The smart grids are confronted to the challenges raised by the increasing uptake of RES and the addition of power electronic converters, such as PV panels and batteries, as well as the development of the power line communication (PLC) for the smart metering. This has led to the emergence of new PQ issues, such as the supraharmic emissions in the frequency range of 2 to 150 kHz [23]. The distortions coming from the RES are generally larger and less regular than the traditional generation sources and loads, making the PQ measurements difficult to perform [23],[32],[33].

The residential equipment, such as the heat pumps, EV chargers (EVC), light emitting diode (LED) lamps, etc. are important sources of the supraharmic emissions [43],[44]. Likewise, the smart meters and PLC, which are significant functionalities of the smart grid technology use waveforms in the frequency range of 9 to 95 kHz. The main effects of the supraharmic emissions include the capacitor overheating, electromagnetic incompatibility, and interference with PLC [23],[44]. As mentioned earlier, these consequences can have significant economic impact. Several case studies involving complaints caused by supraharmic emissions from different customers, such as residential, commercial and industrial customers are described in [45].

Identifying the sources of the supraharmic emissions in the electrical networks with multiple equipment are challenging due to the interactions between the equipment. In these scenarios, the thesis proposes the Design of experiment (DoE) approach for the analysis of the network and is explained in section 4.2.3.1. The existing standards for supraharmic emissions provide guidelines for the measurement and equipment testing, but do not detail the network measurements involving multiple equipment. As more and more PQAs, such as the PQube 3 are designed for measuring the supraharmic emissions in the frequency range of 2 to 150 kHz, a dedicated platform for the characterization of these PQAs in the frequency range of 2 to 150 kHz is required. The thesis aims to develop this waveform platform.

1.7 Thesis Approach

The primary research area of the thesis is PQ in smart grids and focuses on the supraharmic emissions in the frequency range of 2 to 150 kHz. The thesis approach is as follows:

- the studies in the literature indicate the supraharmic emissions as one of the significant PQ issues in the smart grids;
- the measurement system, which can measure the fundamental and supraharmic components of the voltage and current waveforms are designed, fabricated and characterized;
- the measurement campaign 1, which includes the commissioning, individual, and network tests are performed at the Concept Grid, EDF, France;
- the measured waveforms are processed using the discrete Fourier transform (DFT) method, and implemented using the FFT algorithm;
- the voltage and current emissions obtained from the electrical network tests are statistically analyzed using the ANOVA to study the individual effects and interactions between different parameters that influence the supraharmic emissions in the electrical network;
- the outcomes from the measurement campaign 1 are studied and possible improvements to the measurement system and the measurement campaigns are identified;

- the updated measurement system with the modified sensors and Data Acquisition Card (DAQ) is designed, fabricated, and characterized;
- the measurement plan with the additional configurations, such as the multiple equipment tests are performed at the Concept Grid using the updated measurement system. Various factors such as the primary and secondary emissions, influence of cable impedance, etc. are studied during this measurement campaign;
- the measured waveform are analyzed mathematically using the FFT algorithm and statistically using the ANOVA similar to the previous analysis;
- the complex waveform platform, which can create different waveforms including the real network waveforms is designed and implemented;
- the short time stability of the platform, and the influence of different factors, such as the cable length, noise, etc. are calculated and added to the uncertainty budget;
- the commercial PQA is characterized in the frequency range of 2 to 150 kHz using the complex waveform platform.

The important aspects of the thesis approach are shown in Fig. 6.

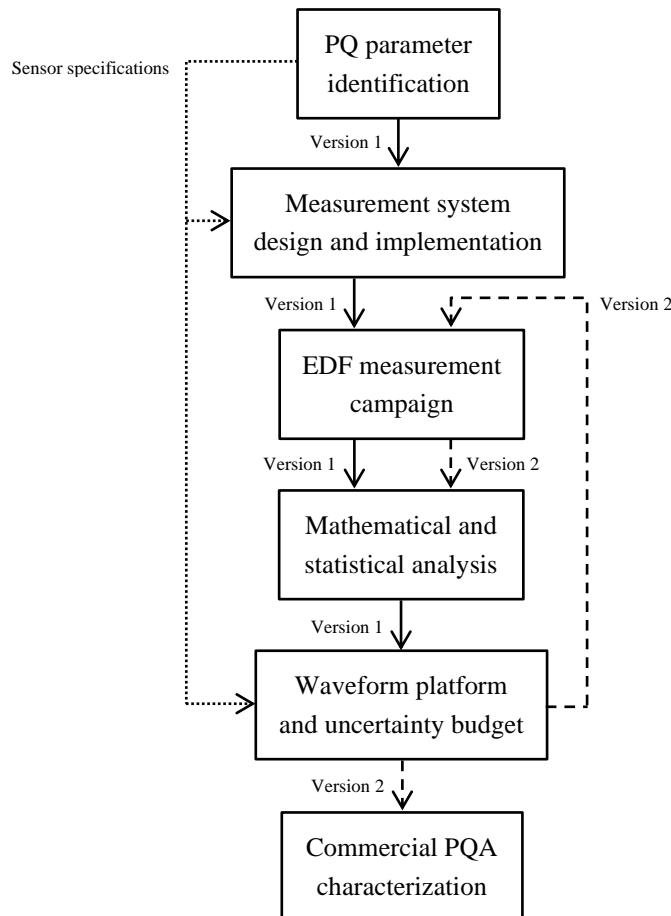


Fig. 6. Thesis approach.

1.8 Thesis Objectives

This thesis aims to contribute to PQ research in smart grids by helping better understand supraharmonic emissions in the frequency range of 2 to 150 kHz. Understanding the underlying faults and causes of the supraharmonic emissions in smart grids will help in shaping a better public policy

towards the implementation of better standards and, in turn, better products and lower economic and health risks. With the increased integration of RES into the traditional grids, it is of great significance to develop a complex waveform platform, which can generate, measure, and acquire the emissions in the frequency range of 2 to 150 kHz to characterize commercial PQA. Commercial PQ instruments measure and analyze the PQ issues, such as harmonics, interharmonics, etc. in the electrical network. Currently, there are no generic waveform platforms available in the market that can perform multiple functions in the frequency range of 2 to 150 kHz, since the current standards do not require these functionalities. Commercial waveform generators available in the market can generate only one disturbance at a time in the frequency range of 2 to 150 kHz per test, whereas the proposed system will generate multiple disturbances per test [46]. The proposed system can be used for research purposes, such as to study the equipment behavior in the presence of supraharmonic emissions, to understand the factors that influence supraharmonic emissions, etc. The proposed system will allow the characterization of PQAs more closely to the real electrical network conditions. The main challenges addressed in the thesis are listed in section 2.7. The manuscript outline is listed below.

1.9 Manuscript Outline

The remainder of the thesis is structured as follows:

- chapter 2 describes the state of the art for the supraharmonic emissions in the smart grids;
- chapter 3 explains the design, implementation, and characterization of the first and second versions of the measurement system;
- chapter 4 outlines the smart grid measurement campaigns. The DoE, schema, configuration, etc. of the measurements are explained in this chapter;
- chapter 5 describes the mathematical and statistical analysis of the measured waveforms. It studies the primary and secondary emissions, effects of cable impedance, and individual effects and interactions between the parameters that influence supraharmonic emissions in an electrical network;
- chapter 6 examines the design of the waveform platform. This chapter includes the hardware design, software interface, platform characterization with uncertainty budget, and PQ analyzer characterization;
- chapter 7 summarizes the conclusions, which includes the contributions of the thesis, and the summary of the results with the possible avenues for the future work;
- references used to prepare the manuscript are added after chapter 7;
- appendix A, B, C, D, and E are added after the references;
- appendix A presents the acquired and processed sensor output waveforms in time and frequency domain from the measurement campaign 1;
- appendix B details the statistical analysis results using ANOVA for the network tests performed during the measurement campaign 1;
- appendix C presents the acquired and processed sensor output waveforms in time and frequency domain from the measurement campaign 2;
- appendix D details the statistical analysis results using ANOVA for the network tests performed during the measurement campaign 2;
- appendix E lists the articles published during the thesis.

CHAPTER 2
SUPRAHARMONIC EMISSIONS

2 SUPRAHARMONIC EMISSIONS

The ever growing presence of the devices connected to the grid through the power electronic converters, such as the PV panels and batteries, as well as the development of the PLC, e.g., for the smart metering, has led to the emergence of new PQ issues [47]. An example of this new PQ issues is those related to the supraharmmonic emissions, limited to the frequency range of 2 to 150 kHz. The supraharmmonic emissions are defined as the emissions from the grid equipment in the frequency range of 2 to 150 kHz [43]-[49]. A review of the literature related to the supraharmmonic emissions in the frequency range of 2 to 150 kHz is summarized below.

2.1 Sources

The supraharmmonic emissions are generated by the electronic converters used in the equipment, such as the PV inverters (PVI), EVC, etc. [50]. The switching of the inverter output circuits in the network generates the supraharmmonic emissions in the frequency range of 2 to 150 kHz. The presence of the inverter circuits can influence the level of supraharmmonic emissions from the other grid equipment, thereby acting as both source and sink [50]. The main equipment that generates the supraharmmonic emissions in the frequency range of 2 to 150 kHz are [23],[45]:

- the PVIs with emissions in the frequency range of 4 to 20 kHz;
- the EVCs with emissions in the frequency range of 15 to 100 kHz;
- the equipment, such as the heat pumps with the emissions in the frequency range of 2 to 150 kHz;
- the industrial size converters with emissions in the frequency range of 9 to 150 kHz;
- the street lamps with emissions in the frequency range of 2 to 20 kHz;
- the PLC for automated meter reading with emissions in the frequency range of 9 to 95 kHz.

Voltage and current supraharmmonic emissions from a PVI measured during the project are shown in Fig. 7 and Fig. 8. The fundamental and supraharmmonic components are portrayed separately in both time domain and frequency domain. The supraharmmonic emission around 20 kHz is visible from the figures for both voltage and current waveforms.

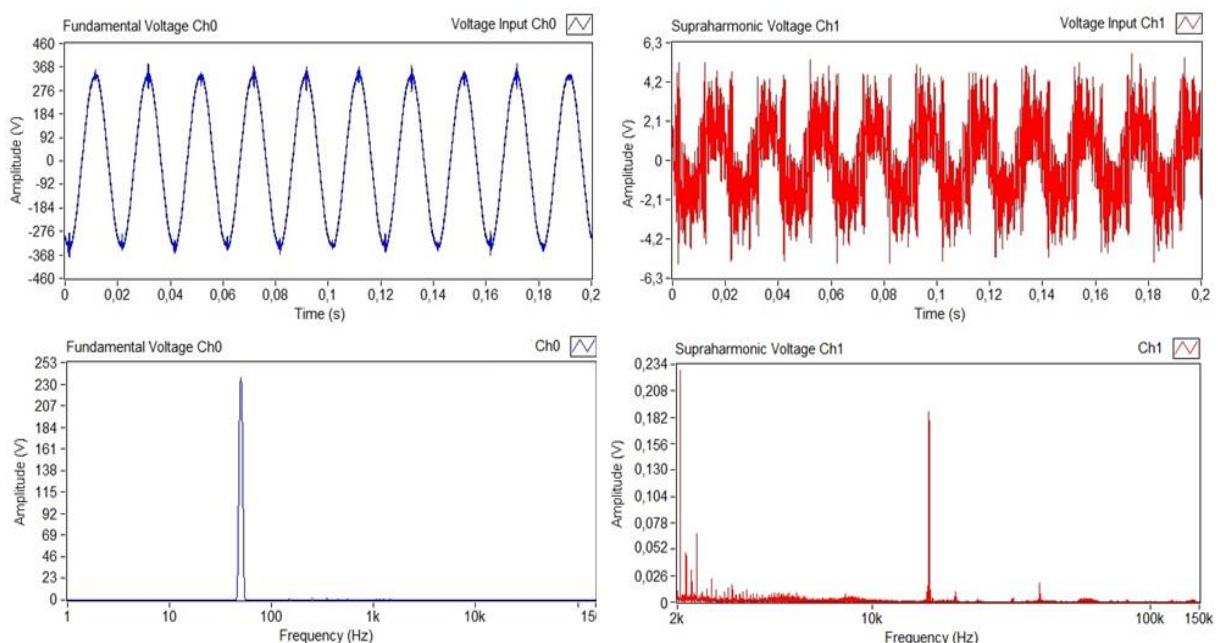


Fig. 7. Voltage measurements from PVI in time and frequency.

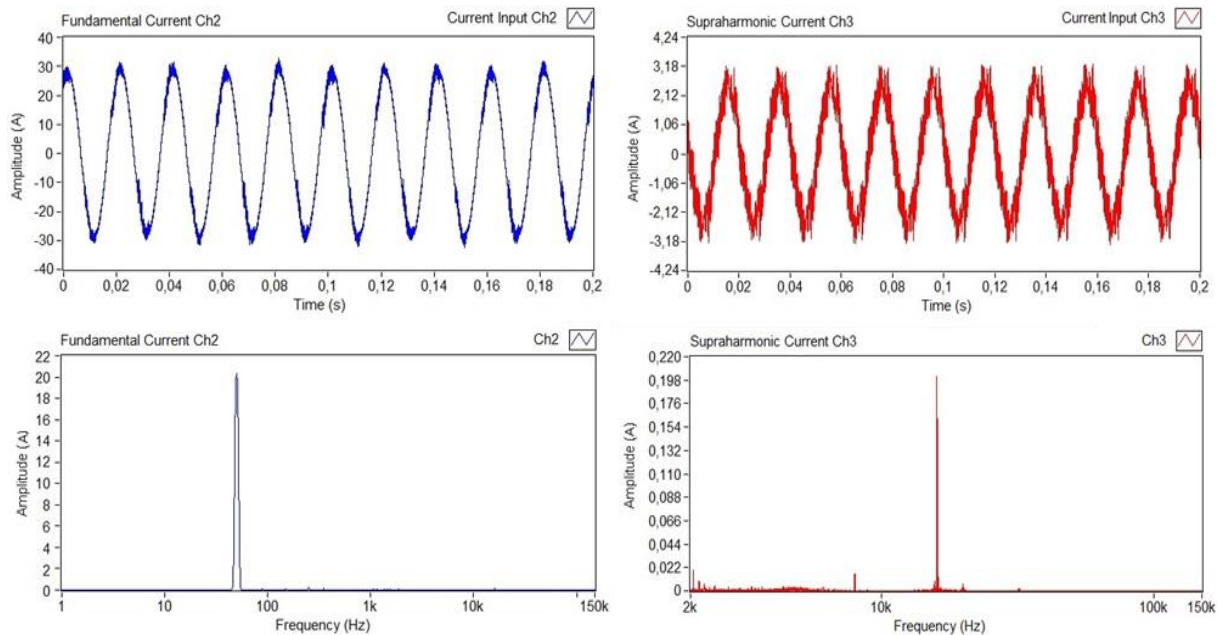


Fig. 8. Current measurements from PVI in time and frequency.

These waveforms were obtained using the measurement system version 2 described in chapter 3. The fundamental waveforms are shown on the left and supraharmonic waveforms are shown on the right side of the figures. The equipment, such as television, refrigerators, etc. which have power electronic converters with active and passive switching are considered as non-intentional sources of supraharmonic emissions, whereas transmitters of PLC are considered as intentional sources of supraharmonic emissions. The grid equipment is designed to satisfy the harmonic emission limits, but this in turn has resulted in the increased emissions at supraharmonic frequencies through, e.g., introduction of self-commutated valves [23]. The propagation of supraharmonic emissions in the frequency range of 2 to 150 kHz in an electrical network from three different angles, such as primary and secondary emissions, propagation between equipment, and resonances are explained below.

2.2 Propagation of Supraharmonic Emissions

The propagation of supraharmonic emissions in electrical networks is analyzed in three different contexts based on the existing studies, which includes the primary and secondary emissions, propagation between the devices, and resonance effect.

2.2.1 Primary and Secondary Emissions

Supraharmonic emissions can be classified into primary and secondary emissions [32],[51],[52]. The Equipment under Test (EuT) generates the primary emissions, whereas the secondary emissions are generated by different equipment in the network, or elsewhere in the network and then propagate towards the EuT due to the low impedance of the equipment terminal. Secondary emissions are rarely present and are not detected when connected to a Line Impedance Stabilization Network (LISN), which creates known impedance for conducted emission measurements [51]-[53]. Secondary emissions may be generated by neighbouring equipment or due to impedance mismatch between the equipment terminals and the network [52]. The equipment connection with rest of the electrical network is shown in Fig. 9.

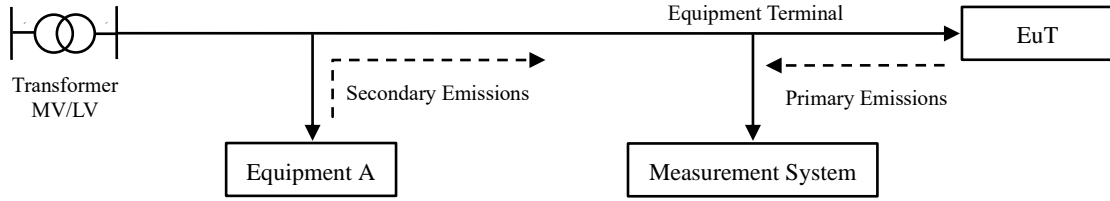


Fig. 9. Equipment connection to the electrical network.

A representation of the primary and secondary emissions in an electrical network with a non-linear source and impedance [51],[52] is shown in Fig. 10, where I is the current emissions, J_1 is the internal emission, Z_E and Z_G are the equipment and grid impedances, and E_B is the background voltage.

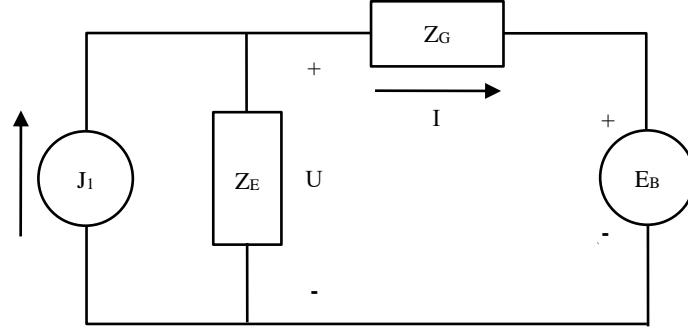


Fig. 10. Primary and secondary emissions [52].

Primary emissions are given as in (1):

$$I_1 = \frac{Z_E}{Z_E + Z_G} \times J_1, \quad (1)$$

Secondary emissions are given as in (2):

$$I_2 = -\frac{1}{Z_E + Z_G} \times E_B, \quad (2)$$

Current emissions are sum of primary and secondary emissions and are given as in (3):

$$I = I_1 + I_2, \quad (3)$$

$$I = \frac{Z_E J_1 - E_B}{Z_E + Z_G},$$

In addition, primary emissions are affected by the presence of secondary emissions in the network. The magnitude of primary emissions from EuT is impacted by the presence of neighbouring equipment. An existing study from [32] analyzes a network with the PVI and residential equipment. The paper states that the 16 kHz emission amplitude from the PVI varies with connection and disconnection of the residential equipment. The amplitude is the highest during the stand-alone operation of the PVI, but the amplitude of the emissions decreases when the neighbouring equipment is connected to the network [32]. It should be noted that in the impedance of the system varies with different measurement locations and can influence the emission variations. Hence the measurements are not reproducible at different locations due to the variable nature of the impedance of the grid.

2.2.2 Propagation between Equipment

The propagation of supraharmmonic emissions between the devices is described in [54]. The studies from [54] show that the current emissions at the supply terminal are much less than the current

emissions at the equipment terminals. In addition, the amplitude of the emissions decrease with the increase in the number of compact fluorescent lamps (CFL) added to the network. It also concludes that the emissions in the frequency range of 9 to 95 kHz propagate among the neighbouring equipment, and not towards the grid.

A similar study involving a low voltage (LV) electrical network with 1 to 48 CFL was conducted in [55] and shows that the current emissions are higher during the operation of a single CFL than when all the other lamps are lit. This shows that the higher frequency emissions are propagating between the lamps [55]. This phenomenon is further explained in [53]. The study uses a test network, shown in Fig. 11, with a constant current source in parallel with a capacitor, which represents an electromagnetic compatibility (EMC) filter in the electrical networks. The capacitor in the network creates a low impedance path for the propagation of current emissions between the current source and equipment [53].

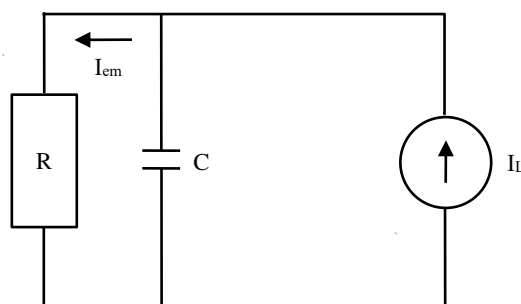


Fig. 11. Simplified model for equipment to grid connection [53].

In addition, according to [33], both simulation-based tests and field measurements confirm that the magnitude of the current flowing towards the grid at the switching frequency of the converter decreases with the increase in the number of similar equipment in the grid. This was studied using EVC of the same type with and without a PV installation.

The interactions between PLC and end user equipment are briefly studied in [56]. The study concludes that attenuation due to shunting in the end user equipment can create communication failure. In addition, this in turn might also result in the communication damaging the end user equipment [56]. All the above studies conclude that the supraharmmonic emissions propagate between the equipment and not towards the distribution grid. It also concludes that the amplitude of the emissions at the equipment terminals is higher than those at the supply terminals.

2.2.3 Resonances

Resonances play an important role in the propagation of supraharmmonic emissions in the frequency range of 2 to 150 kHz. Resonance in an electrical network occurs when the inductive reactance in the network is equal to its capacitive reactance, resulting in minimum impedance in the electrical network. Thus minimum impedance at resonant frequencies can result in the amplification of voltage and current emissions in the network. The studies from [57] show that the emissions around the switching frequencies of a wind turbine are amplified at the point of contact (PoC). However, the emissions from the wind turbines as a whole becomes negligible above the main resonant frequency. Also, the emissions near the resonant frequencies tend to amplify when there is not enough damping in the network. An example for this phenomenon is shown in [58], where there is an oscillation around 2 kHz with a magnitude of 30 to 100% of the fundamental voltage for a 30 kV voltage terminal. In

this case, the underground cables were the main contributors to the resonance. Meanwhile in [59], simulations and measurements show a resonance frequency around 6.7 kHz, when the measurement point is between a power transformer and a 500 m cable.

As discussed earlier, in a LV network, the propagation is between the equipment. In this case, the capacitance and inductance of the equipment plays an important role in the propagation of supraharmonics. An increment or decrement in the number of equipment connected in the network can influence the resonant frequency and thereby, the propagation of supraharmonic emissions in the network. The length of the cable between the transformer and the equipment can have a strong influence on the propagation of supraharmonic emissions. For a cable length of 800 m, the voltage amplitude at frequency of 34.95 kHz is amplified by a factor of 5 according to [60]. On the contrary, the amplitudes of the emissions were highest at the equipment terminal and lowest at the LV transformer bus bar according to measurements from [45]. The field measurements performed at Concept grid, EDF, implied the same phenomenon as discussed in details later. Thus from [45],[60] and field measurements performed, it cannot be concluded that the supraharmonic emissions attenuate with an increase in distance from the source of emissions.

The source of supraharmonic emissions, whether it is intentional or non-intentional, has no relevance with the propagation of these emissions. However, the transfer impedance between the network nodes where the emissions are injected influence the propagation of the supraharmonic emissions.

2.3 Interferences and Effects

Supraharmonic emissions in the frequency range of 2 to 150 kHz create interferences in the electrical network. A number of examples involving the interferences due to voltage and current supraharmonic emissions are detailed in [61]-[65] and are given below. This interference can cause irregularities in the equipment operation and/or decreased functionality as follows [61]:

- degraded output quality of a copy machine due to emissions in the lower kHz;
- control problems with an equipment using 77.5 kHz radio waveform for the internal clocks, due to radiated emission from an interfaced drive with a switching frequency of 3 kHz;
- malfunctioning of dimming control of LED lamps due to emissions from a nearby large rectifier is detailed in [62]. The study concludes that supraharmonic emission impacts light modulation and average light from these LED lamps [63],[63] and are not immune to supraharmonic emissions;
- tripping in earth leakage current breakers located in Japan due to emissions in the frequency range of 2 to 9 kHz is described in [63];

The interference of supraharmonic emissions can also cause complete failure or malfunctioning of equipment in the electrical network and a few examples [61] of this phenomenon are:

- failure of varistor due to presence of voltage supraharmonic emissions;
- regular failure of small drives due to the presence of voltage supraharmonic emissions with an amplitude of 0.9%;
- damage to a precision measurement system, which resulted in an expensive repair due to voltage perturbations in the supraharmonic frequency range.

Supraharmonic emission also creates interferences in PLC systems, which communicates in the frequency range of 9 to 95 kHz. This frequency band coincides with the emissions from equipment, such as PVI's, EVC's, etc. This interaction creates disturbances in the PLC, incorrect equipment operation, and the equipment damage due to high current emissions. This degrades the reliability and

invalidates PLC [56]. Examples of interference between PLC and other equipment, such as malfunctioning of dimmer lamps and data transmission issues in smart meters are described in [62]. In addition, supraharmmonic emission can generate audible noise from the device and/or installation. Studies from [61] show that voltage emissions around 12 kHz generate mechanical oscillation and audible noise in the equipment, such as computer monitors. Audible noise generated from a television is mentioned in [45]. Other effects of supraharmmonic emissions in the frequency range of 2 to 150 kHz [65] include the overheating of the capacitors in the LC filters found in the electrical network. Overheating of the capacitor occurs since the capacitor impedance is a function of inverse of the frequency. Thus with increased frequency components in the network and subsequent decrease of the capacitor impedance, the amount of current flowing through it increases [65]. This high current in the electrical network can destroy the capacitors as shown in Fig. 12. This can also lead to ground fault circuit interrupter (GFCI) trips and other safety issues in the electrical network [65]. In addition, supraharmmonic emission affects the accuracy of the energy meters, unless they are designed to be immune in the frequency range of 2 to 150 kHz as required in International Electrotechnical Commission (IEC) 61000-4-19 [66].



Fig. 12. Capacitor burned due to supraharmmonic emissions [62].

2.4 Mitigation Techniques

Supraharmmonic emissions can be mitigated through several approaches. New switching patterns and control algorithms can be used to reduce supraharmmonic emissions during power electronics switching. Multi-level converters can effectively reduce the supraharmmonic emissions around the switching frequency of the equipment [67]. The most common and established multi-level controller topology is shown in Fig. 13. The multi-level controllers are explained in detail in [68]. The modulation methods used in the multi-level controllers according to the switching frequency, such as the fundamental switching frequency and high switching frequency using the space-vector modulation, are detailed in [69].

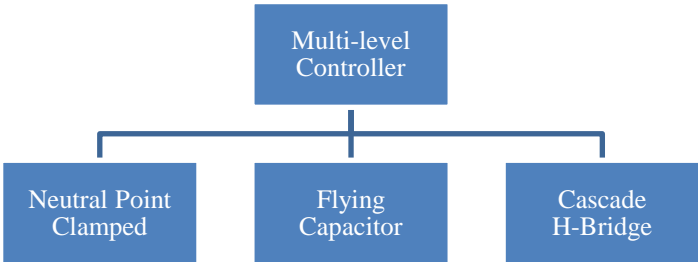


Fig. 13. Multi-level controller topology [67].

Another approach to reduce supraharmonic emissions is to introduce a passive low pass filter between the distribution network and converter [69],[70]. These passive filters, also known as EMC or electromagnetic interference (EMI) filters are a part of much equipment. These filters are usually designed to reduce emissions above 150 kHz. A redesign of these filters to remove supraharmonic emissions in the frequency range of 2 to 150 kHz is a possible solution [69]. The network interface of a high order filter with voltage source converters is briefly explained in [70]. The studies from [70] provide an efficient method for the design of different high order filters, such as LCL filters and multituned traps filters with damping impedances, which can be interfaced with the electrical network to reduce supraharmonic emissions in the frequency range of 2 to 150 kHz.

2.5 Existing Standards

To help minimize the emission of supraharmonics and its consequences, standards have been put in place. IEC 61000-4-7 Annex B [71] provides an analysis method for supraharmonic emissions in the frequency range of 2 to 9 kHz. It specifies the application of DFT on a 0.20 s time window with a 5 Hz resolution. The standard also suggests a bandwidth of 0.20 kHz for mathematical processing in the frequency range of 2 to 9 kHz. It also recommends implementation of a waveform filter to attenuate the fundamental component by 55 dB to minimize the uncertainties in the measurement [71].

Meanwhile, IEC 61000-4-30 [72] Annex C recommends a different analysis method for supraharmonic emissions with a sampling rate of 1 MHz and a high pass filter (HPF) to attenuate the fundamental and lower order harmonics from the measured waveforms. It recommends a time synchronization of 10 cycles each for the measurement interval. Authors from [73] concludes that the measurement of 512 samples at a sampling rate of 1 MHz corresponds to a time interval of 0.5 ms. The 32 measurement intervals of 0.5 ms over 10 fundamental cycles specified in the standard only covers 8% of the total time and this does not comply with the concept of the continuous PQ monitoring.

In addition, the 0.5 ms measurement window yields a frequency resolution of 2 kHz. This frequency resolution does not provide accurate frequency domain information of the emissions. This can be noted from the operation some PQAs, which satisfies the IEC 61000-4-30 requirements [72]. The measurement output from a PQube 3 analyzer when the emission is at 23 kHz is shown in Fig. 14. The analyzer indicates the emission at 22 kHz and 24 kHz.



Fig. 14. PQube 3 output for voltage supraharmonic emission at 23 kHz.

Standard IEC 61000-2-2 Ed 2 A2 defines the supraharmonic emission levels for grid compliance testing [74], whereas Comité International Spécial des Perturbations Radioélectriques (CISPR) 16 provides guidelines for laboratory measurements of supraharmonic emissions from the grid equipment, using a LISN to represent the impedance of the grid [75]. To summarize the standards

mentioned above provides informative guidelines for the measurement and analysis of supraharmonics. On the other hand, the standards do not comply with the real electrical network scenarios and such an example is illustrated in Fig. 13. In this thesis, recommendations from IEC 61000-4-30 [72] and IEC 61000-4-7 [71] are used for the measurements and data analysis. Various standardization committees like IEC are working on developing new supraharmonics standards.

2.6 Measurement and Analysis Approaches

The approaches concerning the measurement and analysis of supraharmonic emissions include both individual equipment and network characterization. The amplitudes of the emissions in the supraharmonic frequency range of 2 to 150 kHz are much smaller compared to emissions in the harmonic frequency range up to 2 kHz [76]. The main challenges [23],[44],[76] in the measurement of supraharmonic emissions in the frequency range of 2 to 150 kHz are:

- lower amplitudes at higher frequencies, which requires measurement sensors with high sensitivity and wide bandwidth to detect these emissions accurately;
- non-invasive sensors for the public electrical networks, which are not always reconfigurable;
- recorder with high resolution and dynamic range to acquire even the smallest emissions.

Supraharmonic measurements using an oscilloscope with multiple inputs are briefly described in [76]. The voltage measurements are performed using an analog filter with an isolation transformer for safety purposes. The current measurements are performed using a Pearson sensor with a sensitivity of 100 mV/A. The frequency range of the current sensor is 1 Hz to 20 MHz. In addition, a HPF is used to filter out the fundamental component and a low pass filter (LPF) is used for anti-aliasing effects. As voltage and current waveforms are analog waveform, there might be a presence of frequencies above Nyquist frequencies, which are half of the sampling frequency. This phenomenon is called aliasing and it is removed by anti-aliasing process [77]. Separate HPF and LPF are used since it is easier to implement than a single band pass filter (BPF). The measurement technology used in [76] can:

- measure multiple channels simultaneously;
- provide the time domain information, which can be used to find the frequency domain characteristics of the supraharmonic emissions;
- create a cost-effective measurement system.

The studies from [45] perform laboratory and network measurements to acquire supraharmonic measurements. A measurement system at the Technical University of Dortmund with a programmable waveform generator, a power amplifier, impedances, PVIs, and a Direct Current (DC) source with programmable voltage-current characteristic from was used for laboratory measurements and is shown in Fig. 15. A number of PVIs from different manufacturers with the same pulse width modulation (PWM) but different carrier frequencies were tested using this configuration [45].

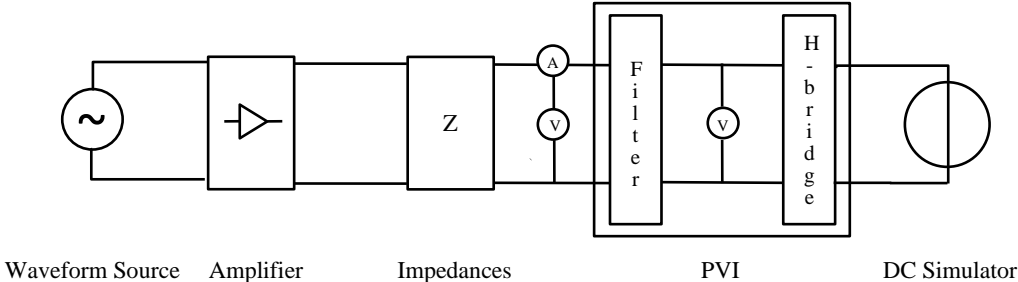


Fig. 15. Laboratory setup for PVI testing [45].

The measurements were performed at the PoC between the inverter and impedances, and inside the inverter between the EMC filter and the switching circuit. The measurements identified supraharmonic emissions around the integer multiples of the carrier frequency. The studies also recommend a 600 Hz voltage band centred on the inverter carrier waveform frequency for laboratory measurement analysis in contrary to 0.20 kHz bandwidth recommended by the standard IEC 61000-4-7 [71]. The supraharmonic emissions from PVI's in a LV network are studied during the network measurements. The studies conclude the presence of high frequency emissions around 17 kHz and a relatively constant emission throughout the day [45].

Meanwhile, the studies from [33] deal with the root causes and interactions between different equipment for the generation of supraharmonic emissions in the frequency range of 2 to 150 kHz in a LV network. According to [33], both simulation-based tests and field measurements with up to five EVs confirm that the magnitude of the current flowing towards the network at switching frequency decreases with the increase in the number of similar equipment in the electrical network. In real electrical networks, the emissions are more random and unpredictable [33] and this reiterates the importance of extended studies concerning the measurement and analysis supraharmonic emissions.

Most of these approaches measures supraharmonic emission in time domain and then use DFT operation to convert it into the frequency domain. In addition, the short time Fourier transform (STFT) algorithm is used to get the information from a join time and frequency domain [44],[55],[76],[77]. During STFT analysis, the sampled waveform is divided into multiple windows and DFT operation is applied on each window. The outcomes from DFT operation are combined to form the changes in the supraharmonic spectrum with time [77]. The measured waveform and DFT/STFT operation of the supraharmonic emission from a LED lamp is shown in Fig. 16, Fig. 17, and Fig. 18.

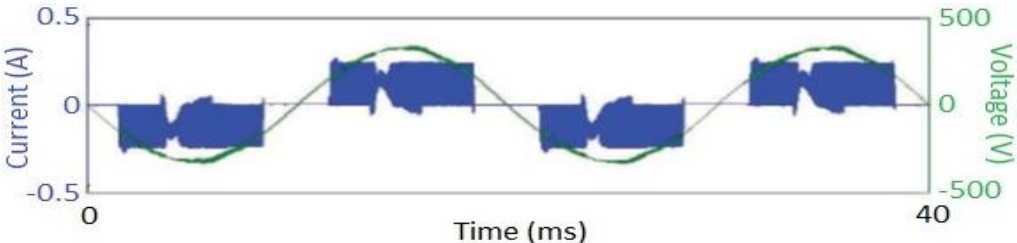


Fig. 16. Measured waveform from a LED lamp [77].

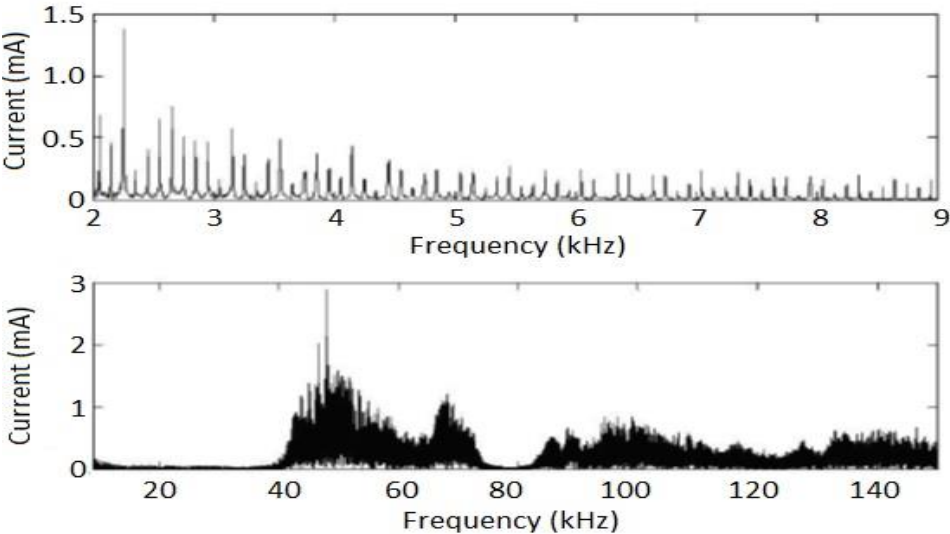


Fig. 17. DFT analysis outcome of current emissions from a LED lamp [77].

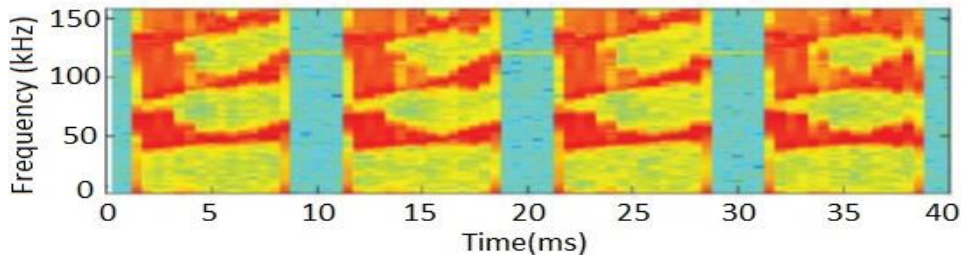


Fig. 18. STFT analysis outcome of current emissions from a LED lamp [77].

The existing measurement system [76] is a 2-channel system which measures the supraharmmonic emissions in the frequency range of 2 to 150 kHz. This measurement system does not provide any information on fundamental voltage and current waveforms in the network. In addition, the current sensor used for the measurements is sealed and is used on a reconfigurable site. However, this is usually not the case in public networks, so the current channel lacks flexibility for the grid measurements. Therefore, it is important to design a flexible measurement system considering safety aspects for actual grid measurements. Other existing studies describe the measurements, but do not explain the measurement system. There is also a lack of information on the performance characteristics of the measurement system in the existing literature.

The network studies from [33] analyze the interaction between equipment, such as PVI and EVCs. This is usually not the case in real electrical networks. The real electrical network is a combination of multiple source and consumption equipment, such as the PVIs, EVCs, heat pumps, refrigerators, etc. The analysis of these networks requires a deeper understanding of both mathematical and statistical processing to establish the cause-effect relationship between the individual effects and interactions between different parameters in the network.

2.7 Research Challenges

A number of research challenges in the field of supraharmmonic emissions in the frequency range of 2 to 150 kHz are described in [43],[44]. The research questions and challenges, which are addressed in this thesis, are listed below:

- to create an accurate and reproducible measurement method for the voltage and current emissions in the supraharmmonic frequency range of 2 to 150 kHz;
- to study the primary and secondary supraharmmonic emissions in the electrical network;
- to evaluate the effects of the sudden connection and disconnection of the load equipment in the network;
- to examine the effects of the cable impedance on the propagation of the supraharmmonic emissions;
- to analyze the individual effects and interactions between the different equipment in the network;
- to estimate the cause-effect relationship between the different generation and load equipment in the network;
- to design and implement a waveform platform for the characterization of the commercial PQ instruments in the supraharmmonic frequency range of 2 to 150 kHz;
- to generate the network emissions in the laboratory using the waveform platform;
- to calculate the uncertainty budget for the waveform platform.

CHAPTER 3
MEASUREMENT SYSTEM

3 MEASUREMENT SYSTEMS

An on-site measurement campaign was conducted to get an idea of the sources of supraharmonic emissions in a residential LV network, and to analyze the importance of these emissions. A 4-channel measurement and acquisition system was therefore designed for the measurement campaign at Concept Grid. Two different measurement systems are designed and developed here. The measurement system version 1 is developed in reference to existing literature from [44],[76]. The measurement system version 2 is designed and developed considering existing literature [44],[76], and the practical knowledge acquired during the electrical network measurements using the measurement system version 1 explained in section 4.2.3. The main challenges of measuring the supraharmonic emissions in the electrical network are discussed in section 2.6. The performance of the measurement systems are analyzed for varying frequencies and amplitudes. The characterization of the measurement system is important as it determines the performance of the measurement system, thereby ensuring the maximum efficiency and accuracy for the measured waveforms. The measurement system 1 was designed at the early stages of the project with available equipment and knowledge sources. The measurement system 2 is designed after the experiences from the network tests using the measurement system 1 during the measurement campaign 1 described in section 4.2. The measurement system is designed with an objective to measure emissions at higher frequencies close to 150 kHz.

3.1 Measurement System Version 1

The design and characterization of the measurement system 1, including 4 channels, are described in detail below. Out of the 4 channels, 2 channels are used for the voltage measurement and remaining 2 channels are used for the current measurements. These channels measure the fundamental and supraharmonic components of the voltage and current waveforms separately in order to maximize the dynamic range of the recording device.

3.1.1 Design

The design of measurement system version 1 is discussed here. The fundamental voltage signal is acquired on channel 1 (see Fig. 19). A 230/16 V, 50/60 Hz step down voltage transformer is used to ensure the electrical isolation among the network and measurement system and to adapt the signal to the recorder inputs [78]. Channel 2, which measures the supraharmonic components of voltage waveforms, consists of a 2nd order passive high pass filter (HPF) with the cut-off frequency of 590 Hz. The HPF is followed by a series connection of Zener diodes with Z_V of 30 V for voltage regulation. A varistor with the cut-off voltage of 30 V is also included in the circuit for overvoltage protection. Then, a voltage divider further attenuates the measured voltage by a factor of 3. In addition, to ensure the isolation, a transformer is added to the voltage circuit. By measuring the fundamental and supraharmonic emissions separately, it is possible to benefit the resolution of the recorder. This design emphasizes on the safety of the user and equipment during the measurements.

The Rogowski coils are used to measure the fundamental and supraharmonic current components in Channels 3 and 4. The Rogowski coils are flexible current sensors, which measure current and convert it into voltage. These sensors can be used for the measurements in the public electrical networks that are not reconfigurable. The fundamental current component is measured using the LFR 06/6 [79]. A different Rogowski coil, CWT015 measures the current component from the frequency of 150 Hz

[80]. In order to further attenuate the lower order frequencies, the 1st order passive HPF is implemented after the sensor output. The electrical schema for the measurement system version 1 is shown in Fig. 19. The technical specifications of the oscilloscope used in the measurement system 1 are as follows [81]:

- maximum bandwidth of 600 MHz;
- maximum sampling of 256 MS/s;
- 4 analog input channels;
- maximum voltage level up to ± 80 V;
- resolution of 12 bits;
- filters with the cut-off frequency of 20, 100, 200, and 300 MHz for noise filtering.

These values represent the maximum possible values of the oscilloscope. The measurements at the electrical network are performed for a window of 200 ms as in [71] and with a sampling rate of 1 MHz to satisfy the Nyquist criteria.

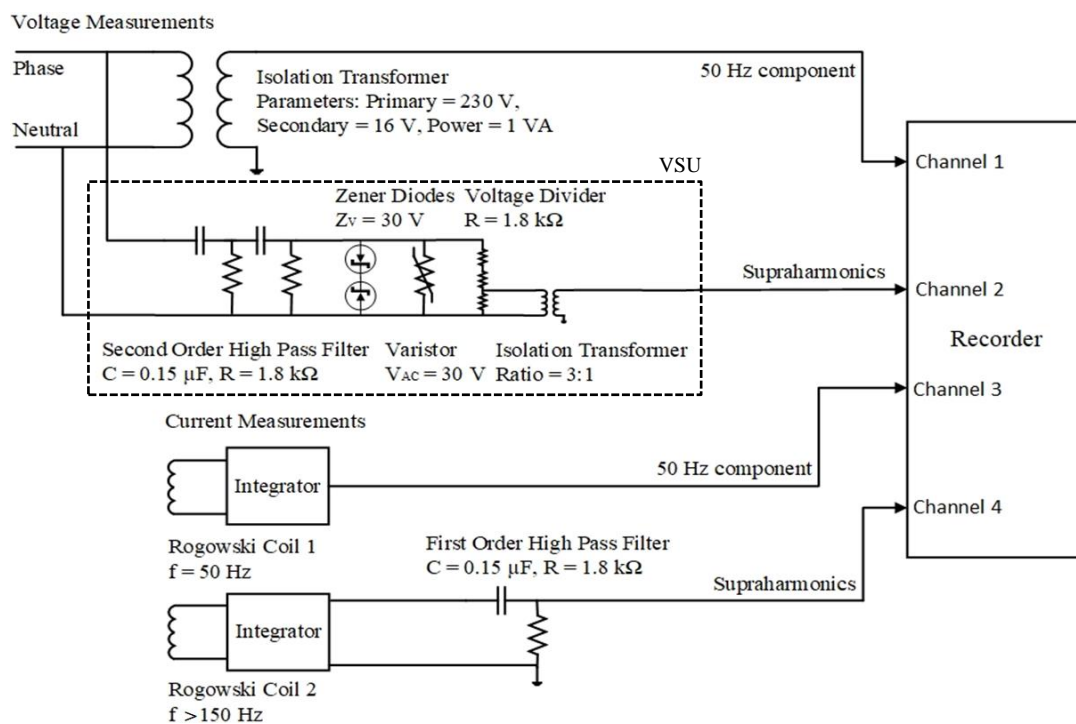


Fig. 19. Measurement system version 1 electrical schema.

The voltage sensors of the measurement system, which includes the voltage transformer (VT) and voltage sensor unit (VSU), are shown in Fig. 20. The sensor is placed inside an insulated box to ensure safety during the operation.

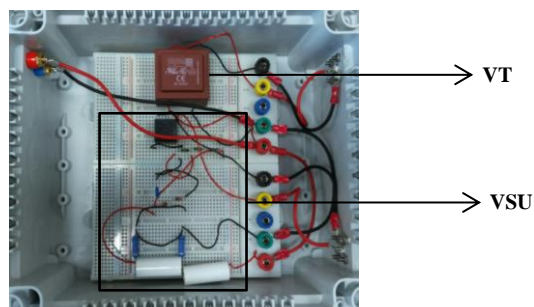


Fig. 20. VT and VSU used in channel 1 and 2.

The Rogowski coils used in the measurement system are shown in Fig. 21.



Fig. 21. LFR 06/6 and CWT015 used in channels 3 and 4.

The performance characteristics of the Rogowski coils, given by the manufacturer [79],[80] are listed in Table 2. The table lists the sensitivity, peak current value, and bandwidth of the Rogowski coils.

Table 2. Performance characteristics of the Rogowski coils [79],[80].

Type	Sensitivity (mV/A)		Peak Current (kA)		LF Bandwidth (3 dB) (Hz)	HF Bandwidth (3 dB) (MHz)
	×10	×1	×10	×1		
LFR 06/6	×10	×1	×10	×1	0.23	1.00
	50	5	0.12	1.20		
CWT015	200		0.03		150	6.00

The oscilloscope used for network measurements is shown in Fig. 22.



Fig. 22. Lecroy Waverunner oscilloscope.

3.1.2 Characterization

The characterization of each component of the measurement system, such as the voltage and current sensors is done for varying frequencies and amplitudes. The characterization tests determine the system performance in the frequency range of 2 to 150 kHz and for the different levels of amplitude.

3.1.2.1 Voltage Transformer

The measurement channel 1 consists of the VT, which steps down the network voltage from 230 to 16 V. This secondary voltage value is compatible with the input voltage range of the oscilloscope used for recording the measurements. In addition, the VT ensures the isolation between the grid and measurement equipment. The characterization of the VT is described below.

Equipment Used

The equipment used for the characterization of the VT are listed in Table 3.

Table 3. Equipment used for characterization of VT.

Equipment	Model	Type	N° id
Waveform Generator	Fluke	5730A	LNE 1019684

VT	Myrra	44201	-
Oscilloscope	Teledyne Lecroy	HDO8108A	LNE 1020886

Characterization Setup

The characterization setup used for channel 1 with the VT is shown in Fig. 23. The setup uses the waveform generator, VT, and oscilloscope for the characterization tests.

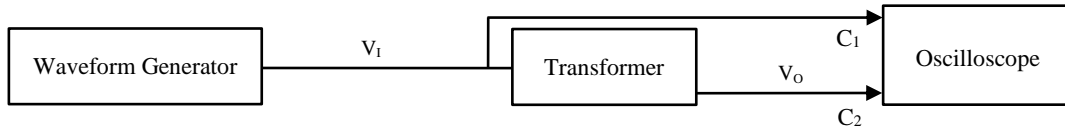


Fig. 23. Characterization schema for VT.

Test Procedure

The test procedure for the frequency characterization of the VT is as follows:

- the voltage waveform of known amplitude is generated using the waveform generator;
- channels 1 and 2 indicate the voltage input and output of the VT;
- the voltage waveform frequency is varied step by step, and the measurements of channels 1 and 2 are recorded;
- the transformer factor is the ratio of the input voltage to the output voltage as in (4).

$$K = \frac{V_I}{V_O}, \quad (4)$$

where K is the transformer factor, V_I is the RMS input voltage, and V_O is the RMS output voltage. The test procedure for the amplitude characterization of the VT is as follows:

- the voltage waveform of known frequency is generated using the waveform generator;
- channels 1 and 2 indicate the voltage input and output of the transformer;
- the voltage waveform amplitude is varied step by step, and the measurements of channels 1 and 2 are recorded;
- the transformer factor is the ratio of the input voltage to the output voltage as in (4).

Characterization Results

The measurement data for the frequency and amplitude characterization of the VT is discussed here. The frequency characterization is limited to 30 kHz, since the VT has a limited bandwidth up to the frequency of 30 kHz. This channel will measure voltage components in the frequency range of 0.05 to 30 kHz, and the voltage emissions above this frequency range will be measured using the channel 2. The voltage waveform of the amplitude of 7 V is used for the frequency characterization. The percentage error is calculated as in (5).

$$\varepsilon (\%) = \frac{\sum K - K_1}{\sum K} \times 100, \quad (5)$$

The characterization curve for the VT in error (%) with respect to the frequency is shown in Fig. 24.

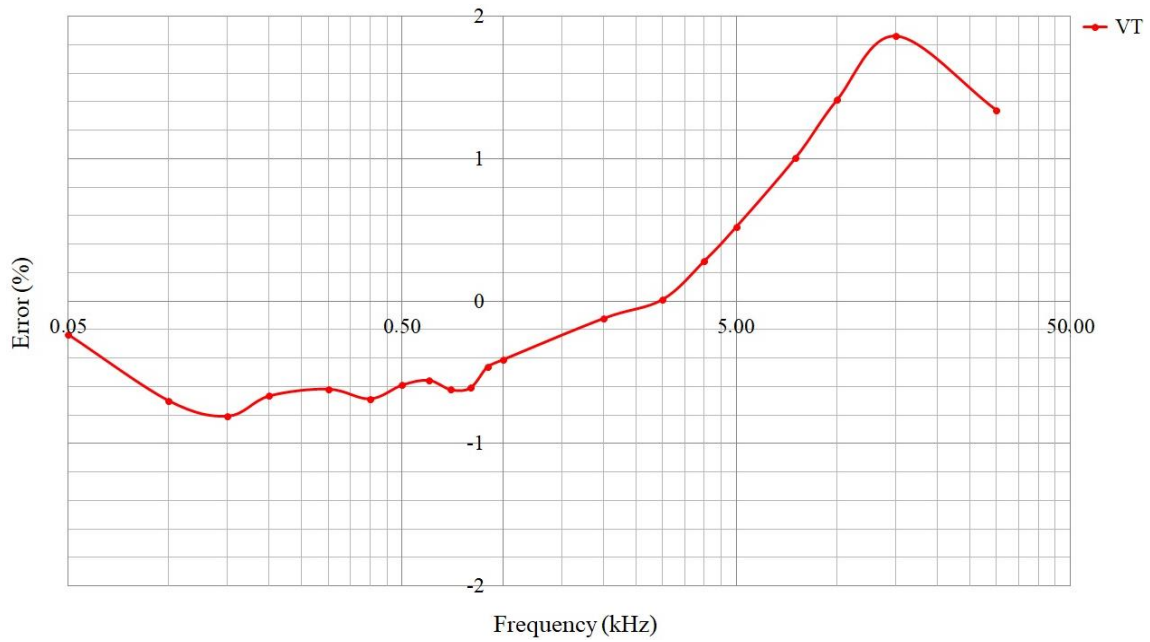


Fig. 24. Frequency characterization curve for VT at at reference voltage of 7 V.

The error value varies from -0.81 to 1.86% in the frequency range of 0.05 to 30 kHz. The error value is within $\pm 1\%$ upto 7.5 kHz. The error value is higher in the frequency range of 7.5 to 30 kHz. This sensitivity values are used to convert the VT output to real value during the mathematical processing of the voltage waveforms.

The characterization curve for the VT in error (%) with respect to the amplitude is shown in Fig. 25. The voltage waveform of the frequency of 50 Hz is used for the amplitude characterization.

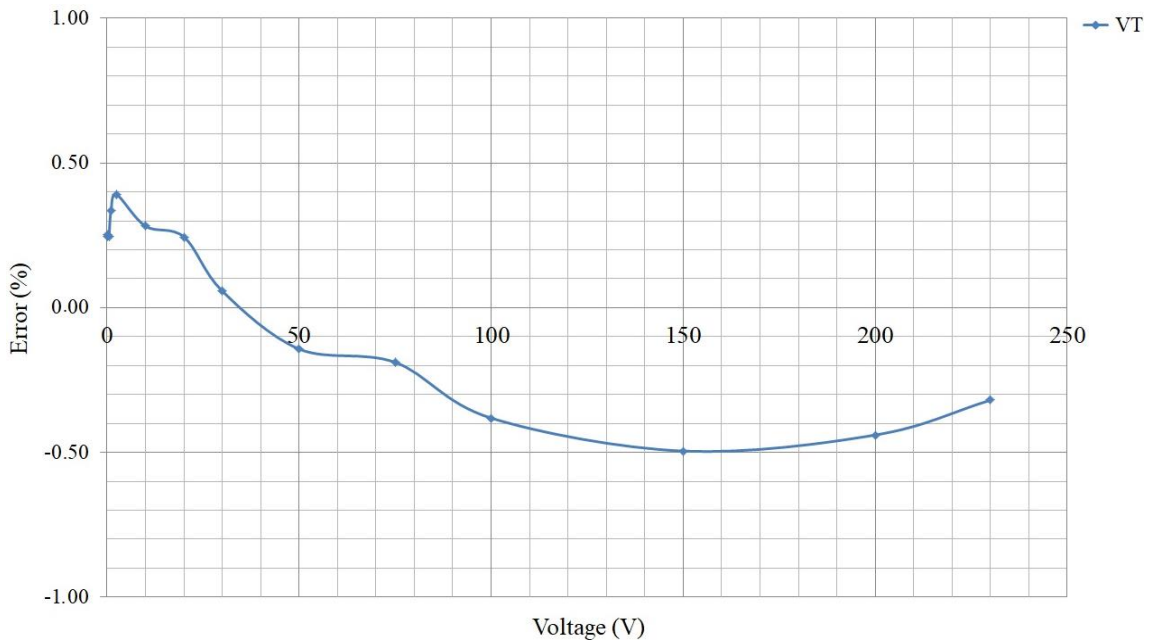


Fig. 25. Amplitude characterization curve for VT at reference frequency of 50 Hz.

The error value varies from -0.50 to 0.39% in the amplitude range of 0.05 to 230 V. The amplitude value varies within $\pm 0.50\%$, which is an acceptable level of variation, and the sensitivity values are used to convert the VT output to real values during the mathematical processing of the voltage waveform.

3.1.2.2 Second Order Passive High Pass Filter

Channel 2 of the measurement system is used to measure the supraharmonic voltage component in the frequency range of 2 to 150 kHz. In order to maximize the resolution of the oscilloscope, it is necessary to attenuate the fundamental voltage component in the electrical network and this is realized by implementing a 2nd order passive HPF in the measurement system. The characterization of the HPF is described below.

Equipment Used

The equipment used for the characterization of the 2nd order passive HPF are listed in Table 4.

Table 4. Equipment used for characterization of HPF.

Equipment	Model	Type	N° id
Waveform Generator	NI	PXIe-5413	LNE 1020904
Waveform Generator	Fluke	5730A	LNE 1019684
2 nd Order Passive HPF	Lab made	RC	-
DAQ	NI	PXIe-6124	LNE 1020904

Characterization Setup

The characterization setup used for 2nd order passive HPF is shown in Fig. 26. The setup uses the PXIe waveform generator, HPF, and PXIe DAQ for the characterization tests.

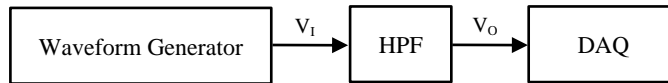


Fig. 26. Characterization schema for HPF.

Test Procedure

The test procedure for the frequency characterization of the HPF is as follows:

- the voltage waveform of known amplitude is generated using the waveform generator;
- channels 1 and 2 indicate the voltage input and output of the HPF;
- the frequency is varied step by step, and the measurements of channels 1 and 2 are recorded;
- the transfer function of the HPF is the ratio of output voltage to input voltage as in (6).

$$TF = \frac{V_o}{V_i}, \quad (6)$$

where TF is the transfer function of the HPF, V_o is the RMS output voltage, and V_i is the RMS input voltage. The test procedure for the amplitude characterization of the HPF is as follows:

- the voltage waveform of known frequency is generated using the waveform generator;
- channels 1 and 2 indicate the voltage input and output of the HPF are recorded;
- the amplitude is varied step by step, and the measurements of channel 1 and 2 are recorded;
- the transfer function of the HPF is the ratio of output voltage to input voltage as in (6).

Characterization Results

The measurement data for the frequency and amplitude characterization of the 2nd order passive HPF is discussed here. The voltage waveform of the amplitude of 3.50 V is used for the frequency

characterization tests from 0.02 to 150 kHz. The characterization curve for the HPF in error (%) with respect to the frequency is shown in Fig. 27. The error value varies from -22.20 to 0.23% in the frequency range of 2 to 150 kHz. The amplitude value varies within $\pm 1.00\%$ except in the frequency range of 2 to 10 kHz, which is an acceptable level of variation, and the sensitivity values are used to convert the HPF output to real values during the mathematical processing of the voltage waveform.

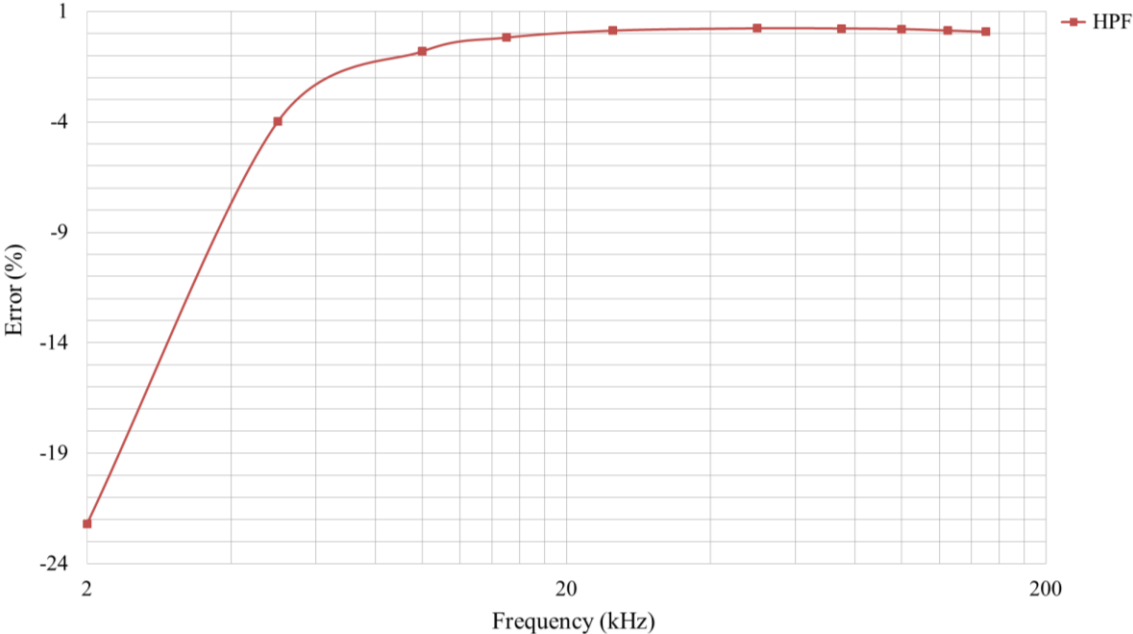


Fig. 27. Frequency characterization curve for HPF at reference voltage of 3.50 V.

The characterization curve for the HPF in error (%) with respect to the amplitude is shown in Fig. 28. The voltage waveform of the frequency of 50 Hz is used for the amplitude characterization. The error value varies from -0.10 to 0.23% in the amplitude range of 3.50 to 230 V. The amplitude value varies within $\pm 0.25\%$, which is an acceptable level of variation, and the sensitivity values are used to convert the HPF output to real values during the mathematical processing of the voltage waveform.

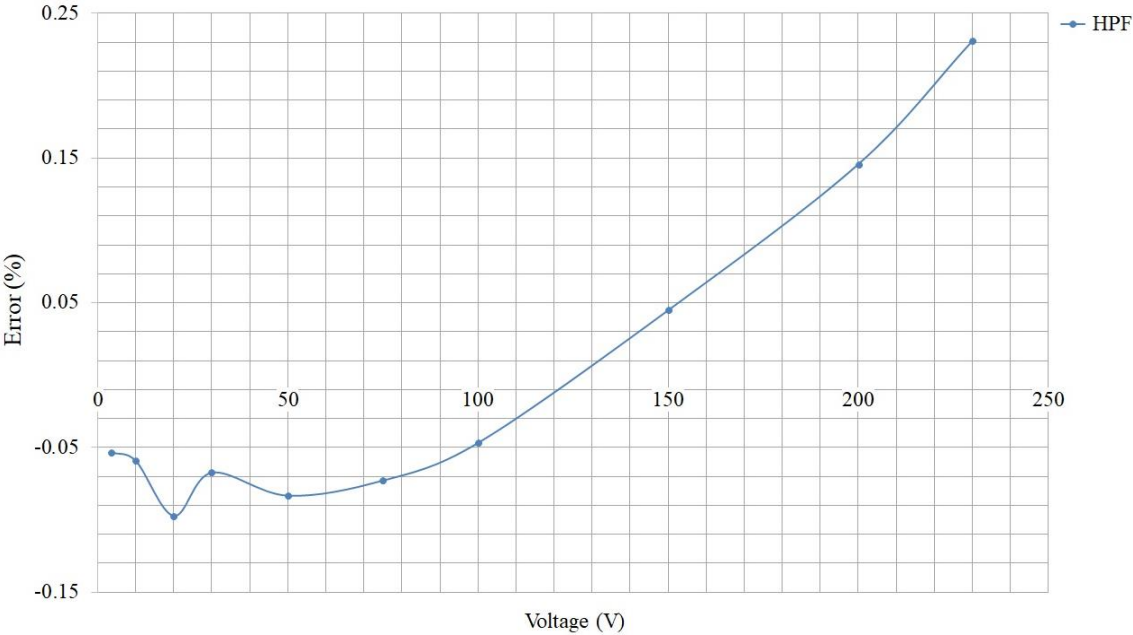


Fig. 28. Amplitude characterization curve for HPF at reference frequency of 50 Hz.

3.1.2.3 Voltage Sensor Unit

The VSU is used to measure the supraharmonic voltage components in the frequency range of 30 to 150 kHz in the electrical network. It consists of the 2nd order passive HPF, series Zener diodes, varistor, voltage divider, and isolation transformer and is shown in Fig. 19. The 2nd order passive HPF with the cut-off frequency of 590 Hz attenuates the fundamental frequency component is used in channel 2. The series Zener diode with Z_V of 30 V and connected in parallel to the HPF, provides voltage regulation for channel 2. The varistor with the cut-off voltage of 30 V ensures overvoltage protection in channel 2. The voltage divider with a resistance of 820 Ω reduces the input voltage to the isolation transformer by a factor of 3. The isolation transformer with a transformer ratio of 3:1 provides the necessary electrical isolation between the network and the measurement system.

Equipment Used

The equipment used for the characterization of VSU are listed in Table 5.

Table 5. Equipment used for characterization of VSU.

Equipment	Model	Type	N° id
Waveform Generator	Keysight	33250A	LNE 1020517
VSU	Lab made	-	-
Oscilloscope	Teledyne Lecroy	HDO8108A	LNE 1020886

Characterization Setup

The characterization setup used for VSU is shown in Fig. 29. The setup uses the waveform generator, VSU, and oscilloscope for the characterization tests.

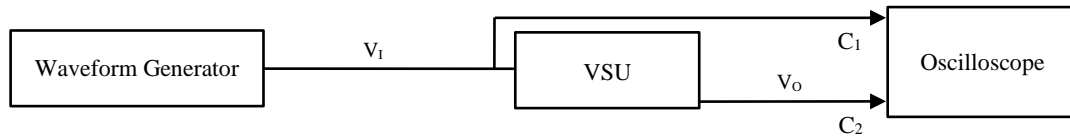


Fig. 29. Characterization schema for VSU.

Test Procedure

The test procedure for the frequency characterization of the VSU is as follows:

- the voltage waveform of known amplitude is generated using the waveform generator;
- channels 1 and 2 indicate the voltage input and output of the VSU;
- the frequency is varied step by step, and the measurements of channels 1 and 2 are recorded;
- the transfer function of the VSU is the ratio of the output voltage to the input voltage as in (6).

The test procedure for the amplitude characterization of the VSU is as follows:

- the voltage waveform of known frequency is generated using the waveform generator;
- channels 1 and 2 indicate the voltage input and output of the VSU;
- the amplitude is varied step by step, and the measurements of channels 1 and 2 are recorded;
- the transfer function of the VSU is the ratio of the output voltage to the input voltage as in (6).

Characterization Results

The measurement data for the frequency and amplitude characterization of the VSU is discussed here. The characterization curve for the VSU in error (%) with respect to the frequency is shown in Fig. 30.

The voltage waveform of the amplitude of 2.80 V is used for the frequency characterization of the VSU. The error value varies from -2.44 to 0.68% in the frequency range of 20 to 150 kHz. This channel will measure voltage emissions in the frequency range of 20 to 150 kHz. The amplitude value varies within $\pm 0.70\%$ except at a frequency of 20 kHz, and the sensitivity values are used to convert the VSU output to real values during the mathematical processing.

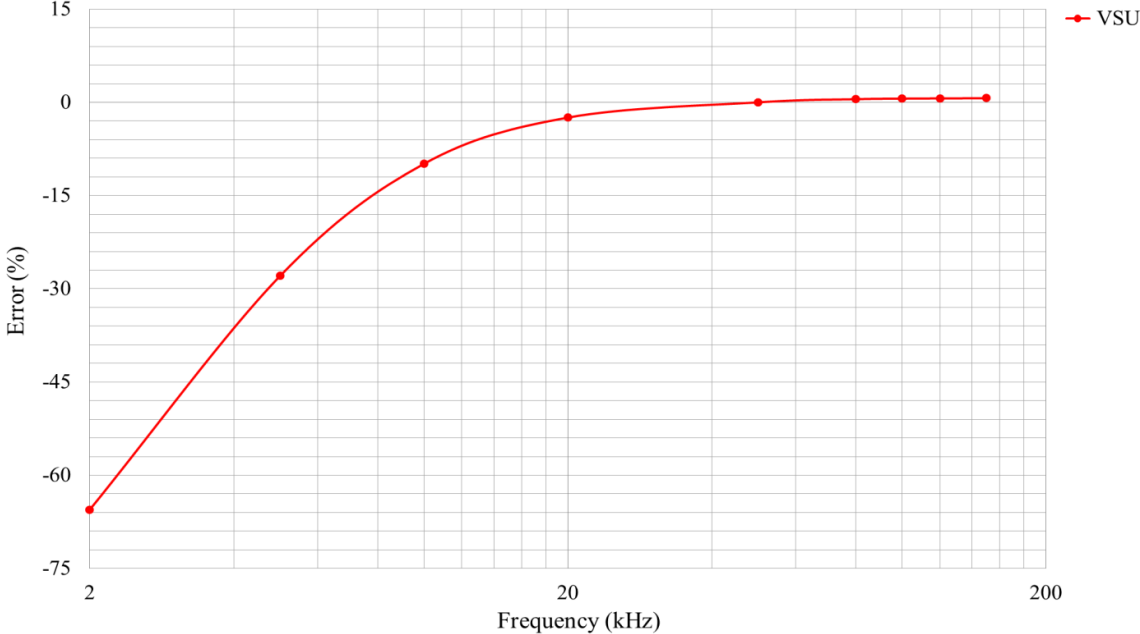


Fig. 30. Frequency characterization curve for VSU at reference voltage of 2.80 V.

The characterization curve for the VSU in error (%) with respect to the amplitude is shown in Fig. 31. The voltage waveform of the frequency of 50 kHz is used for the amplitude characterization. The error value varies from -1.04 to 1.01 in the amplitude range of 0.02 to 6.58 V. This channel will measure voltage emissions in the amplitude range of 0.02 to 6.58 V. The amplitude value varies within $\pm 1.05\%$, which is an acceptable level of variation.

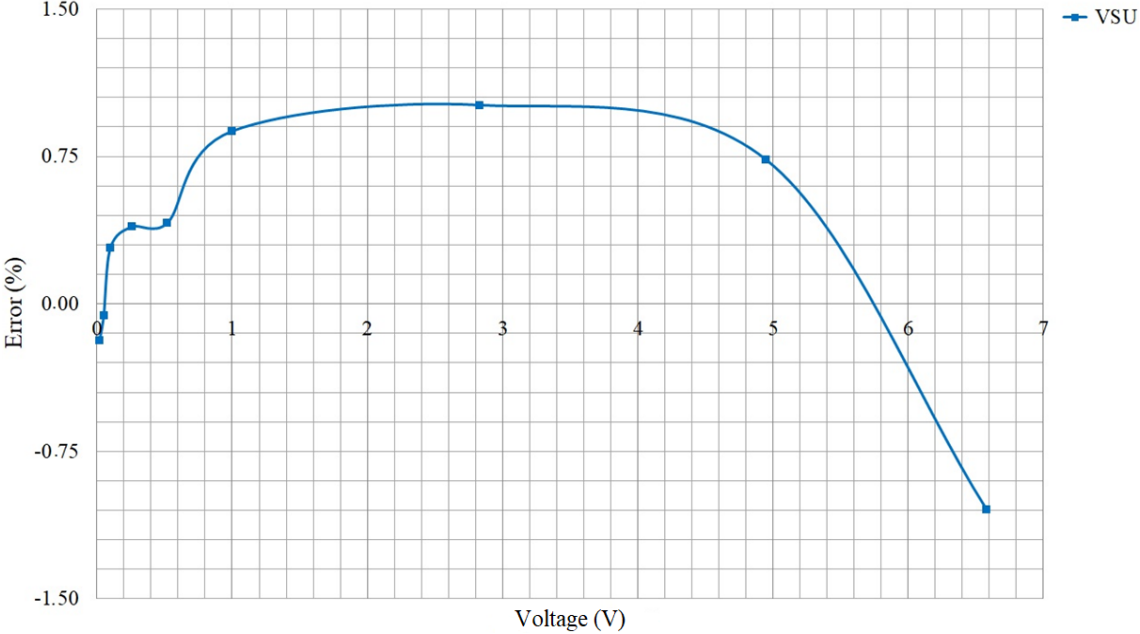


Fig. 31. Amplitude characterization curve for VSU at reference frequency of 50 kHz.

3.1.2.4 Rogowski Coil LFR 06/6

The Rogowski coil LFR 06/6 is used in channel 3 to measure the fundamental current in the electrical network. The performance characteristics of this sensor are listed in Table 6.

Equipment Used

The equipment used for the characterization of the LFR 06/6 are listed in Table 6.

Table 6. Equipment used for characterization of LFR 06/6.

Equipment	Model	Type	N° id
Waveform Generator	Fluke	5730A	LNE 1019684
Function Generator	HP	3325A	LNE 1019988
Power Amplifier	AR	500A250C	
Output Impedance	AR	IT1003	
Current Transformer	Eurocraft	B-0.1	LNE 1019976
Rogowski Coil	PEM	LFR 06/6	LNE 1020872
AC Acquisition Unit	Fluke	5790A	LNE 1020703
DAQ	NI	PXIe-6124	LNE 1020904
Waveform Generator	Fluke	5720A	LNE 1026271
Transconductance Amplifier	Clarke-Hess	8100	LNE 1008742
Current Shunt	SP	CS2D	LNE 1020555
Current Shunt	SP	CS2D	LNE 1020556
Multimeter	Agilent	34401A	LNE 1020754
Multimeter	Agilent	34401A	LNE 1019626

Characterization Setup

Two different characterization setups are used for frequency characterization of the LFR 06/6, since the waveform generator, Fluke 5730A in the first setup has a limited bandwidth of 10 kHz for current waveforms. The Fluke waveform generator is used for characterization up to 10 kHz and is shown in Fig. 32. Meanwhile, for characterization in the frequency range of 10 to 150 kHz, the HP function generator coupled with the AR amplifier is used and is shown in Fig. 33.

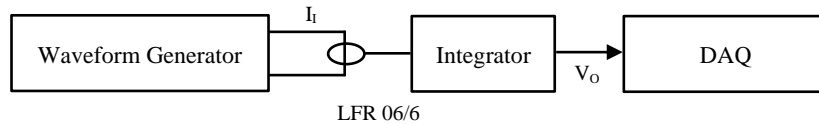


Fig. 32. Frequency characterization schema for LFR 06/6 up to 10 kHz.

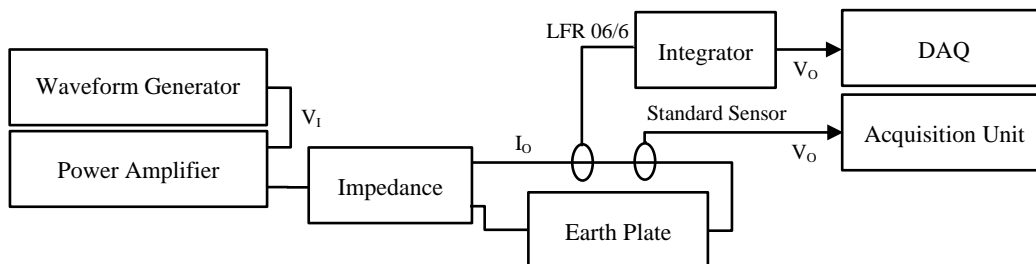


Fig. 33. Frequency characterization schema for LFR 06/6 from 10 to 150 kHz.

A different characterization setup is used for amplitude characterization of the LFR 06/6 according to equipment availability. This characterization setup is shown in Fig. 34.

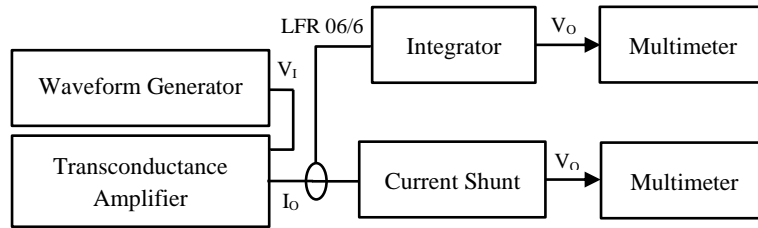


Fig. 34. Amplitude characterization schema for LFR 06/6.

Test Procedure

The test procedure for the frequency characterization of the LFR 06/6 is as follows:

- the connections are made according to Fig. 31 for the characterization up to a frequency of 10 kHz.
- the current waveform of known amplitude is generated by the waveform generator;
- the current waveform is measured by the LFR 06/6, and recorded by the DAQ;
- the sensitivity of the coil is calculated as in (7);

$$S = \frac{V_0}{I_1}, \quad (7)$$

where S is the sensitivity, V_0 is the sensor output, and I_1 is the current input.

- the connections are made according to Fig. 32 for the characterization in the frequency range of 10 to 150 kHz;
- the voltage waveform of known amplitude is generated by the waveform generator, and converted to the current waveform using the power amplifier and the output impedance;
- the input current waveform is measured simultaneously by the characterized sensor and LFR 06/6;
- the sensor output is measured using a characterized AC acquisition unit;
- the LFR 06/6 output is recorded using the DAQ;
- the input current value is calculated from the characterized sensor as in (8);

$$I_1 = \frac{V_0}{S}, \quad (8)$$

where I_1 is the input current, V_0 is the sensor output, and S is the sensitivity.

- the sensitivity is calculated from (7) and (8);
- the test process is repeated for varying frequencies to obtain the frequency behaviour of the LFR 06/6.

The test procedure for the amplitude characterization of the LFR 06/6 is as follows:

- the connections are made according to Fig. 33 for characterization in the amplitude range of 5 to 85 A;
- the voltage waveform of known frequency is generated by the waveform generator, and converted to the current waveform using the transconductance amplifier;
- the input current waveform is measured simultaneously by the characterized current shunt, and the LFR 06/6;
- the sensor outputs are recorded using the characterized multimeters;
- the input current value is calculated from the characterized current shunts, for the different levels of current as in (8);

- the sensitivity is calculated from (7) and (8);
- the test process is repeated for varying amplitudes to obtain the amplitude behaviour of the LFR 06/6.

Characterization Results

The measurement data for frequency and amplitude characterization of the Rogowski coil LFR 06/6 is discussed here. The characterization curve for the LFR 06/6 in error (%) with respect to the frequency is shown in Fig. 35. The current waveform of the amplitude of 1.00 A is used for the frequency characterization of LFR 06/6. The error value varies from -0.37 to 0.20% in the frequency range of 0.02 to 150 kHz. The error value varies within $\pm 0.40\%$, which is an acceptable level of variation, and the sensitivity values are used to convert the LFR 06/6 output to real values during the mathematical processing of the current waveform. The percentage error increases at frequencies higher than 10 kHz. The percentage error varies in the frequency range of 10 to 150 kHz, but this sensor is used to measure the fundamental current component at a frequency of 50 Hz.

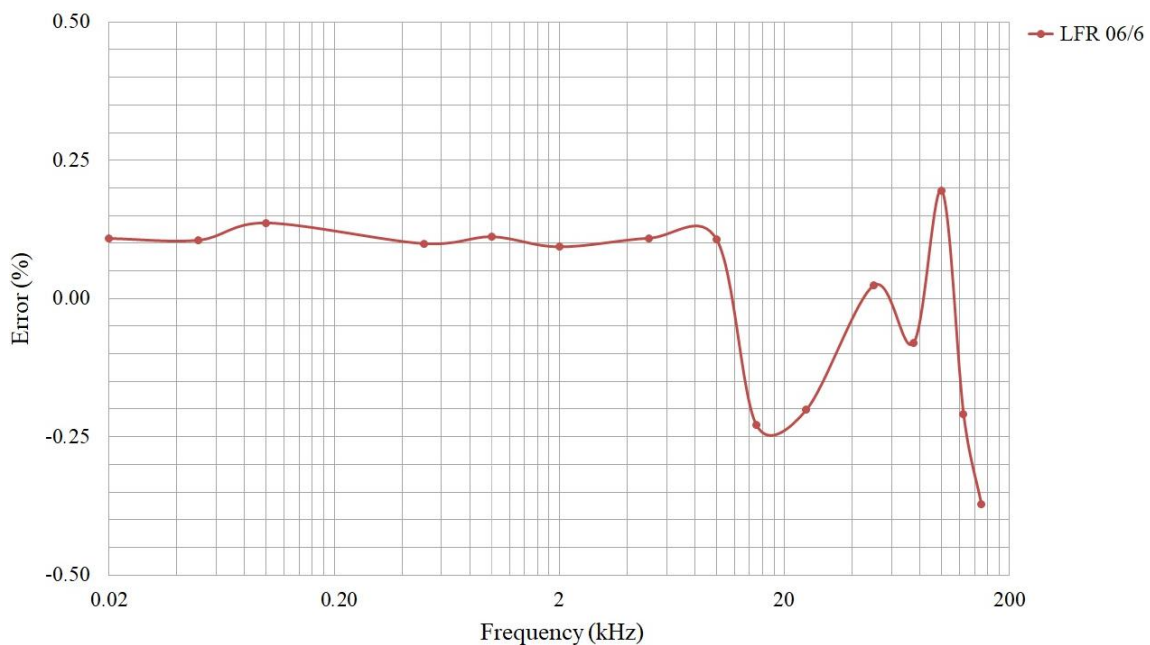


Fig. 35. Frequency characterization curve for LFR 06/6 at reference current of 1 A.

The characterization curve for LFR 06/6 in error (%) with respect to the amplitude is shown in Fig. 36. The voltage waveform of the frequency of 50 Hz, which is converted to the current waveform in the amplitude range of 5 to 85 A by a transconductance amplifier, is used for the amplitude characterization. The error value varies from -0.04 to 0.07% in the amplitude range of 5 to 85 A. The amplitude value varies within $\pm 0.10\%$, which is an acceptable level of variation, and the sensitivity values are used to convert the LFR 06/6 output to real values during the mathematical processing of the current waveform.

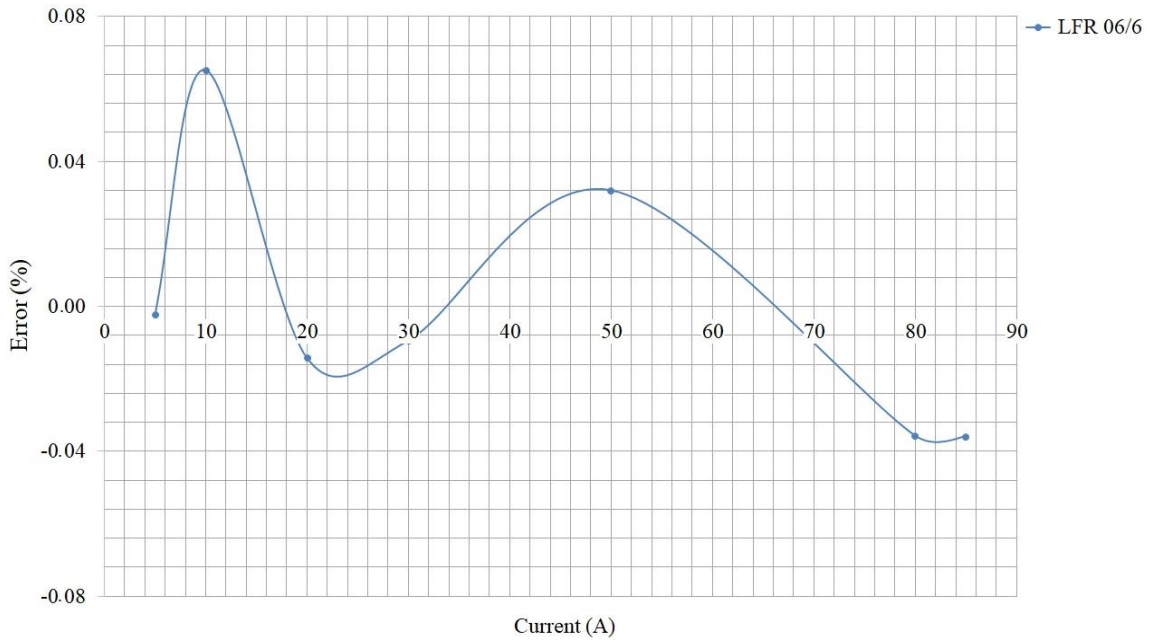


Fig. 36. Amplitude characterization curve for LFR 06/6 at reference frequency of 50 Hz.

3.1.2.5 Rogowski Coil CWT015 + First Order Passive High Pass Filter

The Rogowski coil CWT015 with the 1st order passive HPF is used in channel 4 to measure the supraharmonic current in the frequency range of 2 to 150 kHz in the electrical network. The performance characteristics of this sensor are listed in Table 2.

Equipment Used

The equipment used for the characterization of the CWT015 with the 1st order passive HPF are listed in Table 7 as given below.

Table 7. Equipment used for characterization of CWT015 with HPF.

Equipment	Model	Type	N° id
Waveform Generator	Fluke	5730A	LNE 1019684
Function Generator	HP	3325A	LNE 1019988
Power Amplifier	AR	500A250C	
Output Impedance	AR	IT1003	
Current Transformer	Eurocraft	B-0.1	LNE 1019976
Rogowski Coil	PEM	CWT015	LNE 1020873
1 st Order Passive HPF	Lab made	RC	-
AC Acquisition Unit	Fluke	5790A	LNE 1020703
DAQ	NI	PXIe-6124	LNE 1020904

Characterization Setup

Two different characterization setups are used for frequency characterization of the CWT015 with the HPF. The waveform generator, Fluke 5730A, which has a limited frequency bandwidth is used for

characterization up to the frequency of 10 kHz and is shown in Fig. 37. Meanwhile, for the characterization in the frequency range of 10 to 150 kHz, the HP function generator coupled with the AR amplifier is used and is shown in Fig. 38.

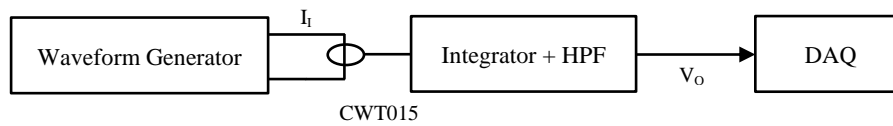


Fig. 37. Frequency characterization schema for CWT015 with HPF up to 10 kHz.

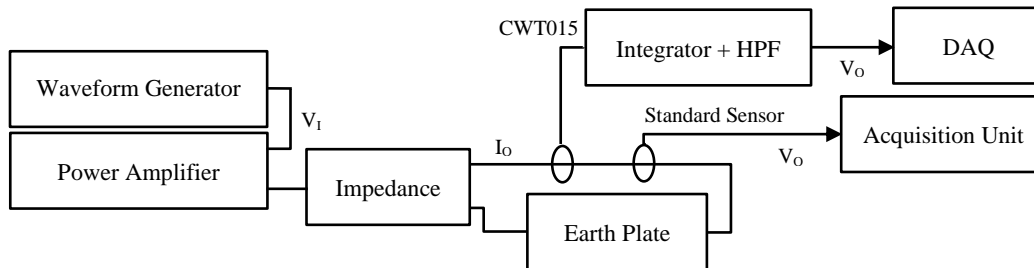


Fig. 38. Frequency characterization schema for CWT015 with HPF from 10 to 150 kHz.

The characterization setup from Fig. 34 is used for amplitude characterization of the CWT015 with the HPF. The test procedure used for frequency and amplitude characterization of the CWT015 with the HPF is detailed below.

Test Procedure

The test procedure for the frequency characterization of the CWT015 with the HPF is as follows:

- the connections are made according to Fig. 37 for the characterization up to a frequency of 10 kHz.
- the current waveform of known amplitude is generated by the waveform generator;
- the current waveform is measured by the CWT015 with the HPF and recorded by the DAQ;
- sensitivity is calculated as in (7);
- the connections are made according to Fig. 38 for the characterization in the frequency range of 10 to 150 kHz;
- the voltage waveform of known amplitude is generated by the waveform generator, and converted to the current waveform using the power amplifier and the output impedance;
- the input current waveform is measured simultaneously by the characterized sensor, and the CWT015 with the HPF;
- the standard sensor output is measured using the characterized AC acquisition unit;
- the CWT015 with the HPF output is recorded using the DAQ;
- the input current value is calculated from the characterized sensor as in (8);
- the sensitivity is calculated as in (7) and (8);
- the test process is repeated for varying frequencies to obtain the frequency behaviour of the CWT015 with the HPF.

The test procedure for the amplitude characterization of the CWT015 with the HPF is as follows:

- the connections are made according to Fig. 36 for the characterization in the amplitude range of 0.02 to 1.00 A;
- the current waveform of the frequency 5 kHz is generated by the waveform generator;

- the current waveform is measured by the CWT015 with the HPF, and recorded by the DAQ;
- the sensitivity is calculated as in (7).

Characterization Results

The measurement data for the frequency and amplitude characterization of the Rogowski coil CWT015 with the 1st order passive HPF is discussed here. The characterization curve for the CWT015 with the HPF in error (%) with respect to the frequency is shown in Fig. 39. The current waveform of the amplitude of 1 A is used for the frequency characterization of the CWT015 with the HPF. The error value varies from -3.21 to 0.68% in the frequency range of 0.02 to 150 kHz. The amplitude value varies within $\pm 0.70\%$ except at 2 kHz, which is an acceptable level of variation. The sensitivity values are used to convert the CWT015 with the HPF output to real values during the mathematical processing of the current waveform.

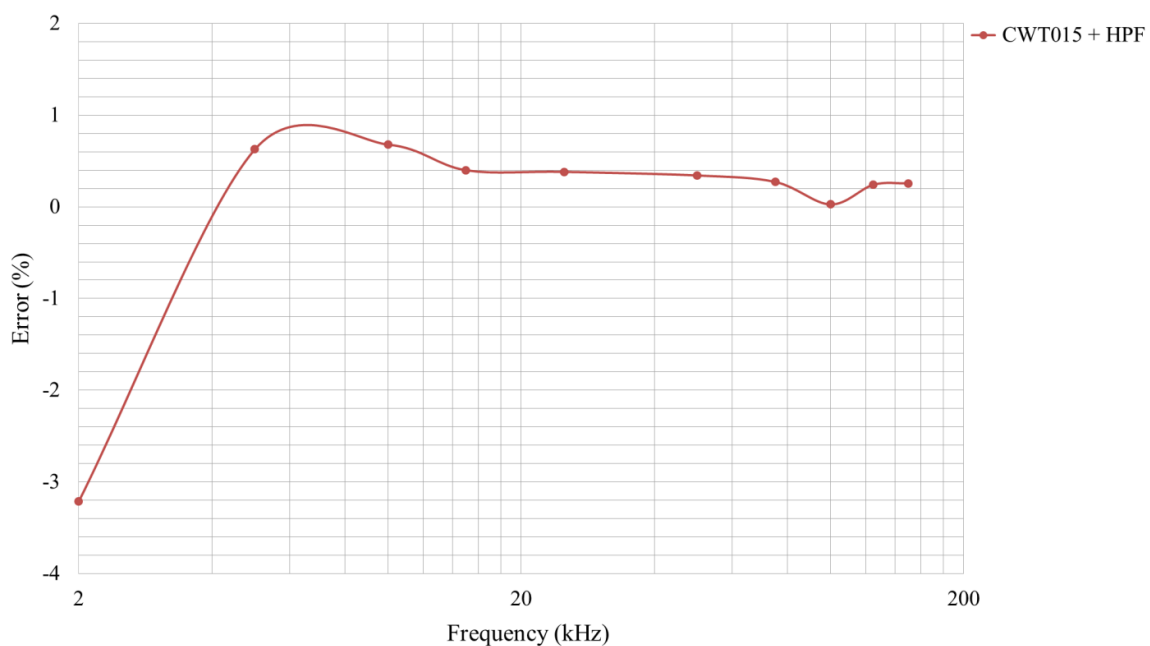


Fig. 39. Frequency characterization curve for CWT015 with HPF at reference current of 1 A.

The characterization curve for the CWT015 with the HPF in error (%) with respect to the amplitude is shown in Fig. 40. The current waveform of the frequency of 5 kHz in the amplitude range of 0.02 to 1.00 A is used for the amplitude characterization. The error value varies from -0.65 to 1.54% in the amplitude range of 0.02 to 1 A. The amplitude value varies within $\pm 0.65\%$ except for 0.02 A, which is an acceptable level of variation, and the sensitivity values are used to convert the VSU output to real values during the mathematical processing of the current waveform.

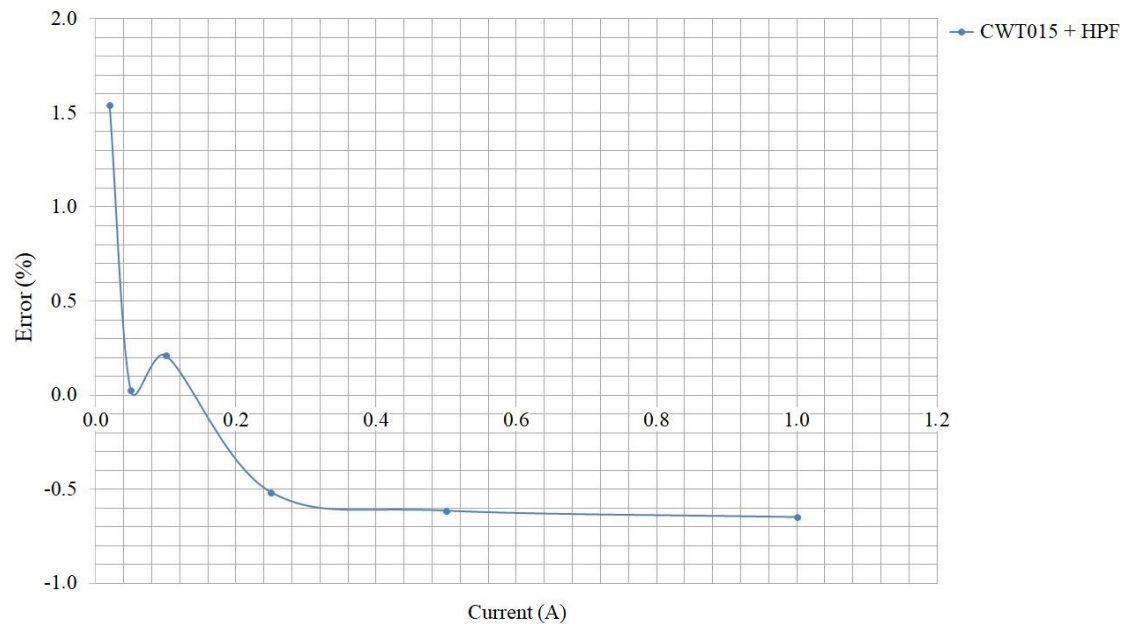


Fig. 40. Amplitude characterization curve for CWT015 with HPF at reference frequency of 5 kHz.

3.2 Measurement System Version 2

The updated version of the measurement system is designed with reference to the results from the laboratory characterization in section 3.1.2. The measurement system 2 is designed after the experiences from the network tests using the measurement system 1 in section 3.1. The measurement system is designed with an objective to measure emissions at higher frequencies close to 150 kHz. The design and characterization of the second version of the measurement system, including all the 4 channels are described in detail below. This version of the measurement system consists of updated sensors and recorder with a better resolution, which can measure supraharmmonic emissions in the frequency range of 2 to 150 kHz in a more efficient manner. This measurement system was used for the second measurement campaign at Concept Grid, EDF.

3.2.1 Design

The design of measurement system version 2 is discussed here. This version uses an updated sensor, the LFR 03/3 with a better frequency response in the frequency range of 2 to 150 kHz, and a recorder, the NI PXIe-6124 with a better resolution of 16 bits compared to the earlier recorder with a resolution of 12 bits. The fundamental voltage component is measured using channel 1, which consists of the VT that step down the voltage from 230 to 10 V at a frequency of 50/60 Hz under no load condition [82]. A voltage divider with ratio 2:1 is added at the secondary side of the transformer to reduce the voltage to 5 V, such that it is compatible with the DAQ input. The supraharmmonic voltage components are measured using channel 2, which consists of a 2nd order passive HPF with the cut-off frequency of 590 Hz. The HPF is followed by an optoisolator, which has a transmitter and receiver connected by an optical fibre. The optoisolator has an input voltage level of 3.5 V and provides isolation between the network and recorder. This ensures the safety of both user and equipment.

The Rogowski coils are used to measure the fundamental and supraharmmonic current components in Channels 3 and 4. The LFR 06/6 is used to measure the fundamental current component [79]. The LFR 03/3 measures the current emissions in the frequency range of 2 to 150 kHz [79]. In order to further attenuate the lower order frequencies, the 1st order passive HPF is implemented after the sensor

output. The electrical schema for the second version of the measurement system is shown in Fig. 41. The technical specifications of the waveform recorder (DAQ PXIe-6124) are as follows [83]:

- maximum bandwidth of 3 MHz;
- maximum sampling rate of 4 MS/s per channel;
- 4 analog input channels;
- maximum voltage level up to ± 11 V;
- resolution of 16 bits.

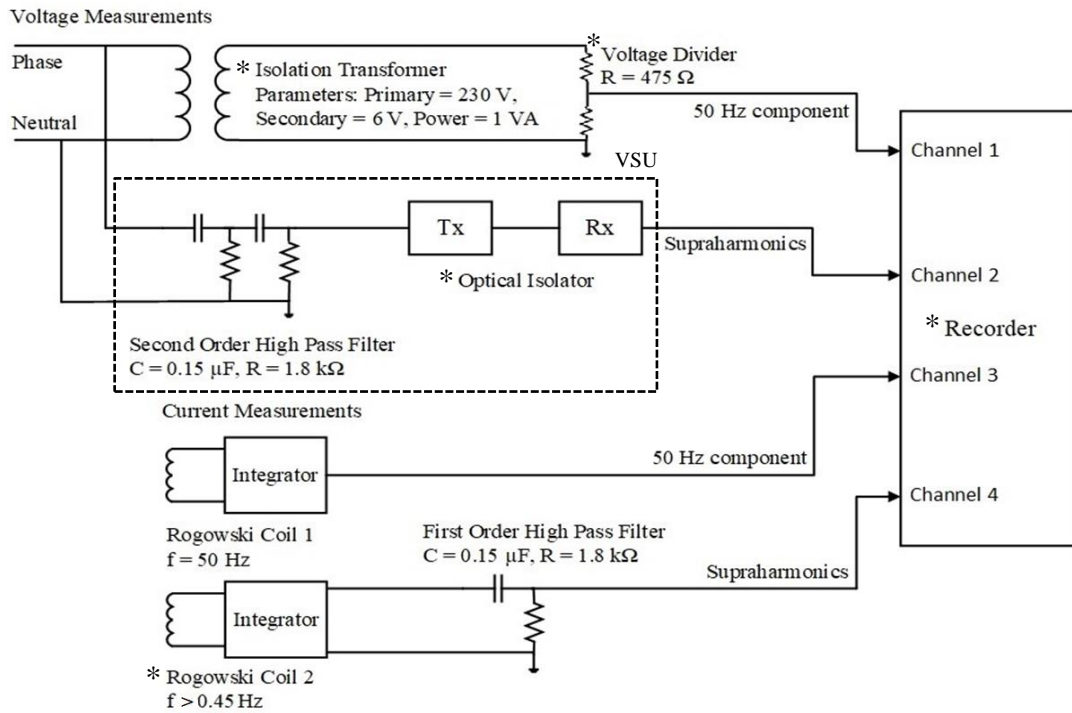


Fig. 41. Measurement system version 2 electrical schema.

* represent the new components in the measurement system. The VT used for measuring the fundamental voltage component is shown in Fig. 42. The VT steps down the voltage input from the LV electrical network.



Fig. 42. VT used in channel 1.

The transmitter and receiver modules of the optoisolator used for the isolation of the electrical network and the recorder in channel 2 are shown in Fig. 43.



Fig. 43. Optoisolator used in channel 2.

The Rogowski coils LFR 06/6 and LFR 03/3 used in the measurement system version 2 are shown in Fig. 20 and Fig. 44.



Fig. 44. LFR 03/3 used in channel 4.

The performance characteristics of the Rogowski coil LFR 03/3, according to the manufacturer [79] are listed in Table 8. The table lists the sensitivity, peak current value, and bandwidth of the coil.

Table 8. Performance characteristics of LFR 03/3 [79].

Type	Sensitivity (mV/A)		Peak Current (kA)		LF Bandwidth (3 dB) (Hz)	HF Bandwidth (3 dB) (MHz)
	$\times 10$	$\times 1$	$\times 10$	$\times 1$		
LFR 03/3	100	10	0.06	0.60	0.45	1.0
	$\times 10$	$\times 1$	$\times 10$	$\times 1$		

3.2.2 Characterization

As for the measurement system version 1, the characterization of each component of the measurement system, such as the sensors, is done for varying frequencies and amplitudes. The characterization tests help to determine the measurement system performance in the frequency range of 2 to 150 kHz and for different levels of amplitude. The characterization of the LFR 06/6 is explained in section 3.1.1.1.

3.2.2.1 Voltage Transformer + Divider

The first measurement channel consists of a VT, which steps down the network voltage from 230 to 10 V at a frequency of 50/60 Hz under no load condition [82]. This secondary voltage value is not compatible with the input voltage range of the DAQ used for recording the measurements. Therefore, the resistive voltage divider with the ratio 2:1 is used to reduce the secondary voltage from the VT. The VT ensures the isolation between the grid and measurement equipment, thereby confirming the safety for both user and equipment. The frequency and amplitude characterization of the VT with divider is described below. This channel is used to measure the fundamental voltage component.

Equipment Used

The equipment used for the characterization of the VT with the voltage divider are listed in Table 9.

Table 9. Equipment used for characterization of transformer with divider.

Equipment	Model	Type	N° id
Waveform Generator	Fluke	5730A	LNE 1019684
VT	Block	VB3.2/50	-
Divider	Lab made	Resistive	-
DAQ	NI	PXIe-6124	LNE 1020904

Characterization Setup

The characterization setup used for channel 1 with the VT with the divider is shown in Fig. 45. The setup uses the waveform generator, transformer, divider, and DAQ for the characterization tests.

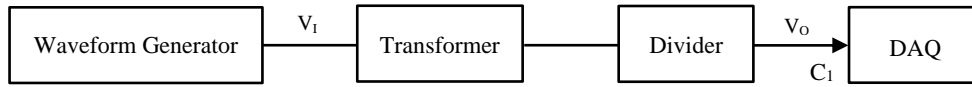


Fig. 45. Characterization schema for VT with divider.

Test Procedure

The test procedure for the frequency characterization of the transformer with the divider is as follows:

- the voltage waveform of known amplitude is generated using the waveform generator;
- channels 1 and 2 are the voltage input and output from the VT with the divider;
- the frequency is varied step by step, and the measurements of channels 1 and 2 are recorded;
- the VT with divider factor is the ratio of the input voltage to the output voltage as in (4).

The test procedure for the amplitude characterization of the VT with the divider is as follows:

- the voltage waveform of known frequency is generated using the waveform generator;
- channels 1 and 2 the voltage input and output from the VT with the divider;
- the amplitude is varied step by step, and the measurements of channels 1 and 2 are recorded;
- the VT with divider factor is the ratio of the input voltage to the output voltage as in (4).

Characterization Results

The measurement data for frequency and amplitude characterization of the VT with the divider is discussed here. The characterization curve for the VT with the divider in error (%) with respect to the frequency is shown in Fig. 46. The voltage waveform of the amplitude of 6 V is used for the frequency characterization. The error value varies from -2.00 to 0.70% in the frequency range of 0.02 to 0.50 kHz. The amplitude value varies within $\pm 0.70\%$ except for a frequency of 0.02 kHz, which is an acceptable level of variation.

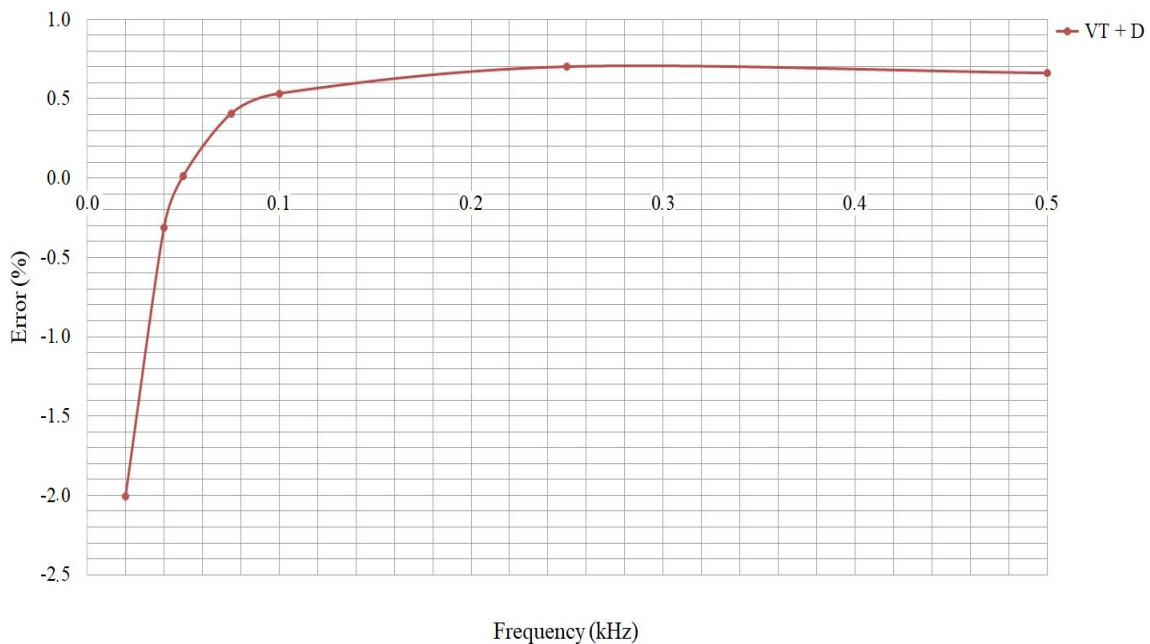


Fig. 46. Frequency characterization curve for VT with divider at reference voltage of 6 V.

The characterization curve for the VT with the divider in error (%) with respect to amplitude is shown in Fig. 47. The voltage waveform of the frequency of 50 Hz is used for the amplitude characterization of the VT with the divider. The error value varies from -0.45 to 0.38% in the amplitude range of 10 to 230 V. The amplitude value varies within $\pm 0.50\%$, which is an acceptable level of variation, and the sensitivity values are used to convert the VT with the divider output to real values during the mathematical processing of the voltage waveform.

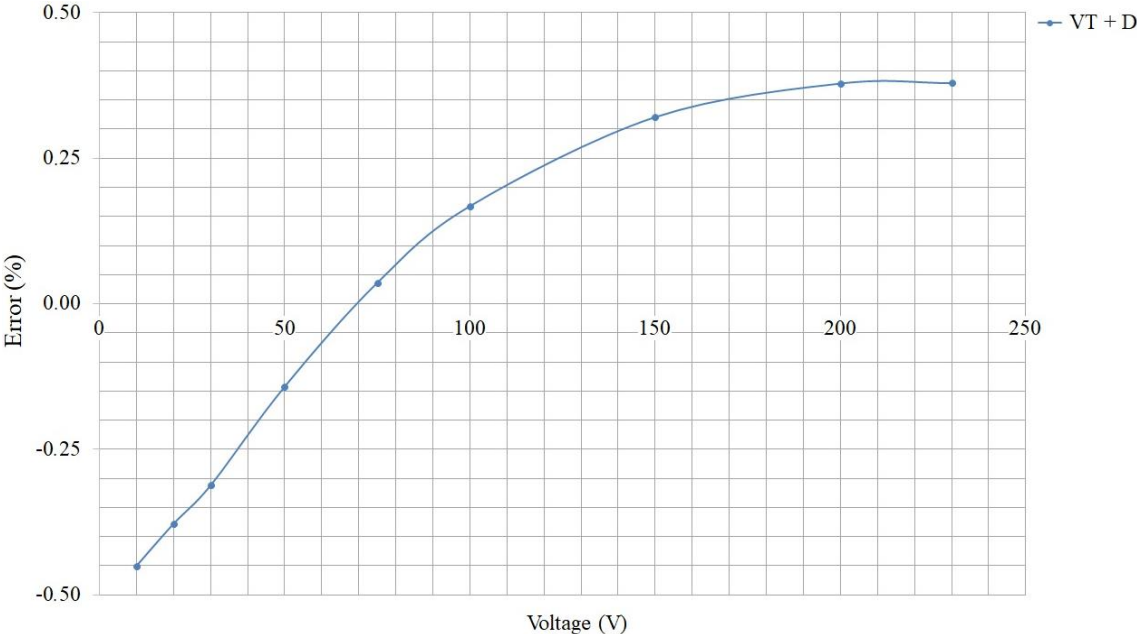


Fig. 47. Amplitude characterization curve for VT with divider at reference frequency of 50 Hz.

3.2.2.2 Optoisolator

The optoisolator with a transmitter and receiver, which are connected using an optical fibre, is used to ensure the electrical isolation in the channel 2 of the measurement system. The characteristics of the optoisolator [83] are given below:

- maximum bandwidth of 12.5 MHz;
- maximum sampling rate of 50 MS/s;
- two voltage levels, ± 5 V and ± 1 V;
- resolution of 12 bits.

The characterization of the optoisolator is described below.

Equipment Used

The equipment used for the characterization of the optoisolator are listed in Table 10.

Table 10. Equipment used for characterization of optoisolator.

Equipment	Model	Type	N° id
Waveform Generator	NI	PXIe-5413	LNE 1020904
Optoisolator	TTI	LTX-5510	-
DAQ	NI	PXIe-6124	LNE 1020904

Characterization Setup

The characterization setup used for the optoisolator is shown in Fig. 48. The setup uses the PXIe waveform generator, optoisolator, and PXIe DAQ for the characterization tests.

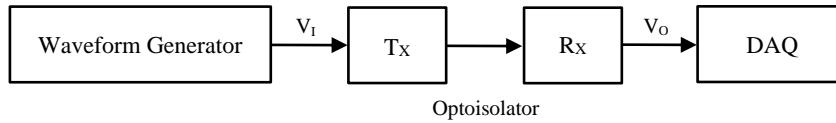


Fig. 48. Characterization schema for optoisolator.

Test Procedure

The test procedure for the frequency characterization of the optoisolator is as follows:

- the voltage waveform of known amplitude is generated using the waveform generator;
- channels 1 and 2 indicate voltage input and output of the optoisolator;
- the voltage waveform frequency is varied step by step, and the measurements of channels 1 and 2 are recorded;
- the transfer function is the ratio of the output voltage to the input voltage of the optoisolator as in (6).

The test procedure for the amplitude characterization of the optoisolator is as follows:

- the voltage waveform of known frequency is generated using the waveform generator;
- channels 1 and 2 indicate the voltage input and output of the optoisolator;
- the voltage waveform amplitude is varied step by step, and the measurements of channels 1 and 2 are recorded;
- the transfer function is the ratio of the output voltage to the input voltage of the optoisolator as in (6).

Characterization Results

The measurement data for the frequency and amplitude characterization of the optoisolator is discussed here. Percentage error is calculated as in (9).

$$\varepsilon (\%) = \frac{V_O - V_I}{V_I} \times 100, \quad (9)$$

where V_O is the RMS output voltage and V_I is the RMS input voltage.

The characterization curve for the optoisolator in error (%) with respect to frequency is shown in Fig. 49. The voltage waveform of the amplitude of 3.50 V is used for the frequency characterization tests from 2 to 150 kHz. The error values vary from -0.61 to -0.17% in the frequency range of 2 to 150 kHz. The amplitude error values vary within $\pm 0.70\%$, which is an acceptable level of variation, and the sensitivity values are used to convert the optoisolator output to real values during the mathematical processing of the voltage waveform.

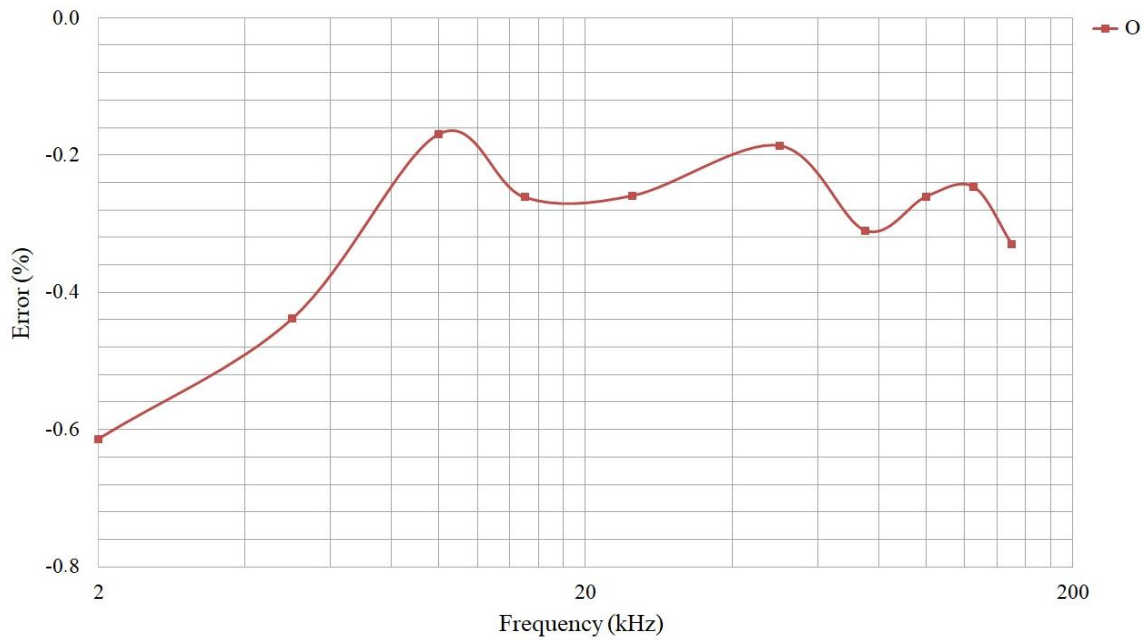


Fig. 49. Frequency characterization curve for optoisolator at reference voltage of 3.50 V.

The characterization curve for the optoisolator in error (%) with respect to the amplitude is shown in Fig. 50. The voltage waveform of the frequency of 20 kHz is used for the amplitude characterization of the optoisolator. The error values vary from -8.94 to 0.44% in the amplitude range of 0.02 to 3.50 V. The error (%) is higher for the lower amplitude waveforms compared to the higher amplitude waveforms. As the amplitude of the voltage waveform increases from 0.02 to 3.50 V, the error decreases from -8.94 to -0.44%. This indicates the importance of applying the corrections to the optoisolator outputs after the measurements in order to obtain accurate measurement data.

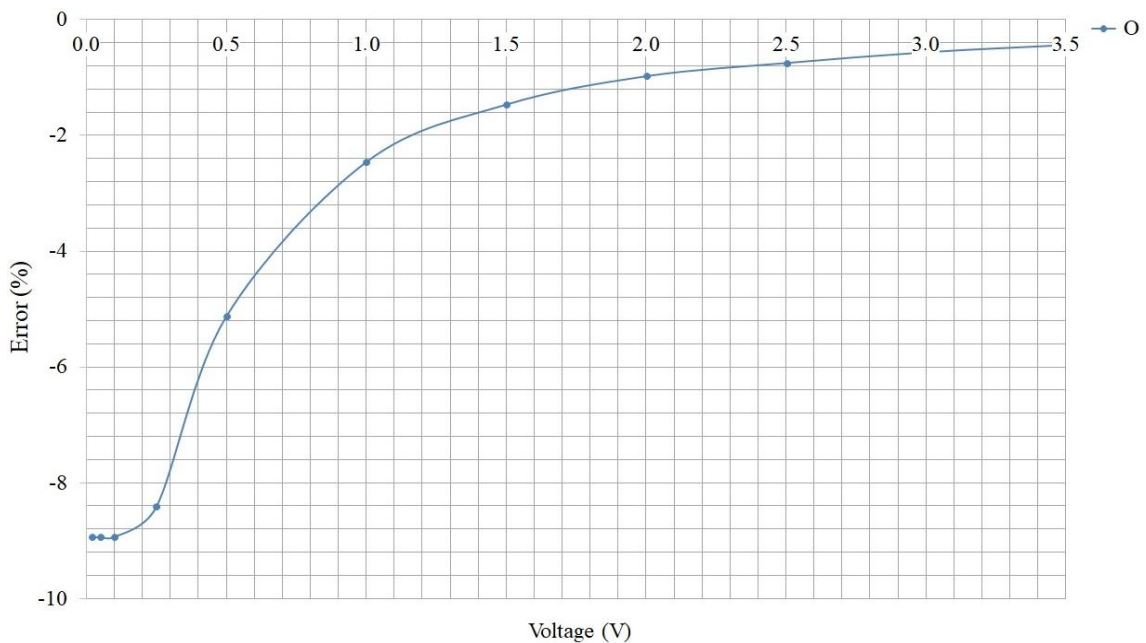


Fig. 50. Amplitude characterization curve for optoisolator at reference frequency of 20 kHz.

3.2.2.3 Second Order Passive High Pass Filter + Optoisolator

Channel 2 is used to measure the supraharmonic voltage component in the frequency range of 2 to 150 kHz. In order to benefit the resolution of the oscilloscope, it is necessary to attenuate the fundamental voltage component in the electrical network. This is realized by implementing the 2nd order passive HPF in the measurement system. The frequency and amplitude characterization of the HPF is explained in section 3.1.1.1. In addition, to ensure the electrical isolation, the optoisolator is used. The characterization of the HPF with the optoisolator is described below.

Equipment Used

The equipment used for the characterization of the 2nd order passive HPF with the optoisolator are listed in Table 11.

Table 11. Equipment used for characterization of HPF with optoisolator.

Equipment	Model	Type	N° id
Waveform Generator	NI	PXIe-5413	LNE 1020904
2 nd Order Passive HPF	Lab made	RC	-
Optoisolator	TTI	LTX-5510	-
DAQ	NI	PXIe-6124	LNE 1020904

Characterization Setup

The characterization setup used for the HPF with the optoisolator is shown in Fig. 51. The setup uses the PXIe waveform generator, optoisolator, and PXIe DAQ for the characterization tests.

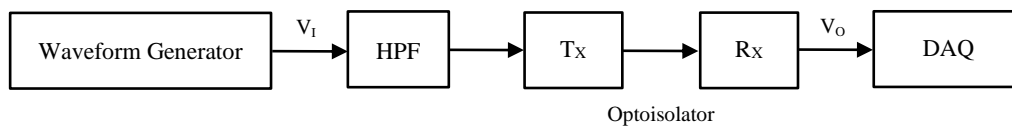


Fig. 51. Characterization schema for HPF with optoisolator.

Test Procedure

The test procedure for the frequency characterization of the HPF with optoisolator is as follows:

- the voltage waveform of known amplitude is generated using the waveform generator;
- channels 1 and 2 indicate the voltage input and output of the HPF with the optoisolator;
- the voltage waveform frequency is varied step by step, and the measurements of channels 1 and 2 are recorded;
- the transfer function is the ratio of the output voltage to the input voltage of the HPF with the optoisolator as in (6).

The test procedure for the amplitude characterization of the HPF with optoisolator is as follows:

- the voltage waveform of known frequency is generated using the waveform generator;
- channels 1 and 2 indicate the voltage input and output of the HPF with the optoisolator;
- the voltage waveform frequency is varied step by step, and the measurements of channels 1 and 2 are recorded;
- the transfer function is the ratio of the output voltage to the input voltage of the HPF with the optoisolator as in (6).

Characterization Results

The measurement data for the frequency and amplitude characterization of the HPF with the optoisolator is discussed here. The characterization curve for the HPF with the optoisolator in error (%) with respect to frequency is shown in Fig. 52. The voltage waveform of the amplitude of 3.50 V is used for the frequency characterization tests in the frequency range of 2 to 150 kHz. The percentage error varies from -20.68 to 0.25% in the frequency range of 2 to 150 kHz. The amplitude value varies within $\pm 0.80\%$ except in the frequency range of 2 to 10 kHz, which is an acceptable level of variation, and the sensitivity values are used to convert the optoisolator output to real values during the mathematical processing of the voltage waveform.

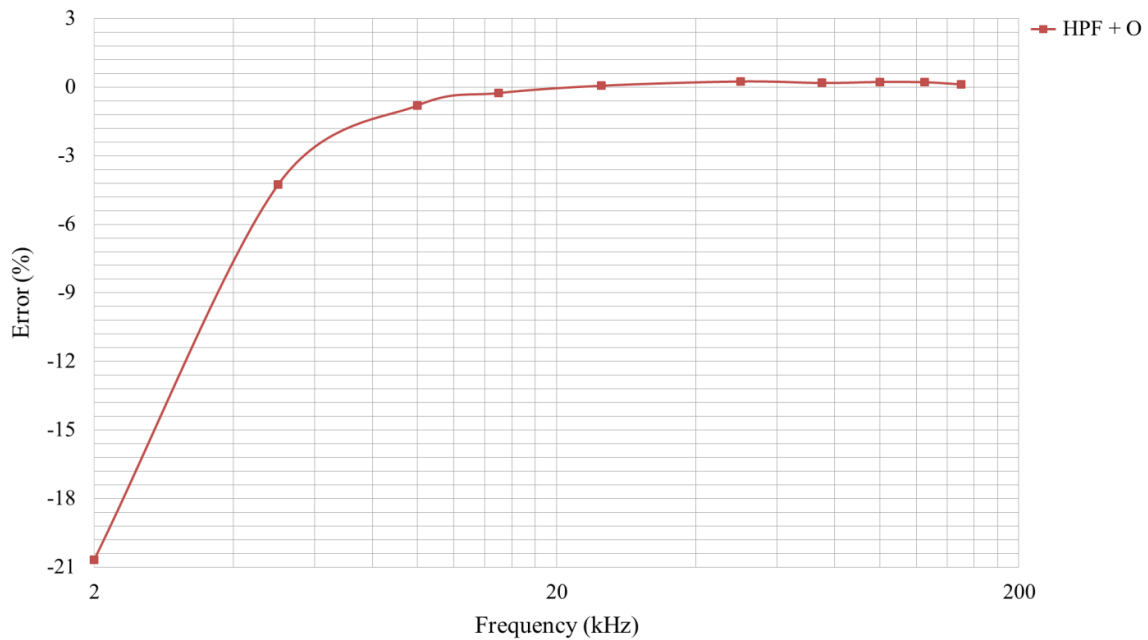


Fig. 52. Frequency characterization curve for HPF with optoisolator at reference voltage of 3.50 V.

The characterization curve for the HPF with the optoisolator in percentage error with respect to the amplitude is shown in Fig. 53. The voltage waveform of the frequency of 20 kHz is used for the amplitude characterization. The error value varies from -8.03 to -0.23% in the amplitude range of 0.02 to 3.50 V. The percentage error is higher for the lower amplitude waveforms compared to the higher amplitude waveforms. As the amplitude of the voltage waveform increases from 0.02 to 3.50 V, the error decreases from -8.03 to -0.23%. This further reiterates the importance of applying the corrections to the optoisolator outputs after the laboratory and electrical network measurements to obtain the accurate measurement data.

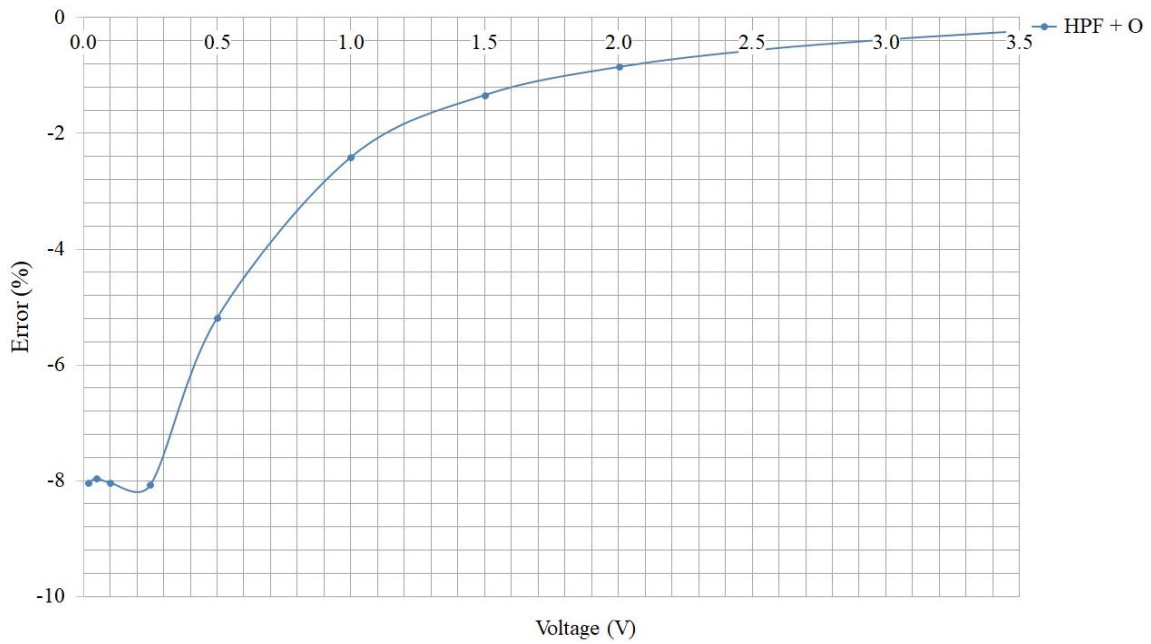


Fig. 53. Amplitude characterization curve for HPF with optoisolator at reference frequency of 20 kHz.

3.2.2.4 Rogowski Coil LFR 03/3 + First Order High Pass Filter

The Rogowski coil LFR 03/3 with the 1st order passive HPF is used in channel 4 to measure the supraharmonic current in the frequency range of 2 to 150 kHz in the electrical network. The performance characteristics of this sensor are listed in Table 18.

Equipment Used

The equipment used for the characterization of the LFR 03/3 with the 1st order passive HPF are listed in Table 12.

Table 12. Equipment used for characterization of LFR 03/3 with HPF.

Equipment	Model	Type	N° id
Waveform Generator	Fluke	5730A	LNE 1019684
Function Generator	HP	3325A	LNE 1019988
Power Amplifier	AR	500A250C	
Output Impedance	AR	IT1003	
Current Transformer	Eurocraft	B-0.1	LNE 1019976
Rogowski Coil	PEM	LFR 03/3	LNE 1020906
1 st Order Passive HPF	Lab made	RC	-
AC Acquisition Unit	Fluke	5790A	LNE 1020703
DAQ	NI	PXIe-6124	LNE 1020904

Characterization Setup

Two different characterization setups are used for the frequency characterization of the LFR 03/3 with the HPF. The waveform generator, Fluke 5730A with limited frequency bandwidth for the current

waveform is used for the characterization up to the frequency of 10 kHz and is shown in Fig. 54. Meanwhile, for the characterization in the frequency range of 10 to 150 kHz, the HP function generator coupled with the AR amplifier is used and is shown in Fig. 55.

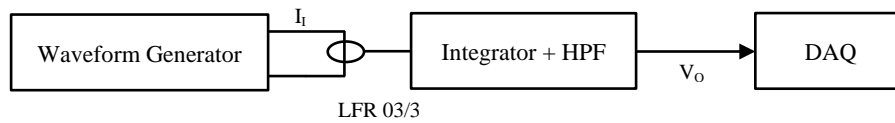


Fig. 54. Frequency characterization schema for LFR 03/3 with HPF up to 10 kHz.

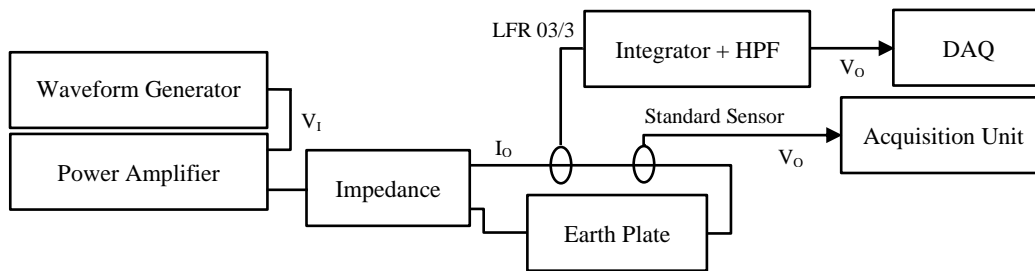


Fig. 55. Frequency characterization schema for LFR 03/3 with HPF from 10 to 150 kHz.

The characterization setup from Fig. 34 is used for amplitude characterization of the LFR 03/3 with the HPF. The test procedure used for frequency and amplitude characterization of the LFR 03/3 with the HPF is detailed below.

Test Procedure

The test procedure for the frequency characterization of the LFR 03/3 with HPF is as follows:

- the connections are made according to Fig. 54 for characterization up to a frequency of 10 kHz.
- the current waveform of known amplitude is generated by the waveform generator;
- the current waveform is measured by the LFR 03/3 with the HPF, and is recorded by the DAQ;
- the sensitivity is calculated as in (7);
- the connections are made according to Fig. 55 for the characterization in the frequency range of 10 to 150 kHz;
- the voltage waveform of known amplitude is generated by the waveform generator, and is converted to the current waveform using the power amplifier and the output impedance;
- the input current waveform is measured simultaneously by the characterized sensor and the LFR 03/3 with the HPF;
- the standard sensor output is measured using the characterized AC acquisition unit;
- the LFR 03/3 with the HPF output is recorded using the DAQ;
- the input current value is calculated from the characterized sensor as in (8);
- the sensitivity is calculated as in (7) and (8);
- the test process is repeated for varying frequencies to obtain the frequency behaviour of the LFR 03/3 with the HPF.

The test procedure for the amplitude characterization of the LFR 03/3 with the HPF is as follows:

- the connections are made according to Fig. 34 for the characterization in the amplitude range of 0.02 to 1.00 A;
- the current waveform with the frequency of 5 kHz is generated by the waveform generator;
- the current waveform is measured by the LFR 03/3 with the HPF, and is recorded by the DAQ;

- the sensitivity is calculated as in (7).

Characterization Results

The measurement data for the frequency and amplitude characterization of the Rogowski coil LFR 03/3 with the 1st order passive HPF is discussed here. The characterization curve for the LFR 03/3 with the HPF in error (%) with respect to frequency is shown in Fig. 56. The current waveform of the amplitude of 1 A is used for the frequency characterization of the LFR 03/3 with the HPF. The error value varies from -2.41 to 0.37% in the frequency range of 2 to 150 kHz. The amplitude value varies within $\pm 0.40\%$ except at a frequency of 2 kHz, which is an acceptable level of variation, and the sensitivity values are used to convert the LFR 03/3 with the HPF output to real values during the mathematical processing of the current waveform.

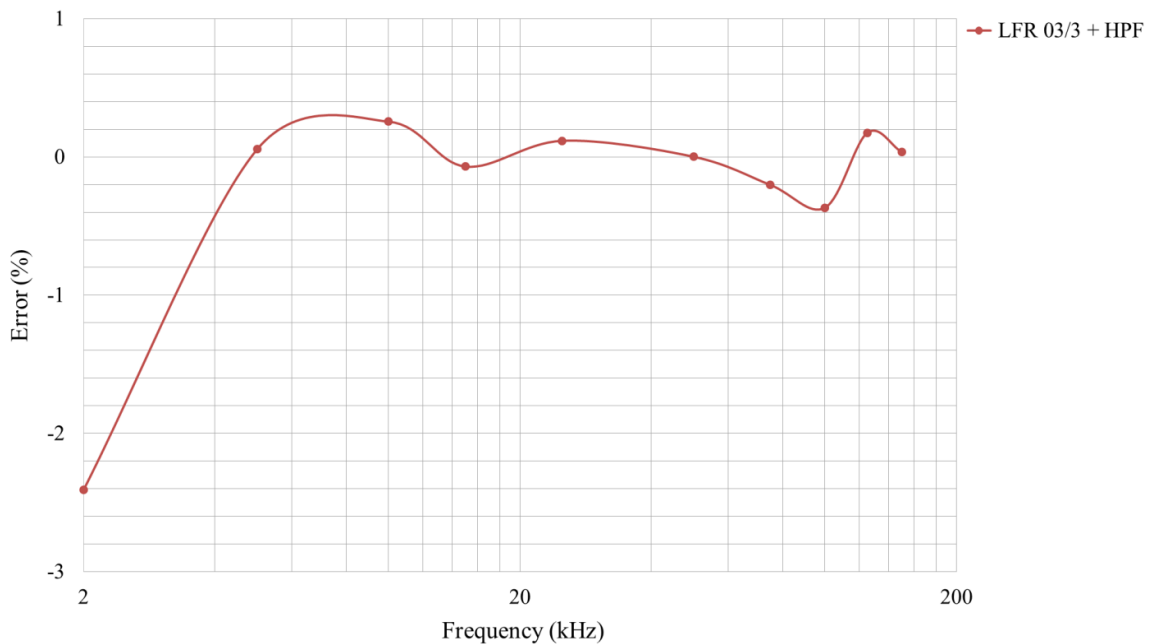


Fig. 56. Frequency characterization curve for LFR 03/3 with HPF at reference current of 1 A.

The characterization curve for the LFR 03/3 with the HPF in error (%) with respect to the amplitude is shown in Fig. 57. The current waveform with a frequency of 5 kHz in the amplitude range of 0.02 to 1.00 A is used for the amplitude characterization. The error value varies from -1.01 to 0.96% in the amplitude range of 0.02 to 1 A. The amplitude value varies within $\pm 1.01\%$, which is an acceptable level of variation, and the sensitivity values are used to convert the LFR 03/3 with the HPF output to real values during the mathematical processing of the current waveform.

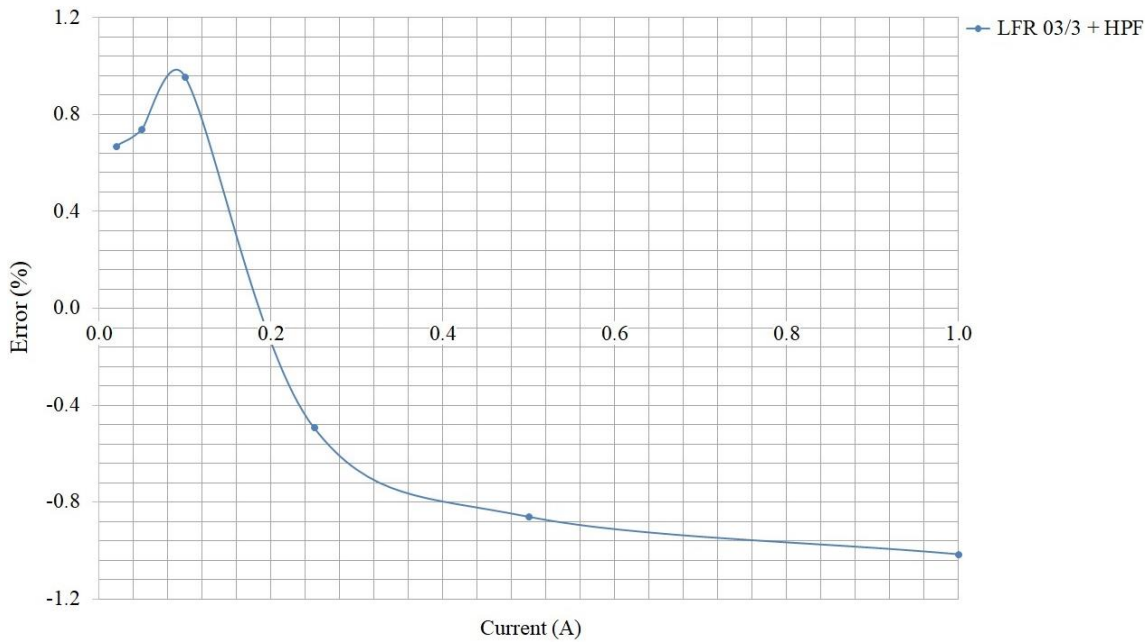


Fig. 57. Amplitude characterization curve for LFR 03/3 with HPF at reference frequency of 5 kHz.

3.3 Summary

The design and characterization of the measurement system versions 1 and 2 are discussed here. The frequency and amplitude characterization of all the 4 channels of the measurement system helps to understand the measurement system behavior. The amplitude and frequency characterization of the measurement systems are explained above. The voltage and current sensors have an acceptable level of the percentage error for the frequency and amplitude characterization. Both versions of the measurement systems use 4 measurement channels, 2 for the voltage waveforms and 2 for the current waveforms. Both systems use the Rogowski coils for the current measurement. The main difference between the two systems are the voltage sensors and recorder. The VSU of the measurement system version 1 has a linear behavior in the frequency range of 30 to 150 kHz, whereas the VSU of the measurement system version 2 has a linear behavior in the frequency range of 2 to 150 kHz. This enables the separate measurement of the fundamental voltage component in the frequency of 50 Hz using channel 1, and the supraharmonic voltage components in the frequency range of 2 to 150 kHz using channel 2. Therefore, the VSU used in the channel 2 of the measurement system version 2 has a better linearity in the frequency range of 2 to 30 kHz compared to the VSU used in the measurement system version 1, as detailed above.

In addition, channel 4 for the measurement of supraharmonic current components in the frequency range of 2 to 150 kHz uses different Rogowski coils in both versions of the measurement system. The Rogowski coil LFR 03/3 used in channel 3 of the second version of the measurement system has better linearity in the frequency range of 2 to 150 kHz. The Rogowski coil CWT015 with the HPF has a better amplitude response compared to the LFR 03/3 in the amplitude range of 0.02 to 1.00 A, where as the LFR 03/3 with the HPF has a better frequency response in the frequency range of 2 to 150 kHz. Hence for the better frequency response, the LFR 03/3 with the HPF is used for measuring the supraharmonic current emissions in the frequency range of 2 to 150 kHz. The DAQ used in the version 2 has a resolution of 16 bits compared to the oscilloscope used in the version 1 that has a resolution of 12 bits. Therefore, the DAQ used in the version 2 is better for recording the supraharmonic emissions

in the frequency range of 2 to 150 kHz, since it has a better resolution of 16 bits. The test signals used for each sensors in the measurement channels varies with the purpose like measurement range of the respective sensor. The electrical network measurements, which include individual and combination tests at the Concept Grid, EDF, using both versions of the measurement systems are described in the chapter 4.

CHAPTER 4
MEASUREMENT CAMPAIGNS

4 MEASUREMENT CAMPAIGNS

The measurements campaigns to identify the supraharmonic emissions in the frequency range of 2 to 150 kHz in real electrical networks are performed at Concept Grid, EDF. Few additional measurements during measurement campaign 1 were performed at laboratory Maison Connecté bas carbone (MCbc), EDF. The EDF Group is one of the leading electricity company and is well established in the EU. EDF along with its different affiliate companies covers electricity-based activities from the generation to retail.

4.1 Concept Grid

Concept Grid is located in the Les Renardières site, south of Paris, France, is a new laboratory designed and dedicated for testing and validating the smart grid equipment, systems, and functions. The platform studies and guides the integration of RES in to the existing electric system, as well as new applications, such as energy storage and EVs. Concept Grid is designed to provide a halfway between the laboratory and electrical network experiments. Therefore, it is possible to conduct the complex testing campaigns at this platform that otherwise would be impossible to perform on a real network system in complete safety. The main objective of the Concept Grid is to reproduce the real operation of the electric network. The platform [86]-[88] consists of:

- a control center to operate the network and monitor the tests;
- a primary substation supplying MV and LV grids;
- a MV network of 3 km including the overhead lines and underground cables supplying a LV network of 7 km;
- an array of RLC cells are added to the network to make an equivalent of additional cable length of 120 km for effective portrayal of the real grid;
- a residential neighbourhood of five houses of an area of 20 m² and these houses are equipped with equipment like smart meters, heat pumps, PV panels, EVCs and storage systems, etc.

The Concept Grid platform schema is shown in Fig. 58.

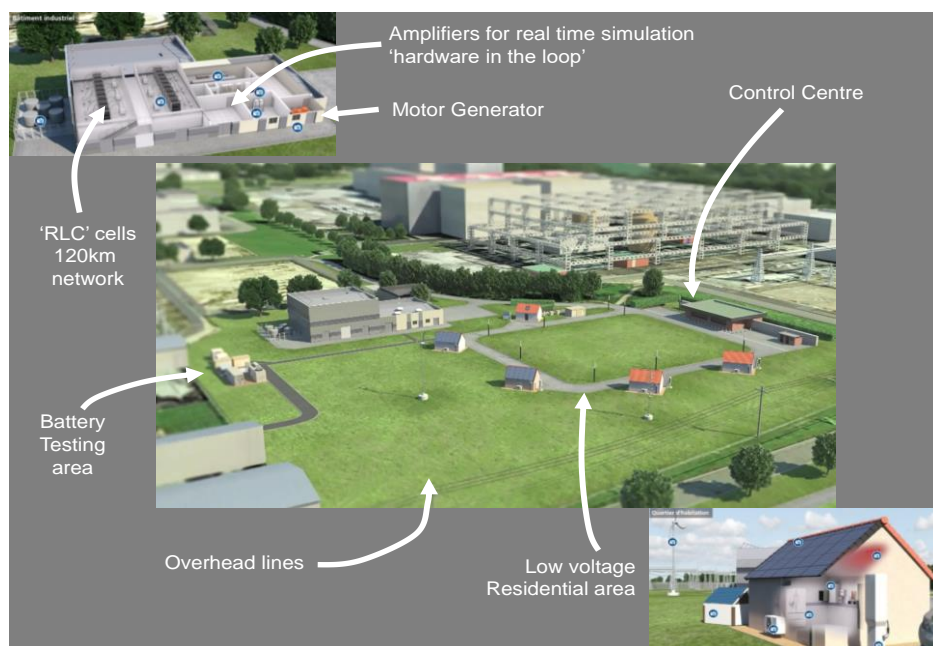


Fig. 58. Concept Grid platform [87].

Concept Grid provides extensive solutions to smart grids issues. The platform allows to reproduce microgrids, islanded systems, and to change the topology according to the tests. It is also possible to perform the configurations and experiments in normal and disturbed conditions. The different measurement points (MP) assigned at Concept Grid, EDF, is shown in Fig. 59.

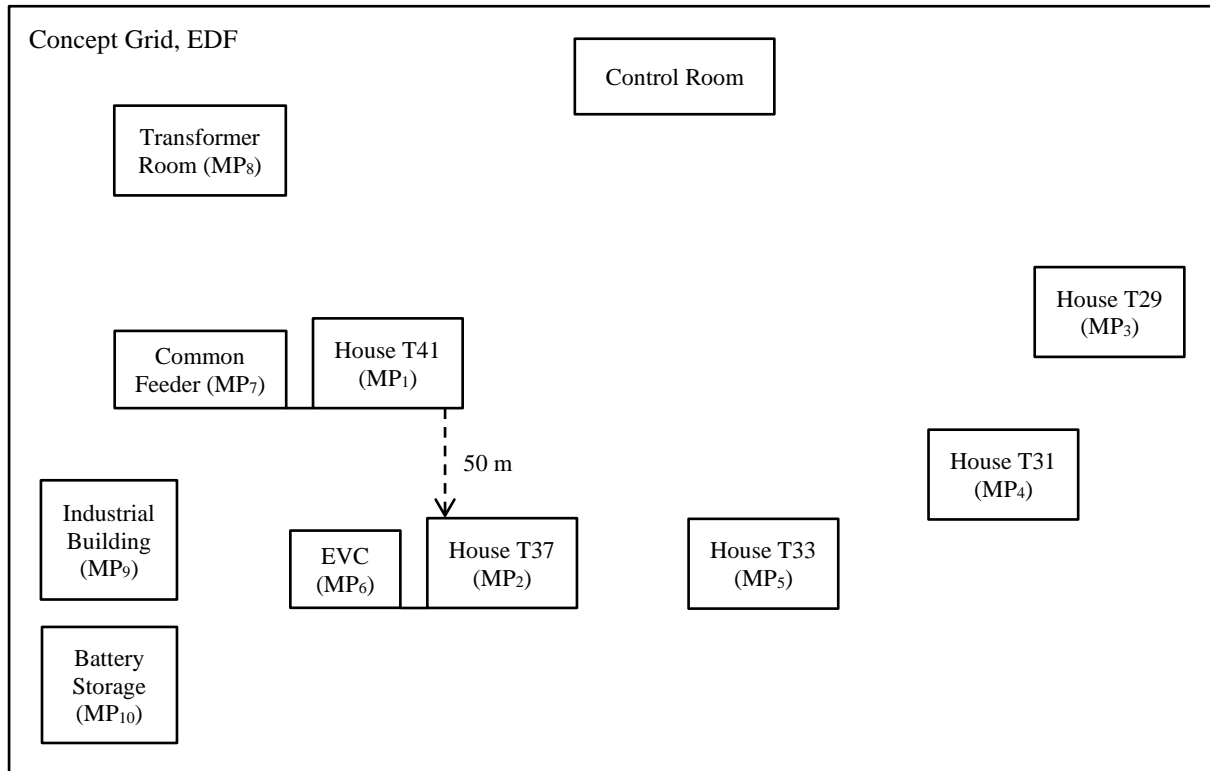


Fig. 59. Concept Grid platform measurement points.

Measurement point, MP₁₁ is located at House A₅ of laboratory MCbc, EDF.

4.2 Measurement Campaign 1

The measurement campaign 1 at Concept Grid, EDF, used measurement system version 1 for the electrical network tests. The objective of the tests is to measure the voltage and current supraharmonic emissions in the frequency range of 2 to 150 kHz. In addition, the fundamental voltage and current waveform at a frequency of 50 Hz is measured during the tests. Three different tests were conducted during the first measurement campaign as follows:

- the commissioning tests to check the performance of the measurement system;
- the individual equipment tests to characterize the test equipment;
- the network tests to analyse the individual effects and interctions between the parameters that influence the emission of supraharmonic emissions. The Design of Experiment (DoE) approach was used for the measurement campaigns to maximize the information obtained with a minimum of tests. This approach is detailed in section 4.2.1.1.

A 4-channel measurement system is used for the waveform acquisition on a single phase circuit. The oscilloscope parameters are set as follows:

- the parameters measured are amplitude and time;
- the sampling rate of 1 MS/s;
- the total duration of one acquisition is 0.20 s.

There is a time lag between each acquisition for saving the file, and to start the next acquisition. This time lag is due to the high sampling rate. This time lag increases or decreases depending on the number of sampling points and is same for the .csv, .txt and .dat file formats. The time lag adds randomness to the acquisitions, which is more closer to real network scenarios. All the above assumptions are deduced from the acquisitions using the above parameters in the laboratory. Each file can be analyzed as soon as the acquisition is completed. The mathematical processing is performed on short windows of 0.20 s as in the standard IEC 61000-4-7 Appendix B [71]. The network parameters, which are adapted on the measurement site are as follows:

- fundamental frequency, f_f of 50 Hz;
- frequency bandwidth, bw_f of 2 to 150 kHz;
- phase to phase voltage, V_{P-P} of 400 V;
- phase to neutral voltage, V_{P-N} of 230 V;
- peak current, I_p of 75 A;
- RMS current, I_{RMS} of 53.03 A.

4.2.1 Commissioning Tests

The main objective of the commissioning tests is to examine the measurement system functionality in the electrical network according to the measurement requirements. Two different configurations are planned for the commissioning of the measurement system. The commissioning tests were performed at the industrial building, which is MP₉ of the Concept Grid, EDF.

4.2.1.1 Configuration 1

The configuration 1 of the commissioning tests is used to test the functionalities of the voltage sensors used in the measurement system version 1. A commercial PQA with a frequency bandwidth up to 2.50 kHz is used alongside the recorder. The PQA is used as a local control for comparisons during the measurements and not as reference equipment [89]. The temperature and other test conditions were within the limits described in the datasheets [78]-[81]. In configuration 1, the local amplifier acts as voltage source with no load in the network.

Electrical Schema

The electrical schema for configuration 1 of the commissioning tests is shown in Fig. 60.

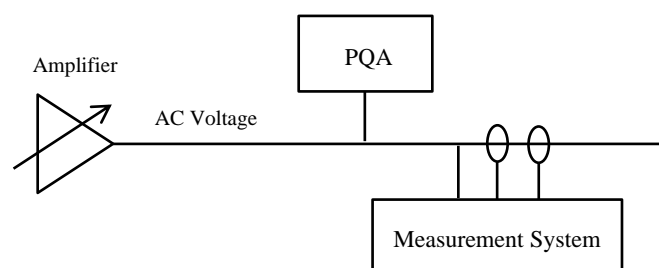


Fig. 60. Configuration 1 for commissioning tests of measurement system version 1.

Test Procedure

The test procedure for the configuration 1 of the commissioning tests is as follows:

- the voltage waveform with an amplitude of 230 V and a frequency of 50 Hz, with and without harmonics of amplitude range of 1.15 to 6.90 V is generated;
- the voltage waveforms are measured simultaneously using PQA and voltage channels of the measurement system;
- the outputs are recorded and compared to confirm the functionality of the voltage sensors used in the measurement system.

4.2.1.2 Configuration 2

The configuration 2 of the commissioning tests is used to test the functionalities of the current sensors used in the measurement system version 1. The positional sensitivity of the RCs was ensured by positioning the conductor through the center of the coil during the measurements. In configuration 2, the main grid is used as the voltage source and the amplifier acts as a current load.

Electrical Schema

The electrical schema for configuration 2 of the commissioning tests is shown in Fig. 61.

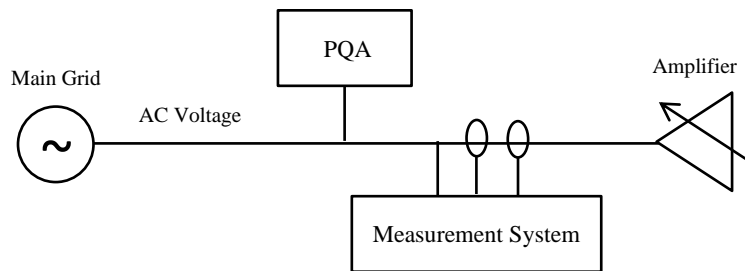


Fig. 61. Configuration 2 for commissioning tests of measurement system version 1.

Test Procedure

The test procedure for the configuration 2 of the commissioning tests is as follows:

- the voltage waveform from the electrical network is used for the tests;
- the current waveform with an amplitude of 25 A and a frequency of 50 Hz, with and without the current harmonics of 0.75 A are generated using the local amplifier;
- the current waveforms are measured simultaneously using the PQA and current channels of the measurement system;
- the outputs are recorded and compared to confirm the functionality of the current sensors used in the measurement system.

4.2.2 Individual Equipment Tests

The main objective of individual equipment tests are to measure the primary emissions from the EuT during individual operation. Primary emissions are defined as the emissions generated from the grid equipment during individual operation [32],[52]. A number of equipment like PVIs, EVCs, heat pumps, etc. are tested during individual equipment tests. The list of equipment tested are given in Table 13. The table contains the equipment type, measurement point and mode of operation of the equipment during the tests. The detailed results of the individual tests are shown in Appendix A.

Table 13. Individual equipment list.

No.	Equipment	Measurement Point	Mode of Operation
1	High power (industrial) PVI A	MP ₂	High Load
		MP ₇	High Load
		MP ₈	High Load
2	High power (industrial) PVI B	MP ₂	High Load
4	High power (industrial) PVI B	MP ₃	High Load
3	Low power (residential) PVI A	MP ₂	High Load
5	Low power (residential) PVI B	MP ₄	High Load
6	Low power (residential) PVI C	MP ₁₁	High Load
7	EV Charger A	MP ₆	High Load
		MP ₆	High Load
8	EV Charger B	MP ₃	High Load
9	EV Charger C	MP ₁₁	High Load
10	EV Charger D	MP ₁₁	High Load
11	Wind Turbine	MP ₅	High Load
12	Heat Pump A	MP ₁	High Load
13	Heat Pump B	MP ₁	High Load
14	Heat Pump C	MP ₃	High Load
15	Alternator	MP ₉ (I/P Side)	10 kW
		MP ₉ (O/P Side)	5 kW
			10 kW
16	Battery Storage	MP ₁₀	Active Power Generation
		MP ₁₀	Active Power Consumption
		MP ₁₀	Reactive Power Generation
		MP ₁₀	Reactive Power Consumption
		MP ₁₀	Active + Reactive Power Generation
		MP ₁₀	Active + Reactive Power Consumption
17	Washing Machine	MP ₁	High Load
18	Refrigerator	MP ₁	High Load
19	Freezer	MP ₄	High Load
21	Television	MP ₁₁	High Load
22	LED Lamps	MP ₁₁	High Load

Electrical Schema

The electrical schema for the individual equipment tests are shown in Fig. 62 and Fig. 63. The schema for PVIs is shown in Fig. 62 and is different from other equipment. The AC side of the PVIs is connected to the main grid. The PVIs can operate at different current levels. The DC side of the PVI can be fed either by the DC simulator or by the PV panels. The PVIs are tested during the high load

conditions, where there is maximum power output from the equipment. The PVIs tested are either industrial or residential Inverters. The main difference between the inverters is the high power (industrial) PVI (PVI_I) has a higher output power rating compared to the low power (residential) PVI (PVI_R).

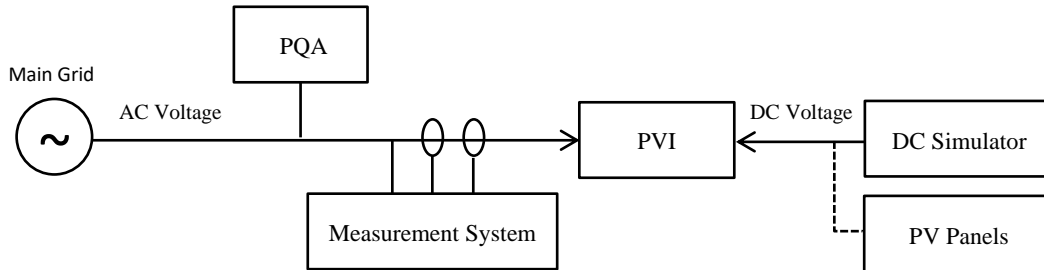


Fig. 62. Individual equipment test schema for PVIs.

The other individual equipment, such as the EVCs, heat pumps, etc., are measured for the high load conditions. The electrical schema for the individual tests of the other equipment is shown in Fig. 63.

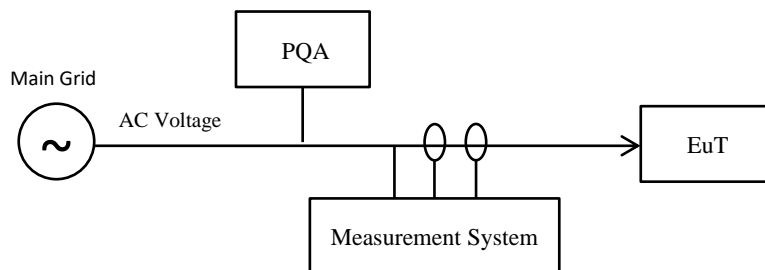


Fig. 63. Individual equipment test schema.

Test Procedure

The test procedure for the individual equipment tests are as follows:

- The main voltage source for the network is the LV grid;
- at Concept Grid, the measurements are performed in the isolated network;
- at laboratory MCbc, measurements are performed in the common electrical network with the external influences;
- for the PVIs, the DC simulator or the PV panels are used to supply the DC side;
- the measurement system is installed on the AC side of the PVI;
- for other equipment, the measurement system is installed at the equipment terminals;
- the measurements are performed for the maximum load conditions;
- the voltage and current waveforms are measured and recorded;
- the measurement and analysis results are explained in chapter 5.

4.2.3 Electrical Network Tests

The main objective of the electrical network tests is to measure the emissions during the operation of combination of different source and load equipment, such as the PVI, EVC, etc. The network is designed to replicate the emissions from the residential unit. The network tests analyze the behavior and interactions between the equipment in the real electrical network scenario.

4.2.3.1 Design of Experiment

The network measurement campaign with multiple factors and high sampling rate is challenging and time consuming due to the large amount of the measured data, and the required subsequent data analysis. Therefore, the DoE approach [90]-[92] was used to identify the different relevant configurations and limit the number of experiments. This approach creates a multi-factor design and analysis with minimum external interference by considering the different factors that contribute to supraharmmonic emissions in the frequency range of 2 to 150 kHz in the test network.

The methodology for building an DoE can be described in 4 steps:

- the definition of the problem is the supraharmmonic emissions and to plan the tests:
 - the objective is to measure the supraharmmonic emissions;
 - the constraints are the parameters that influence generation of supraharmmonic emissions, which are listed in Table 14;
 - the responses are the acquired waveforms from the test network;
 - the model is the design of test network with interaction effects in this case;
 - the experimental protocol includes the random order of the experiments;
- the realization of the tests;
- the statistical analysis of the measured waveforms and the experimental validation of the significant effects;
- the analysis of the results and conclusions.

The DoE applied is a full factorial plan at two levels of operation. Only 2 operational levels of each parameter are chosen. This type of DoE estimates the individual effects and the interactions between the parameters. It consists of all possible combinations of the two levels of each factor, which is 16 in this case and the number of trials increases with increase in the number of parameters.

4.2.3.2 Network Parameters

After the measurement system was designed and correctly characterized, it was installed for obtaining the real network measurements on the Concept Grid, EDF. Based on the existing literature in [23],[33],[93] and the analysis of the Concept Grid architecture, the parameters that influence the generation of the supraharmmonic emissions in the network are considered, and listed in Table 14. These parameters include the generation equipment, such as the PVIs and the load equipment, such as the EVCs, the measurement point, and the modes of operation, which are “High” or “Low”.

Table 14. Test network parameters.

No.	Factors	Mode of Operation	
A	Low power (residential) PVI	High	Low
B	High power (industrial) PVI	High	Low
C	Residential load	High	Low
D	Measurement point	MP ₁	MP ₂

“High” represents the operation in full capacity for the PVIs and residential load, while “Low” represents the off state for the PVIs and sole operation of the light bulbs for the residential load. The measurement points are either at MP₁, which is closer to the residential load, or at MP₂, which is closer to the PVIs.

Electrical Schema

The electrical schema for electrical network tests is shown in Fig. 64.

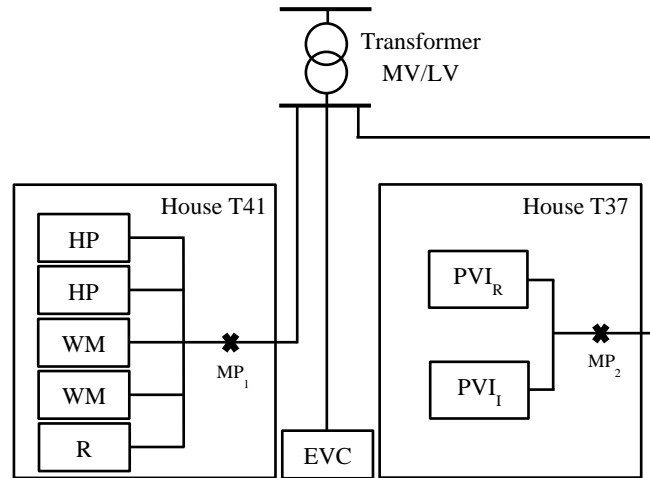


Fig. 64. Electrical network test schema [94].

The generation and load equipment used in the network and in Fig. 64 are as follows:

- Transformer MV/LV is for the medium to low voltage transformer;
- HP is for the heat pump;
- WM is for the washing machine;
- R is for the refrigerator;
- EVC is for the electric vehicle charger;
- PVI_R is for the residential PVI;
- PVI_I is for the industrial PVI;
- MP₁ is the measurement point close to load equipment;
- MP₂ is the measurement point close to source equipment.

The selected configurations for the test network are listed in Table 15. For each configuration, multiple acquisitions of the fundamental and supraharmonic components of the voltage and current waveforms were performed simultaneously.

Table 15. Electrical network test campaign 1 configurations.

No.	PVI _R	PVI _I	Load	Measurement Point
C ₁	High	High	High	MP ₁
C ₂	Low	High	High	MP ₁
C ₃	High	Low	High	MP ₁
C ₄	Low	Low	High	MP ₁
C ₅	High	High	Low	MP ₁
C ₆	Low	High	Low	MP ₁
C ₇	High	Low	Low	MP ₁
C ₈	Low	Low	Low	MP ₁
C ₉	High	High	High	MP ₂
C ₁₀	Low	High	High	MP ₂

C ₁₁	High	Low	High	MP ₂
C ₁₂	Low	Low	High	MP ₂
C ₁₃	High	High	Low	MP ₂
C ₁₄	Low	High	Low	MP ₂
C ₁₅	High	Low	Low	MP ₂
C ₁₆	Low	Low	Low	MP ₂

The electrical network to measurement system connection at the Concept Grid is shown in Fig. 65. The PQA used alongside the recorder and can be seen in Fig. 65.

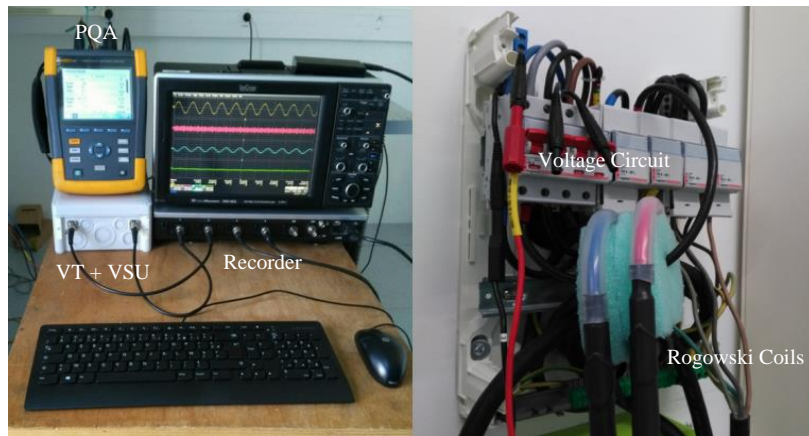


Fig. 65. Electrical network to measurement system connection.

Test Procedure

The test procedure for the electrical network tests are as follows:

- the main voltage source for the network is the LV grid;
- the measurements are performed in an isolated network in concept grid;
- the network test schema is given in Fig. 64.
- the test network is configured according to the configurations listed in Table 33;
- the DC simulator is used to supply the DC side of PVI_I;
- the PV panels are used to supply the DC side of PVI_R;
- the measurements are performed for each configurations at MP₁ and MP₂;
- the multiple acquisitions of duration 0.20 s are performed;
- the measured waveforms are saved and used for mathematical processing;
- the measurement and analysis results are explained in chapter 5.

The measurement and analysis results of individual equipment and electrical network tests are explained in chapter 5. The measurement campaign 1 was performed at the beginning of the thesis to get an idea of the supraharmonics emissions in the residential network with a combination of the source equipment, such as PVI, and the load equipment, such as EVC. The obtained results have been used as guidelines for designing the waveform platform presented in chapter 6. The measurement campaign 2 was planned and performed using the experience from the previous measurement campaign and identifying the short comings from the measurement campaign listed in chapter 5.

4.3 Measurement Campaign 2

The measurement campaign 2 used the measurement system version 2 for the electrical network tests. The objective of the tests is to measure the higher frequency voltage and current supraharmonic emissions. In addition, the fundamental voltage and current waveform at the frequency of 50 Hz was measured during the tests. Three different tests were conducted as follows:

- the individual equipment tests to characterize the test equipment;
- the multiple equipment tests with equipment, such as PVI and EVC;
- the network tests to analyse the individual effects and interactions between the equipment.

The DAQ parameters are set as follows:

- the parameters measured are amplitude and time;
- the sampling rate of 1 MS/s;
- the total duration of one acquisition is varied at the measurement site.

Contrary to the previous measurement campaign, there is no time lag between each acquisition for saving the file and to start the next acquisition. Each file is analysed as the waveform is acquired. A waveform of duration 1 s is processed for each time period of 30 s. The settings are changeable according to the user. The raw and processed waveforms are stored separately for further analysis. The electrical network parameters, which are adapted on the measurement site are similar to the parameters specified before.

4.3.1 Individual Equipment Tests

The main objective of the individual equipment tests are to measure the primary emissions from the EuT during the individual operation. The equipment like the PVI are tested during the individual equipment tests for varying cable length from the equipment terminal to 300 m. The primary emissions from the EVCs are measured close to the equipment terminal. The tests conducted here use the similar electrical schema as in section 4.2.2. The connections are made as in Fig. 62 and Fig. 63.

Test Procedure

The test procedure for the individual equipment tests are as follows:

- the main voltage source for the network is the LV grid;
- the measurements are performed in an isolated network in concept grid;
- for the PVIs, a DC simulator is used to supply the DC side;
- the measurement system is installed on the AC side of the PVI;
- the distance between the PVI and measurement system is varied;
- for the EVC, the measurement system is installed at the equipment terminals;
- the measurements are performed for maximum load conditions;
- the voltage and current waveforms are measured, processed, and recorded;
- the measurement and analysis results are explained in chapter 5.

4.3.2 Multiple Equipment Tests

The main objective of the multiple equipment tests were to measure the primary and secondary emissions between the source equipment, such as the PVI, and the load equipment, such as the EVC. The primary and secondary emissions are defined in section 2.2.1.

Electrical Schema

The electrical schema used for the multiple equipment tests are shown in Fig. 66.

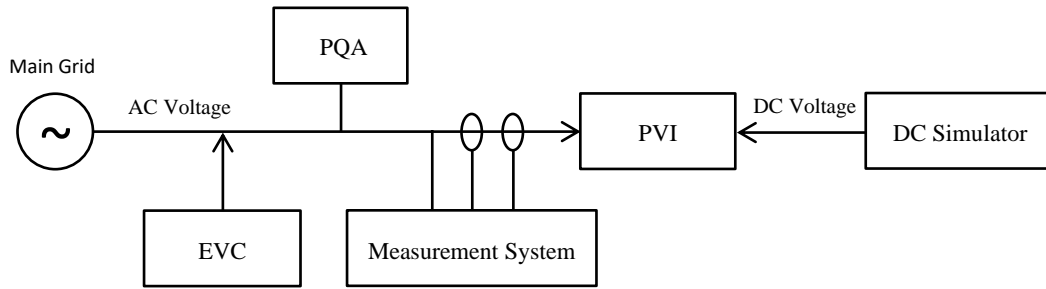


Fig. 66. Multiple equipment test schema for PVI and fast charging EVC.

Test Procedure

The test procedure used for multiple equipment tests are as follows:

- the main voltage source for the network is the LV grid;
- at the Concept Grid, the measurements are performed in the isolated network;
- for the PVIs, a DC simulator is used to supply the DC side;
- the measurement system is installed on the AC side of the PVI;
- the measurements are done for individual operation of the PVI;
- the EVC is connected to the network alongwith the PVI;
- the measurements are performed for maximum load conditions;
- initially, only the PVI is on maximum load condition, and the measurements are acquired using the DAQ;
- the EVC is added to the network during the PVI operation;
- the measurements are performed for the new network conditions;
- the voltage and current waveforms are measured, processed, and recorded;
- the measurement and analysis results are explained in chapter 5.

4.3.3 Electrical Network Tests

The main objective of the electrical network tests is to measure the emissions during the operation of combination of different source and load equipment, such as the PVI, EVC, etc. similar to the tests during the measurement campaign 1. However, only 8 main configuration tests, which are the minimum number of configurations necessary to perform the statistical analysis of the network described in section 5.4.3. The network is designed to replicate the emissions from a residential unit. The network tests analyze the behavior and interactions between different equipment in a real electrical network scenario. The test parameters and network are similar to the measurement campaign 1, as shown in the section 4.2.3.

The main differences in both network tests are the measurement system and the configurations measured. The selected measurement configurations for the electrical network tests are listed in Table 16. The minimum number of configurations that are required to create the cause-effect relationship between the different parameters of the electrical network are performed during the electrical network tests of the measurement campaign 2. The measurements are performed in two different points, MP_1 and MP_2 .

Table 16. Electrical network test campaign 2 configurations.

No.	PVI _R	PVI _I	Load	Measurement Point
C ₁	High	Low	Low	MP ₁
C ₂	Low	High	Low	MP ₁
C ₃	Low	Low	High	MP ₁
C ₄	High	High	High	MP ₁
C ₅	High	Low	High	MP ₂
C ₆	High	High	Low	MP ₂
C ₇	Low	High	High	MP ₂
C ₈	Low	Low	Low	MP ₂

The electrical network to measurement system connection at the Concept Grid, EDF, used during the measurement campaign 2 is shown in Fig. 67.

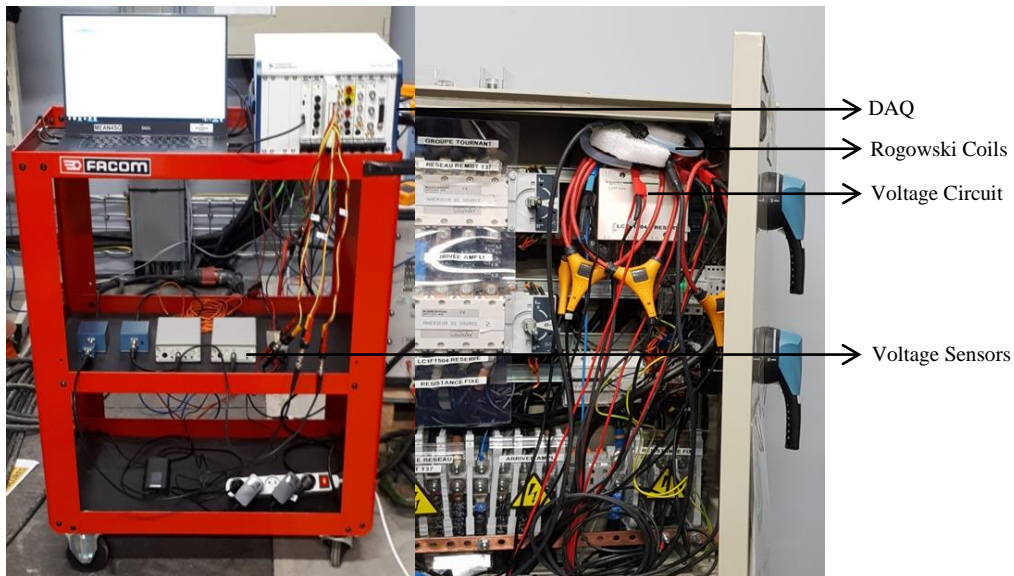


Fig. 67. Electrical network to measurement system connection.

Test Procedure

The test procedure for the electrical network tests are as follows:

- the main voltage source for the network is the LV grid;
 - at the Concept Grid, the measurements are performed in an isolated network;
 - the network test schema is given in Fig. 67.
 - The test network is configured according to the configurations listed in Table 34;
 - the DC simulator is used to supply the DC side of the PVI_I;
 - the PV panels are used to supply the DC side of the PVI_R;
 - the measurements are performed for each configurations at the MP₁ and MP₂;
 - the multiple acquisitions of varying duration for the fundamental and supraharmonic components of the voltage and current waveform are performed;
 - the measured waveforms processed, while the waveforms are acquired;
- the measurement and analysis results are explained in chapter 5.

4.4 Summary

The EDF measurement campaigns were designed to measure and acquire the fundamental components and supraharmmonic components in the frequency range of 2 to 150 kHz of the voltage and current waveforms. The main differences in both the network tests are the measurement system and the configurations measured. The measurement system used for the measurement campaign 2 is updated version of the measurement system used for the measurement campaign 1. The voltage sensor unit used for the measurement of supraharmmonic voltage emissions and the current sensor used for the measurement of the supraharmmonic current emissions in the second version of the measurement system has a better linearity in the frequency range of 2 to 150 kHz.

The measurement campaign 1 tests all the possible configurations of the network as described in section 5.3.3, whereas the measurement campaign 2 tests only the 8 configurations, which are the minimum number of configurations necessary to perform the statistical analysis of the network described in section 5.4.3. The goals of both measurement campaigns are to study and analyze the supraharmmonic emissions in the frequency range of 2 to 150 kHz in the electrical network in an accurate and efficient manner. The measurements from these campaign studies:

- the primary and secondary emissions through network measurements;
- the effects of the sudden connection and disconnection of the load equipment in the network;
- the effects of the cable impedance on the propagation of the supraharmmonic emissions;
- the individual effects and interactions between the different equipment in the network;
- the cause-effect relationship between the different source and load equipment in the network.

The analysis methods, such as the FFT algorithm and ANOVA, and the results are discussed in the chapter 5.

CHAPTER 5
MATHEMATICAL AND STATISTICAL ANALYSIS

5 MATHEMATICAL AND STATISTICAL ANALYSIS

The waveforms acquired from the Concept Grid are processed mathematically and statistically. The waveforms in the time domain are converted to the frequency domain using the FFT algorithm. The frequency domain information is then used for the statistical analysis using the ANOVA. The statistical analysis using ANOVA helps to identify the fluctuations and why it happens in the electrical network with multiple equipment. The mathematical and statistical tools along with their application on the measured waveforms are described below.

5.1 Mathematical Analysis

The mathematical processing of the waveforms acquired from the measurements at the Concept Grid is used to identify the behavior of the supraharmonic emissions in the frequency range of 2 to 150 kHz. The voltage and current waveforms in the time domain is converted into the frequency domain using the FFT algorithm. The FFT algorithm deconstructs the time domain waveform into the frequency domain waveform thereby, making it possible to analyze the different frequency components in the waveform. The processing is performed on the window of duration 0.20 s [71] and uses the Hanning windows to reduce the amplitudes of discontinuities at end of each waveform period. The Hanning windows are preferred window choice during measurement campaign 1, since they are suitable for the sine waves and combination of the sine waves [95]. The current waveform from the heat pump acquired during the measurement campaign 1 in the time and frequency domain is shown in Fig. 68 and Fig. 69.

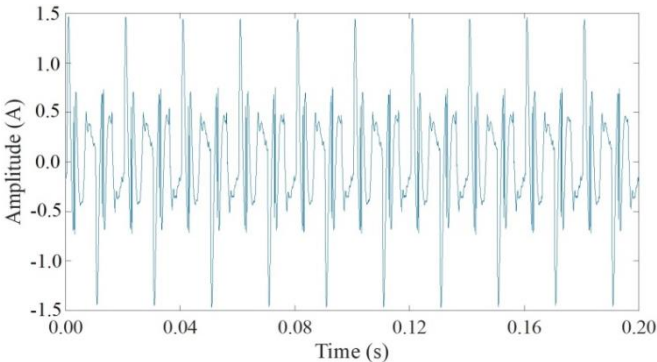


Fig. 68. Current supraharmonic emissions from heat pump in time during campaign 1.

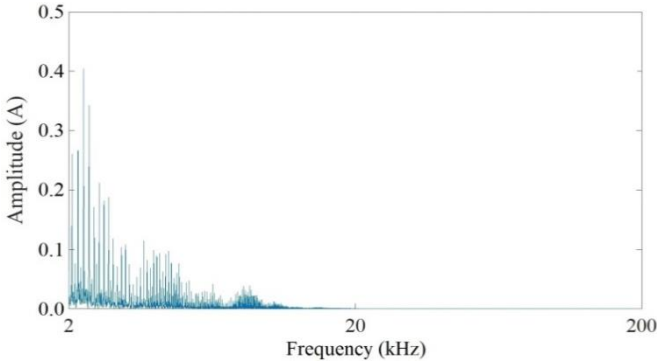


Fig. 69. Current supraharmonic emissions from heat pump in frequency during campaign 1.

From Fig. 69, the current waveform emissions are higher in the frequency range of 2 to 4 kHz. Additional measurement results are presented in Appendix A. The waveforms acquired during the

measurement campaign 2 uses the window duration of 1 s and the flat top windows, since it has better amplitude accuracy compared to the Hanning windows [95]. The current waveform from the EVC in the acquired during the measurement campaign 2 is shown in Fig. 70 and Fig. 71.

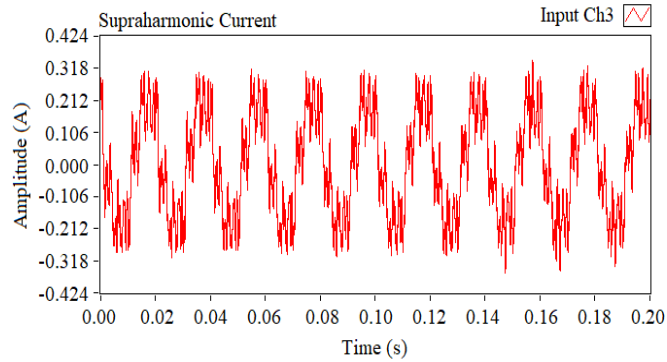


Fig. 70. Current supraharmonic emissions from fast charging EVC in time during campaign 2.

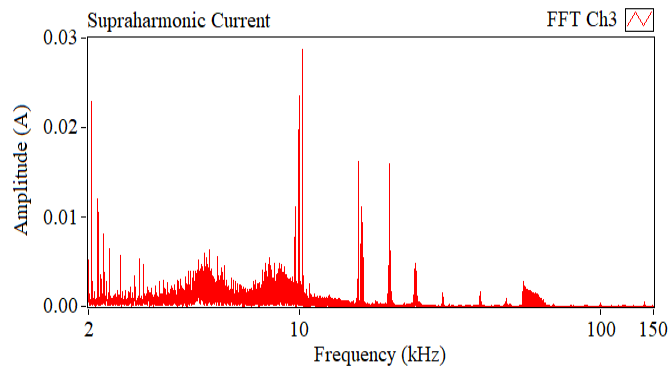


Fig. 71. Current supraharmonic emissions from fast charging EVC in frequency during campaign 2.

From Fig. 71, the current emissions are present throughout the frequency range of 2 to 150 kHz. The emissions are higher in the frequency range of 2 to 4 kHz, 10 to 30 kHz. The lower emissions are observed in the frequency range of 70 to 80 kHz. Additional results are presented in the Appendix C.

5.2 Statistical Analysis

The ANOVA is a collection of statistical models and their associated estimation procedures, such as the variation of response among and between the groups. Among all the alternatives to ANOVA, it is the most adaptive method for detecting the difference among the mean values. The ANOVA is used to test the general difference rather than the specific differences among the means. Some of the most applied models are purely additive model, additive model with interaction effects, or quadratic model. The model applied for the supraharmonic measurement campaigns is additive model with interaction effects. The DoE is designed for the analysis of voltage and current measurements for the fundamental components and supraharmonic components in the frequency range of 2 to 150 kHz in the process of development of tools for accurate study of supraharmonic emissions in smart grids. The objective is to determine a statistical model that explains the influence of a given factors on an output quantity called the response variable, which is denoted as y . The resulting statistical model is only the statistical relationship and does not represent the physical relationship. The statistical model with two factors A and B is designed as in (10).

$$y = b_0 + b_1A + b_2B + b_{12}AB, \quad (10)$$

where, A is PVI_R and B is PVI_I .

The coefficients are:

- b_0 is the emissions when both the inverters are low;
- b_1 is the emissions when only the PVI_R inverter is high;
- b_2 is the emissions when the PVI_I is high;
- b_{12} is the emissions when both the inverters are high.

The products terms, b_0 and b_{12} represent the potential interactions between the two factors. Coefficients b_0 , b_1 , b_2 , b_3 and b_{12} are the coefficients, which are estimated from the results of the experiments in the DoE. The significance of the coefficients is more important than their estimated value as latter is likely to be very high due to the small number of experiments. The significance of coefficients is defined as the measure of statistical difference between the coefficients. The goal is to detect the coefficients that are significantly different from zero. Indeed, in this case, it means that the associated effect of first order or interaction effect is significant, and that the measurement of the response quantity differs according to the value of the effect. The resulting statistical model is only the statistical relationship and does not represent the physical relationship. The practical interpretation of an interaction effect for a statistical model with two factors is shown in Fig. 72.

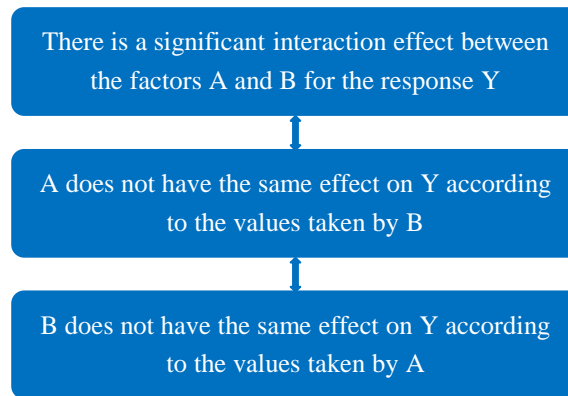


Fig. 72. Interpretation of interaction effects.

In the final statistical model, only the significant effects are considered. The equations (11) to (17) represent the step by step performance of statistical analysis using ANOVA.

The chosen statistical model explains a part of the results. This can be written as in (11):

$$y_i = \hat{y}_i + e_i, \quad (11)$$

where y_i is the measured response, \hat{y}_i is the prediction of the model, and e_i represents the error term.

The analysis relies on the calculation and the analysis of the sum of squares. The total sum of squares is given by (12):

$$\text{Sum of Squares, } SS_{\text{Total}} = \sum (y_i - \bar{y})^2, \quad (12)$$

where \bar{y} is the mean value of the measured responses.

The estimated sum of squares is given by (13):

$$\text{Sum of Squares, } SS_{\text{Estimated}} = \sum (\hat{y}_i - \bar{y})^2, \quad (13)$$

A multiple ANOVA is performed in order to test whether the deviations due to each effect are significant with regard to the residual dispersion [96]. In particular, the Fisher's test is performed for each effect to be tested to determine the p-value of the parameter. The residual quadratic sum is given as in (14). The values in the factorial table [97] are calculated using (14) to (17) as given below:

$$\text{Sum of Squares, } SS_{\text{Residual}} = SS_{\text{Total}} - SS_{\text{Factor}}, \quad (14)$$

$$\text{Degree of Freedom, } df_{\text{total}} = df_{\text{Model}} + df_{\text{Residual}}, \quad (15)$$

$$df_{\text{Residual}} = df_{\text{Total}} - df_{\text{Model}},$$

$$\text{Mean Square, } MS = \frac{SS}{df}, \quad (16)$$

$$F - \text{value} = \frac{MS_{\text{Factor}}}{MS_{\text{Residual}}}, \quad (17)$$

p-value is the measure of similarity between the sample results by assuming that null hypothesis is true. The null hypothesis is rejected when p-value is lower than 0.05. Here, the null hypothesis states that there is no variation between the variables or that a single variable is no different from its mean value [97]. This condition is considered default or true until the statistical evidence nullifies it by an alternative hypothesis. The ANOVA table is summarized in Table 17.

Table 17. ANOVA table.

Source	Sum of Squares	Degrees of freedom	Mean squares	F-statistic
Factor A	SS_A	$k - 1$	MS_A	$\frac{MS_A}{MS_R}$
Factor B	SS_B	$l - 1$	MS_B	$\frac{MS_B}{MS_R}$
Interaction AB	SS_{AB}	$(k - 1)(l - 1)$	MS_{AB}	$\frac{MS_{AB}}{MS_R}$
Residuals	SS_R	$k \times l \times (n - 1)$	MS_R	
Total	SS_T	$m - 1$		

where k is the number of levels of the factor A, l is the number of levels of the factor B, n is the number of repetitions on each treatment, and m is the total number of observations. The ANOVA on the measured waveforms is detailed in section 5.3.3. The results of the campaigns are detailed below.

5.3 Measurement Campaign 1 Results

The measurement campaign 1 results, which include the commissioning test, individual equipment test, and electrical network test analysis and the results are described here. The measurements acquired during the measurement campaign 2 are analysed using the mathematical processing with the FFT algorithm, and the statistical processing using the ANOVA.

5.3.1 Commissioning Tests

The commissioning tests were performed as explained in section 4.2.1. The commissioning test results of the voltage sensors are shown in Table 18. The measurement data from the measurement system and PQA are comparable. Therefore, the functionality of voltage sensors, VT and VSU for the real network measurements is confirmed.

Table 18. Measurement data from configuration 1.

No.	Frequency (kHz)	Fundamental Level (V)		Harmonic Level (V)		Harmonic Level (%)	
		VT	PQA	VSU	PQA	VSU	PQA
1	0.05	232.72	230.22	-	-	-	-
2	0.05 + 2.00	232.72	229.96	2.32	2.32	1.01	1.01
3	0.05 + 2.50	232.35	229.96	1.17	1.15	0.51	0.50

The measurement data for the configuration 2 is listed in Table 19. The results show the measurement data from the measurement system and PQA are comparable. Therefore, the functionality of current sensors, LFR 03/3 and CWT015 for the electrical network measurements is confirmed.

Table 19. Measurement data from configuration 2.

No.	Frequency (kHz)	Fundamental Level (A)		Harmonic Level (A)		Harmonic Level (%)	
		LFR 06/6	PQA	CWT015	PQA	CWT015	PQA
1	0.05	25.03	25.40	-	-	-	-
2	0.05 + 2.50	25.02	25.40	0.75	0.76	3.00	2.98

The commissioning tests were carried out to verify the performance of the voltage and current sensors used in the measurement system version 1 in the real electrical network. The measurement results from Table 18 and Table 19 indicate that the voltage and current sensors used in the measurement system version 1 are confirmed for the electrical network measurements.

5.3.2 Individual Equipment Tests

The individual equipment tests are performed to identify the voltage and current supraharmonic emissions in the frequency range of 2 to 150 kHz from the EuT. The measured waveforms in the time domain are converted to the frequency domain using the FFT algorithm. The network schema and equipment measured during the individual characterization tests are described in section 4.2.2. The supraharmonic voltage and current emissions in the frequency range of 2 to 150 kHz from the generation equipment, PVI_I in the time and frequency domain during high load operation are shown in Fig. 73 to Fig. 76. PVI_I is a major source of supraharmonic emissions in the electrical network. For the PVI_I, higher voltage and current emissions are observed in the frequency range of 2 to 4 kHz, whereas lower current emissions are observed in the frequency of 16 kHz.

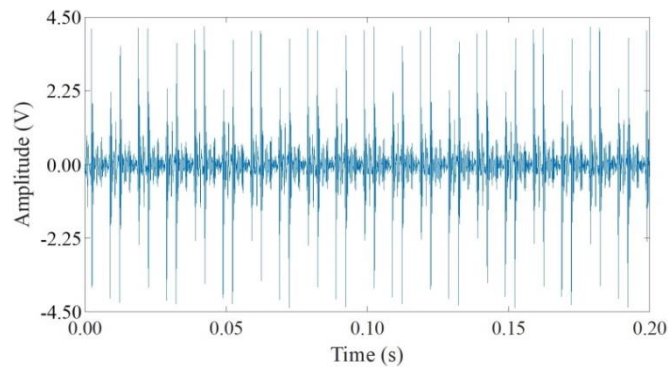


Fig. 73. Voltage supraharmonic emissions from PVI_I in time during campaign 1.

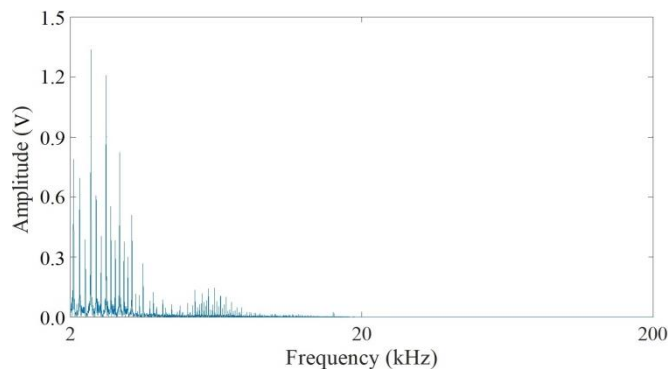


Fig. 74. Voltage supraharmonic emissions from PVI_I in frequency during campaign 1.

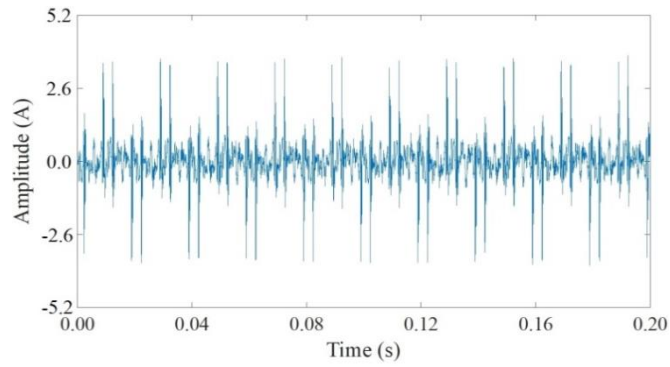


Fig. 75. Current supraharmonic emissions from PVI₁ in time during campaign 1.

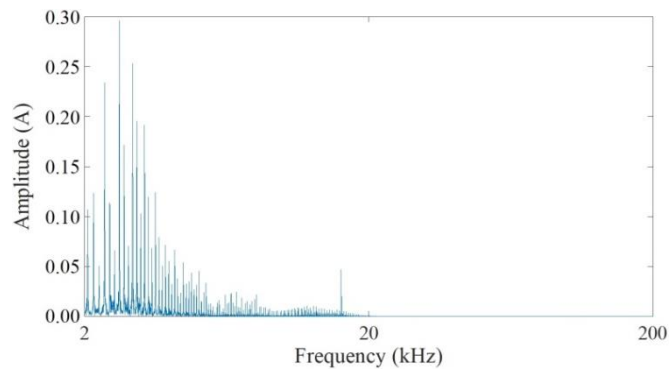


Fig. 76. Current supraharmonic emissions from PVI₁ in frequency during campaign 1.

The supraharmonic voltage and current emissions from the EVC is shown in Fig. 77 to Fig. 80. EVC is a major source of supraharmonic emissions among the load equipment in the electrical network.

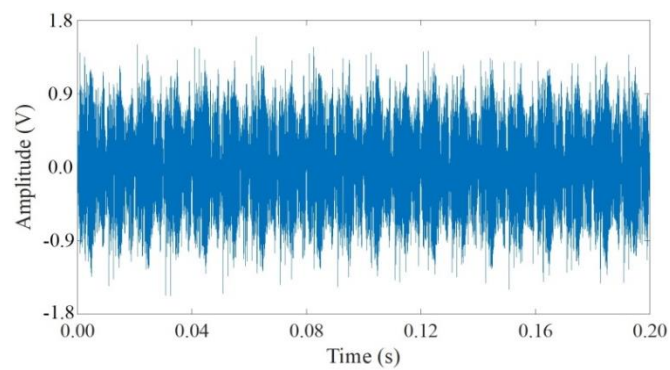


Fig. 77. Voltage supraharmonic emissions from fast charging EVC in time during campaign 1.

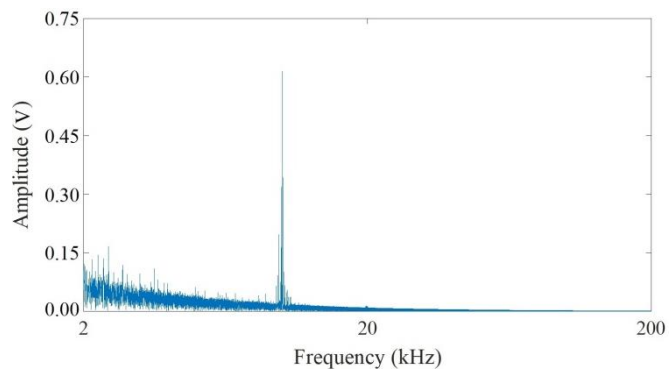


Fig. 78. Voltage supraharmonic emissions from fast charging EVC in frequency during campaign 1.

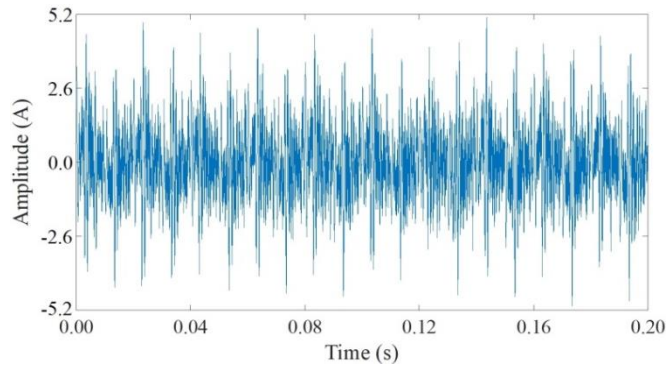


Fig. 79. Current supraharmmonic emissions from fast charging EVC in time during campaign 1.

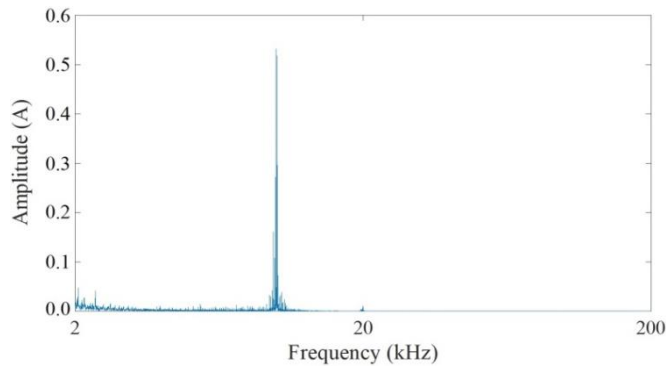


Fig. 80. Current supraharmmonic emissions from fast charging EVC in frequency during campaign 1.

For the ECs, the higher voltage and current emissions are observed in the frequency of 10 kHz, whereas the lower voltage emissions are observed in the frequency range of 2 to 4 kHz. These tests characterize a variety of equipment from the PVI to the EVCs. The individual tests identifies the equipment for the network tests. The results for the other equipment are presented in Appendix A.

5.3.3 Electrical Network Tests

The network schema and the configurations measured during the electrical network tests are described in section 4.2.3. The measured waveforms in the time domain are converted into the frequency domain using the FFT algorithm. Then, the frequency range of 2 to 22 kHz is divided into intervals of 2 kHz. This interval is selected for the studies, as there are no visible emissions above the frequency of 22 kHz. The RMS value of the highest emissions in each interval is obtained by the FFT algorithm. The frequency intervals with no emissions are tabulated as zero. The voltage and current emissions for the configuration C₉ from Table 15 in the time and frequency domain are shown in Fig. 81 to Fig. 84.

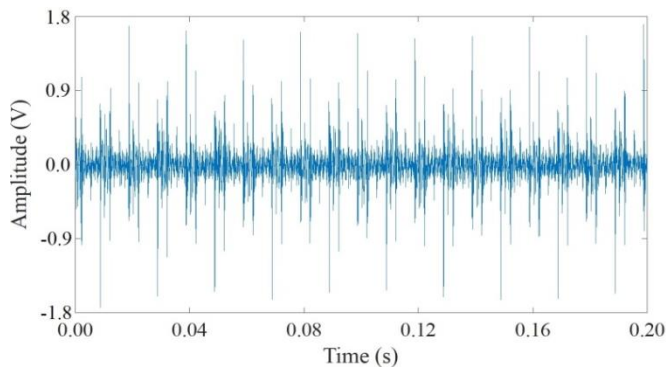


Fig. 81. Voltage supraharmmonic emissions from C₉ in time during campaign 1.

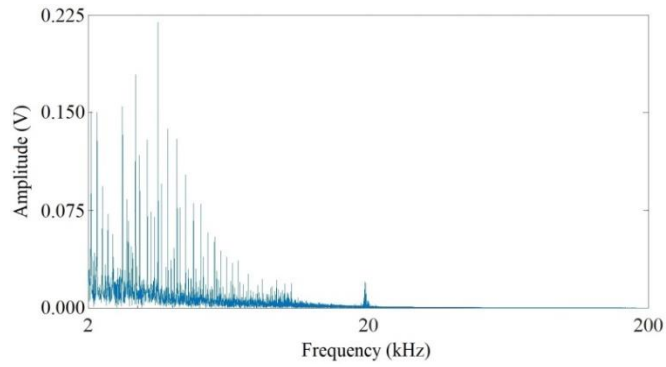


Fig. 82. Voltage supraharmonic emissions from C₉ in frequency during campaign 1.

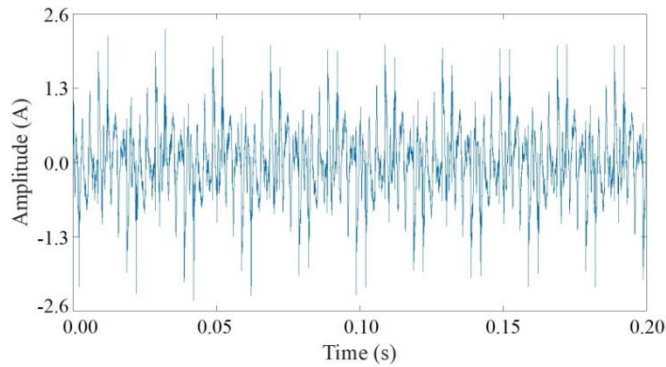


Fig. 83. Current supraharmonic emissions from C₉ in time domain campaign 1.

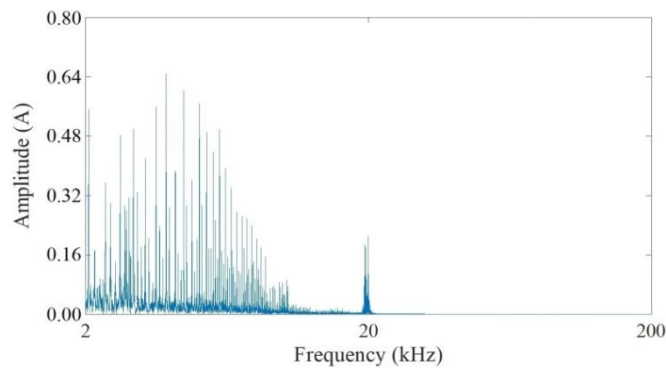


Fig. 84. Current supraharmonic emissions from C₉ in frequency during campaign 1.

The voltage and current supraharmonic emissions in the frequency range of 2 to 22 kHz are observed from Fig. 82 and Fig. 84. The RMS voltage and current values of the highest emissions in each frequency interval is calculated from the processed waveforms, and are shown in Fig. 85 and Fig. 86. The analysis uses the absolute values instead of the normalized values, since some of the configurations have a very low fundamental current component, e.g., C₈. In these cases, the normalized value of the emissions with respect to the fundamental current component is very high. Therefore, using the normalized values for the analysis would not yield the relevant results. Therefore, the absolute value of the measured waveform enables a better comparison as the fundamental current varies over a wide range of values from 0.55 to 27.35 A. The statistical analysis using ANOVA is performed on the absolute values of the emissions. The voltage supraharmonic emissions during the network tests are shown in Fig. 85. The higher peaks are observed in the frequency range of 2 to 6 kHz, where the configurations C₁, C₆, and C₁₄, generate these emissions. The lower peaks are observed

in the frequency range of 10 to 12 kHz. The configurations C₁, C₂, and C₃, generate the emissions in this frequency range. The PVI_I (B) is in “High” state for the configurations C₁ and C₂. The modes of operation of other factors, such as the PVI_R (A), Load (C), and MP (D) vary with these configurations. This indicates the increased influence of the PVI_I (B) on the voltage waveform.

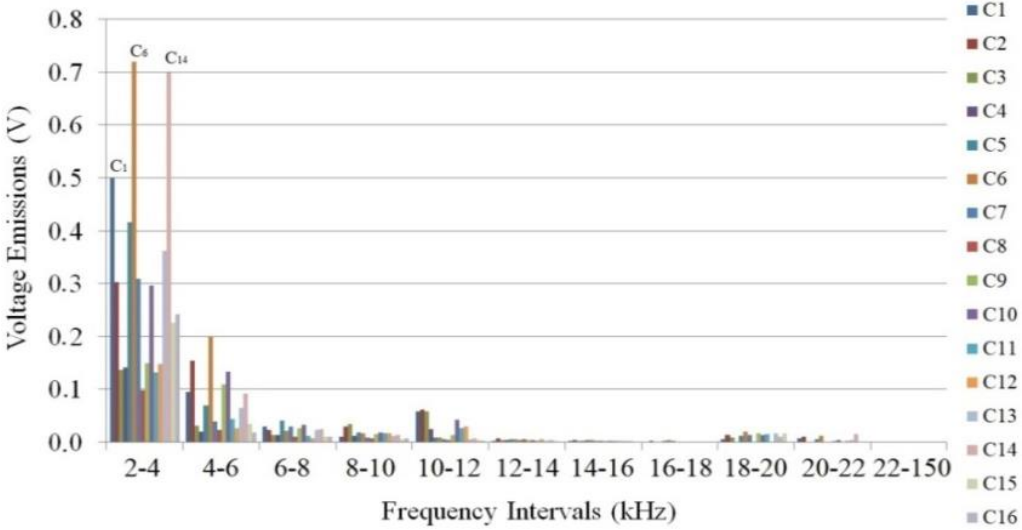


Fig. 85. Voltage supraharmonic emissions from electrical network tests.

The current supraharmonic emissions during the network tests are shown in Fig. 86. The higher emissions are observed in the frequency range of 2 to 4 kHz, where the configurations C₁₃, C₁₄, and C₁₅, generate the highest peak emissions. The PVI_R (A) is in “High” state for C₁₃ and C₁₅. The PVI_I (B) is in “High” state for C₁₃ and C₁₄. The lower peaks are observed in the frequency ranges of 4 to 6, 6 to 12 kHz, and 18 to 22 kHz. This implies that the PVIs generate the higher emissions in the frequency range of 2 to 4 kHz. From Fig. 86, it is observed that the emissions are higher when the MP (D) is closer to the PVIs. Furthermore, the differences in the emissions for the configurations, C₆ and C₁₄, indicate the presence of the higher emissions closer to the equipment terminal.

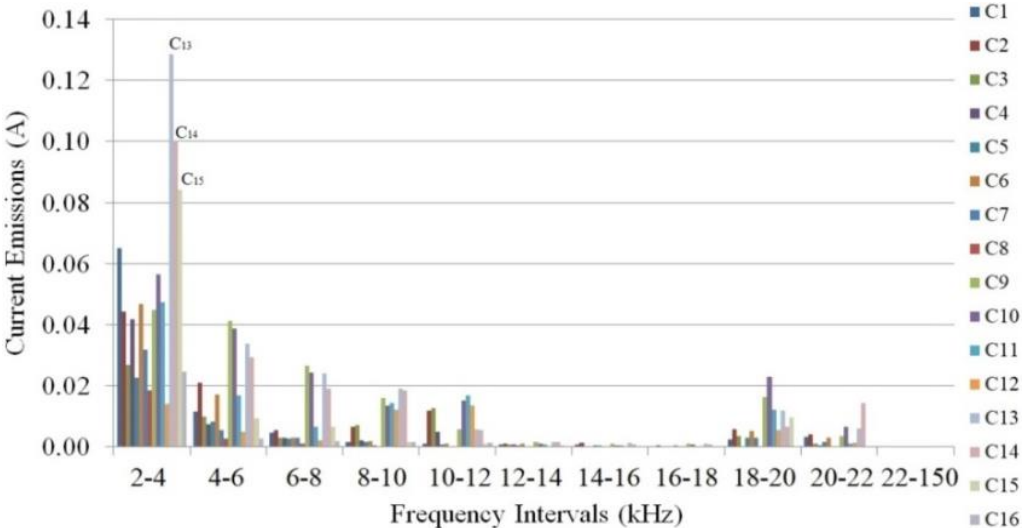


Fig. 86. Current supraharmonic emissions from electrical network tests.

The values from Fig. 85 and Fig. 86 are used for statistical analysis using ANOVA [98]. Let us consider ANOVA for voltage emissions in the frequency range of 2 to 4 kHz.

In this DoE, number of levels of factor A, $p = 2$, and factor B, $q = 2$,
 Number of repetitions, $n = 4$, and total number of observations, $m = 16$,
 From Table 38, overall mean, $\sum_i \sum_j y_{ij} = 0.0721$, where i and j represents the row and columns.

$$\text{Sum of Squares Total, } SS_T = \sum_i \sum_j y_{ij}^2 - \frac{1}{n \times p \times q} (\sum_i \sum_j y_{ij})^2 = 0.04444,$$

$$\text{Sum of Squares of A, } SS_A = \frac{1}{n \times q} \sum_i [\sum_j y_{ij}]^2 - \frac{1}{n \times p \times q} (\sum_i \sum_j y_{ij})^2 = 0.00209,$$

$$\text{Sum of Squares of B, } SS_B = \frac{1}{n \times p} \sum_j [\sum_i y_{ij}]^2 - \frac{1}{n \times p \times q} (\sum_i \sum_j y_{ij})^2 = 0.02892,$$

$$\text{Sum of Squares of Residual, } SS_{Residual} = \sum_i \sum_j y_{ij}^2 - \frac{1}{n} \sum_i [\sum_j y_{ij}]^2 = 0.00778,$$

$$\text{Sum of Squares of AB, } SS_{AB} = SS_T - SS_A - SS_B - SS_{Residual} = 0.00566,$$

$$\text{Sum of Squares of Model, } SS_{Model} = SS_T - SS_{Residual} = 0.03666,$$

$$\text{dof}_A = p - 1 = 1,$$

$$\text{dof}_B = q - 1 = 1,$$

$$\text{dof}_{AB} = (p - 1) \times (q - 1) = 1,$$

$$\text{dof}_{Model} = \text{dof}_A + \text{dof}_B + \text{dof}_{AB} = 3,$$

$$\text{dof}_{Total} = m - 1 = 15,$$

$$\text{dof}_{Residual} = p \times q \times (n - 1) = 12,$$

$$MS_{Model} = \frac{SS_{Model}}{\text{dof}_{Model}} = 0.01222,$$

$$MS_A = \frac{SS_A}{\text{dof}_A} = 0.00209,$$

$$MS_B = \frac{SS_B}{\text{dof}_B} = 0.02892,$$

$$MS_{AB} = \frac{SS_{AB}}{\text{dof}_{AB}} = 0.00566,$$

$$MS_{Residual} = \frac{SS_{Residual}}{\text{dof}_{Residual}} = 0.00065,$$

$$F - \text{value}_{Model} = \frac{MS_{Model}}{MS_{Residual}} = 18.86,$$

$$F - \text{value}_A = \frac{MS_A}{MS_{Residual}} = 3.22,$$

$$F - \text{value}_B = \frac{MS_B}{MS_{Residual}} = 44.49,$$

$$F - \text{value}_{AB} = \frac{MS_{AB}}{MS_{Residual}} = 8.71,$$

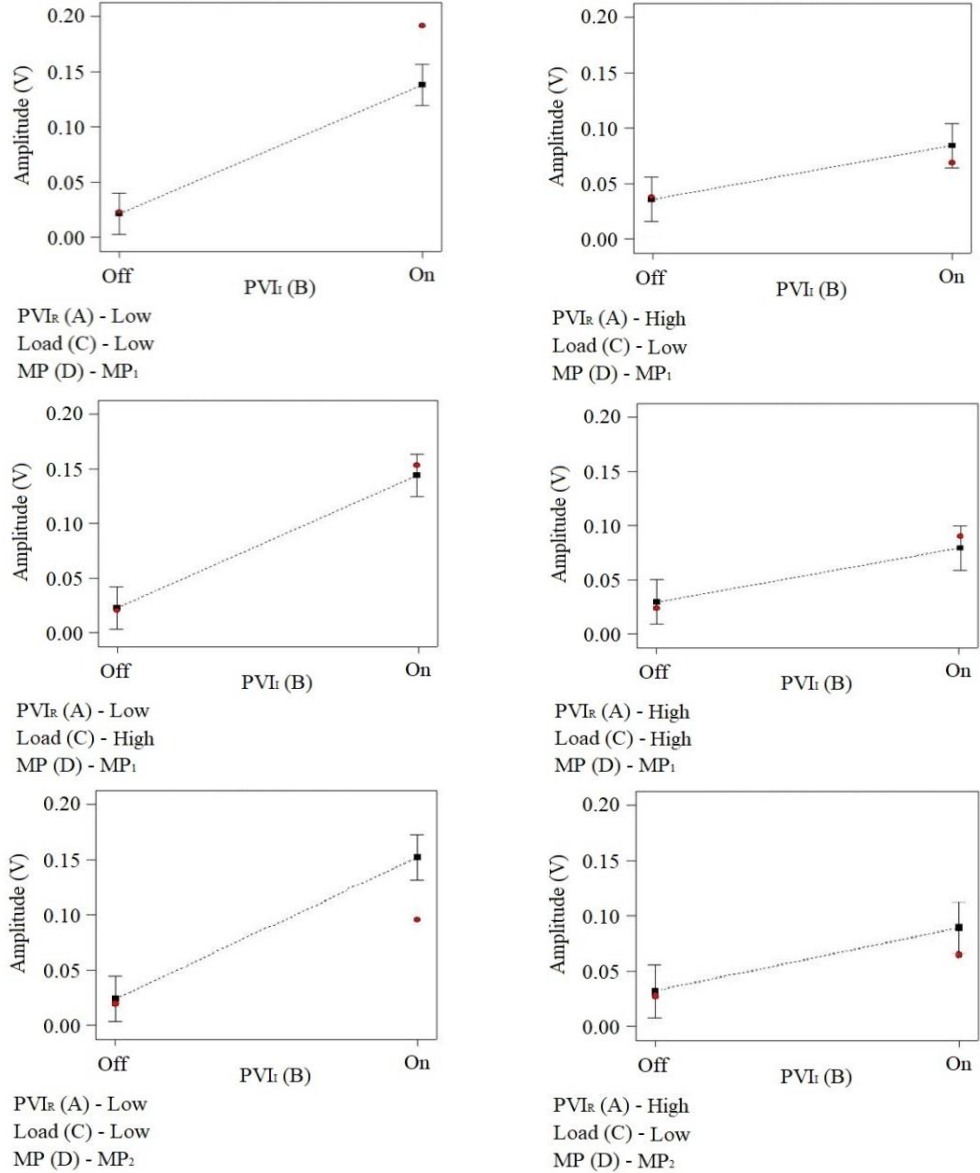
The ANOVA for voltage emissions in the frequency range of 4 to 6 kHz is listed in Table 20.

Table 20. ANOVA Table for voltage emissions from 4 to 6 kHz.

Source	Sum of Squares	df	Mean	F value	p-value prob > F	Remark
Model	0.03666	3	0.01222	18.80	< 0.0001	Highly significant
A - PVI _R	0.00209	1	0.00209	3.22	0.0978	Not significant
B - PVI _I	0.02892	1	0.02892	44.49	< 0.0001	Highly significant
AB	0.00566	1	0.00566	8.71	0.0120	Significant
Residual	0.00778	12	0.00065			
Cor Total	0.04444	15				

The significant parameter means that the particular parameter influences the generation of the supharmonic emissions. The effects represent the individual emissions from the parameters and the

interactions represent the emissions when two different parameters functions together. From Table 20, the analysis model is highly significant for the voltage emissions in the frequency range of 4 to 6 kHz. The most significant parameters of the model are the individual effects of the PVI_I (B) and the interaction between the PVI_R (A) and PVI_I (B). The individual effect of the PVI_R (A) is not significant for this model as the p-value is 0.0978, since it is higher than 0.05. The individual effects and interactions between the parameters for voltage and current emissions in each frequency intervals are mapped using the design expert software. The design of the individual effects of the PVI_I (B) for varying levels of the PVI_R (A), Load (C) and MP (D) are shown in Fig. 87. The levels of the PVI_R (A) and Load (C) are “High” and “Low”. The MPs are MP₁, which is closer to the residential equipment, and MP₂, which is closer to the PVIs. The x-axis represents various levels of the PVI_I (B), which are “Off/Low” and “On/High”. The design of interaction between the PVI_R (A) and PVI_I (B) for various levels of the Load (C) and MP (D) is depicted in Fig. 88. The levels of the Load (C) are “High” and “Low”. The MPs are MP₁ closer to the residential equipment and MP₂ closer to the PVIs. The remaining frequency intervals for voltage and current waveforms in the frequency range of 2 to 22 kHz are analyzed using a similar method. Additional results of the statistical analysis using ANOVA for the emissions in the frequency range of 2 to 22 kHz are presented in Appendix B.



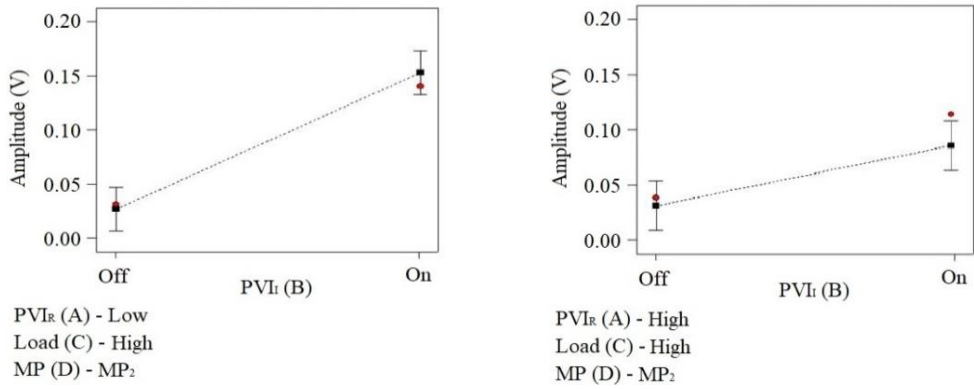


Fig. 87. Individual effects of PVI_I on voltage emissions from 4 to 6 kHz.

The individual effects of the PVI_I (B) in the frequency range of 4 to 6 kHz for various operating level of other parameters, such as the PVI_R (A), Load (C), and MP (D) are shown in Fig. 87. The individual effects of the PVI_I (B) are higher when the PVI_R (A) is “Low”. The effects are lower when the PVI_R (A) is “High”. The other parameters, Load (C) and MP (D) have little to no effect on the PVI_I (B). This is evident from lack of change in the emissions from the PVI_I (B) with change in the levels of the Load (C) and MP (D). The interactions between the PVI_R (A) and PVI_I (B) are shown in Fig. 88.

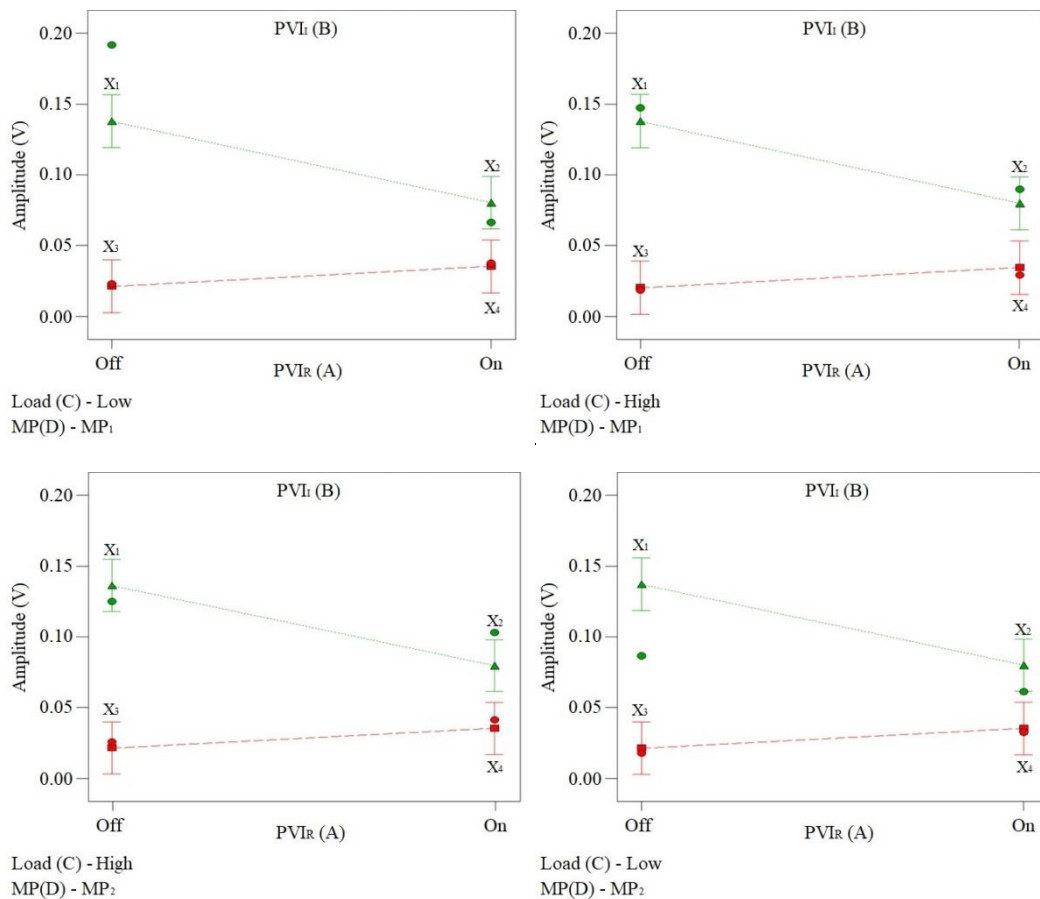


Fig. 88. Interactions between PVI_R and PVI_I on voltage emissions from 4 to 6 kHz.

The design points of the experiment are:

- Load (C) - Low/High;
- MP (D) - MP₁/ MP₂;

- Off/On in the x-axis represents Low/High respectively;
- ▲ - PVI_I (B) - High and ■ - PVI_I (B) - Low;
- x-axis: PVI_R (A) - Off/Low and On/High;
- X₁ - the voltage amplitude when the PVI_R (A) is Low and the PVI_I (B) is High;
- X₂ - the voltage amplitude when the PVI_R (A) is High and the PVI_I (B) is High;
- X₃ - the voltage amplitude when the PVI_R (A) is Low and the PVI_I (B) is Low;
- X₄ - the voltage amplitude when the PVI_R (A) is High and the PVI_I (B) is Low.

The design considers interaction between the PVI_R (A) and PVI_I (B), when the Load (C) is “Low/High” and the MP (D) is “MP₁/ MP₂”. The change in operating levels of the Load (C) and MP (D) does not affect the levels of interactions between the PVI_R (A) and PVI_I (B). From Fig. 88, Points X₃ and X₄ does not differ significantly. This indicates that the PVI_R (A) has no effect on the PVI_I (B), when the PVI_I (B) is “Low”. Therefore, the PVI_R (A) has less to no interaction or influence on the PVI_I (B), when it is “Low” and is represented by the almost horizontal red line. Whereas, X₁ has much higher amplitude compared to X₂, when the PVI_I (B) is “High” and the PVI_R (A) is “Low/High”. This indicates operation of the PVI_R (A) as filter to the PVI_I (B), when the equipment are “High”. Table 21 summarizes the results from the analysis, and indicates the significant factors that create supraharmonic emissions in the grid. The red cells are the highly significant factors with p-value less than 0.01, the yellow cells are the nearly significant factors with p-value between 0.01 and 0.05, and the remaining cells are non-significant factors.

Table 21. Effects and interactions of electrical network parameters 1.

Waveform	Frequency (kHz)	Individual Effects				Parameter Interactions				
		PVI _R	PVI _I	Load	MP	PVI _R /PVI _I	PVI _R /MP	Load/MP	PVI _I /Load	PVI _I /MP
Voltage	2-4		■	■						
	4-6		■			■				
	6-8		■				■			
	8-10			■						
	10-12			■						
	12-14				■					
	14-16		■		■					
	16-18		■	■	■				■	■
	18-20	■	■			■				
	20-22		■							
	22-150									
Current	2-4		■		■			■		
	4-6		■		■				■	
	6-8		■		■				■	
	8-10		■	■	■				■	■
	10-12			■	■					
	12-14		■							
	14-16		■				■			
	16-18		■		■				■	

	18-20									
	20-22									
	22-150									

From the analysis, it is observed that the PVI_I (B) is a major source, as it creates the voltage and current supraharmonics in almost the entire frequency range of 2 to 22 kHz. The MP (D) also plays an important role in the network. The emissions are higher when the MP (D) is closer to the generation equipment like the PVI_R (A) and PVI_I (B) in comparison to other cases. The Load (C) creates supraharmonic emissions in specific frequencies. As mentioned earlier, the Load (C) is a combination of residential equipment, such as the EVCs, heat pumps, washing machines and refrigerators, etc. operating at their maximum capacity. The supraharmonic emissions during the operation of the PVI_R (A) are shown in Fig. 89 to Fig. 92. The higher voltage and current emissions are observed in the frequency range of 2 to 4 kHz, whereas the lower voltage emissions are observed around a frequency of 19.50 kHz and the lower current emissions are observed around a frequency of 16 and 19.50 kHz.

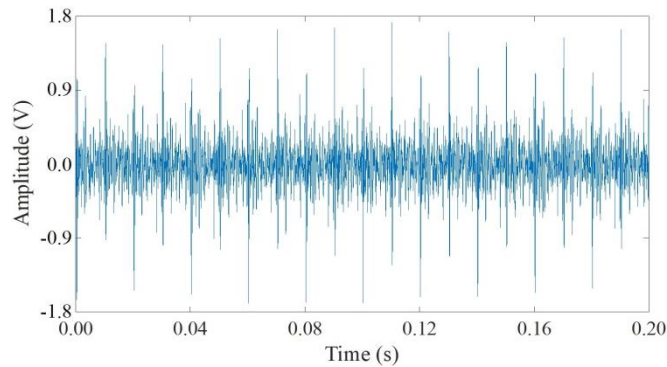


Fig. 89. Voltage supraharmonic emissions from PVI_R in time during campaign 1.

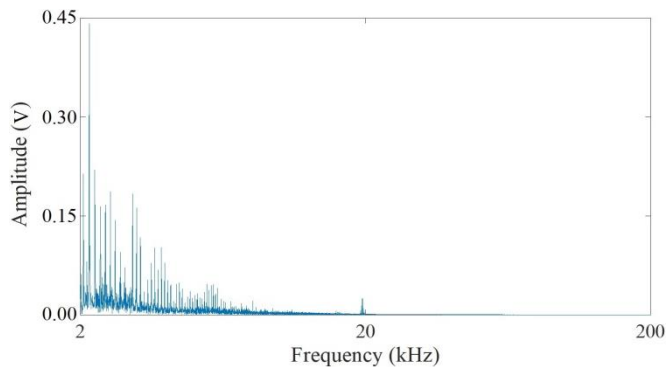


Fig. 90. Voltage supraharmonic emissions from PVI_R in frequency during campaign 1.

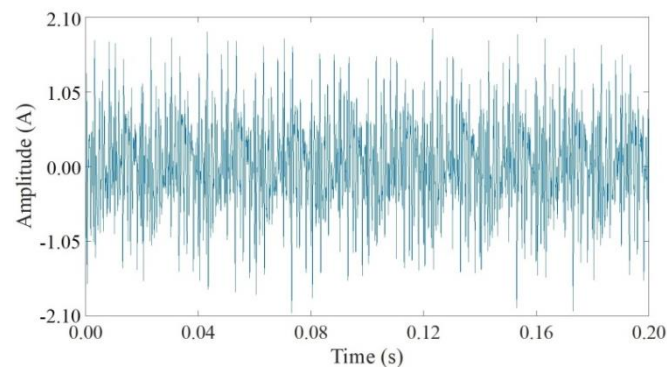


Fig. 91. Current supraharmonic emissions from PVI_R in time during campaign 1.

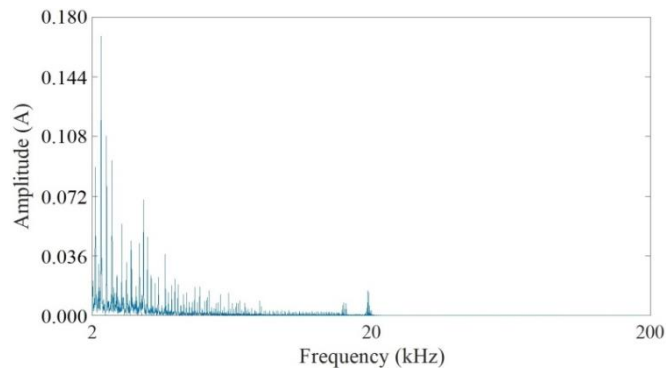


Fig. 92. Current supraharmonic emissions from PVI_R in frequency during campaign 1.

The presence of the supraharmonic emissions are detected during the individual characterization of the PVI_R (A), whereas during the network tests, the effects are limited to the voltage emissions in the frequency range of 18 to 20 kHz. This indicates that the PVI_R (A) acts as the filter for the network emissions when coupled with the PVI_I (B). In addition, the interactions between the parameters vary with the waveforms, e.g., the interactions between the PVI_R (B) and Load (C) are of high significance for the current emissions, but of low significance for the voltage emissions. Furthermore, although the individual factors are significant for a frequency range, this does not necessarily mean that the interactions between these factors are also significant, e.g., the PVI_I (B) and Load (C) are significant, but their interaction is not significant for the voltage emissions in the frequency range of 2 to 4 kHz.

5.4 Measurement Campaign 2 Results

The measurement campaign 2, which include the individual equipment tests, multiple equipment tests, and electrical network tests analysis and results are described here. The measurements acquired are analysed mathematically using FFT algorithm and statistically using ANOVA.

5.4.1 Individual Equipment Tests

Individual equipment tests are performed to identify the voltage and current supraharmonic emissions in the frequency range of 2 to 150 kHz from the EuT. The effects of cable impedance on the propagation of voltage and current supraharmonic emissions are analyzed here. The measured waveforms in time domain are converted to frequency domain using the FFT algorithm. The network schema, equipment measured, and test procedure for the individual characterization tests are described in section 4.2.2. The voltage and current supraharmonic emissions from the PVI_I at equipment terminal in the time and frequency domain are shown in Fig. 93 to Fig. 96.

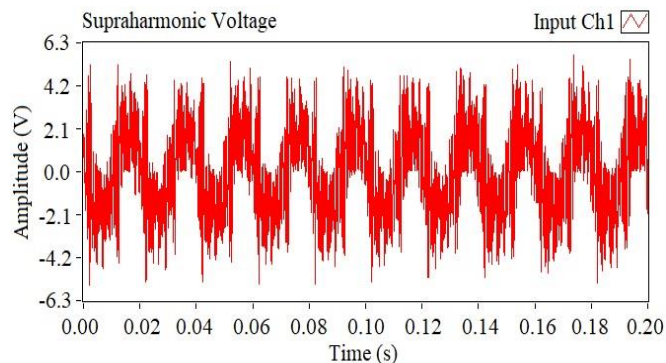


Fig. 93. Voltage supraharmonic emissions from PVI_I at terminal in time during campaign 2.

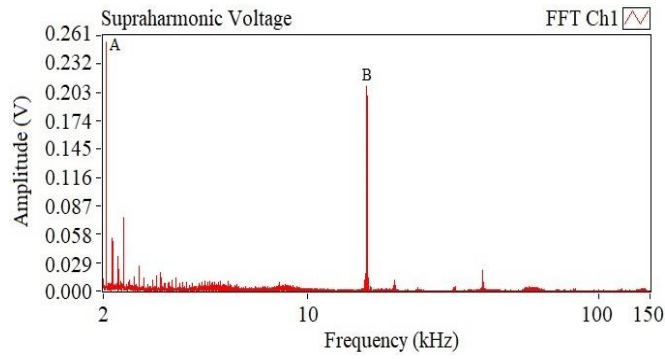


Fig. 94. Voltage supraharmonic emissions from PVI_I at terminal in frequency during campaign 2.

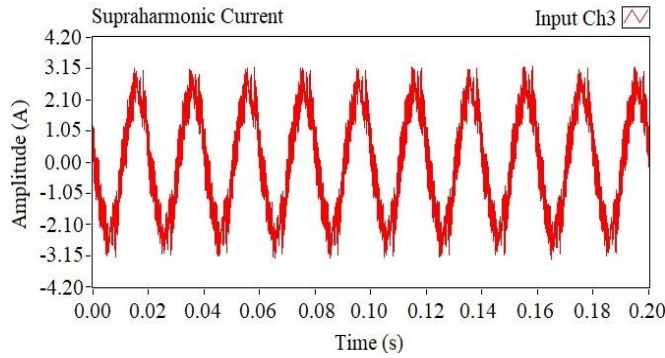


Fig. 95. Current supraharmonic emissions from PVI_I at terminal in time during campaign 2.

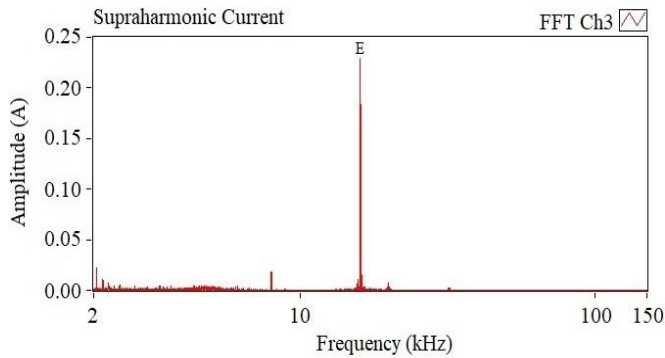


Fig. 96. Current supraharmonic emissions from PVI_I at terminal in frequency during campaign 2.

From Fig. 93, the higher voltage emissions are observed at the frequencies of 2 and 16 kHz, whereas the lower voltage emissions are observed in the frequency range of 2 to 4 kHz. From Fig. 96, the higher current emissions are observed at the frequency of 16 kHz, whereas lower current emissions are observed at the frequency of 8 kHz. The emissions from the PVI_I at a distance of 300 m in the time and frequency domain are shown in Fig. 97 to 100.

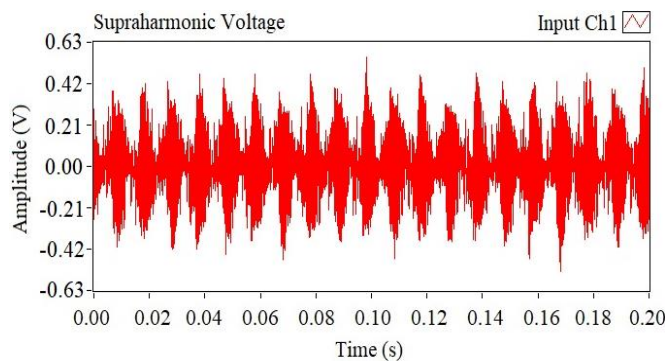


Fig. 97. Voltage supraharmonic emissions from PVI_I at 300 m in time during campaign 2.

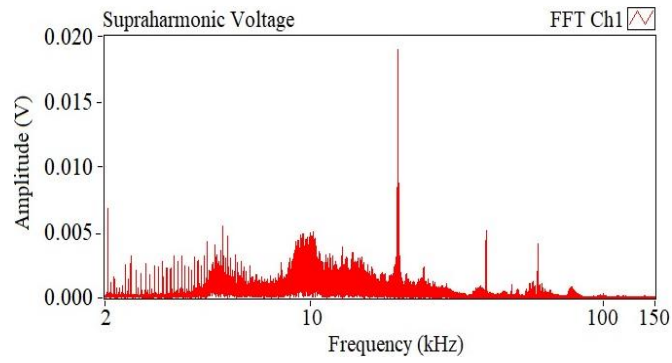


Fig. 98. Voltage supraharmonic emissions from PVI_I at 300 m in frequency during campaign 2.

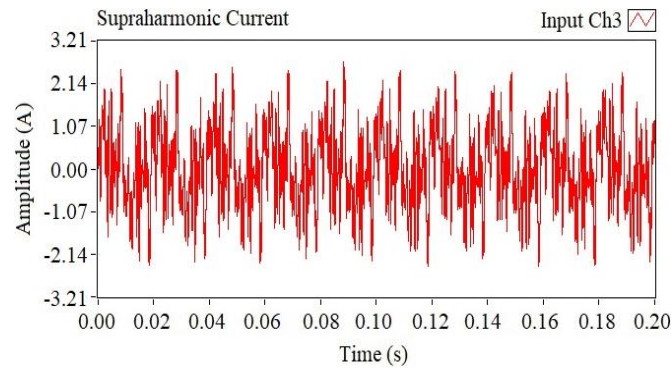


Fig. 99. Current supraharmonic emissions from PVI_I at 300 m in time during campaign 2.

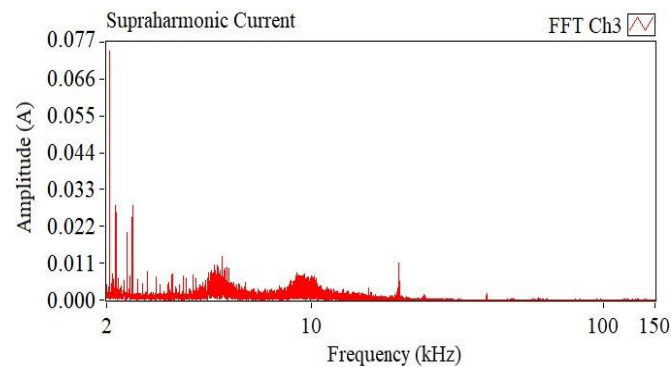


Fig. 100. Current supraharmonic emissions from PVI_I at 300 m in frequency during campaign 2.

Comparing the voltage emissions from Fig. 94 and Fig. 98, and the current emissions from Fig. 96 and Fig. 100, it is observed that the change in the measurement point from the equipment terminal to the distance of 300 m results in the attenuation in the emission amplitudes. The voltage emissions at the frequency of 2 kHz is reduced by the factor of 40, and 16 kHz is reduced by the factor of 11 with the change in the measurement point. The current emissions at 16 kHz is reduced by the factor of 20, whereas the emissions at the frequency of 2 kHz is amplified by the factor of 3. In conclusion, the voltage and current supraharmonic emissions in the frequency range of 2 to 150 kHz tend to attenuate with the increasing distance from the equipment and is maximum at the equipment terminal.

5.4.2 Multiple Equipment Tests

The main objective of multiple equipment tests are to measure the primary and secondary emissions between the source equipment, such as the PVI, and the load equipment, such as the EVC. The tests study the primary and secondary emissions in the electrical network. In addition, the effects of sudden

connection and disconnection of the load equipment in the electrical network are also analyzed. The measured waveforms in the time domain are converted to the frequency domain using the FFT algorithm. The network schema, equipment measured, and test procedure for the multiple equipment tests are described in section 4.3.2.

The individual characterization of the PVI_I is shown in Fig. 93 to Fig. 96. From Fig. 94, higher voltage emissions are observed at a frequencies of 2 and 16 kHz, whereas lower voltage emissions are observed in the frequency range of 2 to 4 kHz. From Fig. 96, higher current emissions are observed at a frequency of 16 kHz, whereas lower current emissions are observed at a frequency of 8 kHz.

The voltage and current supraharmmonic emissions in the electrical network, when the fast charging EVC is connected to the PVI_I is shown in Fig. 101 to Fig. 104. The primary and secondary supraharmmonic emissions, individual effects and interactions between the PVI_I and fast charging EVC are analyzed here. The voltage emissions are observed from Fig. 94 and Fig. 102, and the current emissions are observed from Fig. 96 and Fig. 104.

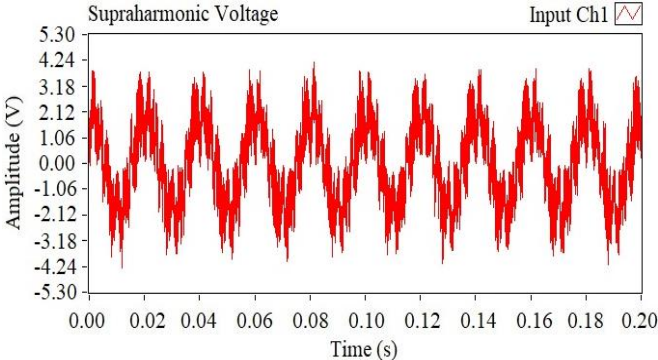


Fig. 101. Voltage supraharmonic emissions from PVI_I with EVC in time during campaign 2.

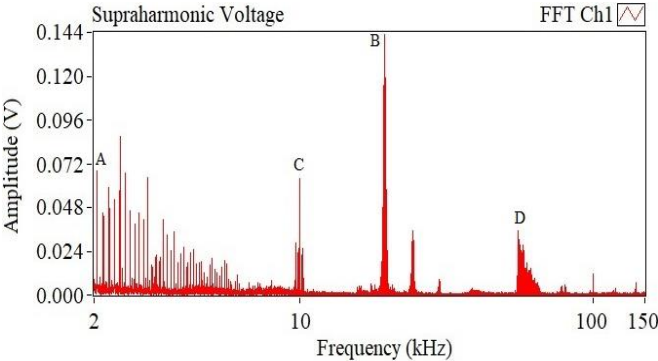


Fig. 102. Voltage supraharmonic emissions from PVI_I with EVC in frequency during campaign 2.

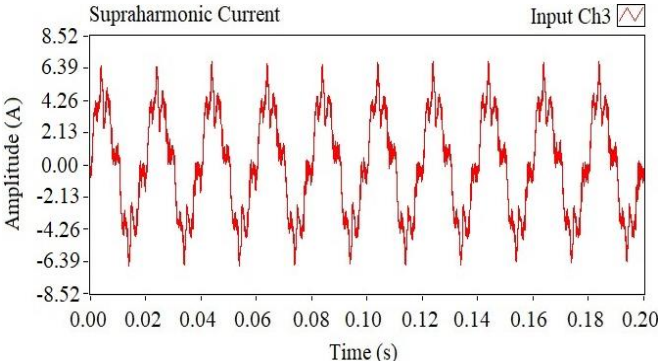


Fig. 103. Current supraharmonic emissions from PVI_I with EVC in time during campaign 2.

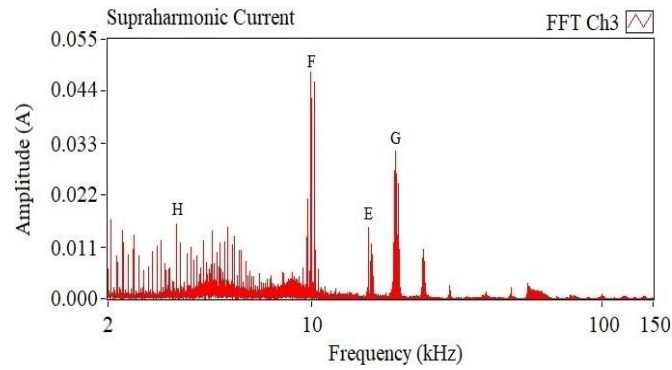


Fig. 104. Current supraharmonic emissions from PVI_I with EVC in frequency during campaign 2.

The voltage supraharmonic emissions from Fig. 94 and Fig. 102 are compared and studied. The voltage emissions, A, B, C, and D are considered here. The voltage emissions, A and B are observed at the equipment terminal of the PVI_I in both scenarios, during the individual operation and when the EVC is connected to the electrical network. This indicates that the voltage emissions, A and B are the primary emissions from the EuT, which is the PVI_I. The voltage emissions, C and D are only observed at the equipment terminal of the PVI_I, when the EVC is connected to the electrical network. These are the secondary emissions from a different source in the electrical network, which is the EVC. The voltage emissions, A and B are the individual effects from the PVI_I. Similarly, the voltage emissions, C and D are the individual effects from the EVC. There is a significant attenuation in the voltage emissions A and B, when the EVC is added to the electrical network. This indicates the interaction between the PVI_I and the EVC in the electrical network.

The current supraharmonic emissions from Fig. 96 and Fig. 104 are also compared and studied. The current emissions, E, F, G, and H are considered here. The current emission, E is observed at the equipment terminal of the PVI_I in both scenarios, during the individual operation and when the EVC is connected to the electrical network. This indicates that the current emission, E is the primary emission from the EuT, which is the PVI_I. The current emissions, F, G, and H are only observed at the equipment terminal of the PVI_I, when the EVC is connected to the electrical network. These are secondary emissions from a different source in the electrical network, which is the EVC. The current emission, E is the individual effect from the PVI_I. Similarly, the current emissions F, G, and H are the individual effects from the EVC. There is a significant attenuation in the current emission E, when the EVC is added to the electrical network. This indicates the interaction between the PVI_I and the EVC in the electrical network. In electrical networks with more parameter effects and interactions influencing the voltage and current supraharmonic emissions in the frequency range of 2 to 150 kHz, a more systematic analysis approach is required. In this case, the electrical network is studied through the statistical analysis using the ANOVA in the frequency range of 2 to 150 kHz and is described below.

5.4.3 Electrical Network Tests

The network schema and configurations measured during electrical network tests are described in section 4.3.3. The measured waveforms in the time domain are converted into the frequency domain using the FFT algorithm. Then, the frequency range of 2 to 150 kHz is divided into frequency intervals with the maximum emissions. The RMS value of the highest emissions in each interval is obtained from the FFT algorithm. The frequency intervals with no emissions are tabulated as zero. The voltage

and current emissions for the configuration C₇ from Table 16 in the frequency range of 2 to 150 kHz in time and frequency domain are shown in Fig. 105 to Fig. 108.

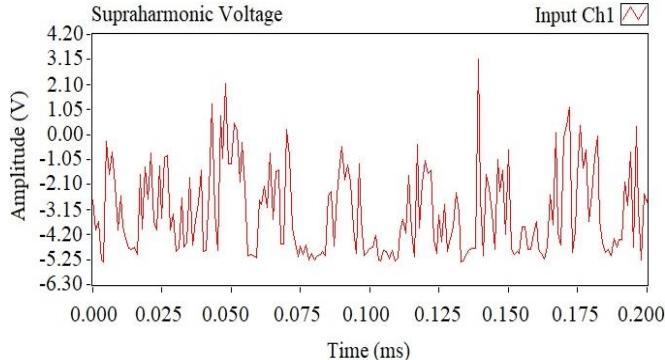


Fig. 105. Voltage supraharmonic emissions from C₇ in time during campaign 2.

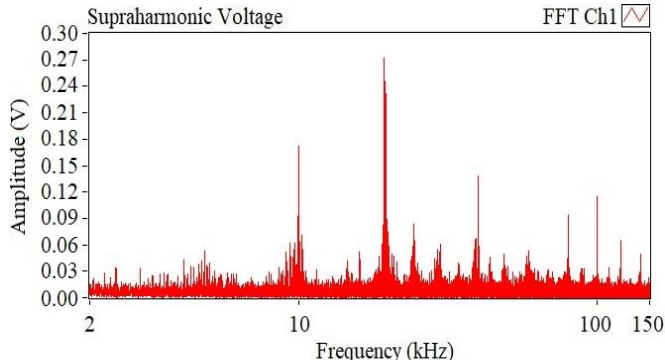


Fig. 106. Voltage supraharmonic emissions from C₇ in frequency during campaign 2.

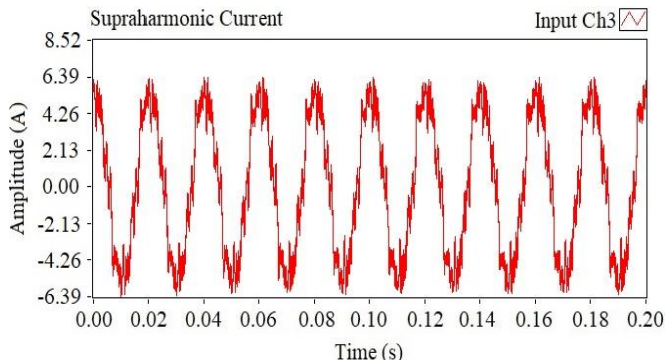


Fig. 107. Current supraharmonic emissions from C₇ in time during campaign 2.

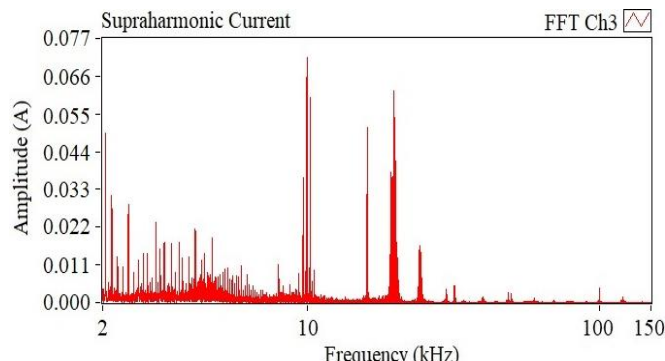


Fig. 108. Current supraharmonic emissions from C₇ in frequency during campaign 2.

The voltage and current supraharmonic emissions in the frequency range of 2 to 150 kHz are observed from Fig. 106 and Fig. 108. The statistical analysis with the ANOVA uses the absolute values instead of normalized values of voltage and current emissions, since some of the configurations have a very low fundamental current component, e.g., C₈. In these cases, the normalized value of the current emissions with respect to the fundamental current component is very high. Therefore, using the normalized values for the analysis would not yield the relevant results. Therefore, the absolute value of the measured waveform enables a better comparison as the fundamental current varies over a wide range of values from 1.76 to 71.52 A.

The statistical analysis with the ANOVA is performed on the absolute values of the voltage and current emissions as explained in section 5.3.3. The RMS values of the highest supraharmonic emissions for the voltage and current waveforms are shown in Fig. 109 and Fig. 110. The voltage supraharmonic emissions during the network tests are shown in Fig. 109. The higher peaks are observed in the frequency range of 9 to 11 and 19 to 21 kHz, where the configurations C₅, C₆, and C₇, generate these emissions. The lower peaks are observed in the frequency range of 39 to 41, 79 to 81 and 99 to 101 kHz. The configurations C₁, C₂, and C₃, generate the emissions in this frequency range. The PVI_R (A) and PVI_I (B) are in “High” state for these configurations. The MP (D) is in MP₂, which is closer to the PVIs for the network configurations mentioned above. This indicates the increased influence of the PVIs on the voltage waveform.

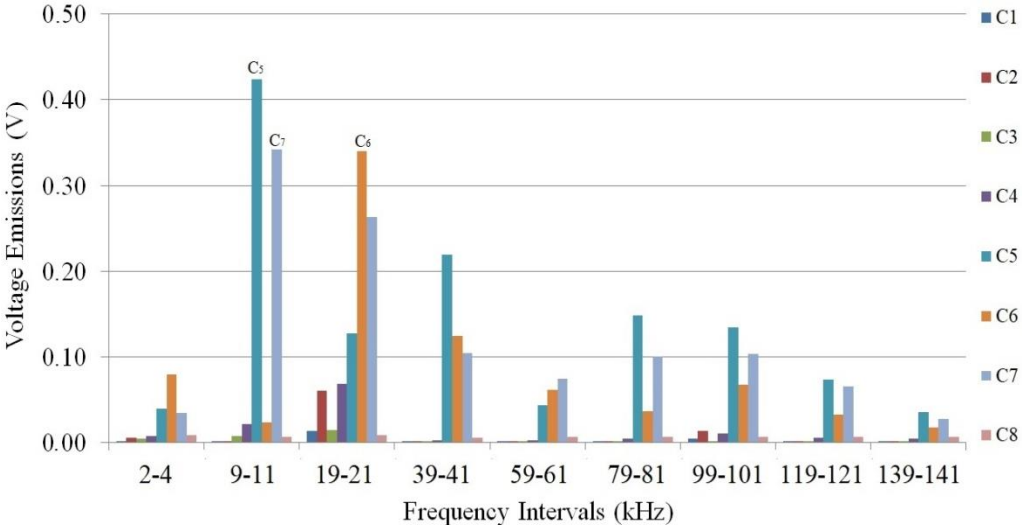


Fig. 109. Voltage supraharmonic emissions from electrical network tests.

The current supraharmonic emissions during the network tests are shown in Fig. 110. The higher emissions are observed in the frequency range of 9 to 11 and 19 to 21 kHz, where the configurations C₅ and C₇, generate the highest peak emissions. The PVI_I (B) is in “High” state for C₅, and the PVI_R (A) is in “High” state for C₇. The Load (C) is in “High” state for C₅ and C₇. The lower peaks are observed in the frequency ranges of 2 to 4 and 99 to 101 kHz. From Fig. 110, it is observed that the emissions are higher when the MP (D) is closer to the PVIs.

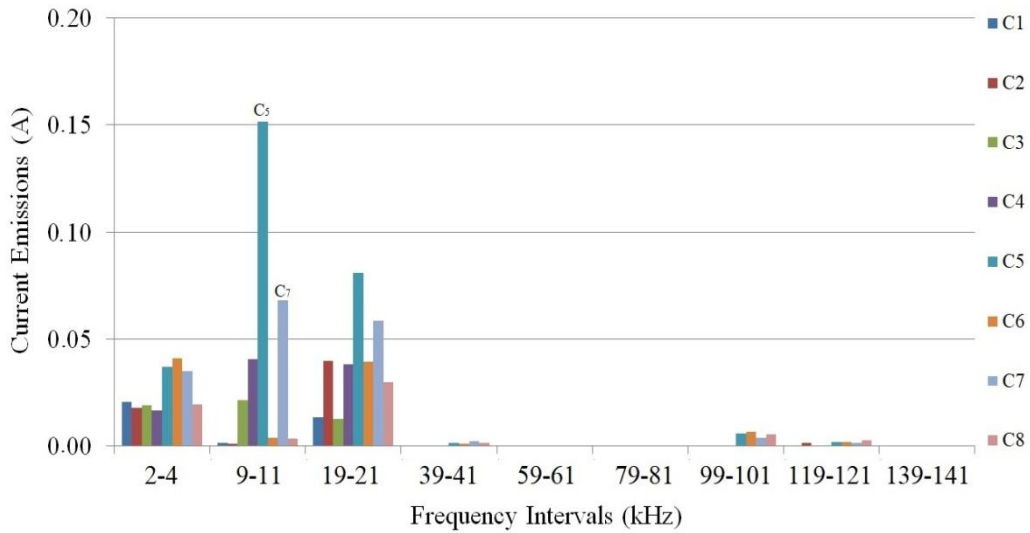


Fig. 110. Current supraharmonic emissions from electrical network tests.

The ANOVA is explained in section 5.3.3. Table 22 summarizes the results and indicates the significant factors that create supraharmonic emissions. The red cells are the highly significant factors with p-value less than 0.01, the yellow cells are the nearly significant factors with p-value between 0.01 and 0.05, and the remaining cells are non-significant factors. These cells are the individual effects and interactions between the factors that influence the supraharmonic emissions in the network.

Table 22. Effects and interactions of electrical network parameters 2.

Waveform	Frequency (kHz)	Individual Effects				Interactions				
		PVI _R	PVI _I	Load	MP	PVI _R /PVI _I	PVI _R /MP	Load/MP	PVI _I /Load	PVI _I /MP
Voltage	2-4				Yellow					
	9-11			Red	Red			Red		
	19-21		Yellow		Yellow					Yellow
	39-41				Yellow					
	59-61		Yellow		Yellow					Yellow
	79-81			Yellow	Red			Yellow		
	99-101			Yellow	Yellow			Yellow		
	119-121			Yellow	Red			Yellow		
	139-141			Yellow	Red			Yellow		
Current	2-4				Yellow					
	9-11			Yellow						
	19-21				Yellow					
	39-41				Red					
	59-61									
	79-81									
	99-101				Red					
	119-121				Yellow					
	139-141									

From Table 22, the analysis studies the higher frequency voltage and current emissions in the frequency range of 2 to 150 kHz in the test network. The voltage emissions are more prevalent at higher frequencies compared to the current emissions. The Load (C) and MP (D) are the main factors, which influence the higher voltage emissions in the frequency range of 2 to 150 kHz. The interactions between the Load (C) and MP (D) are highly significant for the voltage emissions in the frequency range of 9 to 11 kHz, and significant for the voltage emissions in the frequency range of 79 to 150 kHz. There are minimum current emissions at higher frequencies, and the MP (D) influences the existing current emissions in the higher frequency range of 99 to 121 kHz. The results from the statistical analysis using the ANOVA are in line with the analysis from section 5.4.1 and section 5.4.2, where the higher frequency voltage emissions are generated by the EVC, which is included in the Load (C). The analysis outcomes from the measurement campaign 1 and 2 differ as the analyzed frequency intervals vary in both analyses. The first analysis focuses in the frequency range of 2 to 22 kHz, whereas the second analysis focuses on higher frequencies including the frequency range of 39 to 41, 79 to 81, 119 to 121 kHz, etc. In addition, the parameters of the test network, such as the PVIs influence the lower frequencies in the frequency range of 2 to 150 kHz.

5.4.4 Summary

The measurement campaign in the concept grid confirms the presence of the supraharmic emissions in the grid. The equipment, such as the PVIs, EVCs, etc. are the main sources of the supraharmic emissions in the grid. From the measurements performed in the concept grid, it is deduced that the supraharmic emissions tends to attenuate with the increase in the cable length. The emission levels measured closer to the EuT is higher than the emission levels measured at a distance from the EuT. This is evident from the measurement results shown in appendix C. During the network tests of the PVI, the EVC was added and removed from the network to study the effects on the functioning of the PVI. When the EVC was added to the PVI the corresponding measurements showed the peak emissions from the equipment. At frequencies, where both the equipment produced the supraharmic emissions, there was a subsequent attenuation and cancelling out, e.g. the voltage emission peak close to 2 kHz. This emission was visible again once the EVC was removed from the network and is shown in appendix C. Higher frequency emissions close to 150 kHz are visible on the voltage waveforms during the network operations with EVC. The higher level current peaks are visible in the frequency range of 2 to 100 kHz. In addition, the lower level current peaks are visible in the frequency range of 100 to 150 kHz. In short, during the measurement campaign 2, the supraharmic emissions in the frequency range of 2 to 150 kHz were detected for both the voltage and current waveforms as shown in appendix C. The design of the complex waveform generator considering the measurement experience explained above for the laboratory and network measurements is discussed in the chapter 6.

CHAPTER 6
COMPLEX WAVEFORM PLATFORM

6 COMPLEX WAVEFORM PLATFORM

The chapter outlines the design and electrical schema for the complex waveform platform with the characterization system. The components used in the waveform platform and the specifications are explained in this chapter. The components were selected considering the applications in the supraharmonic frequency range of 2 to 150 kHz, like the generation and acquisition. The system is configured with the NI Build your PXI system simulation [99]. With increasing concerns over the effects of the supraharmonic emissions PQAs, such as PQube 3 are designed to measure voltage emissions in the frequency range of 2 to 150 kHz. In this scenario, it is necessary to have a dedicated platform to characterize these PQAs to ensure accuracy and efficiency in the measurement of the supraharmonic emissions in the electrical network. This dedicated platform is realized here. The uncertainty budget of the platform is also calculated. This helps to determine how different factors contribute to the uncertainty of the measurements performed using the waveform platform, thereby ensuring the traceability in the measurements. This gives the idea about the accuracy and quality of the platform and measurement technique. The PQube 3 is used for the tests, since it is one of the few available PQAs, which can measure the voltage emissions in the frequency range of 2 to 150 kHz.

6.1 Objectives

The main objective of the complex waveform generator is to recreate the supraharmonic emissions in the frequency range of 2 to 150 kHz in the laboratory environment. This is realized through the NI PXI system and LabVIEW platform. The LabVIEW platform will be used to communicate with the PXI system. The PXI system consists of 3 NI cards for the following applications:

- the remote control using NI PXIe-8301;
- the waveform generation using NI PXIe-5413;
- the waveform acquisition using NI PXIe-6124.

6.2 Software Architecture

The software architecture of the waveform platform is discussed here [46]. The proposed platform creates the standard and user defined waveforms. The waveform platform has two modes of operation, which are the waveform generation and acquisition. These modes of operation are explained below. The software architecture is shown in Fig. 111.

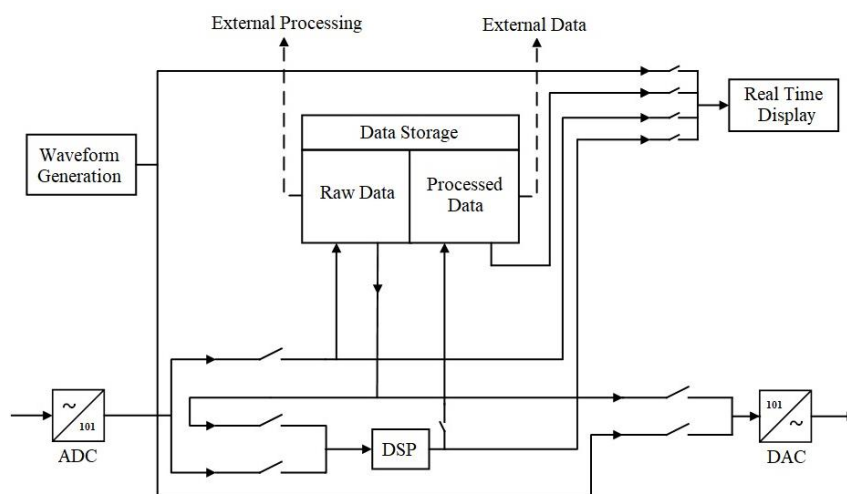


Fig. 111. Waveform platform software architecture [46].

From Fig. 111, the acquired waveforms are either:

- stored in the external memory;
- processed using signal processing algorithms;
- displayed in real time, or;
- stored, processed, and displayed in real time.

The raw and processed waveforms are stored in the external memory, so that if required it could be used for further mathematical processing. The platform can generate the standard waveforms, which are the fundamental signals without any of the supraharmonic components shown in Fig. 112. The standard waveforms include the sine, square, triangle and sawtooth waveforms.

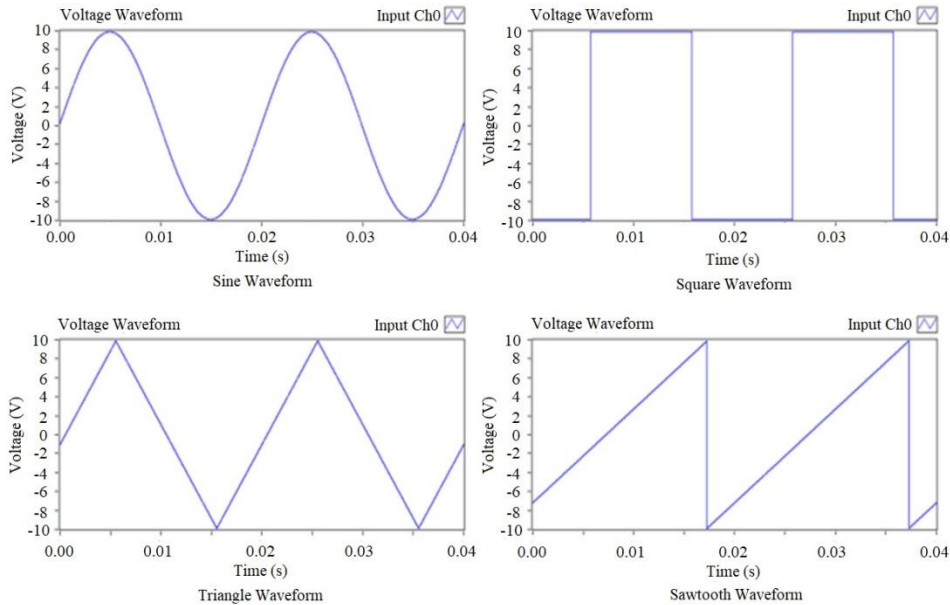


Fig. 112. Standard waveforms.

The complex waveforms, which are the fundamental signals superimposed with the emissions in the frequency range of 2 to 150 kHz can be generated using the platform and is shown in Fig. 113. The amplitude and phase of the emissions with respect to the fundamental waveform can be altered according to the user. In addition, the number of disturbances can be varied from the single emission to multiple emissions.

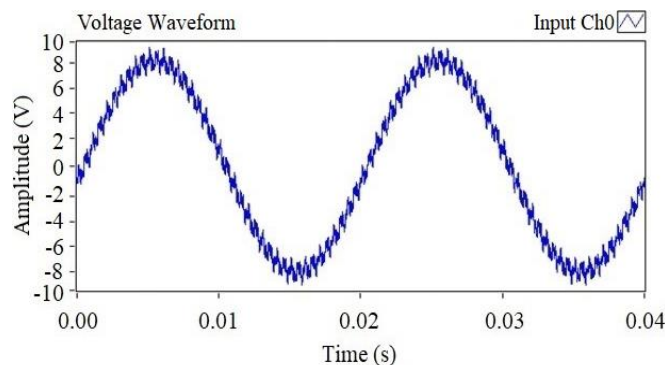


Fig. 113. Complex waveform.

Analog waveforms generated from the files, which are acquired during the electrical network measurements can be recreated in the laboratory using the waveform platform. A current waveform generated by the PVI is shown in Fig. 114.

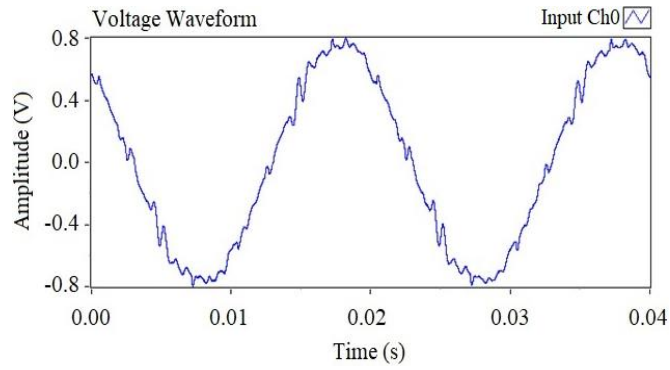


Fig. 114. Current sensor output in voltage from PVI.

Amplitude modulated waveform are generated according to the user definition. Square wave modulation of a sine waveform with 50% duty cycle is shown in Fig. 115.

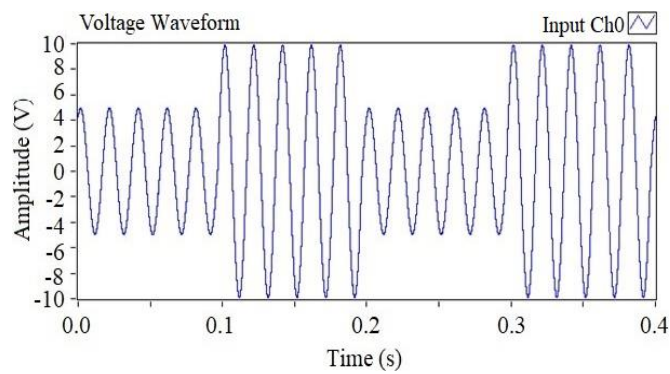


Fig. 115. Modulated waveform.

The waveform platform will also:

- acquire the test waveform in real time. This data is saved as file and also displayed in real time;
- perform FFT algorithm, display, and save the emissions in the frequency domain;
- perform STFT algorithm and display the emissions in the time-frequency domain;
- save the processed waveforms.

The front panel of complex waveform platform is shown in Fig. 116.

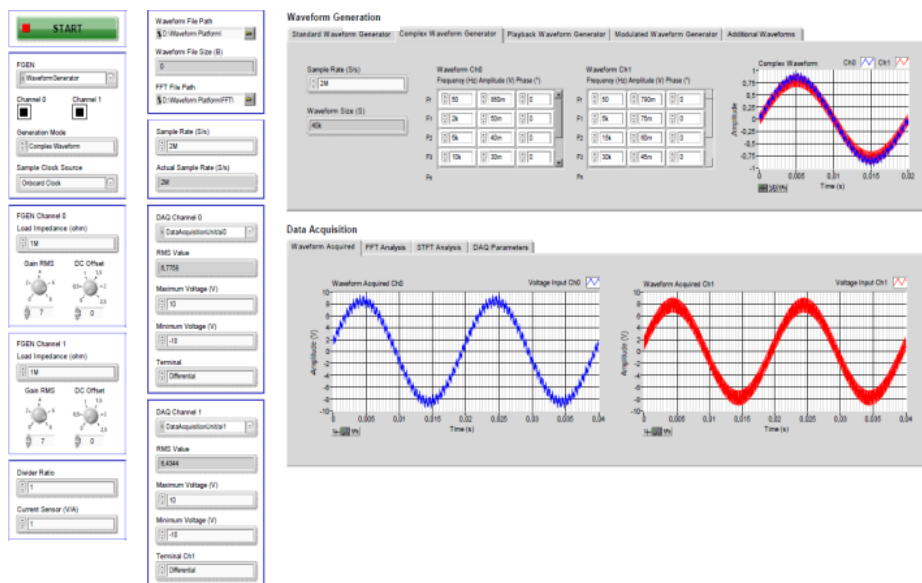


Fig. 116. Waveform platform front panel.

The front panel depicts the complex waveform generated and acquired by the waveform platform. A number of supraharmonic components are superimposed with the fundamental voltage waveform, and the output waveform is acquired by the DAQ.

6.3 Hardware Architecture

The hardware design of the waveform platform is explained below. In addition, the specifications of the waveform platform and the components, which include the voltage and current sensors, are also described. The PXI system is a LabVIEW based measurement and automation system, which consists of both generation and acquisition units [100]. The waveforms are generated and acquired at the sampling rate of 1 MS/s to satisfy Nyquist criteria. The waveform platform specifications are listed in Table 23. The voltage and current specifications are listed in RMS values.

Table 23. Waveform platform specifications.

Function	Parameter	Level	
Generation	Output	8.50 V	
	Resolution	16 bits	
Amplification	Voltage Amplifier	250 V	
	Transconductance Amplifier	70 A	
Measurement and Sensitivity	Lab	VT + Divider	250 V and 46:1
		HPF + Optoisolator	3.50 V
		Rogowski Coil, LFR 06/6	85 A and 0.05 V/A
	Network	VT + Divider	250 V and 46:1
		HPF + Optoisolator	3.50 V
		Rogowski Coil, LFR 06/6	85 A and 0.05 V/A
		Rogowski Coil, LFR 03/3 + HPF	21.21 A and 0.09 V/A
	Acquisition	Input	7.80 V
Resolution		16 bits	

The PXI system with the waveform generator and data acquisition cards (DAQ) are shown in Fig. 117. The PXI chassis is interfaced with the LabVIEW on the computer using the remote controller card with the Thunderbolt 3 connection. The waveform generator has two channels, which can generate two different waveforms. The DAQ has 4 analog input channels, which can be used for the waveform acquisitions.



Fig. 117. Waveform platform.

The waveform platform uses different voltage and current sensors for the laboratory and electrical network applications as listed in Table 23, and these sensors are explained in chapter 3. The characteristics of the NI chassis and cards, such as the model, function, bandwidth, etc. used in the waveform platform are listed in Table 24 to Table 27. These NI cards are selected on the basis of their characteristics, such as the bandwidth, sampling rate, input and output voltage levels, etc.

Table 24. NI chassis specifications [101].

Model	Function	Bandwidth	Slot Count	Power Supply	Equipment
PXIe-1082	Used for housing the NI modules.	24 GB/s per system, 8 GB/s per slot	8	AC Supply	

Table 25. NI remote control specifications [102].

Model	Function	Communication	Bandwidth	Equipment
PXIe-8301	Used for the remote control of the PXIe systems.	Thunderbolt 3.0	2.3 GB/s	

Table 26. NI waveform generator specifications [103].

Model	Function	Bandwidth	Sampling Rate	Equipment
PXIe-5413	Used for the standard, user, and arbitrary waveform generation.	20 MHz	800 MS/s	
Resolution	Memory	O/P Channels	O/P Voltage	
16 bits	256 MB	2	8.50 V	

Table 27. NI DAQ specifications [83].

Model	Function	Bandwidth	Sampling Rate	Equipment
PXIe-6124	Used for the waveform acquisition.	2 MHz	4 MS/s	
Resolution	Overvoltage Protection	I/P Channels	O/P Voltage	
16 bits	±25.50 V	4	7.80 V	

The NI PXIe-6124 DAQ uses the NI TB-2706 terminal block to connect to its analog inputs. The NI TB-2706 terminal block is shown in Fig. 118 and the NI TB-2706 pin layout is shown in Fig. 119. The NI TB-2706 terminal block provides a better analog signal access to the NI PXIe-6124 DAQ [103].



Fig. 118. NI TB-2706 terminal block [103].

PIN#	SIGNAL	PIN#	SIGNAL	PIN#	SIGNAL	PIN#	SIGNAL	PIN#	SIGNAL
68	AI 0+	-	SHIELD						
34	AI 0-	-	SHIELD						
33	AI 1+	66	AI 1-	62	NC	15	D GND	4	D GND
65	AI 2+	31	AI 2-	59	AI 5 GND	14	+5 V	3	PFI 9/CTR 0 GATE
30	AI 3+	63	AI 3-	64	AI 2 GND	13	D GND	2	CTR 0 OUT
28	AI 4+	61	AI 4-	67	AI 0 GND	12	D GND	1	FREQ OUT
60	AI 5+	26	AI 5-	32	AI 1 GND	11	PFI 0/AI START TRIG	35	D GND
25	AI 6+	58	AI 6-	29	AI 3 GND	10	PFI 1/AI REF TRIG	36	D GND
57	AI 7+	23	AI 7-	27	AI 4 GND	9	D GND	37	PFI 8/CTR 0 SOURCE
22	NC	55	NC	24	AI 6 GND	8	+5 V	38	PFI 7/AI SAMP CLK
21	NC	54	NC	18	D GND	7	D GND	39	D GND
20	NC	56	AI 7 GND	17	P0.1	6	PFI 5	40	CTR 1 OUT
53	D GND	19	P0.4	16	P0.6	5	PFI 6	41	PFI 4/CTR 1 GATE
								42	PFI 3/CTR 1 SOURCE
								43	PFI 2/AI CONV CLK
								44	D GND
								45	EXT STROBE*
								46	AI HOLD COMP
								47	P0.3
								48	P0.7
								49	P0.2
								50	D GND
								51	P0.5
								52	P0.0

Fig. 119. NI TB-2706 pin layout [103].

The setup uses the pins AI 0 \pm , AI 1 \pm , AI 2 \pm , AI 3 \pm , for the connections with the voltage and current sensor inputs. The different NI cards are selected based on their characteristics, such as bandwidth, sampling rate, etc. appropriate for the laboratory and electrical network application. The laboratory schema for the characterization of the PQAs, and the electrical network schema for the measurement of the supraharmonic emissions are discussed in the next section.

6.4 Waveform Platform Schema

For the laboratory applications like the characterization of the PQAs, the waveform platform generates the standard waveforms, user defined waveforms, and waveforms that are closely identical to the electrical network waveforms. The waveform generator creates the voltage waveforms in the amplitude range of ± 8.50 V. These waveforms are then increased to the LV network values using the voltage and transconductance amplifiers. The voltage amplifier increases the generator output to higher voltage levels, whereas the transconductance amplifier converts the generator output to the current waveform of required amplitude. These waveforms are measured simultaneously with the waveform platform and EuT. The voltage waveforms are converted to the voltage level adapted to the DAQ input using the VT with the divider, and the HPF. The current waveforms are measured using the Rogowski coils, which converts the current waveforms into the voltage waveforms adapted to the DAQ input. The waveform platform schema used for the characterization of the PQA using the waveform platform is shown in Fig. 120.

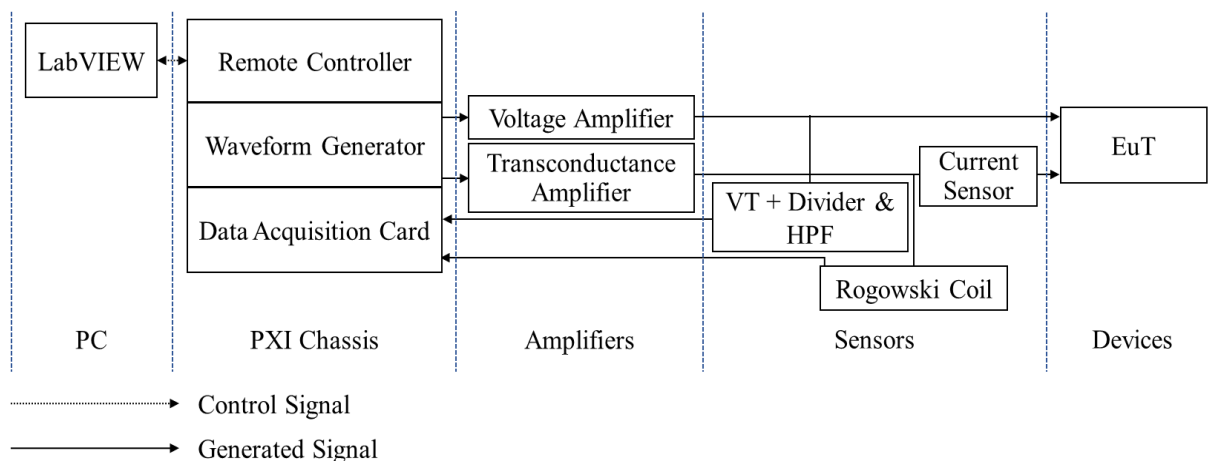


Fig. 120. Waveform platform laboratory schema [46].

For the electrical network measurements, the waveforms from the network are measured through the voltage and current sensors and acquired by the DAQ. The waveform platform schema for the electrical network measurements is shown in Fig. 121. The fundamental and supraharmonic

components of the voltage waveforms are measured using the VT with the divider, and the HPF with the optoisolator. The fundamental and supraharmonic components of the current waveforms are measured using the LFR 06/6, and the LFR 03/3 with the HPF. The results from the electrical network measurements using the waveform platform are explained in section 5.4.3.

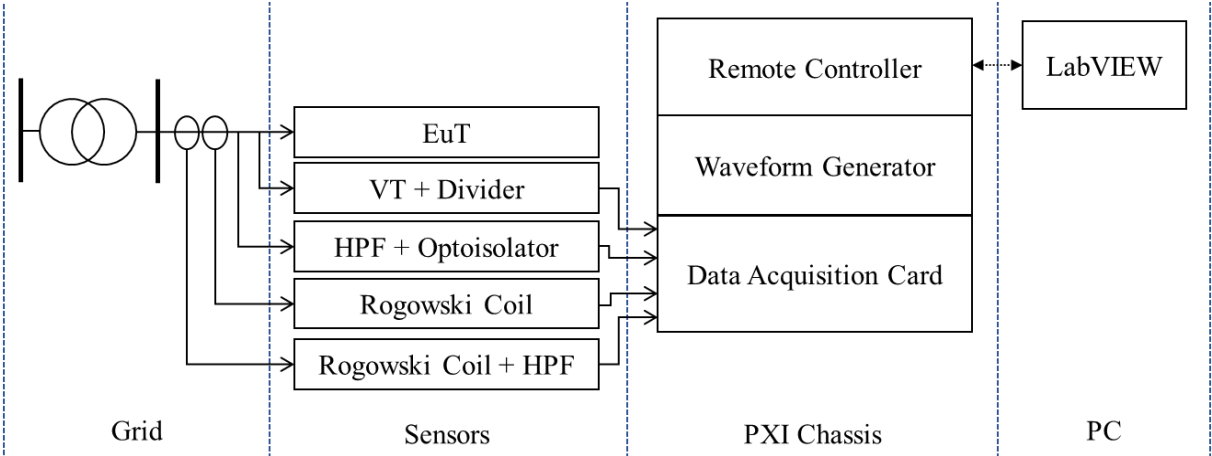


Fig. 121. Waveform platform electrical network schema [46].

The waveform platform characterization, which includes the waveform generator and DAQ in the frequency range of 2 to 150 kHz are described below.

6.5 Waveform Platform Characterization

The characterization of the waveform platform including the waveform generator and DAQ is explained here. The characterization of the waveform platform provides the measurement data, and the characteristic graphs for the varying frequencies and amplitudes. The characterization tests were done in the Low Frequency Electrical Metrology Laboratory in a controlled environment, such as regulated temperature and humidity, and by means of the calibrated references. This guarantees the traceability of the measurement system and a low level of uncertainties. The targeted uncertainty of the waveform platform is set to $\pm 1\%$.

6.5.1 Waveform Generator

The analog output channels of the waveform generator NI PXIe-5413 used for the characterization of PQAs are characterized for the varying frequencies and amplitudes.

Equipment Used

The equipment used for the characterization of the waveform generator are listed in Table 28.

Table 28. Equipment used for characterization of waveform generator.

Designation	Model	Type	N° id
Waveform Generator	NI	PXIe-5413	LNE 1020904
AC Acquisition Unit	Fluke	5790A	LNE 1020703

Schema

The characterization setup used for the waveform generator NI PXIe-5413 is shown in Fig. 122.

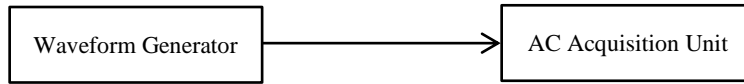


Fig. 122. Characterization schema of waveform generator.

Procedure

The test procedure for the characterization of the waveform generator is as follows:

- the connections are made according to Fig. 122;
- the voltage waveform of known amplitude is generated by the waveform generator;
- the generated voltage waveform is acquired by the AC acquisition unit;
- the AC acquisition unit is a calibrated waveform recorder with the correction factors;
- the correction factors are the adjustments applied to compensate for the variations in the recorder;
- the correction factors of the AC acquisition unit is applied to the displayed voltage values;
- the measurements are performed for the waveforms of the amplitudes of 0.02, 3.50, and 6.00 V;

The measurement data and results are explained below.

Characterization Results

The measurement results for the frequency and amplitude characterization of the waveform generator is discussed here. The frequency characterization of the waveform generator Ch₀ in the frequency range of 0.02 to 150 kHz for the voltage waveforms of the amplitude of 0.02, 3.50, and 6.00 V, are explained here. The difference between the generated and acquired values is calculated as in (18).

$$\varepsilon (\%) = \frac{V_0 - V_1}{V_1} \times 100, \tag{18}$$

where $\varepsilon (\%)$ is the percentage error, V_0 is RMS displayed voltage, and V_1 is the RMS generated voltage. The characterization curve for the waveform generator Ch₀ in error (%) with respect to the frequency is shown in Fig. 123. The waveform generator Ch₀ is characterized in the frequency range of 0.02 to 150 kHz for the voltage waveforms of the amplitude of 0.02, 3.50, and 6.00 V. The error values vary within the value of $\pm 0.15\%$, which is within the targeted limit.

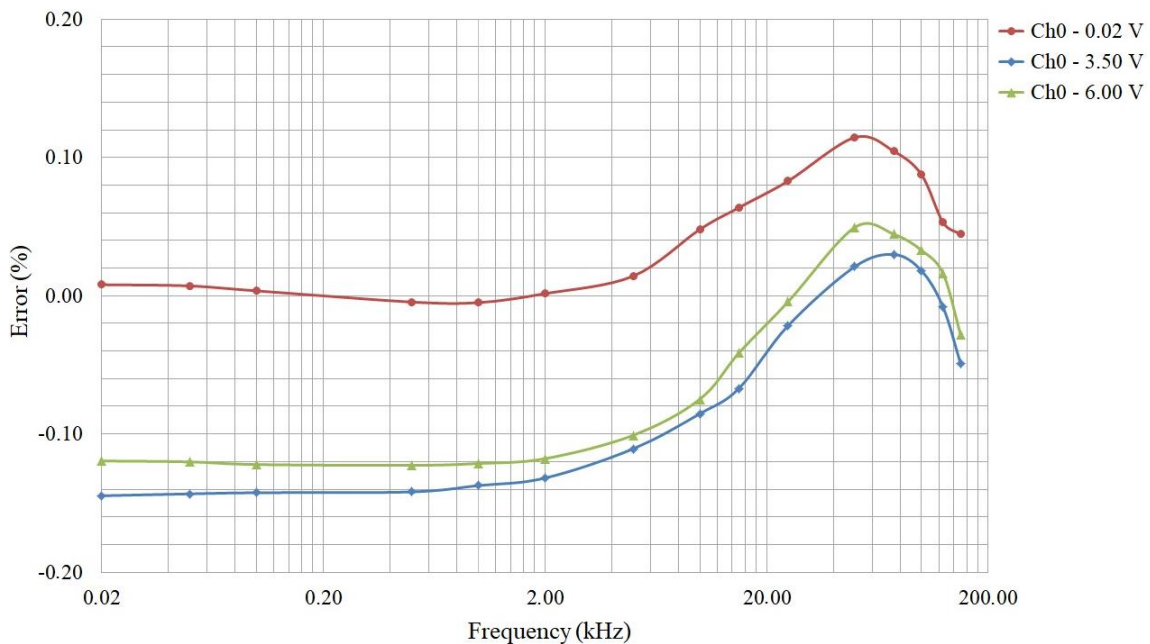


Fig. 123. Characterization curve of waveform generator Ch₀.

The frequency characterization of the waveform generator channel Ch₁ in the frequency range of 0.02 to 150 kHz for the voltage waveforms of the amplitude of 0.02, 3.50, and 6.00 V, are explained below. The difference between the generated and displayed values is calculated as in (15). The characterization curve for the waveform generator Ch₁ in error (%) with respect to the frequency is shown in Fig. 124. The waveform generator channel Ch₁ is characterized in the frequency range of 0.02 to 150 kHz for the voltage waveforms of the amplitude of 0.02, 3.50, and 6.00 V. The error values vary within the value of $\pm 0.13\%$, which is within the targeted limit. The generated waveform can be composed numerically with the amplitudes corrected with the coefficients from the characterization curves.

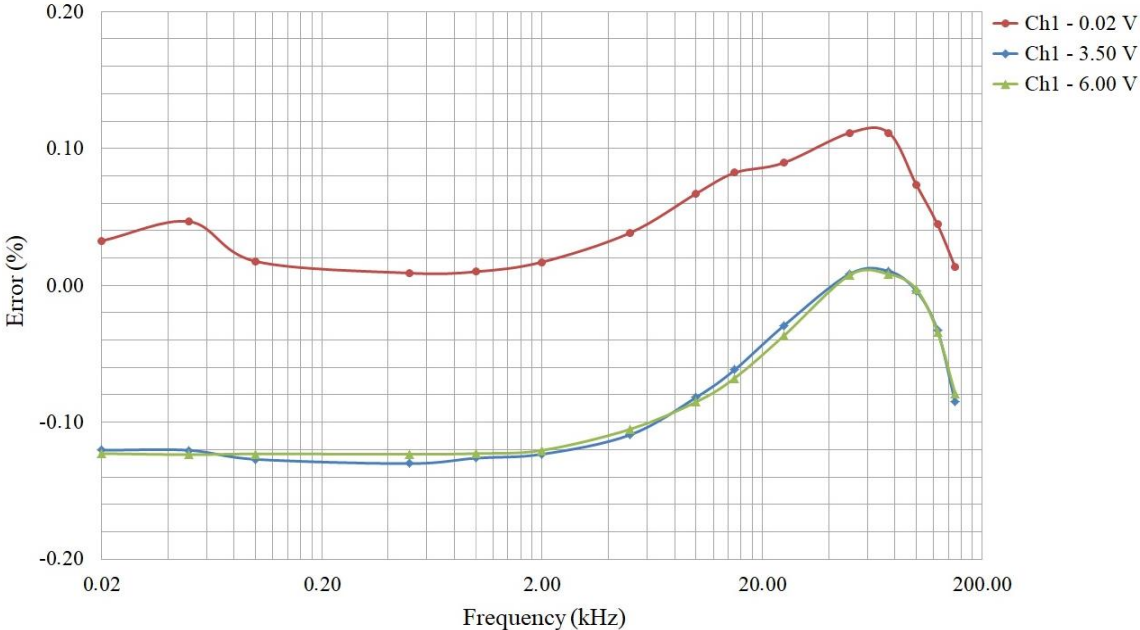


Fig. 124. Characterization curve of waveform generator Ch₁.

The characterization curves for the waveform generator channels Ch₀ and Ch₁, has similar characteristics in the frequency range of 2 to 150 kHz for the voltage waveforms of the amplitude of 0.02, 3.50, and 6.00 V. The error values of the waveform generator channels varies from the value of $\pm 0.15\%$ for the Ch₀, and from $\pm 0.13\%$ for the Ch₁. The frequency characterization of the DAQ analog input channels for varying amplitudes are described below.

6.5.2 Data Acquisition Card

The analog input channels of the DAQ NI PXIe-6124 used for the waveform acquisition are characterized for the varying frequencies and amplitudes.

Equipment Used

The equipment used for the characterization of the DAQ are listed in Table 29.

Table 29. Equipment used for characterization of DAQ.

Designation	Model	Type	N° id
Waveform Generator	FLUKE	5730A	LNE 1019684
DAQ	NI	PXIe-6124	LNE 1020904

Schema

The characterization setup used for the DAQ NI PXIe-6124 is shown in Fig. 125.

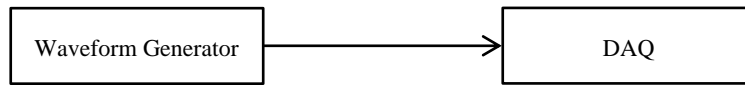


Fig. 125. Characterization schema of DAQ.

Procedure

The test procedure for the characterization of the DAQ is as follows:

- The connections are made according to Fig. 125;
- the voltage waveform of known amplitude is generated by the waveform generator;
- the generated voltage waveform is acquired by the DAQ;
- the waveform generator is a calibrated generator with the correction factors;
- the correction factors are the adjustments applied to compensate for the variations in the generator;
- the correction factors of the waveform generator is applied to the generated voltage waveform;
- the acquisitions are performed for the voltage waveforms of the amplitudes of 0.02 and 6.00 V;

The measurement data and results are explained below.

Characterization Results

The measurement results for the frequency and amplitude characterization of the waveform generator is discussed here. The frequency characterization of the DAQ analog input AI₀ to AI₄, in the frequency range of 0.02 to 150 kHz for the voltage waveforms of the amplitude of 0.02 V is shown in Fig. 126. The error values between the generated and acquired values are calculated as in (15). The characterization curve for the DAQ in error (%) with respect to the frequency is shown in Fig. 126. The DAQ is characterized in the frequency range of 0.02 to 150 kHz for the voltage waveforms of the amplitude of 0.02 V. The error values of the channels vary within the value of $\pm 0.25\%$, which is within the targeted uncertainty.

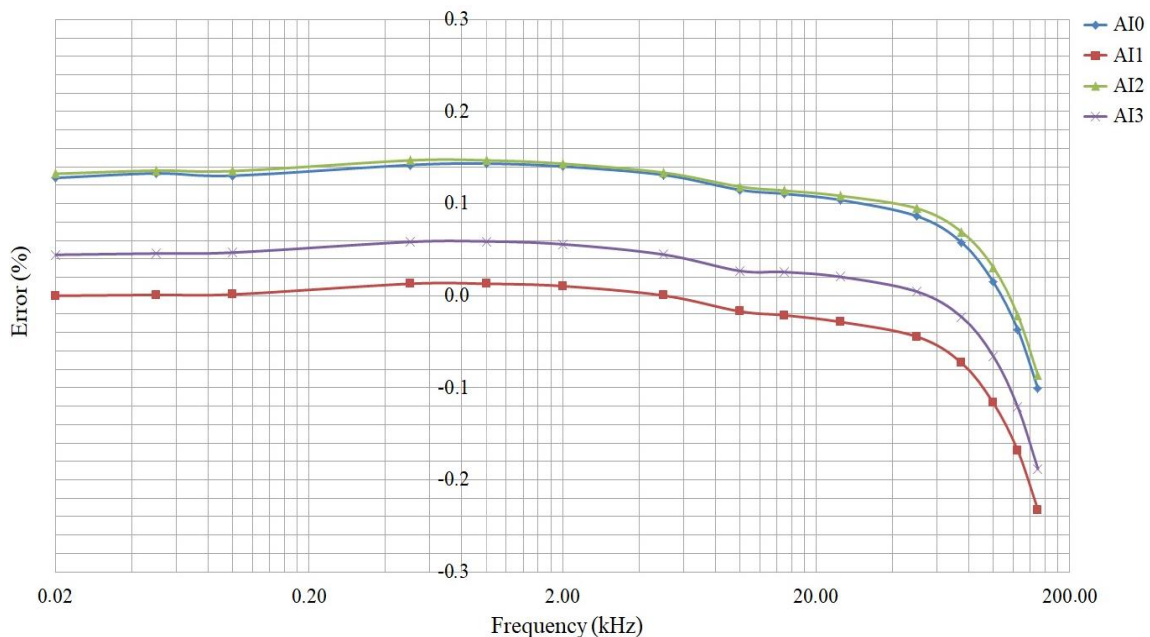


Fig. 126. Characterization curve of DAQ for 20 mV.

The characterization of the DAQ analog input AI₀ to AI₄, in the frequency range of 0.02 to 150 kHz for the voltage waveforms of the amplitude of 6.00 V is shown in Fig. 127. The DAQ is characterized in the frequency range of 0.02 to 150 kHz for the voltage waveforms of the amplitude of 6.00 V. The error values vary within the value of $\pm 0.21\%$, which is within the targeted uncertainty.

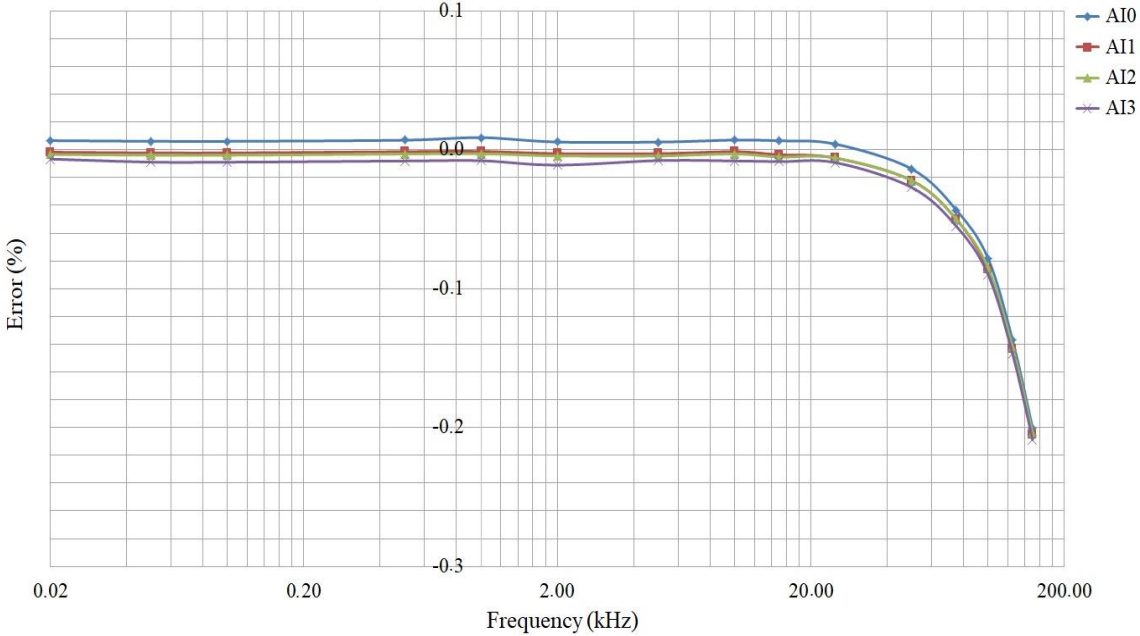


Fig. 127. Characterization curve of DAQ for 6 V.

As stated earlier the target uncertainty for the supraharmonics measurement is $\pm 1\%$. Therefore, the values obtained for the DAQ channels are less than the target uncertainty. Additionally, let’s suppose that the emissions at the frequency of 150 kHz have the amplitude of 100 mA. A measurement error of 0.25% means an error of 250 μ A. This will indicate a measured value between the value of 99.75 mA and 100.25 mA. The characterization curves for the DAQ analog input channels AI₀ to AI₄, has similar characteristics in the frequency range of 2 to 150 kHz for the voltage waveforms of the amplitude of 6.00 V. The characterization curves for the DAQ analog input channels AI₀ to AI₄, has varying characteristics in the frequency range of 2 to 150 kHz for the voltage waveforms of the amplitude of 0.02 V. The error values of the analog input channels varies from the value of $\pm 0.25\%$ for the DAQ. The waveform platform uncertainty budget with respect to factors, such as the FFT windowing, noise, and cable length are described below.

6.5.3 Waveform Uncertainty Budget

The uncertainty budget of the waveform platform is determined here. In addition, the influences of the factors, such as the FFT windows, noise, and cable length on the waveform platform are studied. All along these studies, the waveform was generated and acquired by the waveform platform. The uncertainty budget helps to determine the measurement accuracy performed using the waveform platform. The uncertainty budget procedure will ensure the traceability of the conducted tests.

Equipment Used

Table 30 lists the equipment used for the tests conducted to calculate the uncertainty of the various components of the waveform platform.

Table 30. Equipment used for characterization of waveform generator.

Designation	Model	Type	N° id
Computer	Dell	Precision 5520	LNE 1055082
Remote Control Module	NI	PXIe-8301	LNE 1020904
Voltage Generator	NI	PXIe-5413	LNE 1020904
Voltage Amplifier	N4L	LPA400	-
	SPS	6100 PAS 1000	-
Transconductance Amplifier	Clarke-Hess	8100	LNE 1008742
VT	Block	VB 3.2/50	-
Divider	Lab made	Resistive	-
2 nd Order Passive HPF	Lab made	RC	
Optoisolator	TTI	LTX-5510	-
Rogowski Coil	PEM	LFR 06/6	LNE 1020872
Rogowski Coil	PEM	LFR 03/3	LNE 1020906
1 st Order Passive HPF	Lab made	RC	-
Terminal Block	NI	TB-2706	LNE 1020904
DAQ	NI	PXIe-6124	LNE 1020904
PQ Analyzer	PSL	PQube 3	LNE 1020905

Procedure

The laboratory schema in Fig. 120 is used here. The short time stability of the waveform platform is calculated for the fundamental voltage waveform at the frequency of 50 Hz, superimposed with a supraharmonic voltage component at the frequency of 20 kHz. The procedure is as follows:

- the measurements are performed for 20 samples with the time period of 5 minutes;
- the measured values are recorded;
- the samples are recorded for 3 days;
- the repeatability of the tests is found by calculating the standard deviation of the 20 samples;
- the day vs day reproducibility of the tests is found by first calculating the mean of the first two test samples, and then calculating the standard deviation of the mean values;
- the stability of the tests is found by calculating the standard deviation between the calculation from 3 days of the test;
- the average daily drift is found by calculating the differences between the mean values in each test;
- the resolution is the smallest change in the measured waveform.

The measurement data and results are explained below.

Measured Data

Each measurement samples are acquired for the time period of 5 mins for the duration of 3 days.

The arithmetic mean and standard deviation of the measurement samples are calculated as given in (19) and (20).

$$\text{Arithmetic Mean, } \bar{y} = \frac{1}{n} \sum_{i=1}^{20} (y_i), \quad (19)$$

Where n is the number of samples and y_i is the sample values.

$$\text{Standard deviation, } \sigma = \sqrt{\frac{1}{n} \sum_{i=1}^{20} (y_i - \bar{y})^2}, \quad (20)$$

For day 1,

$\bar{y} = 230.00$, for the voltage waveform of the frequency of 50 Hz, and the amplitude of 230 V.

$\bar{y} = 2.62$, for the voltage waveform of the frequency of 20 kHz, and the amplitude of 2.60 V.

$\sigma = 6.11 \times 10^{-3}$, for the voltage waveform of the frequency of 50 Hz, and the amplitude of 230 V.

$\sigma = 2.56 \times 10^{-3}$, for the voltage waveform of the frequency of 20 kHz, and the amplitude of 2.60 V.

For day 2,

$\bar{y} = 229.99$, for the voltage waveform of the frequency of 50 Hz, and the amplitude of 230 V.

$\bar{y} = 2.62$, for the voltage waveform of the frequency of 20 kHz, and the amplitude of 2.60 V.

$\sigma = 6.17 \times 10^{-3}$, for the voltage waveform of the frequency of 50 Hz, and the amplitude of 230 V.

$\sigma = 2.56 \times 10^{-3}$, for the voltage waveform of the frequency of 20 kHz, and the amplitude of 2.60 V.

For day 3,

$\bar{y} = 229.99$, for the voltage waveform of the frequency of 50 Hz, and the amplitude of 230 V.

$\bar{y} = 2.62$, for the voltage waveform of the frequency of 20 kHz, and the amplitude of 2.60 V.

$\sigma = 6.17 \times 10^{-3}$, for the voltage waveform of the frequency of 50 Hz, and the amplitude of 230 V.

$\sigma = 2.56 \times 10^{-3}$, for the voltage waveform of the frequency of 20 kHz, and the amplitude of 2.60 V.

The uncertainty parameters, such as the repeatability, reproducibility, etc. are listed in Table 31.

Table 31. Parameters of waveform platform uncertainty.

Parameter	Fundamental at 50 Hz, 230 V	Supraharmonics at 20 kHz, 2.60 V
Repeatability	6.17×10^{-3}	2.56×10^{-3}
Reproducibility	4.60×10^{-3}	8.48×10^{-4}
Stability	6.42×10^{-3}	7.35×10^{-4}
Average Daily Drift	-6.50×10^{-3}	1.20×10^{-3}
Resolution	2.00×10^{-2}	1.00×10^{-2}

The effects of other parameters like the FFT windows, noise, and cable length are described below. The waveform characteristics for the different FFT windows like, Hanning, Hamming, etc. for the voltage waveform of the frequency of 50 Hz, and the amplitude of 6 V, superimposed step by step with the supraharmonic voltage waveforms of the frequency of 2, 20, and 150 kHz, and the amplitude of 0.12 V, is listed in Table 32.

Table 32. Waveform platform uncertainties from FFT windows.

Window	Fundamental at 50 Hz, 6 V		Supraharmonics at 2 kHz, 0.12 V	
	Amplitude	Error (%)	Amplitude	Error (%)
No Windows	6.00	-0.03	0.12	-0.03
Hanning	6.00	-0.04	0.12	-0.02
Hamming	6.00	-0.04	0.12	-0.03
Blackman-Harris	6.00	-0.04	0.12	-0.02
Exact Blackman	6.00	-0.04	0.12	-0.02
Blackman	6.00	-0.04	0.12	-0.02

Flat Top	6.00	-0.03	0.12	-0.01
4 Term B-Harris	6.00	-0.04	0.12	-0.03
7 Term B-Harris	6.00	-0.04	0.12	-0.02
Low Sidelobe	6.00	-0.04	0.12	-0.03
	Fundamental at 50 Hz, 6 V		Supraharmonics at 20 kHz, 0.12 V	
Window	Amplitude	Error (%)	Amplitude	Error (%)
No Windows	6.00	-0.03	0.12	-2.17
Hanning	6.00	-0.04	0.12	-0.81
Hamming	6.00	-0.04	0.12	-1.01
Blackman-Harris	6.00	-0.04	0.12	-0.64
Exact Blackman	6.00	-0.03	0.12	-0.65
Blackman	6.00	-0.04	0.12	-0.62
Flat Top	6.00	-0.03	0.12	0.08
4 Term B-Harris	6.00	-0.04	0.12	-0.45
7 Term B-Harris	6.00	-0.04	0.12	-0.25
Low Sidelobe	6.00	-0.04	0.12	-0.36
	Fundamental at 50 Hz, 6 V		Supraharmonics at 150 kHz, 0.12 V	
Window	Amplitude	Error (%)	Amplitude	Error (%)
No Windows	6.00	-0.03	0.12	-11.70
Hanning	6.00	-0.04	0.12	-4.69
Hamming	6.00	-0.04	0.12	-5.64
Blackman-Harris	6.00	-0.03	0.12	-3.75
Exact Blackman	6.00	-0.04	0.12	-3.66
Blackman	6.00	-0.04	0.12	-3.58
Flat Top	6.00	-0.04	0.12	-0.14
4 Term B-Harris	6.00	-0.04	0.12	-2.83
7 Term B-Harris	6.00	-0.04	0.12	-1.74
Low Sidelobe	6.00	-0.03	0.12	-2.32

As in Table 32, the error values are the lowest for the Flat Top windows while performing the FFT algorithm. Therefore, the Flat Top windows are used for the mathematical analysis using the FFT algorithm in the waveform platform. The effects of noise from 0 to 5% of the waveform amplitude, on the voltage fundamental waveform of the frequency of 50 Hz, and the amplitude of 6 V are shown in Fig. 128. These voltage waveforms are superimposed with the voltage waveforms of the frequency of 20 and 150 kHz, and the amplitude of 0.12 and 0.06 V.

From Fig. 128, the noise signals appear to have very low effect on the fundamental voltage waveform, whereas the effects on the supraharmonic components increase with the level of the noise. The effects of the noise on the supraharmonic components also increase with the frequency range of 2 to 150 kHz. The effects are more visible when the noise levels are up to 5% of the fundamental signal, which is not usually the case in real electrical network scenarios, where the noise signal ranges only upto few millivolts as seen from the network measurements.

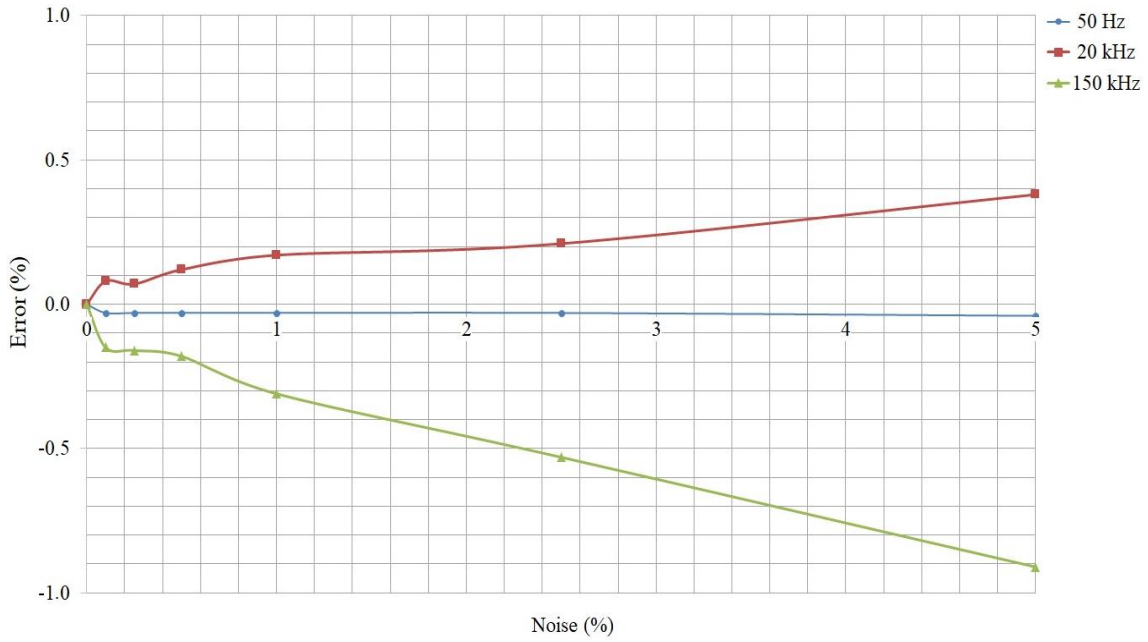


Fig. 128. Effects of noise on the waveform platform.

The effects of the cable length 0.25 and 1.00 m, for the voltage waveform of the frequencies of 0.05, 2.00, 20.00, and 150.00 kHz, and the amplitudes of 0.02, 3.50, and 6.00 V, on the waveform platform is listed in Table 33.

Table 33. Waveform platform uncertainty from cable length.

Length (m)	Voltage Waveform - 0.02 V							
	0.05 kHz	Error	2 kHz	Error	20 kHz	Error	150 kHz	Error
0.25	0.02	-0.11	0.02	-0.12	0.02	-0.09	0.02	0.17
1.00	0.02	-0.12	0.02	-0.13	0.02	-0.10	0.02	0.15
Length (m)	Voltage Waveform - 3.50 V							
	0.05 kHz	Error	2 kHz	Error	20 kHz	Error	150 kHz	Error
0.25	3.50	-0.11	3.50	-0.11	3.50	-0.11	3.49	0.12
1.00	3.50	-0.11	3.50	-0.12	3.50	-0.12	3.49	0.12
Length (m)	Voltage Waveform - 6.00 V							
	0.05 kHz	Error	2 kHz	Error	20 kHz	Error	150 kHz	Error
0.25	6.00	-0.10	6.00	-0.11	6.00	-0.10	5.99	0.13
1.00	6.00	-0.11	6.00	-0.12	6.01	-0.11	5.99	0.12

The cable length has a very low effect on the waveform platform uncertainty for the voltage waveform in the frequency range of 0.05 to 150 kHz, and in the amplitude range of 0.02 to 6.00 V. The uncertainty error for the cable length of 0.25 m has a maximum variation of $\pm 0.17\%$ for the voltage waveform of the frequency of 150 kHz, and the amplitude of 0.02 V, whereas the uncertainty error for the cable length of 1.00 m has a maximum variation of $\pm 0.15\%$ for the voltage waveform of the frequency of 150 kHz, and the amplitude of 0.02 V. Table 34 to Table 39 lists the performance of the various components of the waveform platform, such as the VT with the divider, the HPF, the optoisolator, the Rogowski coils etc. as given below.

Table 34. Waveform Generator + DAQ performance.

Amplitude (V)	Frequency (kHz)							
	0.05		2.00		20.00		150.00	
	Relative Stability	Error (%)						
0.02	1.24×10^{-5}	0.12	1.26×10^{-5}	0.12	1.28×10^{-5}	0.11	1.28×10^{-5}	-0.15
3.50	5.08×10^{-5}	0.11	5.41×10^{-5}	0.11	5.69×10^{-5}	0.12	5.76×10^{-5}	-0.12
6.00	4.88×10^{-5}	0.11	4.56×10^{-5}	0.12	4.97×10^{-5}	0.11	4.60×10^{-5}	-0.13

Table 35. Waveform Generator + VT + Divider + DAQ performance.

Amplitude (V)	Frequency (kHz) - 0.05	
	Relative Stability	Error (%)
6.00	1.21×10^{-5}	-0.14
230.00	4.59×10^{-5}	-0.01

Table 36. Waveform Generator + HPF + DAQ performance.

Amplitude (V)	Frequency (kHz)					
	2 kHz		20 kHz		150 kHz	
	Relative Stability	Error (%)	Relative Stability	Error (%)	Relative Stability	Error (%)
0.02	5.18×10^{-5}	0.11	5.43×10^{-5}	-0.40	5.57×10^{-5}	-0.55
3.50	4.76×10^{-5}	0.14	4.94×10^{-5}	-0.31	4.53×10^{-5}	-0.44
6.00	4.49×10^{-5}	0.14	4.27×10^{-5}	-0.31	4.67×10^{-5}	-0.45

Table 37. Waveform Generator + Optoisolator + DAQ performance.

Amplitude (V)	Frequency (kHz)					
	2 kHz		20 kHz		150 kHz	
	Relative Stability	Error (%)	Relative Stability	Error (%)	Relative Stability	Error (%)
0.02	8.71×10^{-4}	0.26	1.22×10^{-3}	0.68	1.47×10^{-3}	-0.51
3.50	1.07×10^{-4}	-0.24	1.20×10^{-4}	-0.54	1.16×10^{-4}	-0.59

Table 38. Rogowski Coil LFR 06/6 performance with the conductor positioning.

Amplitude (A)	Frequency - 0.05 kHz			
	Conductor through the Centre		Conductor through the Edge	
	Relative Stability	Error (%)	Relative Stability	Error (%)
10	4.27×10^{-4}	-0.14	6.41×10^{-4}	0.15
5	4.48×10^{-4}	-0.15	6.71×10^{-4}	0.14

Table 39. Rogowski Coil CWT015 performance.

Amplitude (A)	Frequency (kHz)					
	2 kHz		20 kHz		150 kHz	
	Relative Stability	Error (%)	Relative Stability	Error (%)	Relative Stability	Error (%)
1	3.89×10^{-4}	0.33	4.31×10^{-3}	-0.34	3.75×10^{-3}	0.57

The error values in percentage of different components used in the waveform platform are listed above. Table 40 lists the uncertainty budget [106] for each channel of the waveform platform. The uncertainties of the various measurement channels for voltage and current waveforms are calculated as in (18). The factors that influence uncertainty are as follows:

$$(\delta_{Ch})^2 = (\delta_W)^2 + (\delta_N)^2 + (\delta_L)^2 + (\delta_S)^2,$$

$$(\delta_{Ch}) = ((\delta_W)^2 + (\delta_N)^2 + (\delta_L)^2 + (\delta_S)^2)^{\frac{1}{2}}, \quad (18)$$

where,

- δ_{Ch} is the total uncertainty of the measurement channel;
- δ_W is the value of the FFT windowing;
- δ_N is the value of the noise signals;
- δ_L is the value of the cable length;
- δ_{AI0} , δ_{AI1} , δ_{AI2} , and δ_{AI3} are the values of the DAQ analog input channels;
- δ_S is the value of the sensors from the waveform platform channels;
 - δ_{S1} is the value of the VT with the divider and the DAQ from Ch₁;
 - δ_{HPF} is the value of the 2nd order HPF with the DAQ from Ch₂;
 - δ_O is the value of the optoisolator with the DAQ from Ch₂;
 - δ_{S1} is the value of the 2nd order HPF with the optoisolator and the DAQ from Ch₂;
 - δ_{S3} is the value of the LFR 06/6 with the DAQ from Ch₃;
 - δ_{S4} is the value of the LFR 03/3 with the DAQ from Ch₄.

The uncertainty values are calculated for 3 parameters as follows:

- time, where the measurement samples are recorded over a period of time;
- amplitudes, where the measurements are recorded for the different voltage and current amplitudes depending the channel used;
- frequency, where the measurements are performed in the frequency range of 2 to 150 kHz for the Ch₂ used for the supraharmonic voltage measurement, and the Ch₄ used for the supraharmonic current measurement. For the Ch₁ used for the fundamental voltage measurement, and the Ch₃ used for the fundamental current measurement, the measurements are performed at the frequency of 50 Hz.

The methodology uses:

- the relative standard uncertainty;
- the normal A probability distribution, which is calculated from the standard deviation of the measured values;
- the sensitivity coefficient of 1.

Table 40. Waveform platform uncertainty budget [106].

Channel 1 - Fundamental Voltage - 50 Hz			
Source	Time	Amplitude	
FFT Windowing (δ_w)	4.40×10^{-5}		
Noise Level (δ_N)	5.56×10^{-5}	6.03×10^{-5}	
Cable Length (δ_L)	4.67×10^{-5}	7.66×10^{-5}	
DAQ AI ₀ (δ_{AI0})	4.88×10^{-5}	7.26×10^{-5}	
VT + Divider + DAQ AI ₀ (δ_{S1})	4.59×10^{-5}	9.13×10^{-4}	
Combined Standard Uncertainty	9.65×10^{-5}	9.19×10^{-4}	
Channel 2 - Supraharmonic Voltage - 2 to 150 kHz			
Source	Time	Amplitude	Frequency
FFT Windowing (δ_w)	5.25×10^{-5}	8.46×10^{-4}	1.12×10^{-3}
Noise Level (δ_N)	8.07×10^{-4}	4.19×10^{-4}	3.53×10^{-3}
Cable Length (δ_L)	5.01×10^{-5}	2.60×10^{-4}	1.59×10^{-3}
DAQ AI ₁ (δ_{AI1})	1.28×10^{-4}	1.74×10^{-4}	1.55×10^{-3}
2 nd order HPF + DAQ AI ₁ (δ_{HPF})	5.57×10^{-5}	5.73×10^{-4}	3.46×10^{-3}
Optoisolator + DAQ AI ₁ (δ_O)	1.47×10^{-3}	6.06×10^{-4}	5.99×10^{-3}
2 nd order HPF + Optoisolator + DAQ AI ₁ (δ_{S2})	1.47×10^{-3}	8.21×10^{-4}	6.74×10^{-3}
Combined Standard Uncertainty	1.68×10^{-3}	1.28×10^{-3}	7.85×10^{-3}
Channel 3 - Fundamental Current - 50 Hz			
Source	Time	Amplitude	
FFT Windowing (δ_w)	4.40×10^{-5}		
Noise Level (δ_N)	5.56×10^{-5}	6.03×10^{-5}	
Cable Length (δ_L)	4.67×10^{-5}	7.66×10^{-5}	
DAQ AI ₂ (δ_{AI2})	4.88×10^{-5}	7.26×10^{-5}	
LFR 06/6 + DAQ AI ₂ (δ_{S3})	4.27×10^{-4}	8.24×10^{-5}	
Combined Standard Uncertainty	4.35×10^{-4}	1.35×10^{-4}	
Channel 4 - Supraharmonic Current - 2 to 150 kHz			
Source	Time	Amplitude	Frequency
FFT Windowing (δ_w)	5.25×10^{-5}	8.46×10^{-4}	1.12×10^{-3}
Noise Level (δ_N)	8.07×10^{-4}	4.19×10^{-4}	3.53×10^{-3}
Cable Length (δ_L)	4.64×10^{-5}	2.60×10^{-4}	1.59×10^{-3}
DAQ AI ₃ (δ_{AI3})	1.28×10^{-4}	1.74×10^{-4}	1.55×10^{-3}
LFR 03/3 + 1 st order HPF + DAQ AI ₃ (δ_{S4})	4.31×10^{-4}	8.94×10^{-3}	4.73×10^{-3}
Combined Standard Uncertainty	9.18×10^{-4}	8.99×10^{-3}	6.21×10^{-3}

The parameters of the calculation are described above. The uncertainties from the channels Ch₁ and Ch₃ with respect to the time and amplitude, and the channels Ch₂ and Ch₃ with respect to the time, amplitude, and frequency are listed here. The waveform platform is designed for the laboratory characterization of commercial PQAs in the frequency range of 2 to 150 kHz and this is discussed below.

6.5.4 Power Quality Analyzer Characterization

The main objective is to characterize the commercial PQAs, such as the PQube 3 in the frequency range of 2 to 150 kHz for the voltage waveforms using the developed waveform platform. The PQube 3 is an indicative device for conducted emissions in the frequency range of 2 to 150 kHz and is designed according to IEC 61000-4-30 [72].

Equipment used

The equipment used for the characterization of commercial PQA in the frequency range of 2 to 150 kHz using the waveform platform are given in Table 41.

Table 41. Equipment used for characterization of waveform generator.

Designation	Model	Type	N° id
Computer	Dell	Precision 5520	LNE 1055082
Remote Control	NI	PXIe-8301	LNE 1020904
Voltage Generator	NI	PXIe-5413	LNE 1020904
Voltage Amplifier	N4L	LPA400	-
	SPS	6100 PAS 1000	-
VT	Block	VB 3.2/50	-
Divider	Lab made	Resistive	-
2 nd Order Passive HPF	Lab made	RC	-
DAQ	NI	PXIe-6124	LNE 1020904
Terminal Block	NI	TB-2706	LNE 1020904
PQA	PSL	PQube 3	LNE 1020905

Electrical Schema

The electrical schema for the characterization of the PQube 3 is shown in Fig. 129.

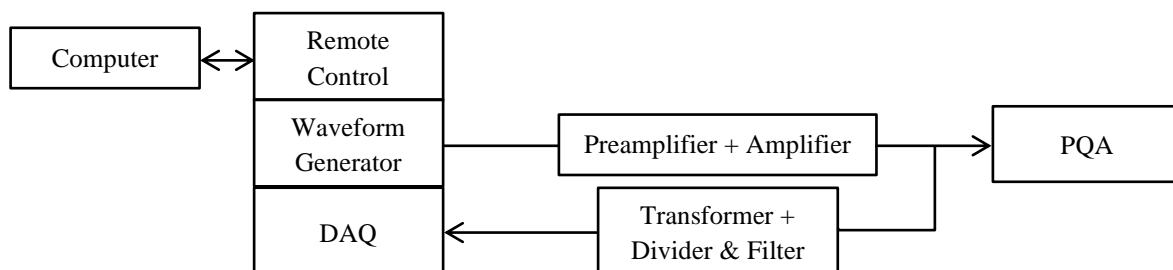


Fig. 129. Electrical schema for waveform generator characterization.

Measurement Parameters

Table 42 lists the test parameters, such as the sampling rate, frequencies, and amplitudes for the characterization of the PQube 3 in the frequency range of 2 to 150 kHz.

Table 42. PQube 3 measurement parameters.

Parameters	Level
Sampling Rate	512 samples per cycle

Fundamental Frequency	50 Hz
Voltage Amplitude	$L_1 - N$, 230 V
Supraharmonic Emissions	2 - 150 kHz
Voltage Amplitude	$L_1 - E$, ~ 2.30 V

Procedure

The test procedure for the characterization of the PQube 3 is as follows:

- the connections are made according to Fig. 129;
- the distorted waveforms with varying frequencies from the waveform generator are amplified using the preamplifier with the amplifier;
- the amplified voltage waveform is measured by the waveform platform and PQube 3;
- the waveform platform voltage sensor outputs are processed with the FFT algorithm using the flat top window;
- the processed value is converted to the real value after applying the characterization values obtained from section 3.2.2;
- the characterization curve is formed with respect to percentage error between the values from the waveform platform and PQube 3;
- the amplitude characterization is performed with varying amplitudes of the supraharmonic component at a frequency of 20 kHz.

The laboratory setup for the PQube 3 characterization in the frequency range of 2 to 150 kHz using the waveform platform is shown in Fig. 130.

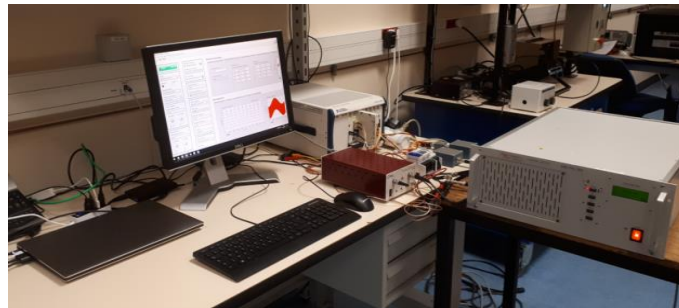


Fig. 130. Laboratory setup for waveform generator characterization.

The commercial PQA, PQube 3 used for the characterization tests is shown in Fig. 131.



Fig. 131. PQube 3 [107].

The PQube 3 has following characteristics [108]:

- auto-detect the mains frequency, configuration, and nominal voltage upto 690 V;
- measure and record the AC power disturbances, such as the flicker, supraharmonics, etc.;

- measure in real time and record the voltage emissions in the frequency range of 2 to 150 kHz;
- certified for the Class A PQ measurements according to IEC 61000-4-30 [72].

Measurement Results

The measurement results for the characterization of the PQube 3 in the frequency range of 2 to 150 kHz are discussed here. The characterization curve for the PQube 3 in percentage error with respect to the sample numbers at the frequency of 50 Hz is shown in Fig. 132. The error value varies from -0.0087 to 0.0121 % at the frequency of 50 Hz, which is an acceptable level of variation with respect to the class of the device and according to the manufacturer specifications [108].

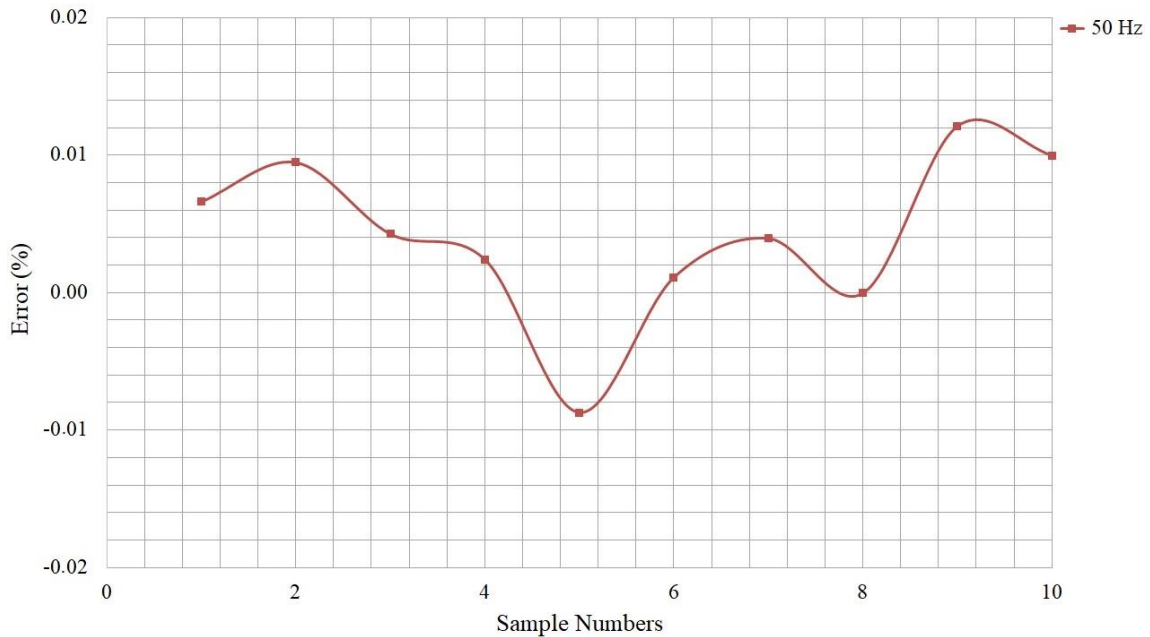


Fig. 132. Frequency characterization of PQube 3 at fundamental frequency.

The characterization curve for the PQube 3 in the percentage error with respect to the frequency in the frequency range of 2 to 150 kHz is shown in Fig. 133. The error value varies from -5.97 to 4.43 % at the frequency range of 2 to 150 kHz. The amplitude error values vary within $\pm 6.00\%$, when the supraharmonic component is 1% of the fundamental waveform, which is an acceptable level of variation according to the manufacturer specifications [108].

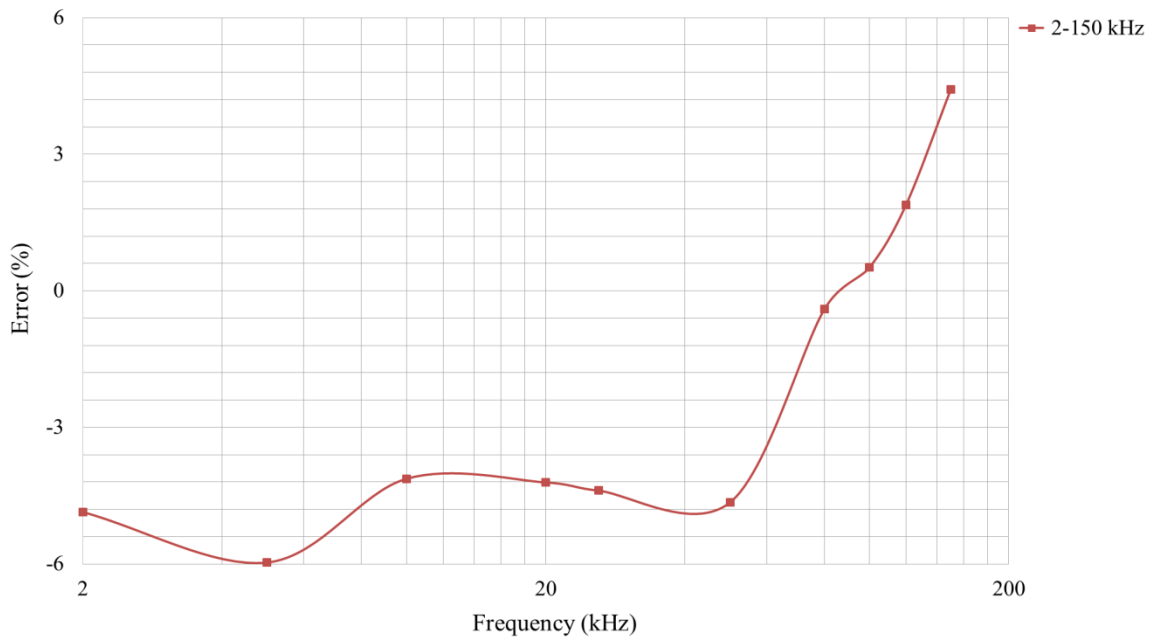


Fig. 133. Frequency characterization of PQube 3 at supraharmonic frequency.

The characterization curve for PQube 3 in the percentage error with respect to the sample number is shown in Fig. 134. The fundamental waveform of the frequency 50 Hz and the amplitude of 50 V are superimposed with a supraharmonic component of the frequency 20 kHz and varying amplitudes from 1 to 10% of the fundamental waveform. The percentage error values of the supraharmonic component tend to decrease with increase in the amplitude. The error values of the fundamental waveform vary from -0.30 to -0.27% at the frequency of 50 Hz and the amplitude of 50 V.

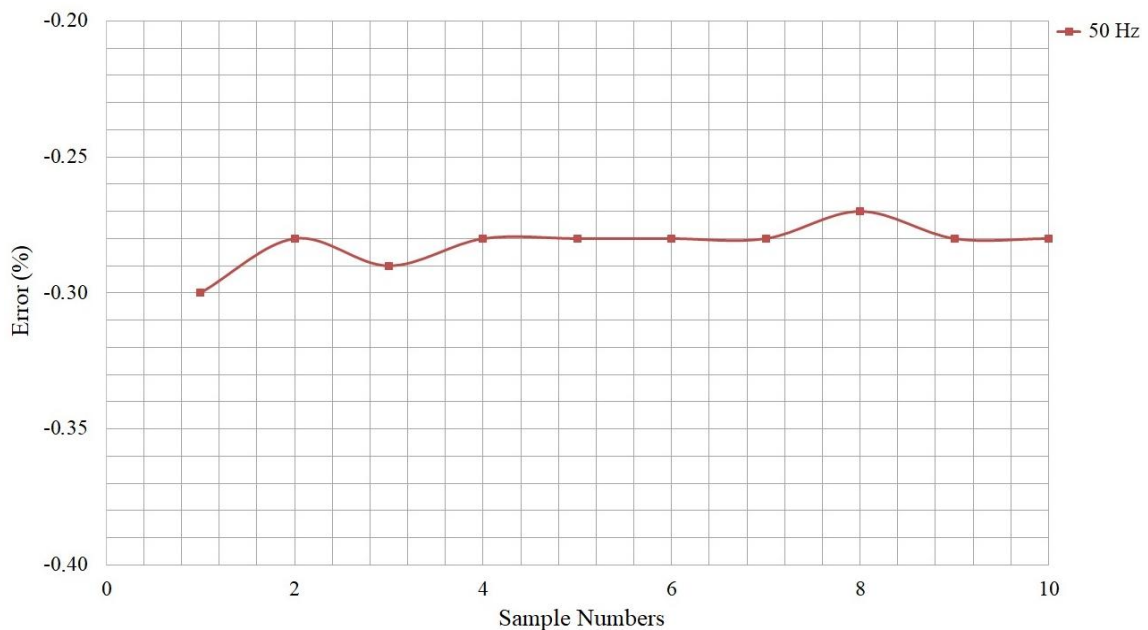


Fig. 134. Amplitude characterization of PQube 3 at fundamental frequency.

The percentage error remains linear for the fundamental waveform at the frequency of 50 Hz and the amplitude of 50 V. The characterization curve for the PQube 3 in the percentage error with respect to the amplitude at the frequency of 20 kHz is shown in Fig. 135. The error values of the supraharmonic component vary from 4.64 to 6.13% at the amplitude of 1 to 10% of the fundamental waveform.

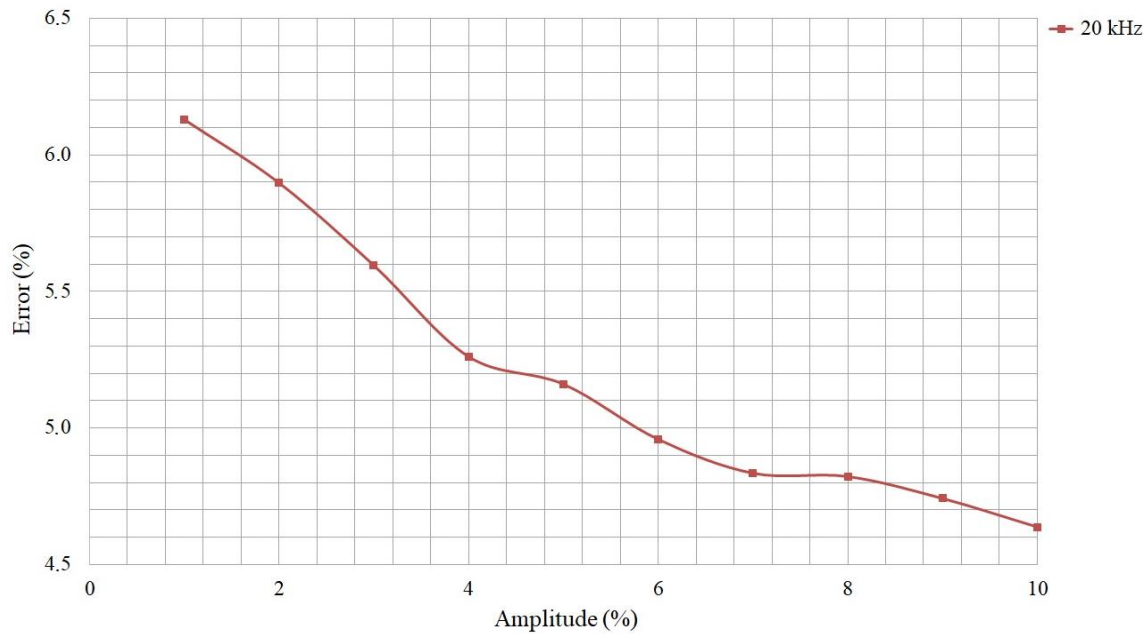


Fig. 135. Amplitude characterization of PQube 3 at supraharmic frequency.

Therefore, the PQube 3 is characterized in the frequency range of 2 to 150 kHz and for varying amplitudes for voltage waveforms. The PQA measure the current waveforms upto the amplitude order of 50, and is not capable of measuring supraharmic current emissions [107]. The variations of the PQube 3 while measuring the voltage emissions in the frequencies such as 23 kHz is shown in Fig. 14. Therefore, PQube 3 can be used as an indication device for the supraharmic voltage emissions in the frequency range of 2 to 150 kHz. Hence, the laboratory applications of the waveform platform are realized. The electrical network applications of the waveform platform are realized in section 5.4.3.

6.6 Summary

The waveform platform is designed for the generation and acquisition of the supraharmic emissions in the frequency range of 2 to 150 kHz. The chapter describes the software and hardware design of the waveform platform. The components, such as the waveform generator, DAQ, etc. used for the construction of the waveform platform are also listed here. The components are selected on the basis of the parameters, such as the bandwidth, sampling rate, etc. which are appropriate for the applications in the frequency range of 2 to 150 kHz. The waveform platform is designed as a generation and acquisition system for the laboratory applications, and as a stand-alone acquisition system for the electrical network applications. The existing generators in the market are designed according to the existing standards and are not equipped to perform multitasks, such as the generation and acquisition like the developed waveform platform.

The uncertainty budget of the waveform platform is calculated for the different parameters, such as cable length, noise, etc. The uncertainties are calculated separately for each of the 4 measurement channels of the waveform platform. The commercial PQA was characterized for voltage waveforms in the frequency range in the frequency range of 2 to 150 kHz. In addition, the PQA was characterized for the voltage waveforms for varying amplitudes of supraharmic emissions in the frequency range of 2 to 150 kHz. The PQA has a percentage error of $\pm 6.00\%$ for varying frequencies, and $\pm 6.13\%$ for varying amplitudes in the frequency range of 2 to 150 kHz. The error values are within the acceptable

levels of variation specified according to the manufacturer specifications. Therefore, the waveform platform can be used for the frequency and amplitude characterization of the PQAs in the frequency range of 2 to 150 kHz. The conclusions, which include the summary, contributions, and future work of the thesis are discussed in chapter 7.

CHAPTER 7
CONCLUSIONS

7 CONCLUSIONS

As discussed in the previous chapters, the supraharmmonic emissions in the frequency range of 2 to 150 kHz are on a rise in the smart grids due to the increasing integration of the power electronic converters, such as the PV panels and batteries, as well as the development of the PLC, e.g. for the smart metering. This chapter discusses the results of the thesis, reviews the contributions of the thesis, and lists the possible avenues for the future work.

7.1 Summary

The primary research area of the thesis is PQ in smart grids. It focuses on the quantification and reproduction of the supraharmmonic emissions in the frequency range of 2 to 150 kHz. In the end, the thesis deals with the objectives explained as follows. The PQ issues, which are present in the smart grids, are identified. From these studies, the supraharmmonic emissions in the frequency range of 2 to 150 kHz are identified as one of the significant PQ issues in smart grids. In addition, the measurement system that can be used for the supraharmmonic measurements and analysis in the electrical networks are designed and realized, since there are no commercial systems available that satisfy all the requirements, such as low uncertainty, wide bandwidth, non-invasive sensors, adapted resolution both for fundamental and supraharmonics components, etc. The topic of the supraharmmonic emissions in the frequency range of 2 to 150 kHz has been receiving interest from the scientific community getting interest since the year 2000. However, there are only few research groups studying this phenomenon and there are only few details concerning the existing measurement system. The electrical network tests are carried out in the Concept Grid platform that can create different smart grid configurations to study the individual effects and interactions between the parameters.

The waveform data acquired from the Concept Grid, EDF, is processed using the mathematical and statistical tools. The waveform data from the electrical network are processed using the FFT algorithm to quantify the emissions. The quantified waveform data is then analysed using the ANOVA to identify the individual effects and interactions between different parameters in the network that influence the supraharmmonic emissions in the frequency range of 2 to 150 kHz. These tools extract the emission patterns, and analyze the behavior of the electrical network parameters. The statistical analysis of the electrical network using ANOVA identified the PVI_I as the one of the major sources of supraharmmonic emissions. The analysis also identified the operation of the PVI_R as a filter to the PVI_I during the coupled operation. The design and realization of the complex waveform platform for the generation and acquisition of the supraharmmonic emissions in the frequency range of 2 to 150 kHz is based on the results from the measurement campaign 1. This phase included the electronic design and hardware construction of the waveform platform. The platform interface is developed using the LabVIEW software. The NI PXI system is used for the waveform generation and acquisition. The platform can create low voltage electrical network test scenario in the laboratory. It can also act as a stand-alone recording device for the electrical network measurements.

The development of the waveform platform for the generation and acquisition of the supraharmmonic emissions in the frequency range of 2 to 150 kHz is based on the electrical network measurements. The measurement campaign in the concept grid confirms the presence of the supraharmmonic emissions in the grid. The platform is used for the laboratory and electrical network applications. For the

laboratory applications, such as the characterization of the PQ analyzers, the platform is used for the waveform generation, measurement, and acquisition. For the electrical network applications, such as the measurement and acquisition of the supraharmic emissions in the frequency range of 2 to 150 kHz, the waveform platform is used exclusively as the waveform acquisition unit. In addition, the corresponding characterization procedure and uncertainty budget of the waveform platform considering different sources of uncertainty such as, the noise, cable length, etc. are developed. The commercial PQA is characterized for varying frequencies and amplitudes using the waveform platform. The drawbacks of the PQA, such as the measurement variation in the frequency range of 9 to 150 kHz are explained in the document.

The emission levels measured closer to the EuT is higher than the emission levels measured at a distance from the EuT. This is evident from the measurement results obtained from measurement campaign 2. During the network tests of the PVI, the EVC was added and removed from the network to study the effects on the functioning of the PVI. When the EVC was added to the PVI the corresponding measurements showed the peak emissions from the equipment. At frequencies, where both the equipment are in operation, there was a subsequent attenuation and cancelling out of the supraharmic emissions, e.g. the voltage emission peak close to 2 kHz. This emission was visible again once the EVC was removed from the electrical network. The higher frequency emissions close to 150 kHz are visible on the voltage waveforms during the network operations with the EVC. The higher level current peaks are visible in the frequency range of 2 to 100 kHz. In addition, the measurement campaigns indicate that the supraharmic emissions will attenuate with increase in the distance from the source of emissions. The contributions of the thesis are detailed below.

7.2 Contributions

The main contributions of the thesis are given below:

- the state of the art on the existing literature on the supraharmic emissions in the frequency range of 2 to 150 kHz;
- the 4-channel measurement system for the accurate and reproducible measurement of the voltage and current emissions in the supraharmic frequency range of 2 to 150 kHz;
- the thesis analyzes:
 - the primary and secondary emissions in the electrical network;
 - the effects of sudden connection and disconnection of load equipment in the network;
 - the effects of cable impedance on the propagation of supraharmic emissions;
 - the effects of the different parameters, such as the PVIs, residential equipment, etc. in the network;
- the cause-effect relationship between the different parameters, such as the PVIs, residential equipment, etc. in the network;
- the design and implementation of the waveform platform for the characterization of the commercial PQ instruments in the supraharmic frequency range of 2 to 150 kHz;
- the network measurements using the waveform platform;
- the recreation of the electrical network waveform in the laboratory using the waveform platform;
- the uncertainty budget for the waveform platform within the range of $\pm 1\%$ for all the measurement channels.

Overall, these contributions are expected to help in the future studies concerning the reliable measurement and characterization of supraharmonic emissions in the frequency range of 2 to 150 kHz. These contributions can contribute to further development of new standards in the field of supraharmonic emissions in the frequency range of 2 to 150 kHz. The thesis provides the real network emissions profiles and the laboratory methods for the characterization of these emissions. The possible avenues for future work are discussed below.

7.3 Future Work

The thesis has developed a reliable waveform platform with the uncertainty budget for the generation, measurement, and acquisition of the supraharmonic emissions in the frequency range of 2 to 150 Hz. The waveform platform can be used for the laboratory applications, such as the characterization of the commercial PQAs, and the electrical network applications, such as the measurement of the supraharmonic emissions. The future work could include the development of the voltage sensors with better linearity and isolation in the frequency range of 2 to 150 kHz. The sensors with better linearity will make the creation of the network signals in the laboratory more straightforward. In addition, further analysis of the data should be done on the effects of the various factors, such as the effects of the cable impedance on the propagation of the supraharmonic emissions. The existing PQAs, such as the PQube 3 do not measure the current emissions in the frequency range of 2 to 150 kHz. Once the commercial PQAs develop this possibility, the current channels can be characterized in the frequency range of 2 to 150 kHz using the waveform platform. The standards should be developed in order to incorporate the emission profiles in the electrical networks. The waveform platform should be kept up to date with changes and developments in the existing and possible new standards, which defines the measurement and testing in the supraharmonic frequency range of 2 to 150 kHz. As of now numerous national metrology institutes are realizing the importance of standardization of measurement and analysis of supraharmonic emissions in the electrical networks and are working on development of waveform platform. The waveform platform developed in the thesis can be used as the basis for the new developments in the field of supraharmonic emissions.

CHAPTER 8
REFERENCES

8 REFERENCES

- [1] “MEAN4SG - Metrology Excellence Academic Network for Smart Grids,” *H2020 - Marie Skłodowska-Curie ITN*. [Online]. Available: www.mean4sg-itn.eu. [Accessed: Sep. 25, 2018].
- [2] V. Giordano and G. Fulli, “A Business Case for Smart Grid Technologies: A Systemic Perspective,” *Energy Policy*, vol. 40, pp. 252-259, Jan. 2012.
- [3] “Sustainable Development,” *International Institute for Sustainable Development (IISD)*. [Online]. Available: www.iisd.org/topic/sustainable-development/. [Accessed: Feb. 08, 2019].
- [4] “Sustainable Development Goals - Sustainable Development Knowledge Platform.” *United Nations Department of Economic and Social Affairs (UNDESA)*. [Online]. Available: www.sustainabledevelopment.un.org. [Accessed: Apr. 03, 2019].
- [5] IEA, “Global Energy & CO₂ Status Report,” *International Energy Agency*, pp. 1-14, Mar. 2018.
- [6] N. Y. Amponsah, M. Troldborg, B. Kington, I. Aalders, and R. L. Hough, “Greenhouse Gas Emissions from Renewable Energy Sources: A Review of Lifecycle Considerations,” *Renewable and Sustainable Energy Reviews*, vol. 39, pp. 461-475, Nov. 2014.
- [7] R. Hledik, “How Green is the Smart Grid?” *The Electricity Journal*, vol. 22, no. 3, pp. 29-41. Apr. 2009.
- [8] “Vision and Strategy for Europe’s Electricity Networks of the Future,” *ETP Smart Grids*, pp. 4-33, Apr. 2006.
- [9] C. P. Vineetha and C. A. Babu, “Smart Grid Challenges, Issues and Solutions,” in *International Conference on Intelligent Green Building and Smart Grid (IGBSG)*, Taipei, Taiwan, 2014, pp. 1-4.
- [10] A. Zahedi, “Developing a System Model for Future Smart Grid,” in *IEEE PES Innovative Smart Grid Technologies (ISGT)*, Perth, Australia, 2011, pp. 1-5.
- [11] T. Atasoy, H. E. Akinç, and Ö. Erçin, “An Analysis on Smart Grid Applications and Grid Integration of Renewable Energy Systems in Smart Cities,” in *4th International Conference on Renewable Energy Research and Applications (ICRERA)*, Palermo, Italy, 2015, pp. 547-550.
- [12] “Distributed Generation,” *Virginia Tech*. [Online]. Available: www.dg.history.vt.edu. [Accessed: Apr. 19, 2019].
- [13] “Community Microgrid,” *Clean Coalition*. [Online]. Available: www.clean-coalition.org/community-microgrids/. [Accessed: Apr. 19, 2019].
- [14] J. V. H. Sanderson, “Whole System Approach to Future Power Operations Comprising a Majority of Distributed Generation,” in *IET Power in Unity: A Whole System Approach*, London, UK, 2013, pp. 1-5.
- [15] A. Esmailian and M. Kezunovic, “Prevention of Power Grid Blackouts using Intentional Islanding Scheme,” *IEEE Transactions on Industry Applications*, vol. 53, no. 1, pp. 622-629, Jan. 2017.
- [16] H. H. Zeineldin, K. Bhattacharya, E. F. El-Saadany, and M. M. A. Salama, “Impact of Intentional Islanding of Distributed Generation on Electricity Market Prices,” *IEEE Proceedings - Generation, Transmission and Distribution*, vol. 153, no. 2, pp. 147-154, Mar. 2006.
- [17] I. Kim and R. G. Harley, “A Study on the Intentional Island formed by the Residential Photovoltaic System and the Challenges to Island Operation,” in *North American Power Symposium (NAPS)*, Charlotte, USA, 2015, pp. 1-5.

- [18] G. P. Verbong, S. Beemsterboer, and F. Sengers, "Smart Grids or Smart Users? Involving Users in Developing a Low Carbon Electricity Economy," *Energy Policy*, vol. 52, pp. 117-125, Jan. 2013.
- [19] E. Zio and T. Aven, "Uncertainties in Smart Grids Behavior and Modeling: What are the Risks and Vulnerabilities? How to Analyze them?" *Energy Policy*, vol. 39, no. 10, pp. 6308-6320, Oct. 2011.
- [20] R. Fares, "Renewable Energy Intermittency Explained: Challenges, Solutions, and Opportunities," *Scientific American*. [Online]. Available: blogs.scientificamerican.com/plugged-in/renewable-energy-intermittency-explained-challenges-solutions-and-opportunities/. [Accessed: Mar. 16, 2017].
- [21] D. Amaripadath, "Effects of Diffuse Radiation to the Operation of Photovoltaic Power Plants," Master Thesis, Department of Electrical Engineering, Tampere University of Technology, Tampere, Finland, 2015.
- [22] S. S. Kaddah, K. M. Abo-Al-Ez, T. F. Megahed, and M. G. Osman, "Probabilistic Power Quality Indices for Electric Grids with Increased Penetration Level of Wind Power Generation," *International Journal of Electrical Power & Energy Systems*, vol. 77, pp. 50-58, May 2016.
- [23] S. Rönnerberg and M. Bollen, "Power Quality Issues in the Electric Power System of the Future," *The Electricity Journal*, vol. 29, no. 10, pp. 49-61, Dec. 2016.
- [24] O. P. Mahela and A. G. Shaik, "Topological Aspects of Power Quality Improvement Techniques: A Comprehensive Overview," *Renewable and Sustainable Energy Reviews*, vol. 58, pp. 1129-1142, May 2016.
- [25] "What are Voltage Sags, Dips, Swells and Transients?" *Fluke Corporation*. [Online]. Available: www.fluke.com/en-us/learn/best-practices/measurement-basics/power-quality/voltage-sags-dips-transients. [Accessed: Apr. 03, 2019].
- [26] M. Didden, "Voltage Sags in Continuous Processes - Case Study," *Copper Development Association*, pp. 1-8, Jun. 2003.
- [27] D. Chapman, "The Cost of Poor Power Quality," *Copper Development Association*, pp. 1-4, Mar. 2001.
- [28] Z. Hanzelka and A. Bien, "Voltage Disturbances: Flicker Measurement," *Copper Development Association*, pp. 1-8, Oct. 2005.
- [29] "What is Voltage and Current Unbalance?" *Fluke Corporation*. [Online]. Available: www.fluke.com/en-us/learn/best-practices/measurement-basics/power-quality/what-is-voltage-unbalance. [Accessed: Apr. 05, 2019].
- [30] P. V. S. Valois, C. M. V. Tahan, N. Kagan, and H. Arango, "Voltage Unbalance in Low Voltage Distribution Networks," in *16th International Conference and Exhibition on Electricity Distribution (CIRED)*, Amsterdam, The Netherlands, 2001, pp. 1-5.
- [31] "How to Find Harmonics in Electrical Systems," *Fluke Corporation*. [Online]. Available: www.fluke.com/en/learn/best-practices/measurement-basics/power-quality/how-to-find-harmonics-in-electrical-systems. [Accessed: Apr. 12, 2019].
- [32] S. Rönnerberg and M. Bollen, "Measurements of Primary and Secondary Emission in the Supraharmonic Frequency Range 2-150 kHz," in *23rd International Conference and Exhibition on Electricity Distribution (CIRED)*, Lyon, France, 2015, pp. 1-4.
- [33] C. Waniek, T. Wohlfahrt, J. M. Myrzik, J. Meyer, M. Klatt, and P. Schegner, "Supraharmonics: Root Causes and Interactions between Multiple Devices and the Low Voltage Grid," in *IEEE PES Innovative Smart Grid Technologies (ISGT)*, Torino, Italy, 2017, pp. 1-6.

- [34] Z. Hanzelka and A. Bien, "Harmonics: Interharmonics," *Copper Development Association*, pp. 1-10, Jul. 2004.
- [35] H. G. Beleiu, I. N. Beleiu, S. G. Pavel, and C. P. Darab, "Management of Power Quality Issues from an Economic Point of View," *Sustainability*, vol. 10, no. 7, pp. 1-16, Jul. 2018.
- [36] R. Targosz and J. Manson, "Cost of Poor Power Quality," in *Handbook of Power Quality*, New York, NY, USA: John Wiley & Sons, Ltd., 2008, pp. 545-592.
- [37] S. Elphick, P. Ciufo, V. Smith, and S. Perera, "Summary of the Economic Impacts of Power Quality on Consumers," in *Australasian Universities Power Engineering Conference (AUPEC)*, Wollongong, Australia, 2015, pp. 1-6.
- [38] R. S. Jangid, K. Parkh, and P. Anjana, "Reducing the Voltage Sag and Swell Problem in Distribution System Using Dynamic Voltage Restorer with PI Controller," *International Journal of Soft Computing and Engineering*, vol. 3, no. 6, pp. 193-202, Jan. 2014.
- [39] "Symmetrical Components," *Wikinow*. [Online]. Available: www.wikinow.co/topic/symmetrical-components. [Accessed: Apr. 29, 2019].
- [40] "Latest BS 7671 Wiring Regulations & Surge Protection." *Luckinslive*. [Online]. Available: www.luckinslive.com/product-news/fursesurgeprotection/. [Accessed: Apr. 29, 2019].
- [41] "What are Harmonics?" *Electricalfact*. [Online]. Available: www.electricalfact.com/2019/01/what-are-harmonics-how-generated. [Accessed: Apr. 30, 2019].
- [42] "Effects of Interharmonics Presence," *Emerich Power Quality Experts*. [Online]. Available: blog.emerich.in/2019/01/. [Accessed: Apr. 30, 2019].
- [43] S. Rönnberg and M. Bollen, "Propagation of Supraharmonics in the Low Voltage Grid", *Energiforsk*, rep. 461, pp. 10-50, Dec. 2017.
- [44] A. Larsson, "High Frequency Distortion in Power Grids due to Electronic Equipment," Licentiate Thesis, Department of Applied Physics and Mechanical Engineering, Luleå University of Technology, Luleå, Sweden, 2006.
- [45] M. Klatt, J. Meyer, P. Schegner, A. Koch, J. Myrzik, T. Darda, and G. Eberl, "Emission Levels Above 2 kHz - Laboratory Results and Survey Measurements in Public Low Voltage Grids," in *22nd International Conference and Exhibition on Electricity Distribution (CIRED)*, Stockholm, Sweden, 2013, pp. 1-4.
- [46] D. Amaripadath, R. Roche, L. Joseph-Auguste, D. Istrate, D. Fortuné, J. P. Braun, and F. Gao, "Design of Versatile Waveform Platform for Supraharmonic Testing and Calibration," in *25th International Conference and Exhibition on Electricity Distribution (CIRED)*, Madrid, Spain, 2019, pp. 1-4.
- [47] S. Rönnberg, M. Bollen, A. Larsson, and M. Lundmark, "An Overview of the Origin and Propagation of Supraharmonics (2-150 kHz)," in *Nordic Conference on Electricity Distribution System Management and Development (NORDAC)*, Stockholm, Sweden, 2014, pp. 1-12.
- [48] A. Novitskiy, S. Schlegel, and D. Westermann, "Analysis of Supraharmonic Propagation in a MV Electrical Network," in *19th International Scientific Conference on Electric Power Engineering (EPE)*, Brno, Czech Republic, 2018, pp. 1-6.
- [49] D. Agudelo-Martínez, M. Limas, A. Pavas, and J. Bacca, "Supraharmonic Bands Detection for Low Voltage Devices," in *17th International Conference on Harmonics and Quality of Power (ICHQP)*, Belo Horizonte, Brazil, 2016, pp. 1003-1009.
- [50] M. Rycroft, "Supraharmonics in Transmission and Distribution Networks," *EE Publishers*. [Online]. Available: www.ee.co.za/article/supraharmonics-transmission-distribution-networks. [Accessed: May 10, 2019].

- [51] S. Rönnberg, M. Bollen, H. Amaris, G. W. Chang, I. Y. Gu, Ł. H. Kocewiak, J. Meyer, M. Olofsson, P. F. Ribeiro, and J. Desmet, "On Waveform Distortion in the Frequency Range of 2 kHz-150kHz - Review and research challenges," *Electric Power Systems Research*, vol. 150, pp. 1-10, Sep. 2017.
- [52] M. Bollen and S. Rönnberg, "Primary and Secondary Harmonics Emission; Harmonic Interaction - a Set of Definitions," in *17th International Conference on Harmonics and Quality of Power (ICHQP)*, Belo Horizonte, Brazil, 2016, pp. 703-708.
- [53] S. Rönnberg, A. Larsson, M. Bollen, and J. Schanen, "A Simple Model for Interaction between Equipment at a Frequency of Some Tens of kHz," in *21st International Conference on Electricity Distribution (CIRED)*, Frankfurt, Germany, 2011, pp. 1-4.
- [54] S. Rönnberg, M. Wahlberg, M. Bollen, A. Larsson, and M. Lundmark, "Measurements of Interaction between Equipment in the Frequency Range 9 to 95 kHz," in *20th International Conference on Electricity Distribution (CIRED)*, Prague, Czech Republic, 2009, pp. 231-234 .
- [55] A. Larsson and M. Bollen, "Measurement Result from 1 to 48 Fluorescent Lamps in the Frequency Range 2 to 150 kHz," in *14th International Conference on Harmonics and Quality of Power (ICHQP)*, Bergamo, Italy, 2010, pp. 1-8.
- [56] S. Rönnberg, M. Bollen, and M. Wahlberg, "Interaction between Narrowband Power-Line Communication and End-User Equipment," *IEEE Transactions on Power Delivery*, vol. 26, no. 3, pp. 2034-2039, Jul. 2011.
- [57] K. Yang, M. Bollen, and A. Larsson, "Aggregation and Amplification of Wind-Turbine Harmonic Emission in a Wind Park," *IEEE Transactions on Power Delivery*, vol. 30, no. 2, pp. 791-799, 2014.
- [58] C. Unger, "Current Developments for the Reduction of Power Quality Related Disturbances in Industrial Installations," in *8th International Conference on Advances in Power System Control, Operation and Management (APSCOM)*, Hong Kong, China, 2009, pp. 1-5.
- [59] K. Temma, F. Ishiguro, N. Toki, I. Iyoda, J.J. Paserba, "Clarification and Measurements of High Frequency Harmonic Resonance by a Voltage Sourced Converter," *IEEE Transactions on Power Delivery*, vol. 20, no. 1, pp. 450-457, Jan. 2005.
- [60] C. Leroi and E. De Jaeger, "Conducted Disturbances in the Frequency range 2-150 kHz: Influence of the LV Distribution Grids," in *23rd International Conference on Electricity Distribution (CIRED)*, Lyon, France, 2015, pp. 1-5.
- [61] C. Unger, K. Krüger, M. Sonnenschein, and R. Zurowski, "Disturbances due to Voltage Distortion in the kHz Range - Experiences and Mitigation Measures," in *18th International Conference and Exhibition on Electricity Distribution (CIRED)*, Turin, Italy, 2005, pp. 1-4.
- [62] "Electromagnetic Interference between Electrical Equipment/Systems in the Frequency Range below 150 kHz," NSAI Standards, Dublin, Ireland, Tech. Report. CLC/TR 50627, Nov. 2015.
- [63] F. Zavoda, S. Rönnberg, M. Bollen, J. Meyer, and J. Desmet, "Power Quality and EMC Issues with Future Electricity Networks," in *23rd International Conference and Exhibition on Electricity Distribution (CIRED)*, Lyon, France, 2015, pp. 1-5.
- [64] G. Singh, E.R. Collins, S. Rönnberg, A. Larsson, and M. Bollen, "Impact of High Frequency Conducted Voltage Disturbances on LED Driver Circuits," in *IEEE Power & Energy Society General Meeting*, Chicago, IL, USA, 2017, pp. 1-5.
- [65] Power Sensors Limited, "Conducted Emissions in the 2kHz-150kHz Band Supra-harmonics," PQube 3 Application Note, ver. 3.0, Alameda, CA, USA.

- [66] Electromagnetic Compatibility (EMC) - Part 4-19: Testing and Measurement Techniques - Test for Immunity to Conducted, Differential Mode Disturbances and Signalling in the Frequency Range 2 kHz to 150 kHz at A.C. Power Ports, IEC 61000-4-19, 2014.
- [67] A. Moreno-Munoz, A. Gil-de-Castro, S. Rönnerberg, M. Bollen, and E. Romero-Cadval, "Ongoing Work in CIGRE Working Groups on Supraharmonics from Power-Electronic Converters," in *23rd International Conference and Exhibition on Electricity Distribution (CIRED)*, Lyon, France, 2015, pp. 1-5.
- [68] J. Rodriguez, L. G. Franquelo, S. Kouro, J. I. Leon, R. C. Portillo, M. A. M. Prats, and M. A. Perez, "Multilevel Converters: An Enabling Technology for High-Power Applications," *Proceedings of the IEEE*, vol. 97, no. 11, pp. 1786-1817, Nov. 2009.
- [69] M. Malinowski, K. Gopakumar, J. Rodriguez, and M. A. Perez, "A Survey on Cascaded Multilevel Inverters," *IEEE Transactions on Industrial Electronics*, vol. 57, no. 7, pp. 2197-2206, Jul. 2010.
- [70] R. N. Beres, X. Wang, F. Blaabjerg, M. Liserre, and C. L. Bak, "Optimal design of high-order passive-damped filters for grid-connected applications," *IEEE Transactions on Power Electronics*, vol. 31, no. 3, pp. 2083-2098, Mar. 2016.
- [71] Electromagnetic Compatibility (EMC) - Part 4-7: Testing and Measurement Techniques - General Guide on Harmonics and Interharmonics Measurements and Instrumentation, IEC 61000-4-7, 2003.
- [72] Electromagnetic Compatibility (EMC) - Part 4-30: Testing and Measurement Techniques - Power Quality Measurement Methods, IEC 61000-4-30, 2015.
- [73] M. Klatt, J. Meyer, and P. Schegner, "Comparison of Measurement Methods for the Frequency Range of 2 kHz to 150 kHz," in *16th International Conference on Harmonics and Quality of Power (ICHQP)*, Bucharest, Romania, 2014, pp. 818-822.
- [74] Electromagnetic Compatibility (EMC) - Part 2-2 Ed2 A2: Environment - Compatibility Levels for Low-Frequency Conducted Disturbances and Signalling in Public Low-Voltage Power Supply Systems, IEC 61000-2-2 Ed2 A2, 2018.
- [75] CISPR - Specification for Radio Disturbance and Immunity Measuring Apparatus and Methods - Part 2-1: Methods of Measurement of Disturbances and Immunity - Conducted Disturbance Measurements, CISPR 16-2-1, 2014.
- [76] A. Larsson, "On High-frequency Distortion in Low-voltage Power Systems," PhD Thesis, Department of Engineering Sciences and Mathematics, Luleå University of Technology, Luleå, Sweden, 2011.
- [77] S. Rönnerberg, "Emission and Interaction from Domestic Installations in the Low Voltage Electricity Network, up to 150 kHz," PhD Thesis, Department of Engineering Sciences and Mathematics, Luleå University of Technology, Luleå, Sweden, 2013.
- [78] *Datasheet 44123*, Myrra, Collégien, France, 2004.
- [79] *LFR Specification*, Power Electronics Measurements Ltd., Nottingham, UK, 2018.
- [80] *CWT Specification*, Power Electronics Measurements Ltd., Nottingham, UK, 2018.
- [81] *HRO 12-bit High Resolution Oscilloscopes*, Teledyne Lecroy, New York, USA, 2014.
- [82] *PCB Transformers*, Block, Verden, Germany, 2018.
- [83] *NI PXIe-6124 Specifications*, National Instruments, Texas, USA, 2008.
- [84] LTX-5510 Analog/Digital Fiber Optic Link, Terahertz Technologies Inc., New York, USA, 2018.

- [85] “Electricité de France,” *EDF*. [Online]. Available: www.edf.fr. [Accessed: Nov. 15, 2017].
- [86] “Préparer les Systèmes Électriques de Demain,” *EDF*. [Online]. Available: www.edf.fr/groupe-edf/premier-electricien-mondial/activites/recherche-et-developpement/nos-projets-phares/preparer-les-systemes-electriques-de-demain. [Accessed: Nov. 17, 2017].
- [87] B. Puluhen, “Concept Grid: Préparer Aujourd’hui les Systèmes Électriques de Demain,” *EDF*, Moret-sur-Loing, France, Apr. 2015.
- [88] B. Puluhen, L. Joseph-Auguste, S. Vilbois, T. Drizard, C. Lebosse, and G. Diquerreau, “Islanding Tests with Li-ion Storage System on the EDF Concept Grid,” in *International Conference and Exhibition on Electricity Distribution (CIRED) workshop*, Helsinki, Finland, 2016, pp. 1-4.
- [89] A. N. Mortensen and G.L. Johnson, “A Power System Digital Harmonic Analyzer,” *IEEE Transactions on Instrumentation and Measurements*, vol. 37, no. 4, pp. 537-540, Dec. 1988.
- [90] W. G. Cochran and G. M. Cox, *Experimental Designs*, 2nd ed., New York, NY, USA: John Wiley & Sons, Ltd., 1992, pp. 1-43.
- [91] D. C. Montgomery, *Design and Analysis of Experiments*, 7th ed., New York, NY, USA: John Wiley & Sons, 2008, pp. 12-13.
- [92] The Writing Studio, “Experimental and Quasi-experimental Research,” *Colorado State University*, [Online]. Available: www.writing.colostate.edu/guides/guide.cfm. [Accessed on Feb. 11, 2019].
- [93] S. Schöttke, J. Meyer, P. Schegner, and S. Bachmann, “Emission in the Frequency Range of 2 kHz to 150 kHz caused by Electrical Vehicle Charging,” in *IEEE International Symposium on Electromagnetic Compatibility (ISEMC-Europe)*, Gothenburg, Sweden, 2014, pp. 620-625.
- [94] D. Amaripadath, R. Roche, L. Joseph-Auguste, D. Istrate, D. Fortuné, J. P. Braun, and F. Gao, “Measurement of Supraharmonic Emissions (2 - 150 kHz) in Real Grid Scenarios,” in *Conference on Precision Electromagnetic Measurements (CPEM)*, Paris, France, 2018, pp. 1-2.
- [95] NI, “Understanding FFTs and Windowing,” *National Instruments*, pp. 1-15, May 2019.
- [96] G. Zwanenburg, H.C. Hoefsloot, J. A. Westerhuis, J. J. Jansen, and A. K. Smilde, “ANOVA - Principal Component Analysis and ANOVA - Simultaneous Component Analysis: A Comparison,” *Journal of Chemometrics*, vol. 25, no. 10, pp. 561-567, Jul. 2011.
- [97] Penn State University, “Stat 502: Analysis of Variance and Design of Experiments,” *Pennsylvania State Eberly College of Science*, [Online]. Available: www.onlinecourses.science.psu.edu/stat502/node/137. [Accessed on Apr. 15, 2018].
- [98] CEA, *Statistique Appliquée à l'Exploitation des Mesures*, 2nd ed., Paris, France: Masson, 1986, pp. 1-125.
- [99] “Build your own PXI System,” *NI*. [Online]. Available: ohm.ni.com/advisors/pxi/pages/common/intro. [Accessed: Mar. 23, 2018].
- [100] “Configuring PXI Systems using MXI-Express,” *NI*. [Online]. Available: www.ni.com/tutorial/4811/en/. [Accessed: Jan. 05, 2018].
- [101] *NI PXIe-1082 User Manual*, National Instruments, Texas, USA, 2016.
- [102] *User Manual PXIe-830*, National Instruments, Texas, USA, 2017.
- [103] *Specifications PXIe-5413*, National Instruments, Texas, USA, 2018.
- [104] “NI TB-2706 Direct Connectivity Terminal Block with Screw Terminals,” *NI*. [Online]. Available: sine.ni.com/nips/cds/view/p/lang/en/nid/201812. [Accessed: Jan. 11, 2018].

- [105] R. Hogan, “8 Sources of Uncertainty in Measurement for every Uncertainty Budget,” *Isobudgets*, [Online]. Available: www.isobudgets.com/8-sources-of-uncertainty-in-measurement-for-every-uncertainty-budget/. [Accessed on Jan. 16, 2019].
- [106] D. Istrate, D. Fortuné, A. Porée, and I. Blanc, “Measurement Traceability for High Impulse Currents up to 50 kA,” *Revue Française de Métrologie*, vol. 3, no. 39, pp. 15-28, Jun. 2015.
- [107] “PQube 3”, *PSL*, [Online]. Available: www.powerstandards.com/product/pqube-3/highlights/. [Accessed on Jul. 31, 2019].
- [108] *PQube 3 Power Analyzer*, Power Standards Lab, California, USA, 2018.

APPENDIX A
MEASUREMENT CAMPAIGN 1
MATHEMATICAL ANALYSIS RESULTS

APPENDIX A

The individual measurements of the network equipment with respect to the measurement points listed in Table 13 as discussed earlier and are shown here with the acquired and processed sensor output waveforms in time and frequency domain. The measurement and analysis process is described in section 4.2 and 5.3.

Industrial PV Inverter A Waveforms Measurement Point MP₂

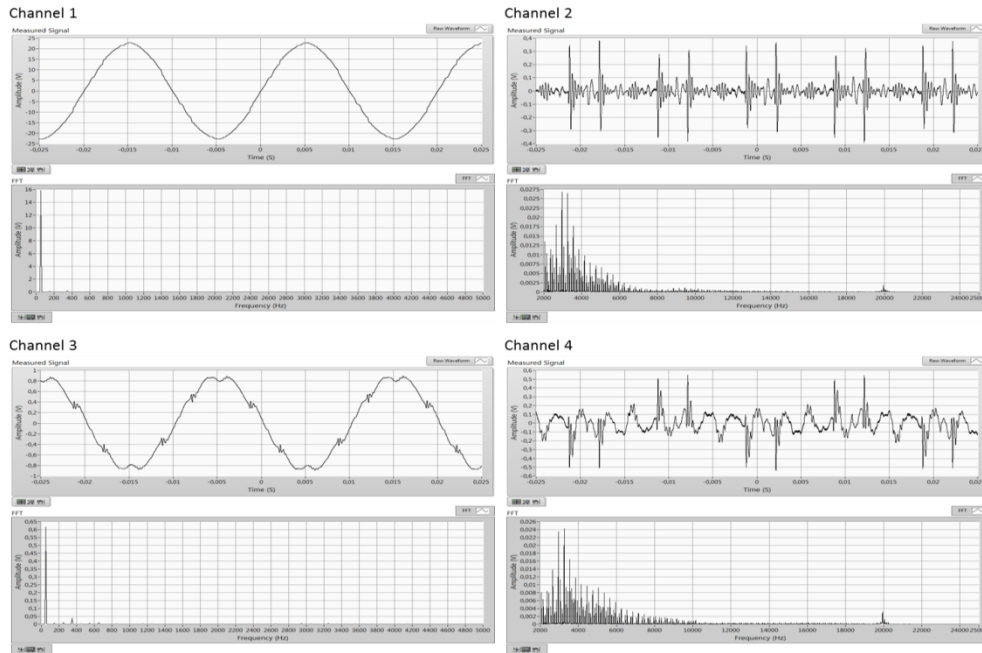


Fig. A.1. Acquired and processed waveforms.

Waveforms for Measurement Point MP₇

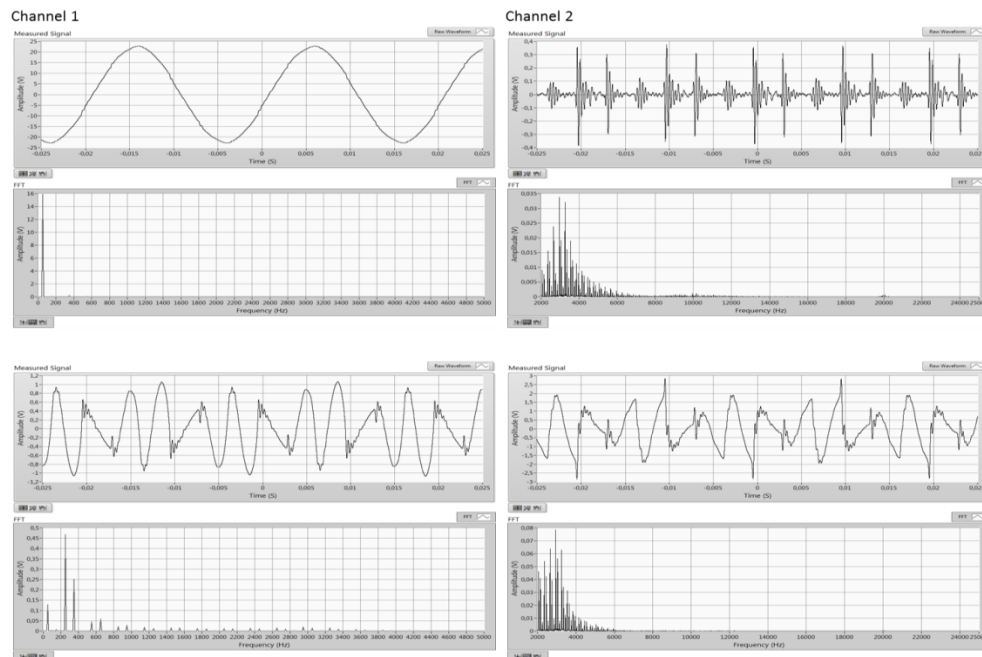


Fig. A.2. Acquired and processed waveforms.

Waveforms for Measurement Point MP₈

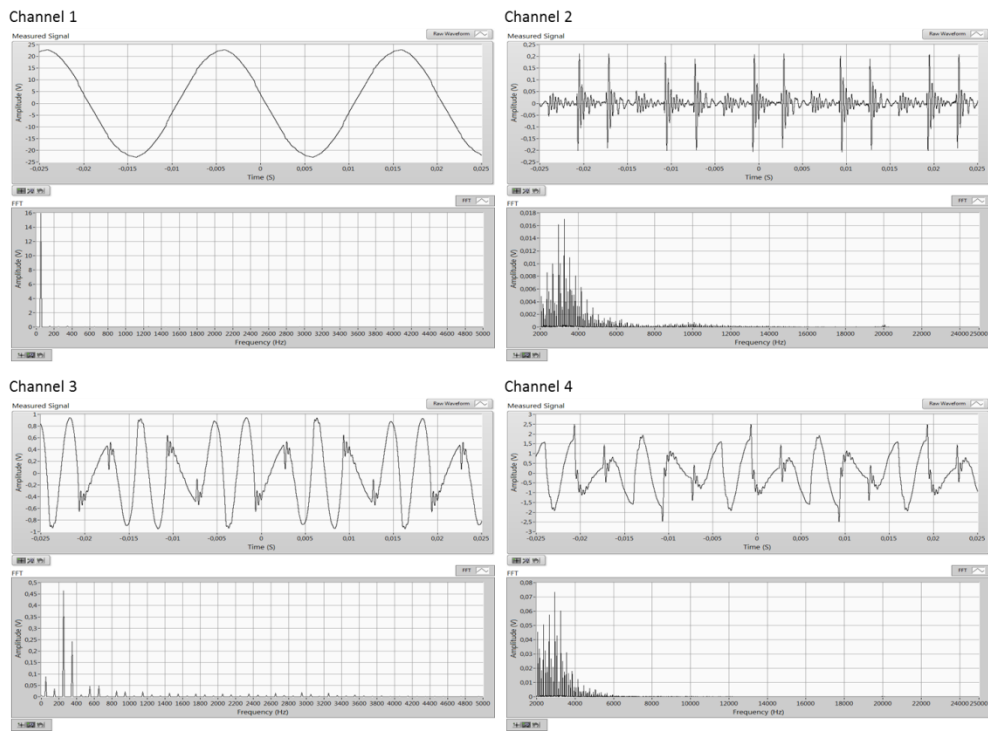


Fig. A.3. Acquired and processed waveforms.

Industrial PV Inverter B

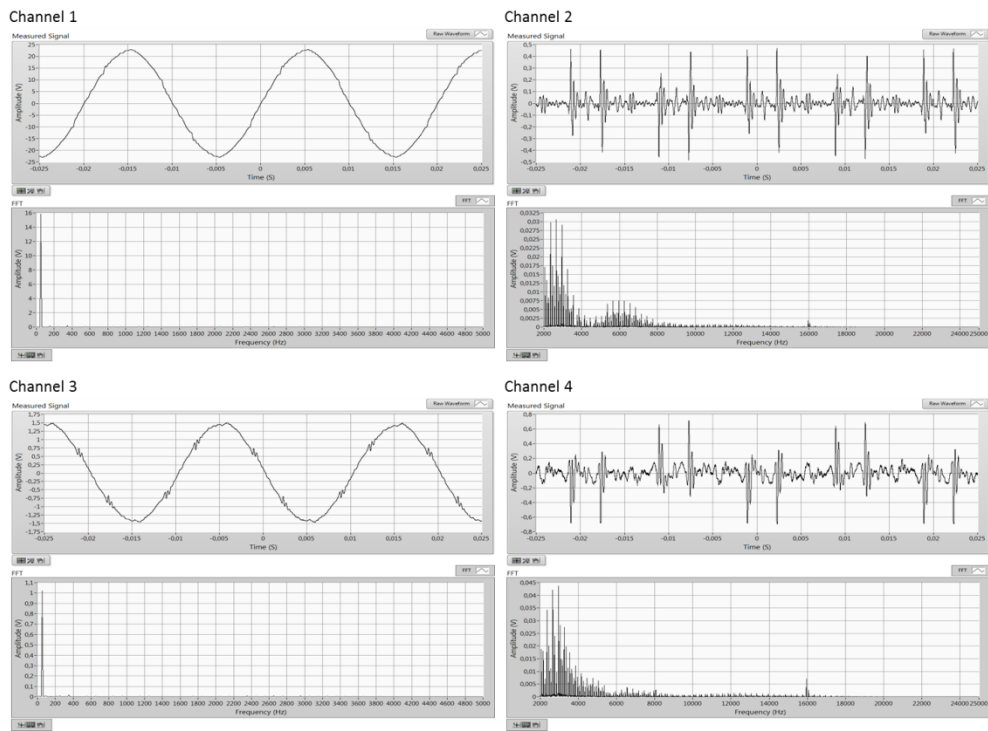


Fig. A.4. Acquired and processed waveforms.

Industrial PV Inverter C

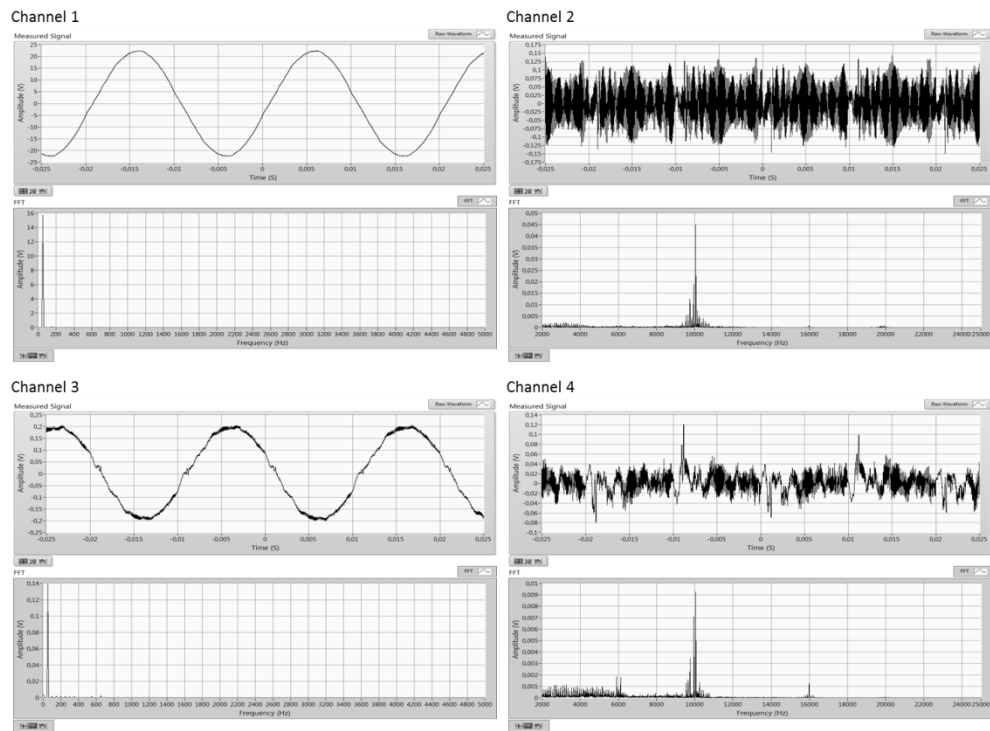


Fig. A.5. Acquired and processed waveforms.

Residential PV Inverter A

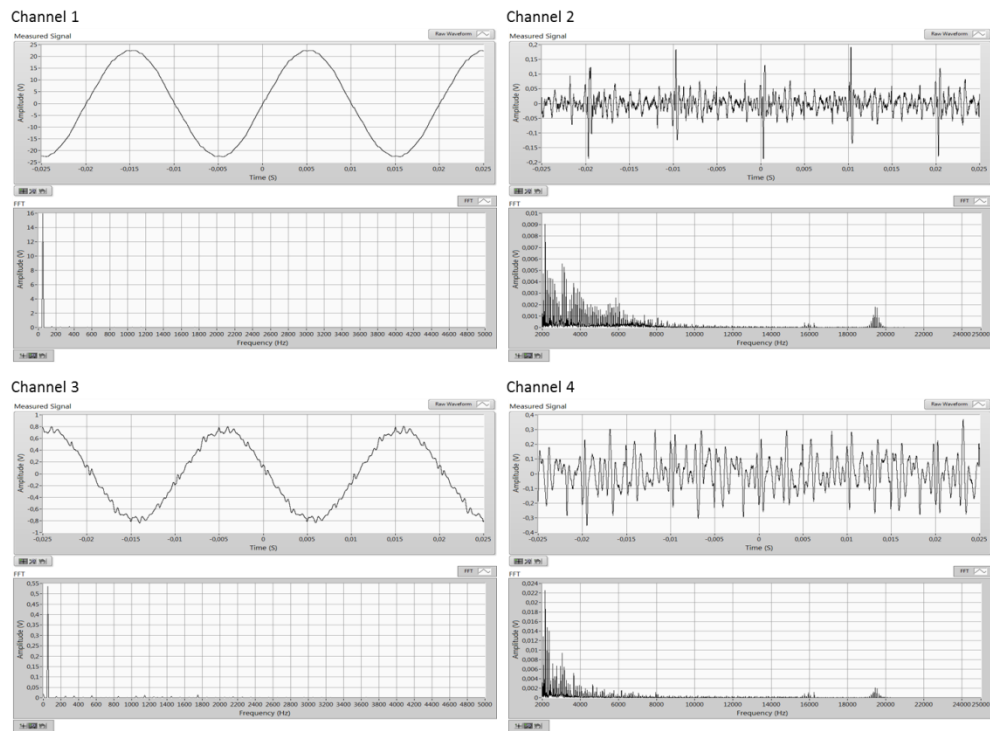


Fig. A.6. Acquired and processed waveforms.

Residential PV Inverter B

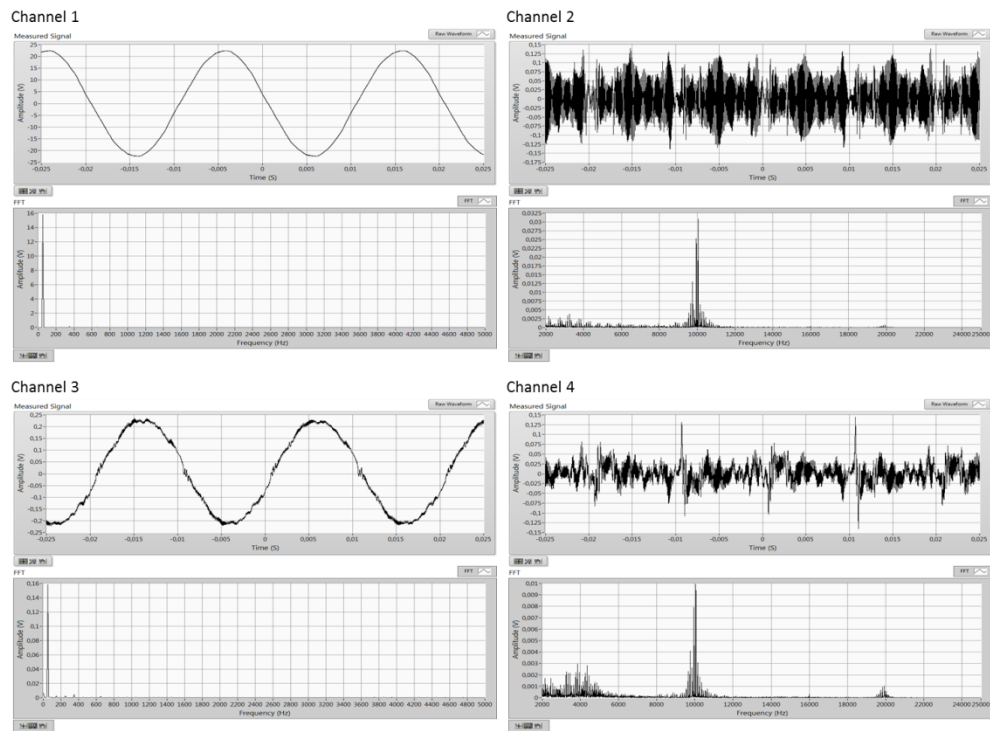


Fig. A.7. Acquired and processed waveforms.

Residential PV Inverter C

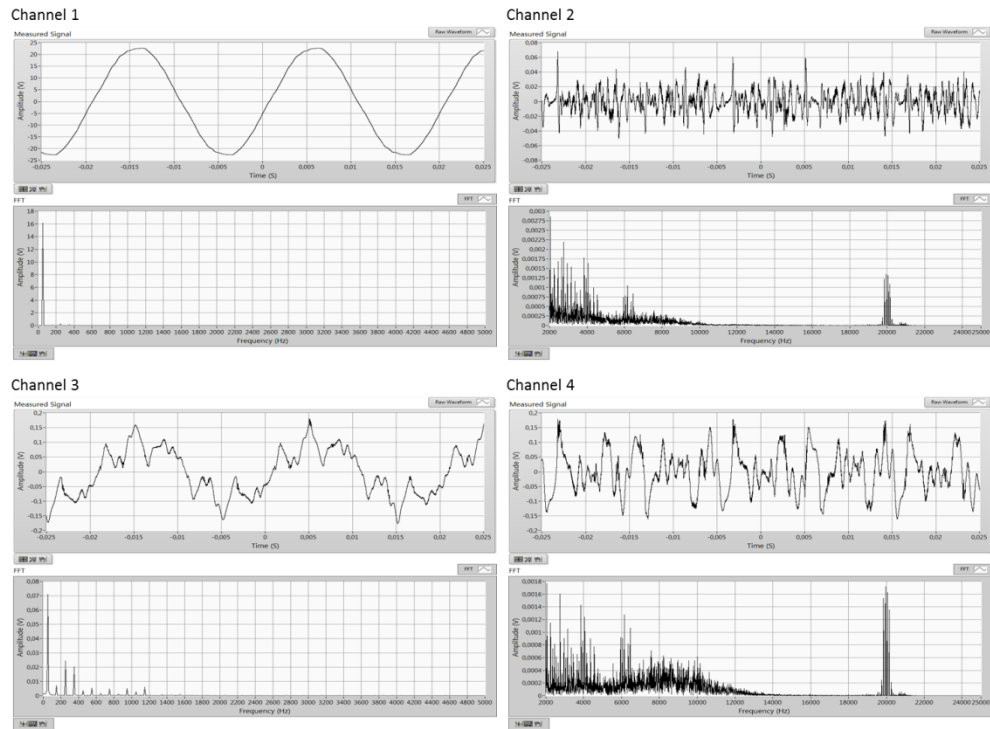


Fig. A.8. Acquired and processed waveforms.

Fast Charging EV Charger

Waveforms from Measurement Point MP₆

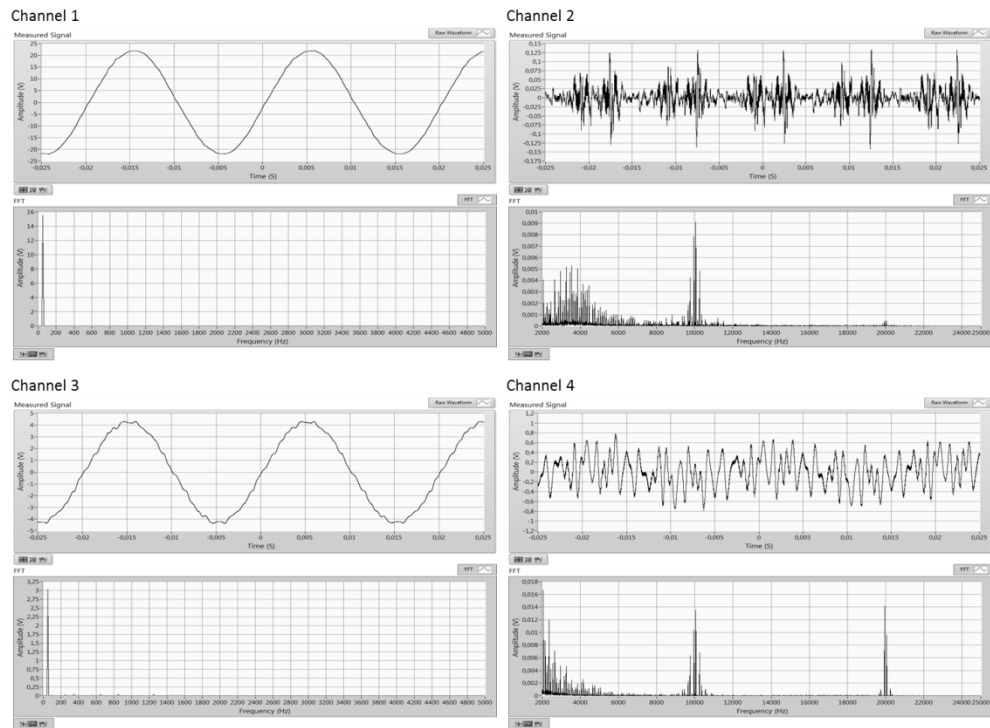


Fig. A.9. Acquired and processed waveforms.

Waveforms from Measurement Point MP₇

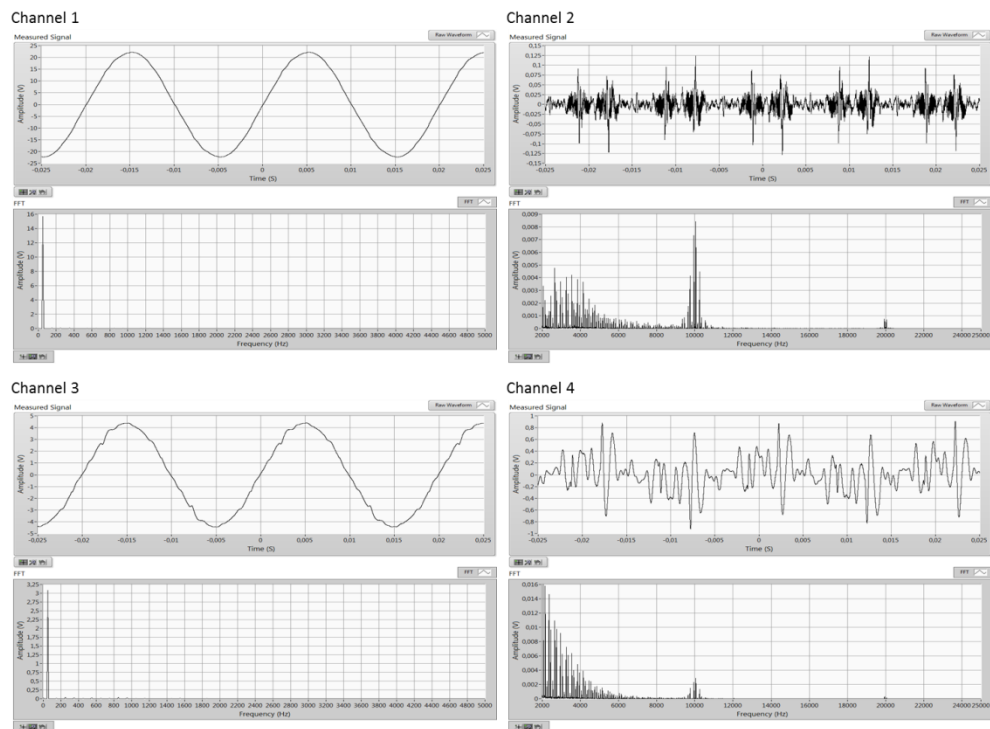


Fig. A.10. Acquired and processed waveforms.

Slow Charging EV Charger A

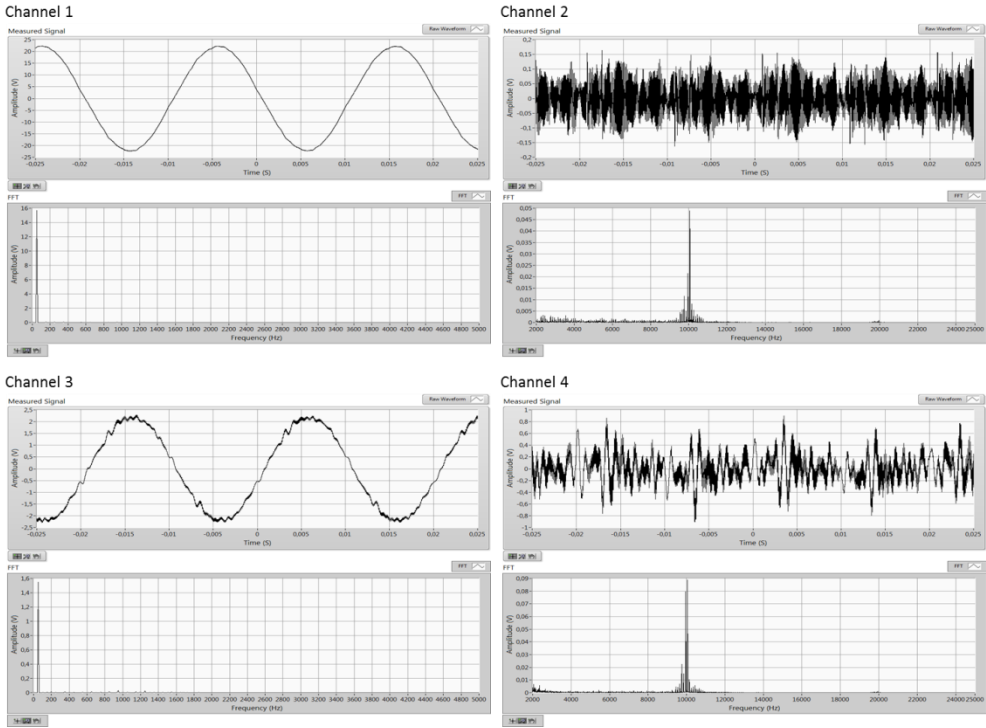


Fig. A.11. Acquired and processed waveforms.

Slow Charging EV Charger B

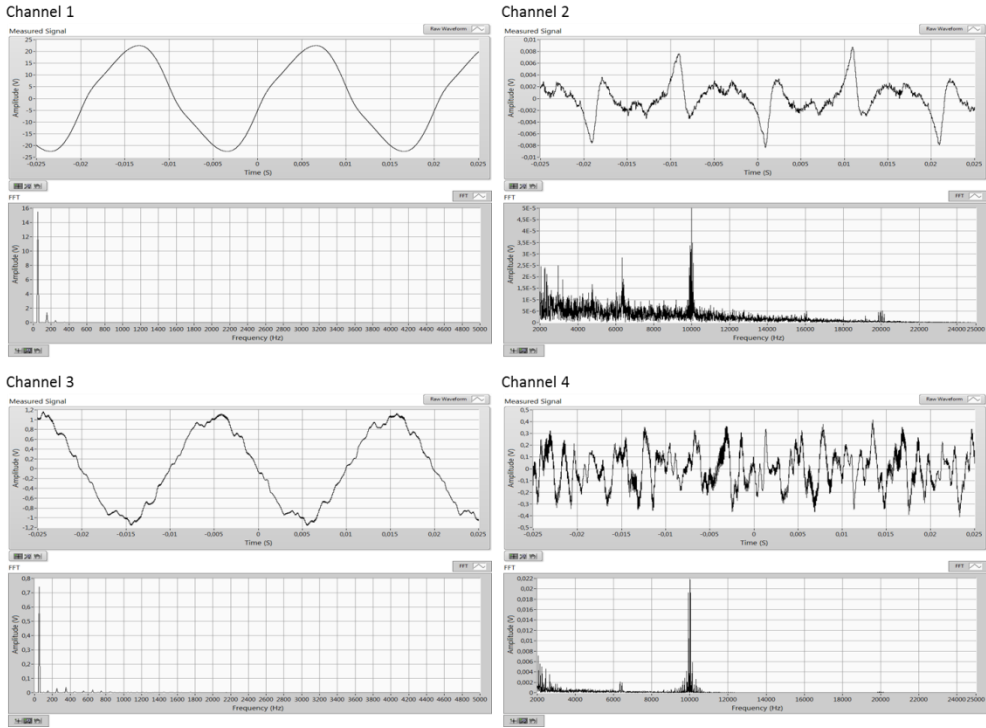


Fig. A.12. Acquired and processed waveforms.

Slow Charging EV Charger C

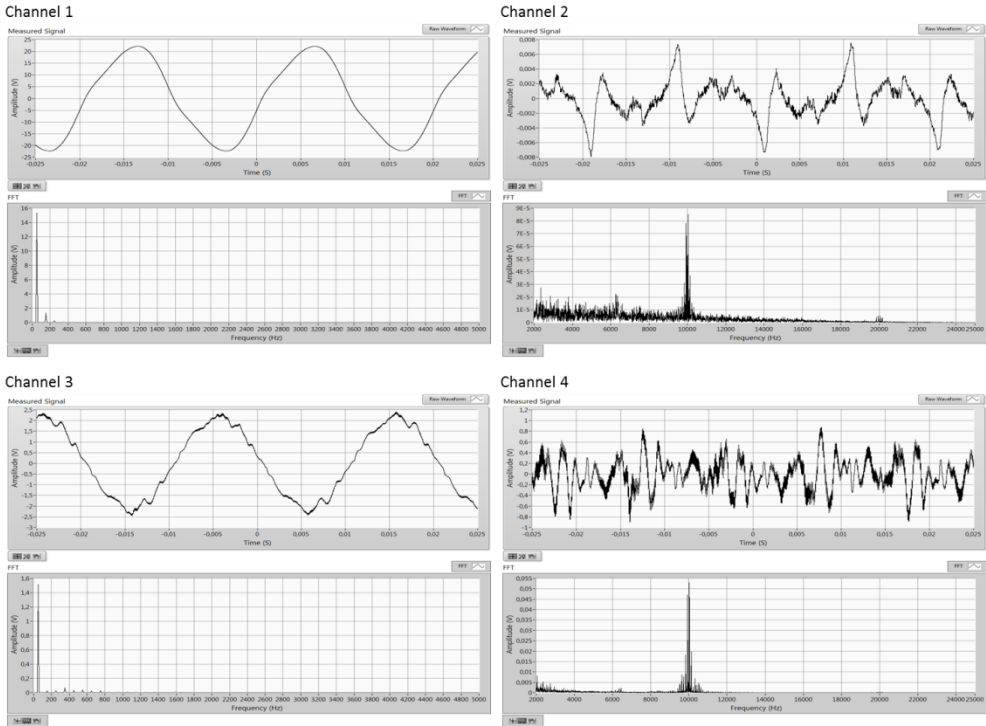


Fig. A.13. Acquired and processed waveforms.

Wind Turbine

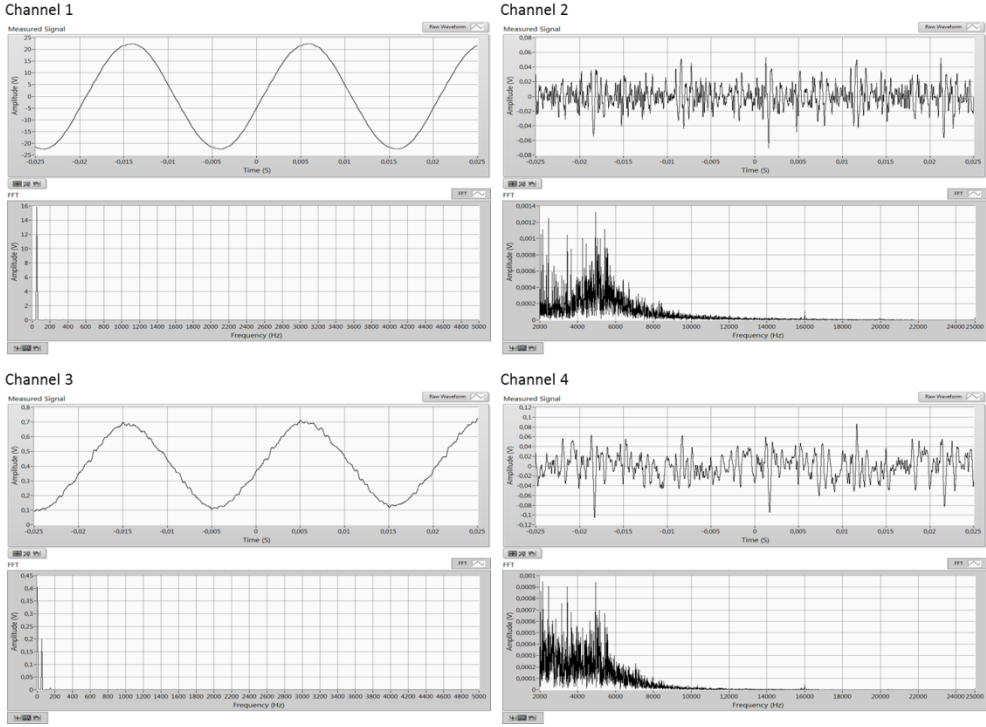


Fig. A.14. Acquired and processed waveforms.

Heat Pump A

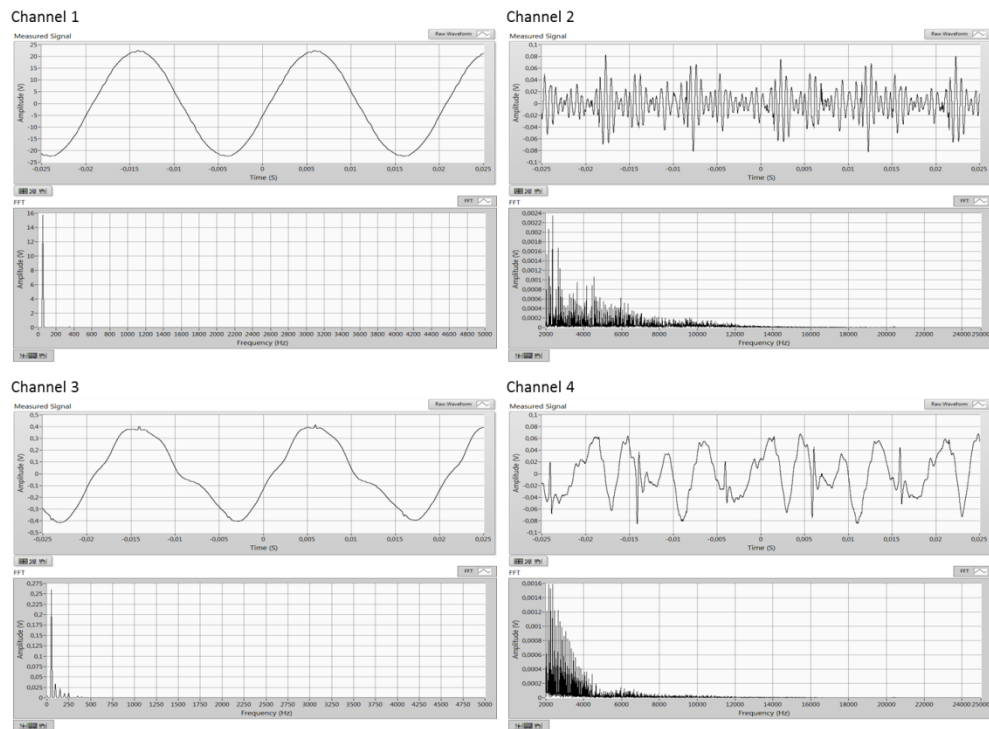


Fig. A.15. Acquired and processed waveforms.

Heat Pump B

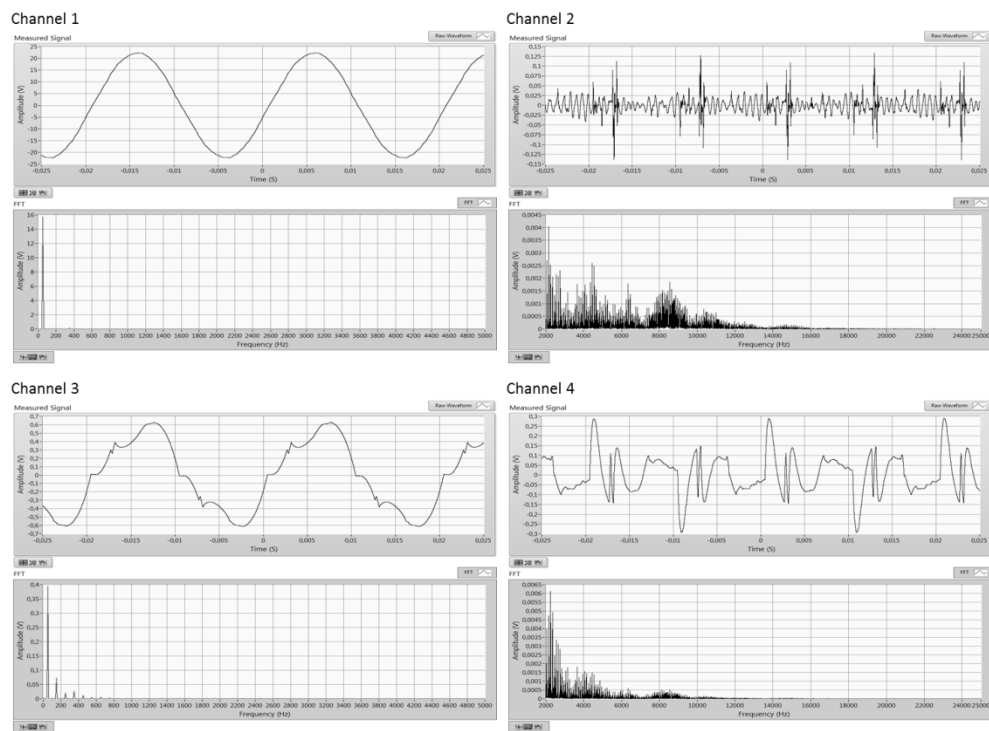


Fig. A.16. Acquired and processed waveforms.

Heat Pump C

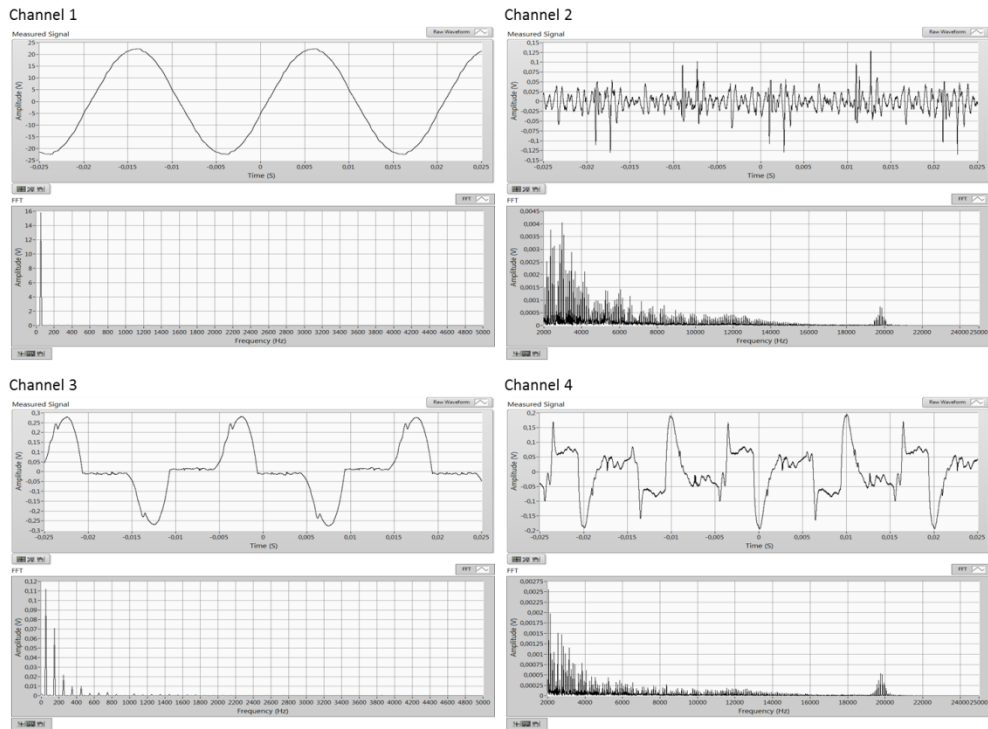


Fig. A.17. Acquired and processed waveforms.

Alternator

Waveforms for Input Side for 10 kW

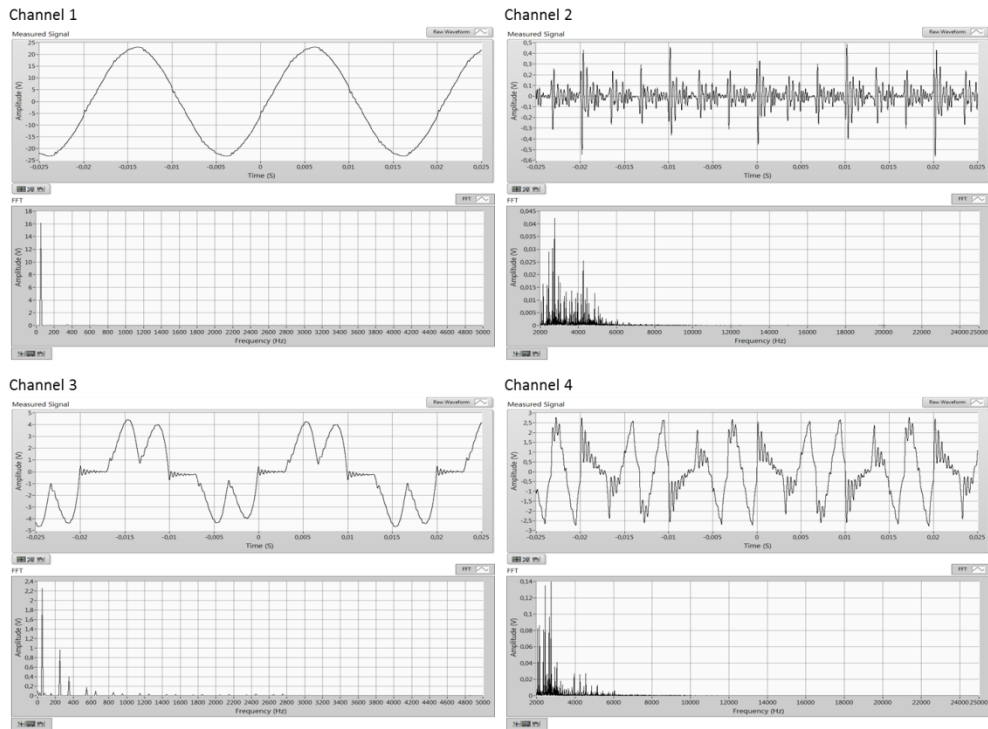


Fig. A.18. Acquired and processed waveforms.

Waveforms for Output Side for 5 kW

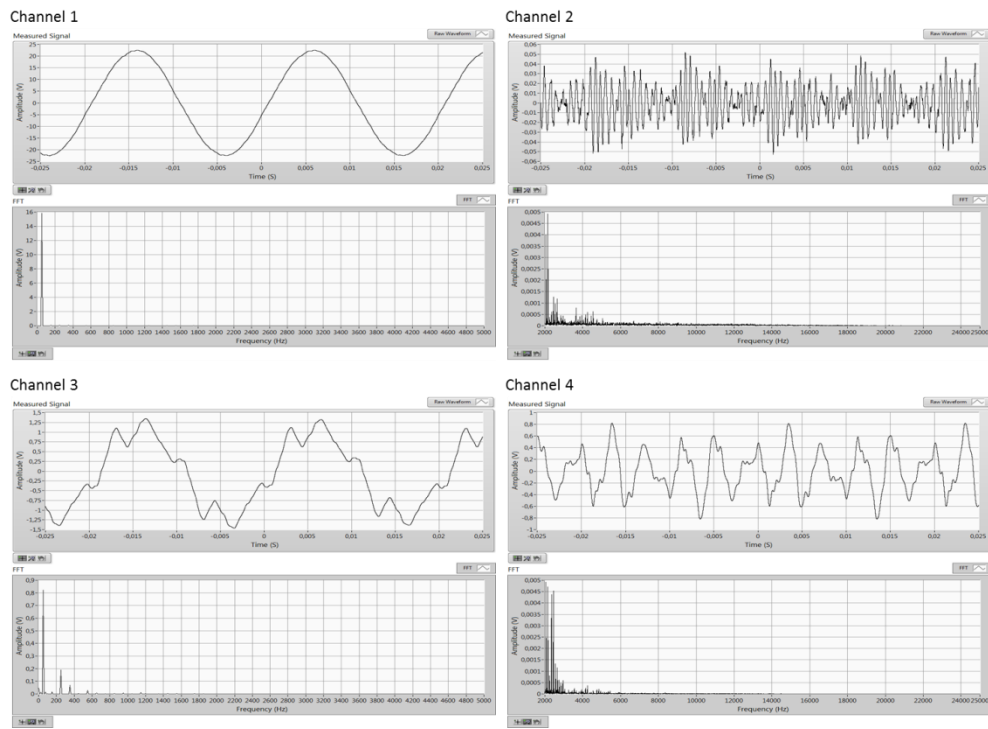


Fig. A.19. Acquired and processed waveforms.

Waveforms for Output Side for 10 kW

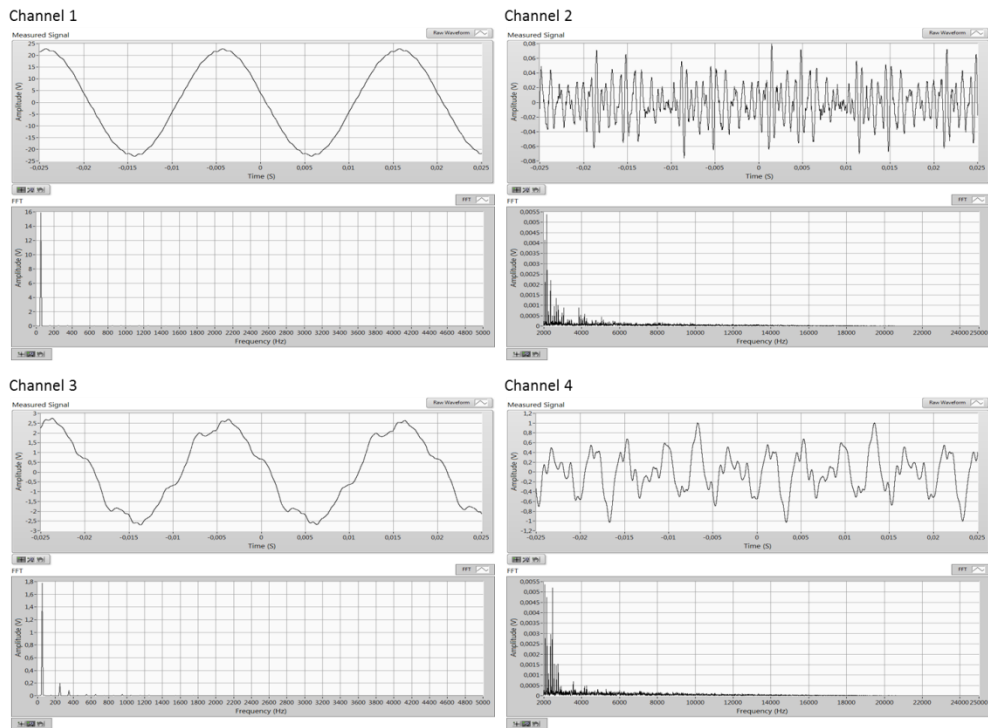


Fig. A.20. Acquired and processed waveforms.

Battery Storage

Waveforms for Active Power Generation

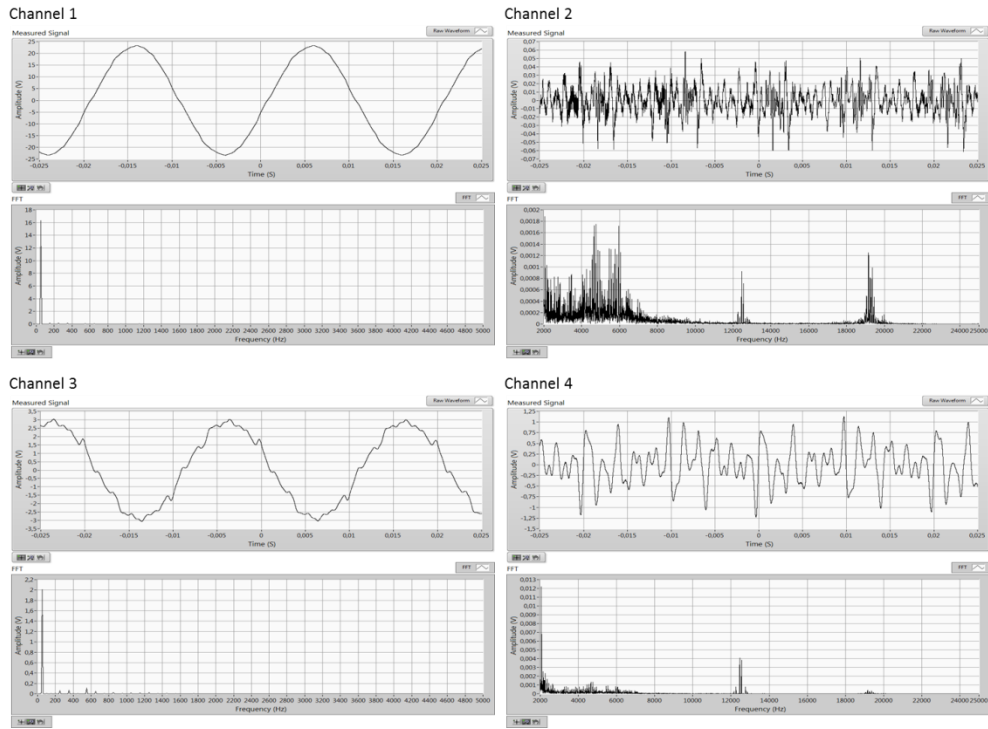


Fig. A.21. Acquired and processed waveforms.

Waveforms for Active Power Consumption

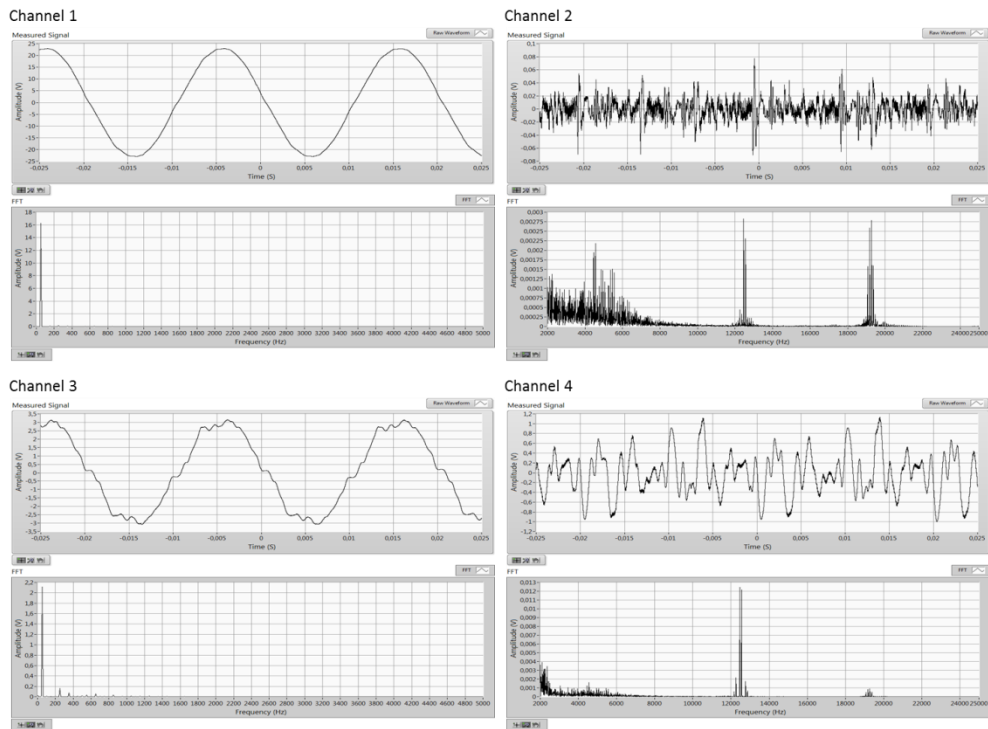


Fig. A.22. Acquired and processed waveforms.

Waveforms for Reactive Power Generation

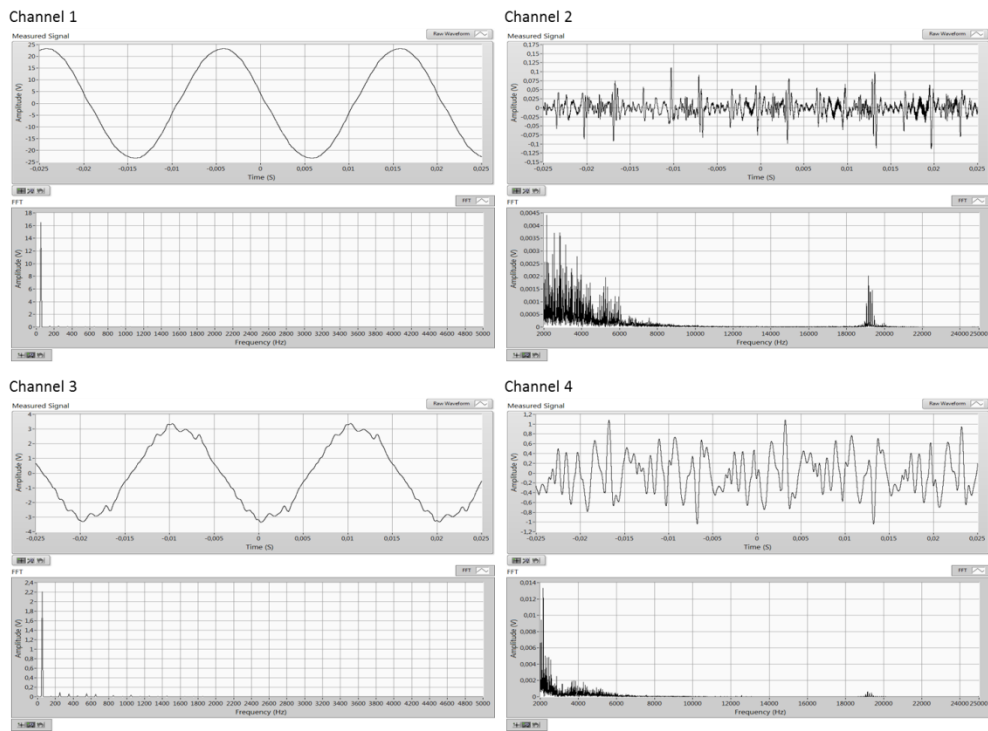


Fig. A.23. Acquired and processed waveforms.

Waveforms for Reactive Power Consumption

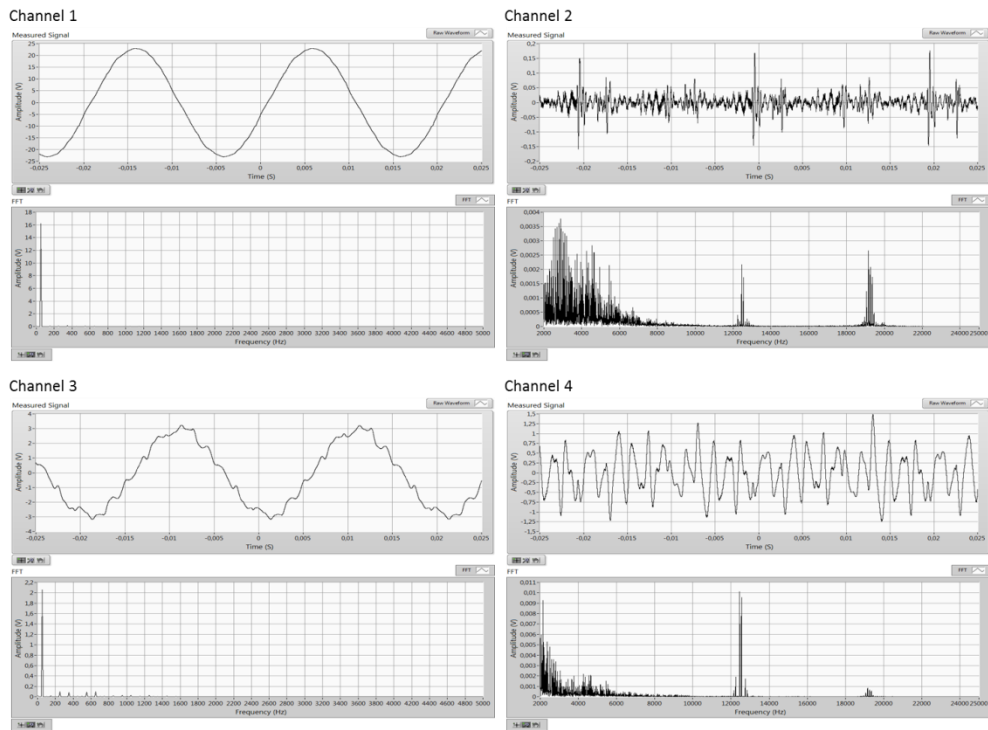


Fig. A.24. Acquired and processed waveforms.

Waveforms for Active + Reactive Power Generation

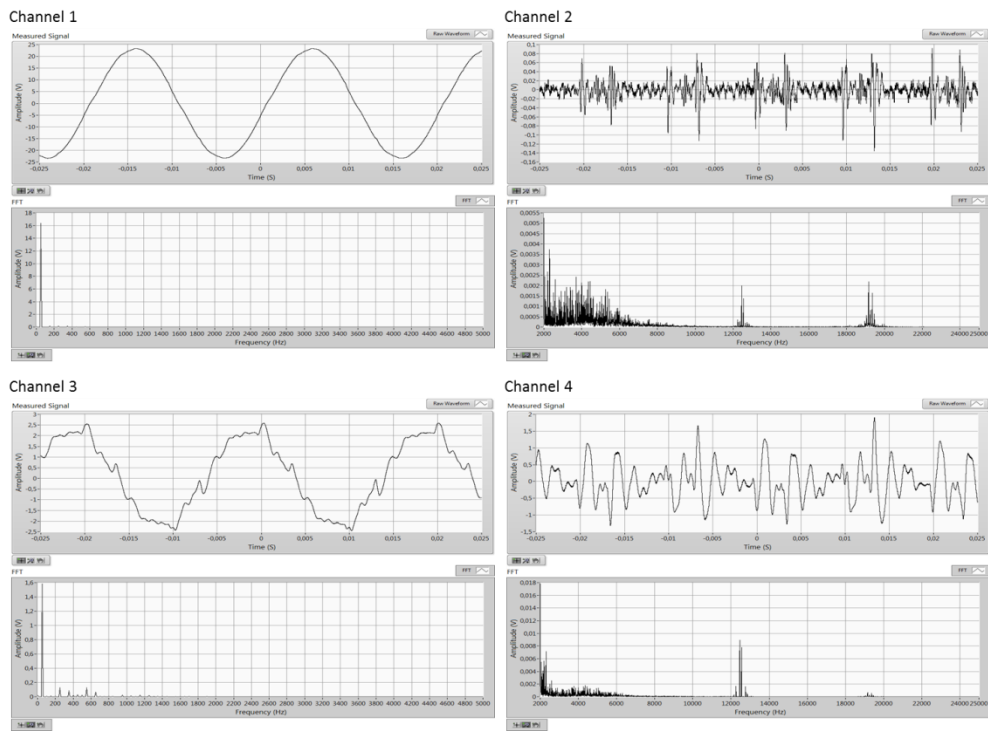


Fig. A.25. Acquired and processed waveforms.

Waveforms for Active + Reactive Power Consumption

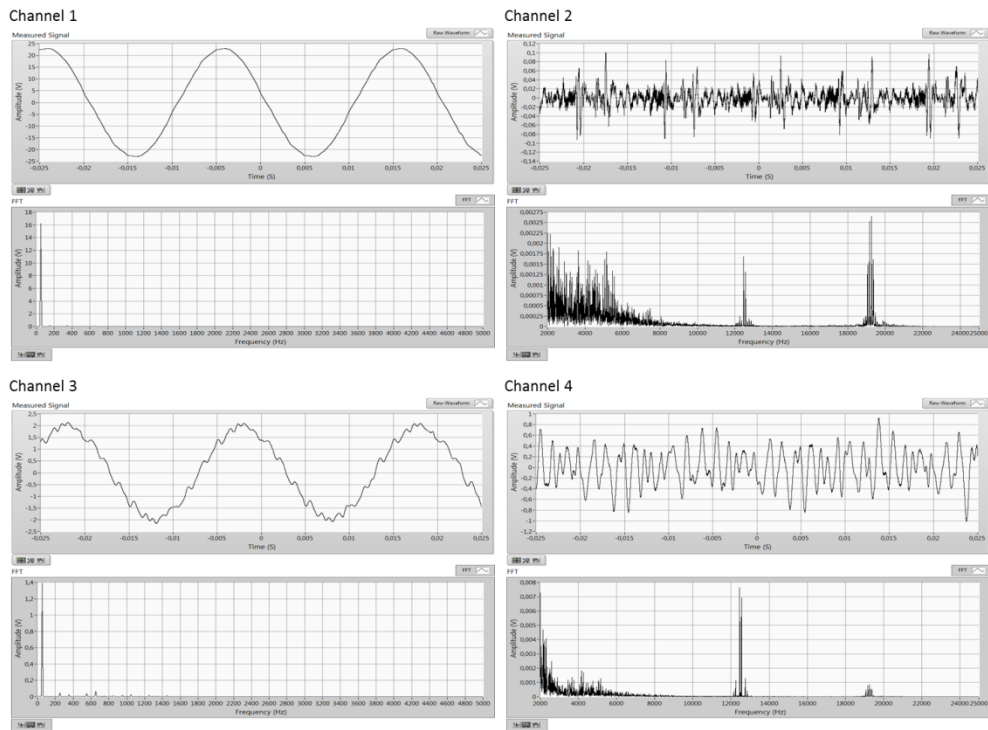


Fig. A.26. Acquired and processed waveforms.

Washing Machine

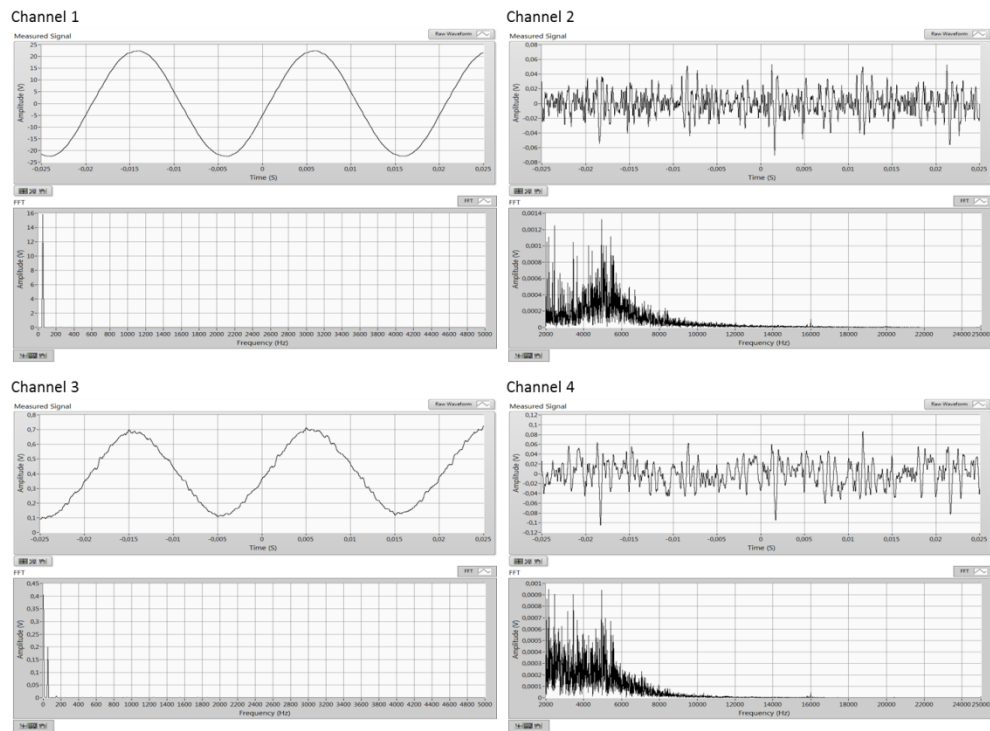


Fig. A.27. Acquired and processed waveforms.

Refrigerator

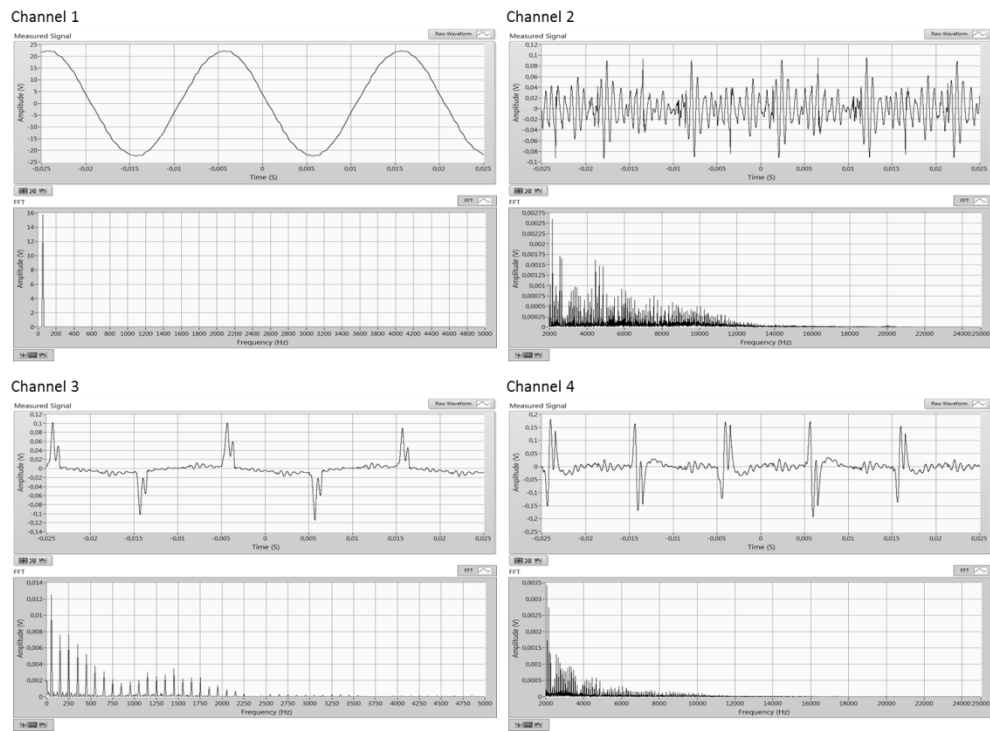


Fig. A.28. Acquired and processed waveforms.

Freezer

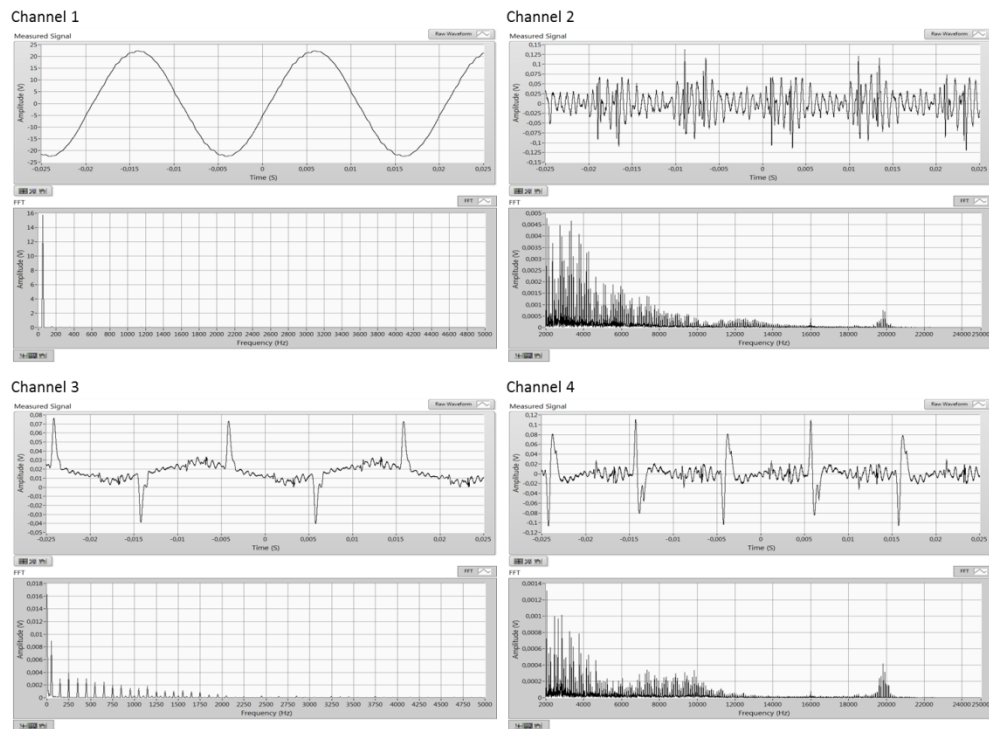


Fig. A.29. Acquired and processed waveforms.

Television

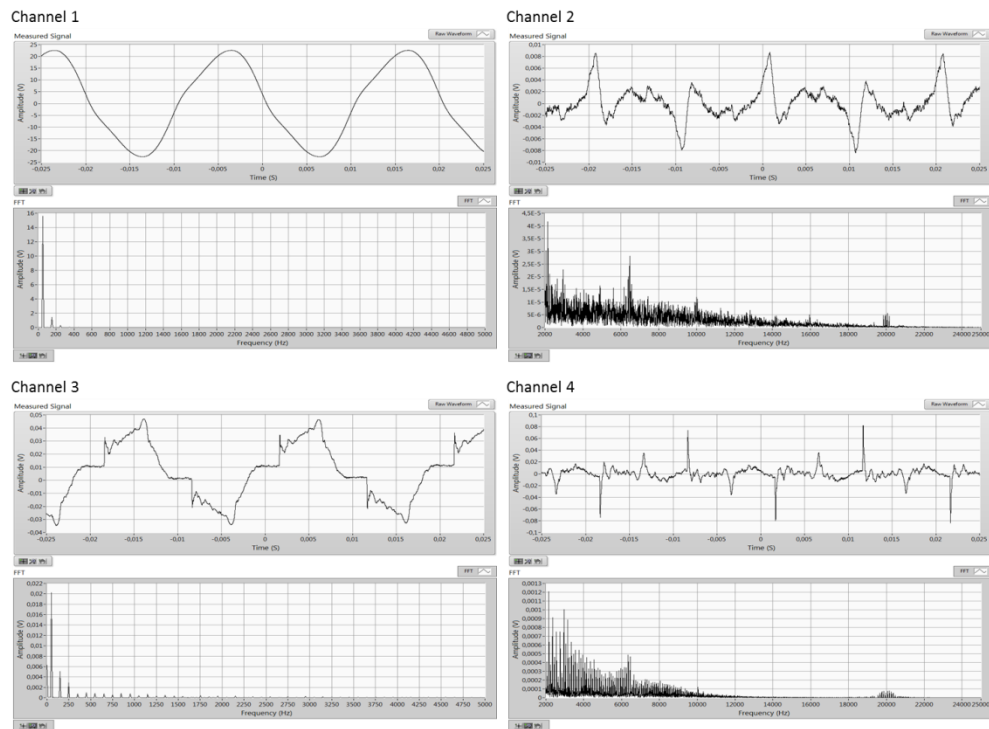


Fig. A.30. Acquired and processed waveforms.

LED Lamps - 14 no's.

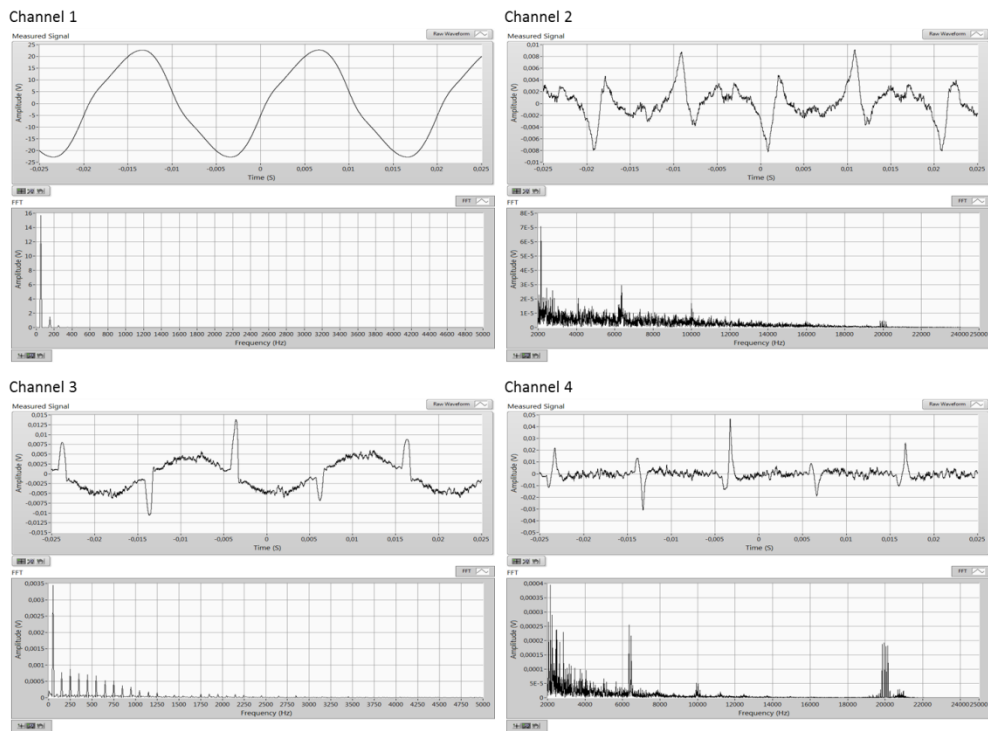


Fig. A.31. Acquired and processed waveforms.

APPENDIX B
MEASUREMENT CAMPAIGN 1
STATISTICAL ANALYSIS RESULTS

APPENDIX B

The statistical analysis results using the ANOVA for the voltage and current waveforms acquired during the measurement campaign 1 are listed here. The analysis process is explained in section 5.3.3.

Voltage Waveforms for Absolute Measurements

Table B.1. ANOVA table for the voltage waveform in the frequency range of 2 to 4 kHz.

Analysis of Variance					
Source	Sum of Squares	df	Mean Square	F Value	p-value Prob > F
Model	0.3532	2	0.1766	10.72	0.0018
B-Industrial PV Inverter	0.2531	1	0.2532	15.36	0.0018
C-Load	0.1001	1	0.1001	6.07	0.0284
Residual	0.2143	13	0.0165		
Cor Total	0.5675	15			

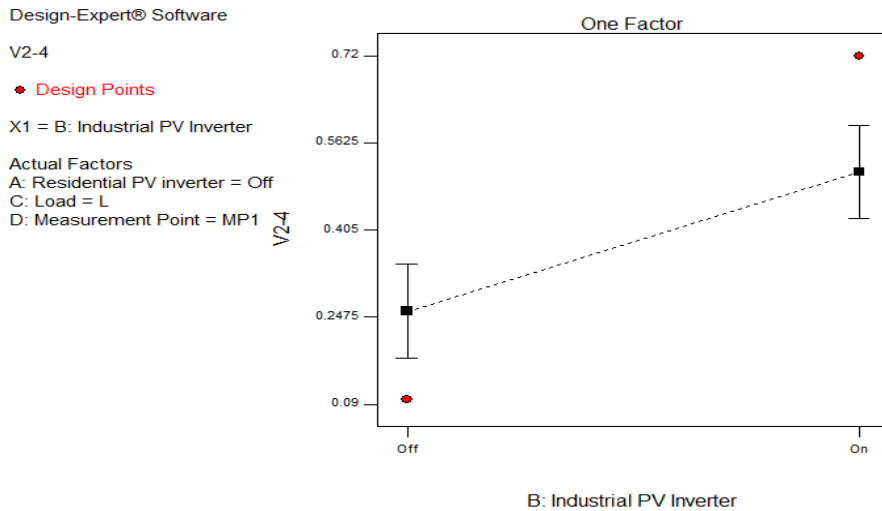


Fig. B.1. Effect of the PVI_R on the voltage waveform in the frequency range of 2 to 4 kHz.

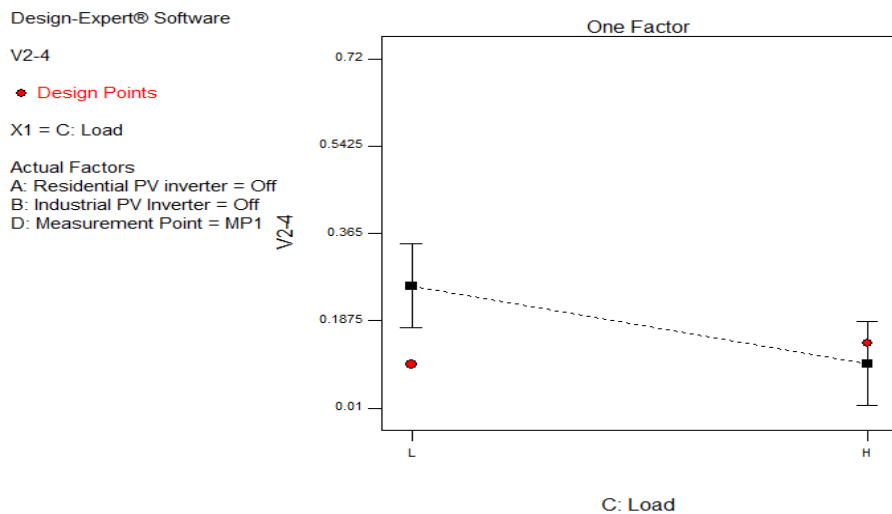


Fig. B.2. Effect of the load on the voltage waveform in the frequency range of 2 to 4 kHz.

Table B.2. ANOVA table for the voltage waveform in the frequency range of 4 to 6 kHz.

Analysis of Variance					
Source	Sum of Squares	df	Mean Square	F Value	p-value Prob > F
Model	0.0367	3	0.0122	18.86	< 0.0001
A-Residential PV inverter	0.0021	1	0.0021	3.22	0.0978
B-Industrial PV Inverter	0.0289	1	0.0289	44.63	< 0.0001
AB	0.0057	1	0.0057	8.73	0.0120
Residual	0.0078	12	0.0007		
Cor Total	0.0444	15			

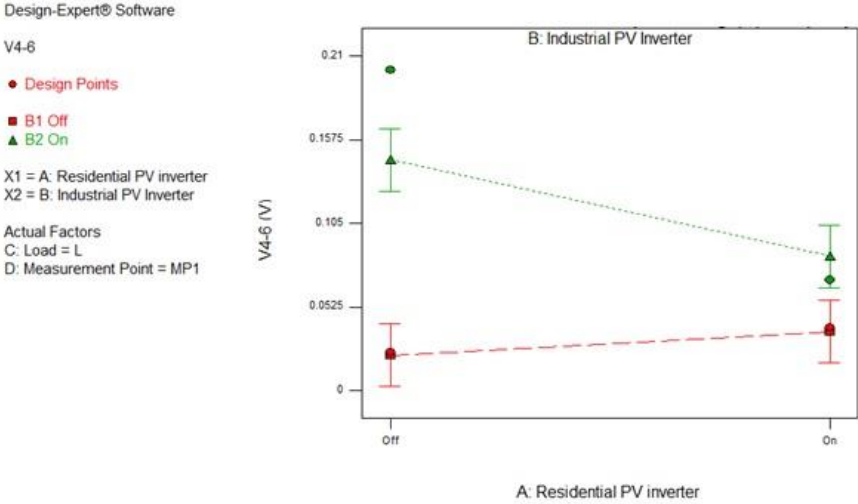


Fig. B.3. Effect of interaction between the PVI_R and PVI_I on the voltage waveform in the frequency range of 4 to 6 kHz.

Table B.3. ANOVA table for the voltage waveform in the frequency range of 6 to 8 kHz.

Analysis of Variance					
Source	Sum of Squares	df	Mean Square	F Value	p-value Prob > F
Model	0.0011	4	2.84E-04	11.35	0.0007
A-Residential PV inverter	0.0001	1	1.09E-04	4.36	0.0609
B-Industrial PV Inverter	0.0008	1	8.18E-04	32.63	0.0001
D-Measurement Point	0.0001	1	6.89E-05	2.75	0.1256
AD	0.0001	1	1.42E-04	5.65	0.0367
Residual	0.0003	11	2.51E-05		
Cor Total	0.0014	15			

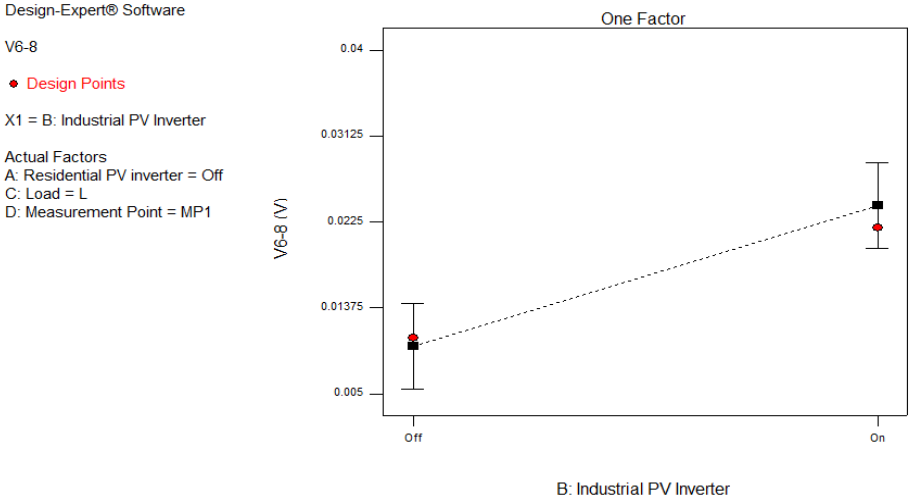


Fig. B.4. Effect of the PVI_I on the voltage waveform in the frequency range of 6 to 8 kHz.

Table B.4. ANOVA table for the voltage waveform in the frequency range of 8 to 10 kHz.

Analysis of Variance					
Source	Sum of Squares	df	Mean Square	F Value	p-value Prob > F
Model	2.76E-04	1	2.76E-04	5.62	0.0327
C-Load	2.76E-04	1	2.76E-04	5.62	0.0327
Residual	6.89E-04	14	4.92E-05		
Cor Total	9.65E-04	15			

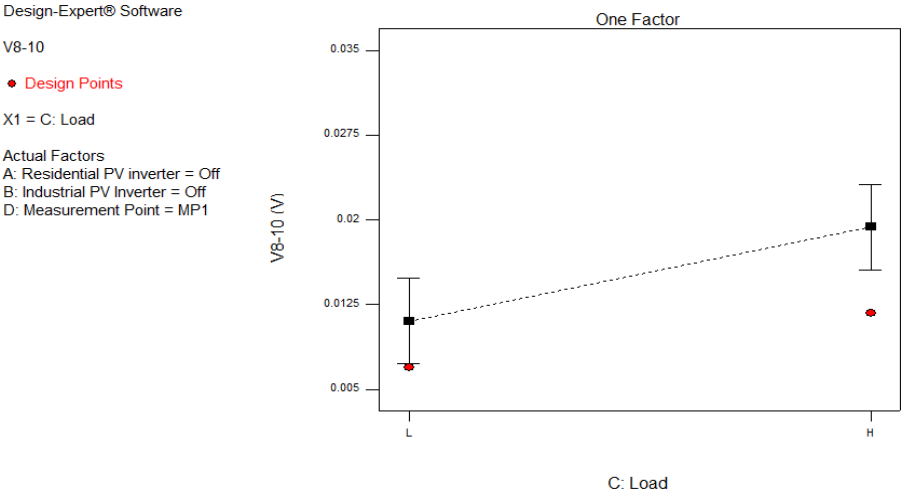


Fig. B.5. Effect of the load on the voltage waveform in the frequency range of 8 to 10 kHz.

Table B.5. ANOVA table for the voltage waveform in the frequency range of 10 to 12 kHz.

Analysis of Variance					
Source	Sum of Squares	df	Mean Square	F Value	p-value Prob > F
Model	0.0045	1	0.0045	26.36	0.0002
C-Load	0.0045	1	0.0045	26.36	0.0002
Residual	0.0024	14	0.0002		
Cor Total	0.0069	15			

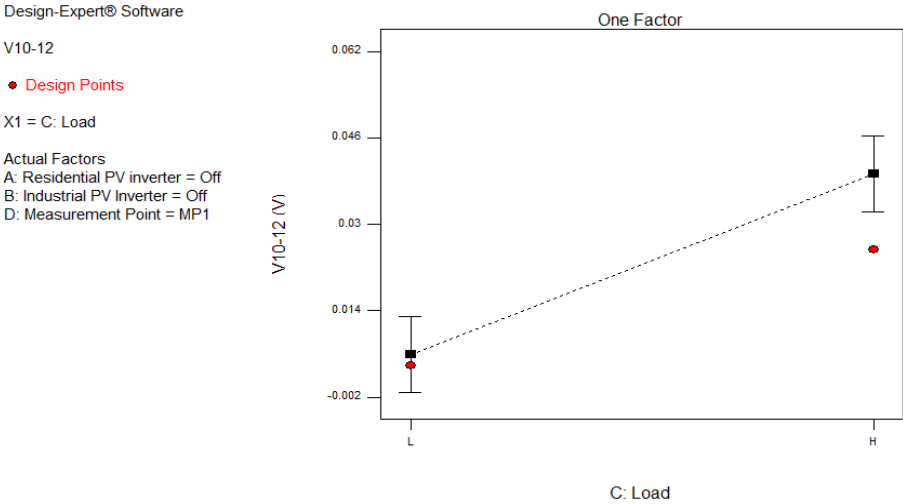


Fig. B.6. Effect of the load on the voltage waveform in the frequency range of 10 to 12 kHz.

Table B.6. ANOVA table for the voltage waveform in the frequency range of 12 to 14 kHz.

Analysis of Variance					
Source	Sum of Squares	df	Mean Square	F Value	p-value Prob > F
Model	1.35E-05	1	1.35E-05	6.41	0.0240
D-Measurement Point	1.35E-05	1	1.35E-05	6.41	0.0240
Residual	2.95E-05	14	2.11E-06		
Cor Total	4.30E-05	15			

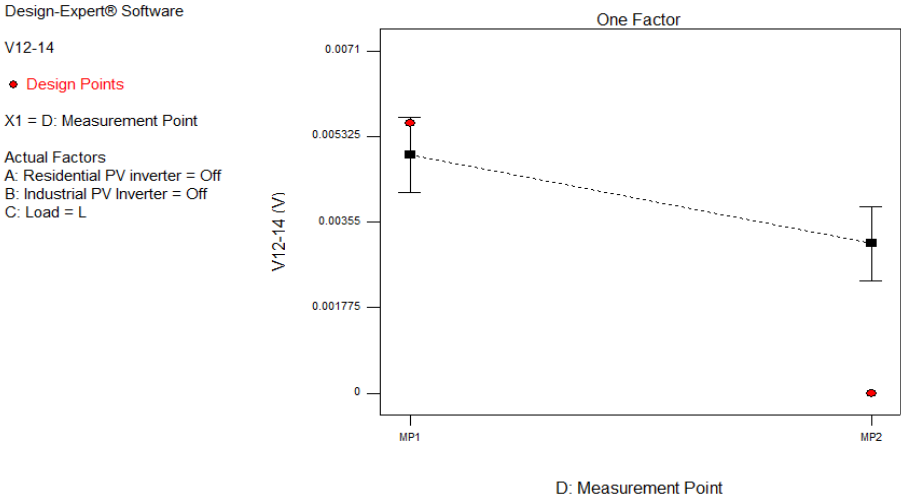


Fig. B.7. Effect of the measurement point on the voltage waveform in the frequency range of 12 to 14 kHz.

Table B.7. ANOVA table for the voltage waveform in the frequency range of 14 to 16 kHz.

Analysis of Variance					
Source	Sum of Squares	df	Mean Square	F Value	p-value Prob > F
Model	1.00E-05	2	5.00E-06	10.24	0.0021
B-Industrial PV Inverter	6.10E-06	1	6.10E-06	12.51	0.0036
D-Measurement Point	3.90E-06	1	3.90E-06	7.97	0.0144
Residual	6.40E-06	13	4.90E-07		
Cor Total	1.60E-05	15			

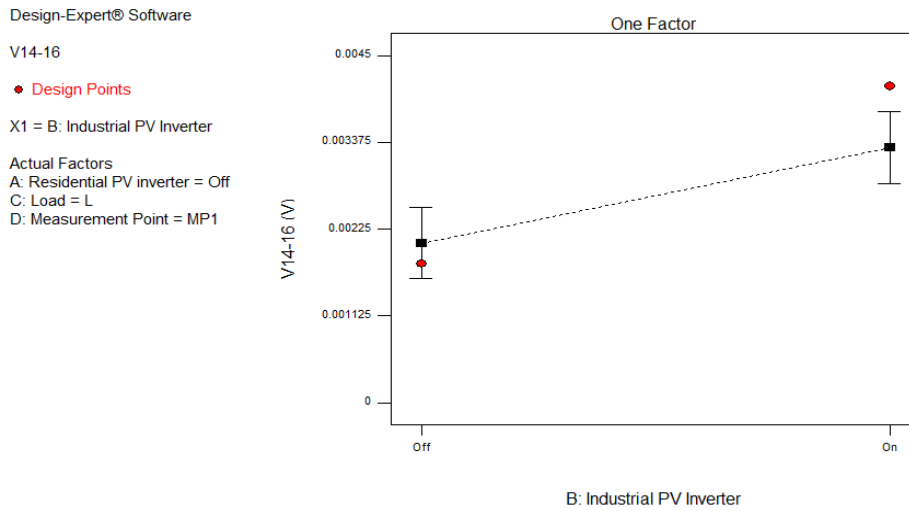


Fig. B.8. Effect of the PVI_I on the voltage waveform in the frequency range of 14 to 16 kHz.

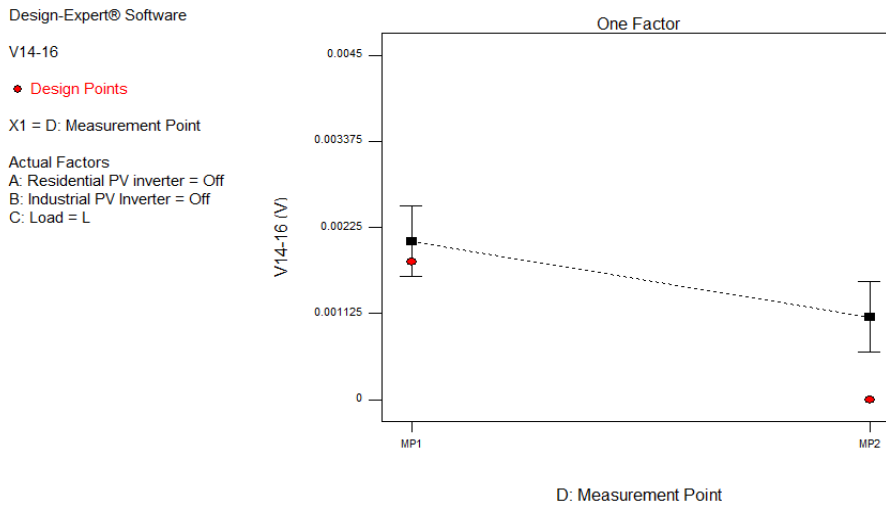


Fig. B.9. Effect of the measurement point on the voltage waveform in the frequency range of 14 to 16 kHz.

Table B.8. ANOVA table for the voltage waveform in the frequency range of 16 to 18 kHz.

Analysis of Variance					
Source	Sum of Squares	df	Mean Square	F Value	p-value Prob > F
Model	1.38E-05	5	2.80E-06	5.70	0.0096
B-Industrial PV Inverter	2.25E-06	1	2.30E-06	4.66	0.0563
C-Load	2.10E-06	1	2.10E-06	4.35	0.0635
D-Measurement Point	5.06E-06	1	5.10E-06	10.48	0.0089
BD	2.25E-06	1	2.30E-06	4.66	0.0563
CD	2.10E-06	1	2.10E-06	4.35	0.0635
Residual	4.83E-06	10	4.80E-07		
Cor Total	1.86E-05	15			

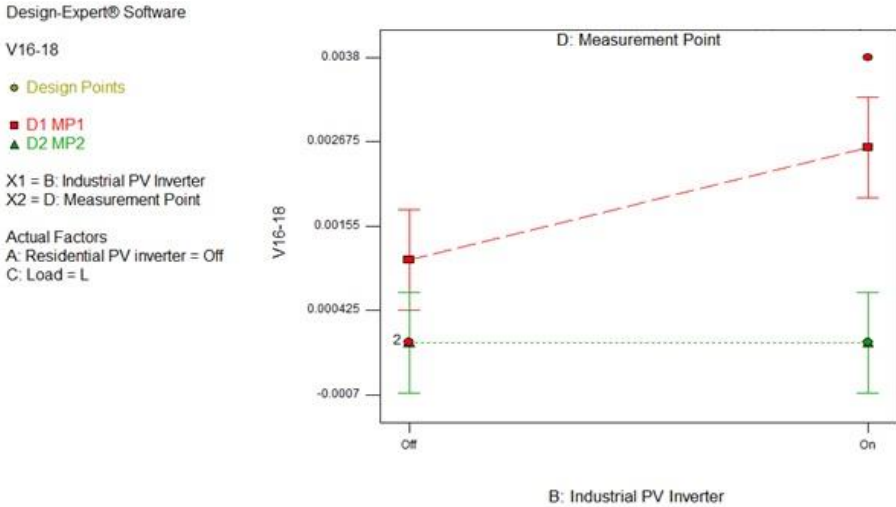


Fig. B.10. Interaction effect between the PVI_I and measurement point on the voltage waveform in the frequency range of 16 to 18 kHz.

Table B.9. ANOVA table for the voltage waveform in the frequency range of 18 to 20 kHz.

Analysis of Variance					
Source	Sum of Squares	df	Mean Square	F Value	p-value Prob > F
Model	5.50E-04	3	1.83E-04	14.38	0.0003
A-Residential PV inverter	1.41E-04	1	1.41E-04	11.05	0.0061
B-Industrial PV Inverter	1.91E-04	1	1.91E-04	14.98	0.0022
AB	2.18E-04	1	2.18E-04	17.10	0.0014
Residual	1.53E-04	12	1.28E-05		
Cor Total	7.04E-04	15			

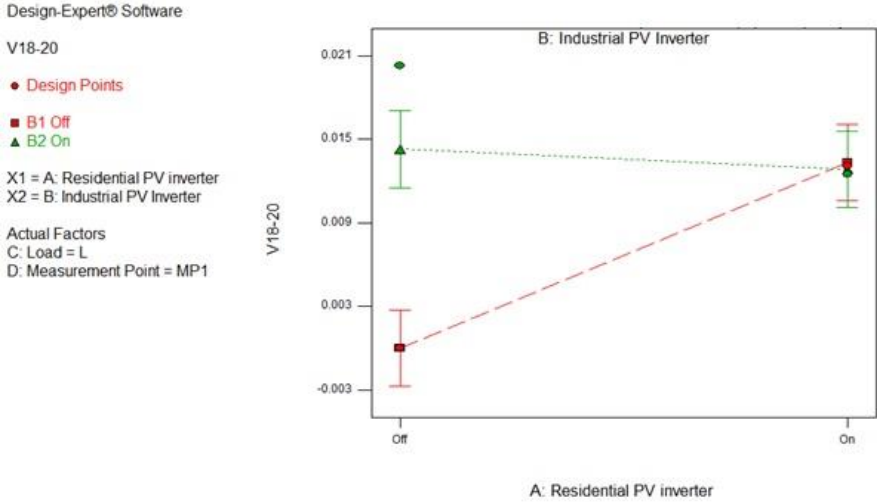


Fig. B.11. Interaction effect between the PVI_R and PVI_I on the voltage waveform in the frequency range of 18 to 20 kHz.

Table B.10. ANOVA table for the voltage waveform in the frequency range of 20 to 22 kHz.

Analysis of Variance					
Source	Sum of Squares	df	Mean Square	F Value	p-value Prob > F
Model	2.15E-04	1	2.15E-04	23.2011	0.0003
B-Industrial PV Inverter	2.15E-04	1	2.15E-04	23.2011	0.0003
Residual	1.30E-04	14	9.25E-06		
Cor Total	3.44E-04	15			

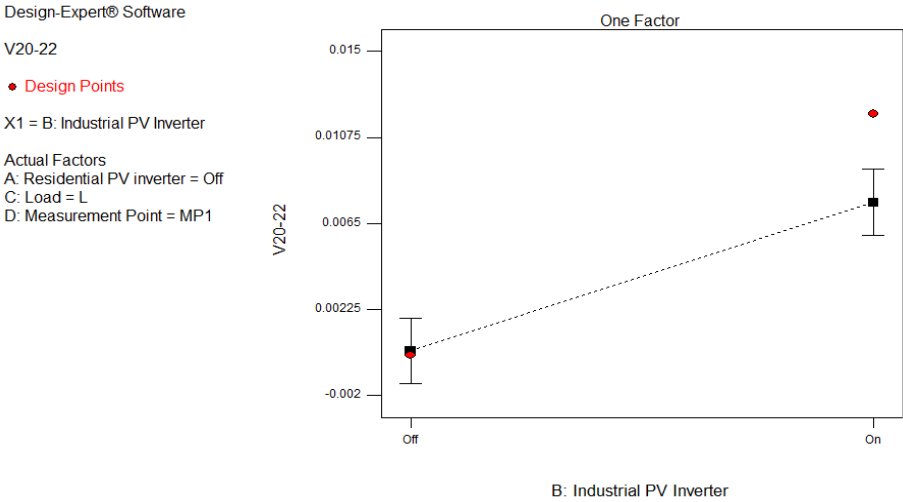


Fig. B.12. Effect of the PVI_I on the voltage waveform in the frequency range of 18 to 20 kHz.

Current Waveforms for Absolute Measurements

Table B.11. ANOVA table for the current waveform in the frequency range of 2 to 4 kHz.

Analysis of Variance					
Source	Sum of Squares	df	Mean Square	F Value	p-value Prob > F
Model	0.0098	4	0.0025	5.41	0.0117
B-Industrial PV Inverter	0.0030	1	0.0030	6.63	0.0258
C-Load	0.0009	1	0.0009	1.88	0.1972
D-Measurement Point	0.0026	1	0.0026	5.65	0.0367
CD	0.0034	1	0.0039	7.46	0.0195
Residual	0.0050	11	0.0005		
Cor Total	0.0148	15			

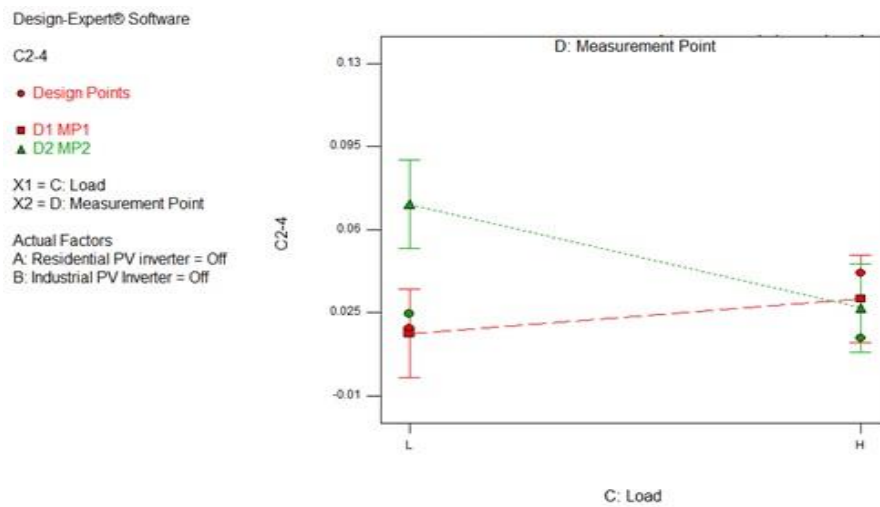


Fig. B.13. Interaction effect between the load and measurement point on the current waveform in the frequency range of 2 to 4 kHz.

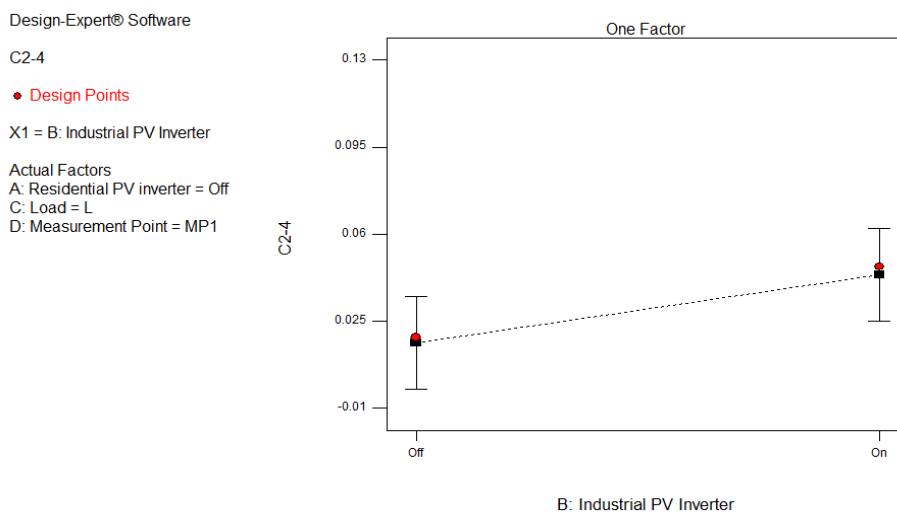


Fig. B.14. Effect of the PVI on the current waveform in the frequency range of 2 to 4 kHz.

Table B.12. ANOVA table for the current waveform in the frequency range of 4 to 6 kHz.

Analysis of Variance					
Source	Sum of Squares	df	Mean Square	F Value	p-value Prob > F
Model	0.00	3	0.00	26.41	< 0.0001
B-Industrial PV Inverter	0.00	1	0.00	45.74	< 0.0001
D-Measurement Point	0.00	1	0.00	20.24	0.0007
BD	0.00	1	0.00	13.25	0.0034
Residual	0.00	12	0.00		
Cor Total	0.00	15			

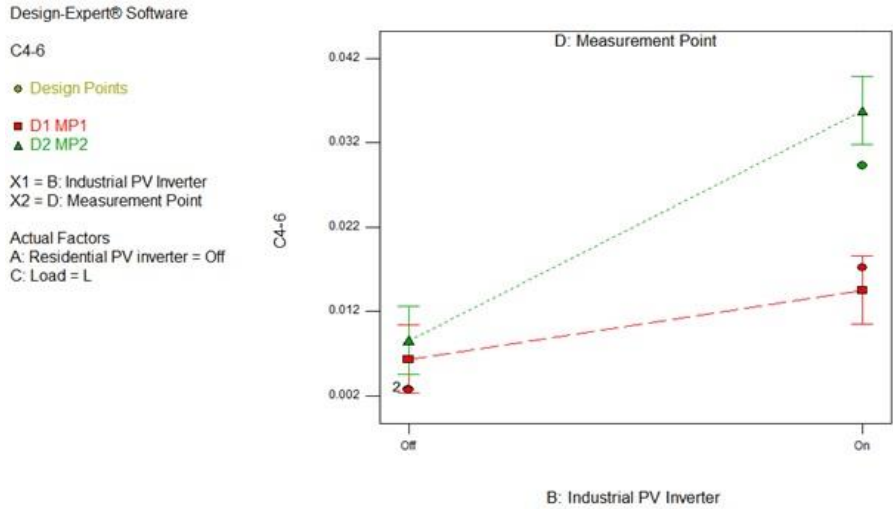


Fig. B.15. Interaction effect between the PVI_I and measurement point on the current waveform in the frequency range of 2 to 4 kHz.

Table B.13. ANOVA table for the current waveform in the frequency range of 6 to 8 kHz.

Analysis of Variance					
Source	Sum of Squares	df	Mean Square	F Value	p-value Prob > F
Model	0.001	3	4.00E-04	85.10	< 0.0001
B-Industrial PV Inverter	0.000	1	4.30E-04	92.24	< 0.0001
D-Measurement Point	0.000	1	4.50E-04	96.27	< 0.0001
BD	0.000	1	3.10E-04	66.79	< 0.0001
Residual	0.000	12	4.70E-06		
Cor Total	0.001	15			

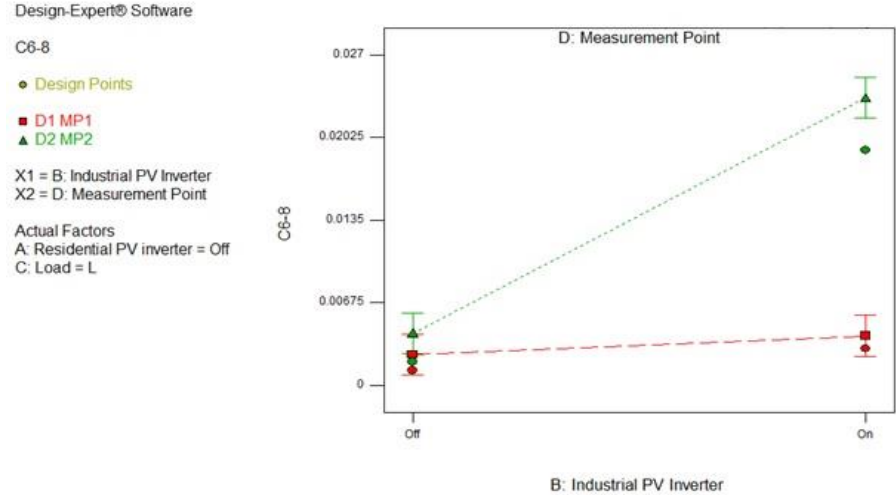


Fig. B.16. Interaction effect between the PVI_I and measurement point on the current waveform in the frequency range of 6 to 8 kHz.

Table B.14. ANOVA table for the current waveform in the frequency range of 8 to 10 kHz.

Analysis of Variance					
Source	Sum of Squares	df	Mean Square	F Value	p-value Prob > F
Model	6.53E-04	5	1.31E-04	17.29	0.0001
B-Industrial PV Inverter	9.46E-05	1	9.46E-05	12.52	0.0054
C-Load	5.22E-05	1	5.22E-05	6.91	0.0252
D-Measurement Point	3.49E-04	1	3.48E-04	46.16	< 0.0001
BC	7.79E-05	1	7.79E-05	10.31	0.0093
BD	7.97E-05	1	7.97E-05	10.54	0.0088
Residual	7.56E-05	10	7.55E-06		
Cor Total	7.25E-04	15			

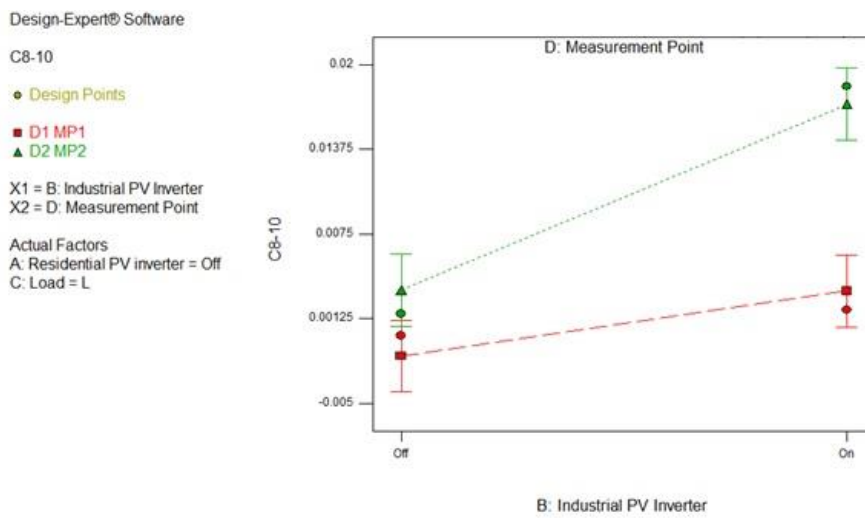


Fig. B.17. Interaction effect between the PVI_I and measurement point on the current waveform in the frequency range of 8 to 10 kHz.

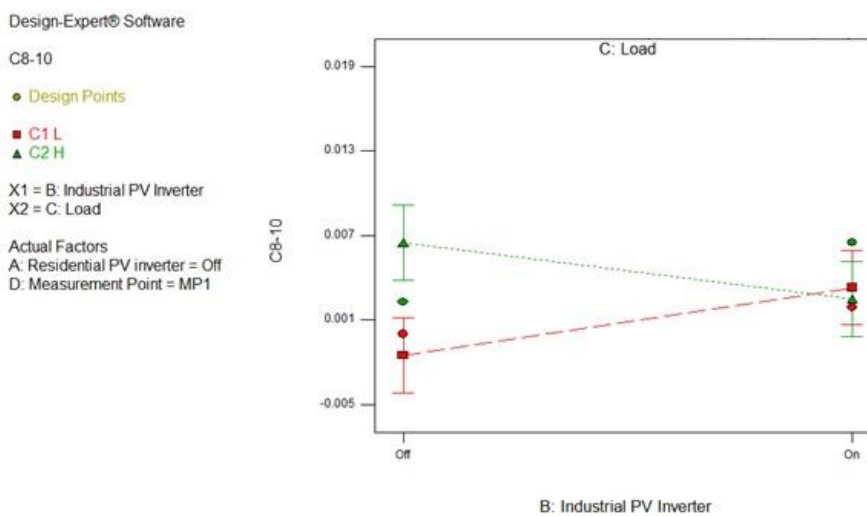


Fig. B.18. Interaction effect between the PVI_I and load on the current waveform in the frequency range of 8 to 10 kHz.

Table B.15. ANOVA table for the current waveform in the frequency range of 10 to 12 kHz.

Analysis of Variance					
Source	Sum of Squares	df	Mean Square	F Value	p-value Prob > F
Model	0.0003	2	2.00E-04	11.68	0.0013
C-Load	0.0003	1	3.00E-04	18.83	0.0008
D-Measurement Point	0.0001	1	6.60E-05	4.52	0.0531
Residual	0.0002	13	1.46E-05		
Cor Total	0.0005	15			

Design-Expert® Software

C10-12

◆ Design Points

X1 = C: Load

Actual Factors
 A: Residential PV inverter = Off
 B: Industrial PV Inverter = Off
 D: Measurement Point = MP1

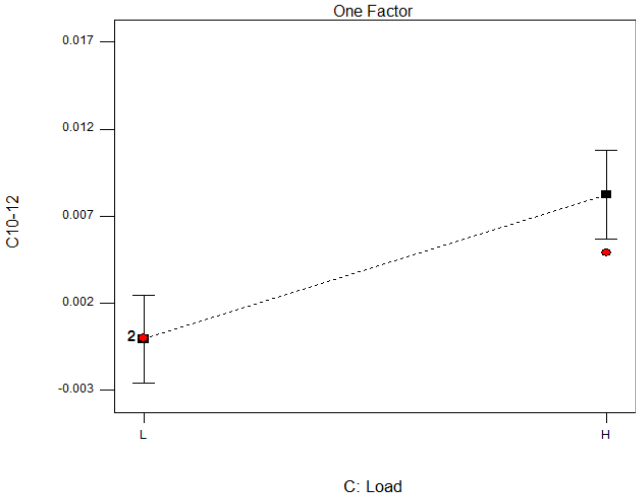


Fig. B.19. Effect of the load on the current waveform in the frequency range of 10 to 12 kHz.

Table B.16. ANOVA table for the current waveform in the frequency range of 12 to 14 kHz.

Analysis of Variance					
Source	Sum of Squares	df	Mean Square	F Value	p-value Prob > F
Model	0.0000	1	0.0000	19.70	0.0006
B-Industrial PV Inverter	0.0000	1	0.0000	19.70	0.0006
Residual	0.0000	14	0.0000		
Cor Total	0.0000	15			

Design-Expert® Software
 C12-14
 ● Design Points
 X1 = B: Industrial PV Inverter
 Actual Factors
 A: Residential PV inverter = Off
 C: Load = L
 D: Measurement Point = MP1

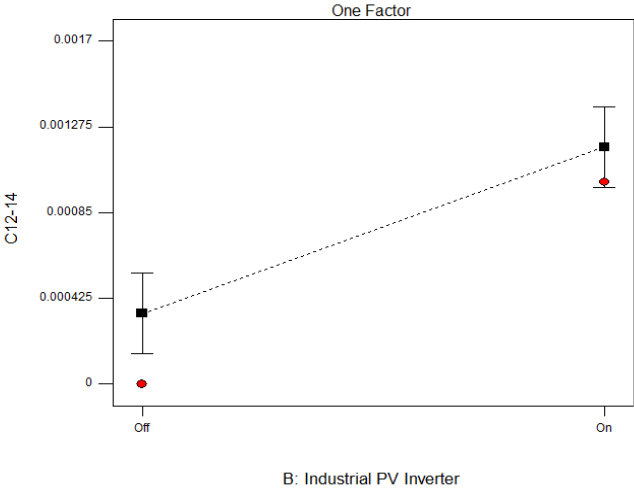


Fig. B.20. Effect of the PVI on the current waveform in the frequency range of 12 to 14 kHz.

Table B.17. ANOVA table for the current waveform in the frequency range of 14 to 16 kHz.

Analysis of Variance					
Source	Sum of Squares	df	Mean Square	F Value	p-value Prob > F
Model	2.96E-06	4	7.41E-07	15.32	0.0002
A-Residential PV inverter	7.56E-08	1	7.56E-08	1.56	0.2370
B-Industrial PV Inverter	2.48E-06	1	2.48E-06	51.30	< 0.0001
D-Measurement Point	7.56E-08	1	7.56E-08	1.56	0.2370
AD	3.31E-07	1	3.31E-07	6.84	0.0240
Residual	5.32E-07	11	4.84E-08		
Cor Total	3.49E-06	15			

Design-Expert® Software
 C14-16
 • Design Points
 X1 = B: Industrial PV Inverter
 Actual Factors
 A: Residential PV inverter = Off
 C: Load = L
 D: Measurement Point = MP1

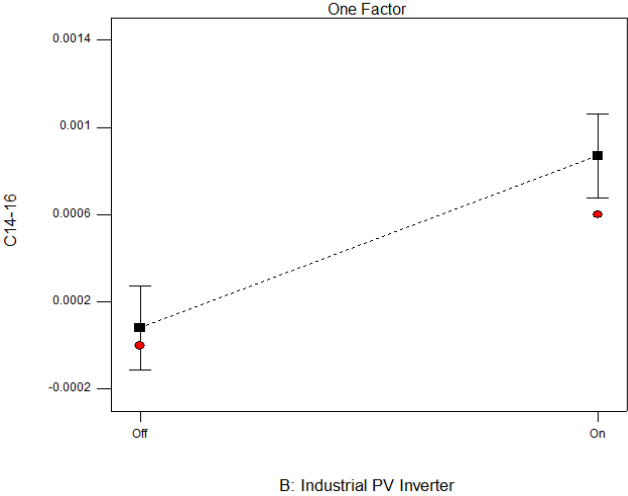


Fig. B.21. Effect of the PVI_I on the current waveform in the frequency range of 14 to 16 kHz.

Table B.18. ANOVA table for the current waveform in the frequency range of 16 to 18 kHz.

Analysis of Variance					
Source	Sum of Squares	df	Mean Square	F Value	p-value Prob > F
Model	2.28E-06	3	7.61E-07	35.8039	< 0.0001
B-Industrial PV Inverter	1.56E-06	1	1.56E-06	73.5294	< 0.0001
D-Measurement Point	3.60E-07	1	3.60E-07	16.9412	0.0014
BD	3.60E-07	1	3.60E-07	16.9412	0.0014
Residual	2.55E-07	12	2.13E-08		
Cor Total	2.54E-06	15			

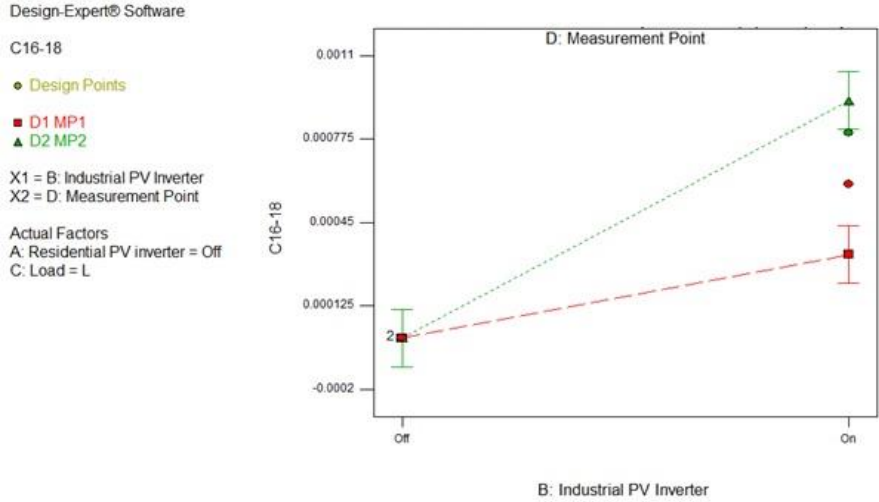


Fig. B.22. Interaction effect between the PVI and measurement point on the current waveform in the frequency range of 16 to 18 kHz.

Table B.19. ANOVA table for the current waveform in the frequency range of 18 to 20 kHz.

Analysis of Variance					
Source	Sum of Squares	df	Mean Square	F Value	p-value Prob > F
Model	3.42E-04	2	1.71E-04	8.02	0.0054
B-Industrial PV Inverter	1.01E-04	1	1.01E-04	4.72	0.0489
D-Measurement Point	2.41E-04	1	2.41E-04	11.30	0.0051
Residual	2.77E-04	13	2.13E-05		
Cor Total	6.18E-04	15			

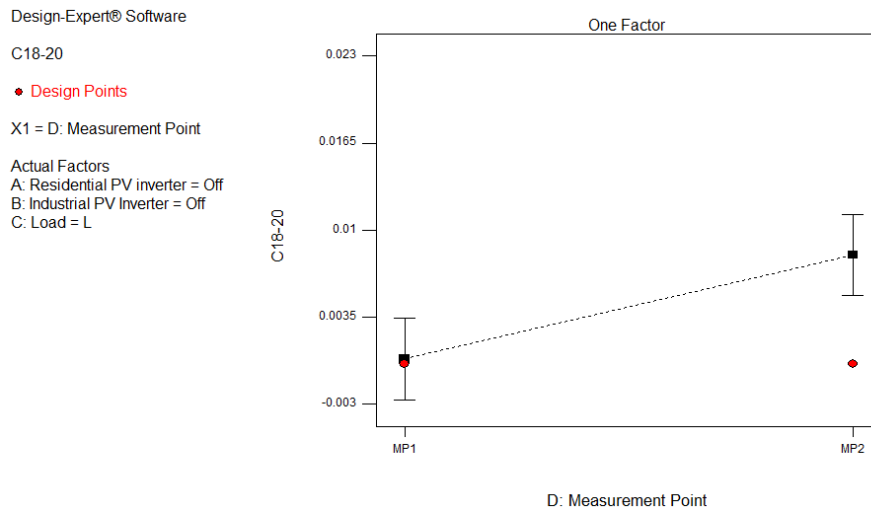


Fig. B.23. Effect of the measurement point on the current waveform in the frequency range of 18 to 20 kHz.

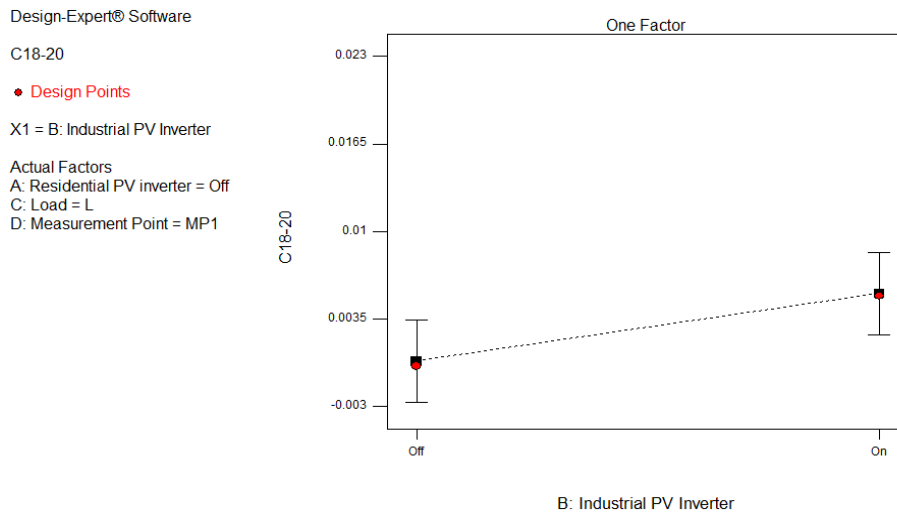


Fig. B.24. Effect of the PVI on the current waveform in the frequency range of 18 to 20 kHz.

Table B.20. ANOVA table for the current waveform in the frequency range of 20 to 22 kHz.

Analysis of Variance					
Source	Sum of Squares	df	Mean Square	F Value	p-value Prob > F
Model	9.22E-05	1	9.22E-05	11.1265954	0.0049
B-Industrial PV Inverter	9.22E-05	1	9.22E-05	11.1265954	0.0049
Residual	1.16E-04	14	8.28E-06		
Cor Total	2.08E-04	15			

Design-Expert® Software
 C20-22
 • Design Points
 X1 = B: Industrial PV Inverter
 Actual Factors
 A: Residential PV inverter = Off
 C: Load = L
 D: Measurement Point = MP1

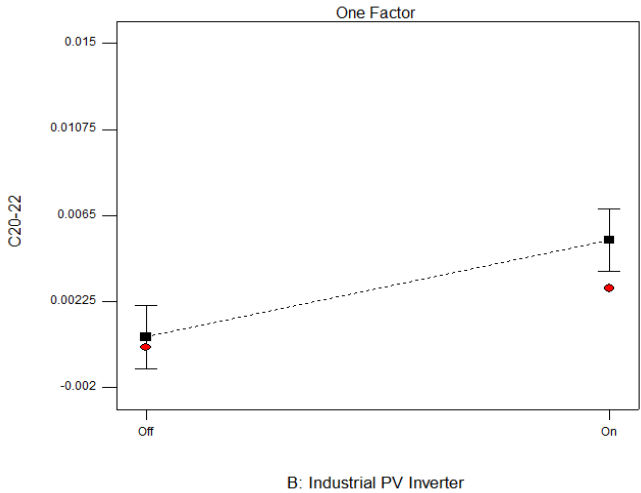


Fig. B.25. Effect of the PVI_I on the current waveform in the frequency range of 20 to 22 kHz.

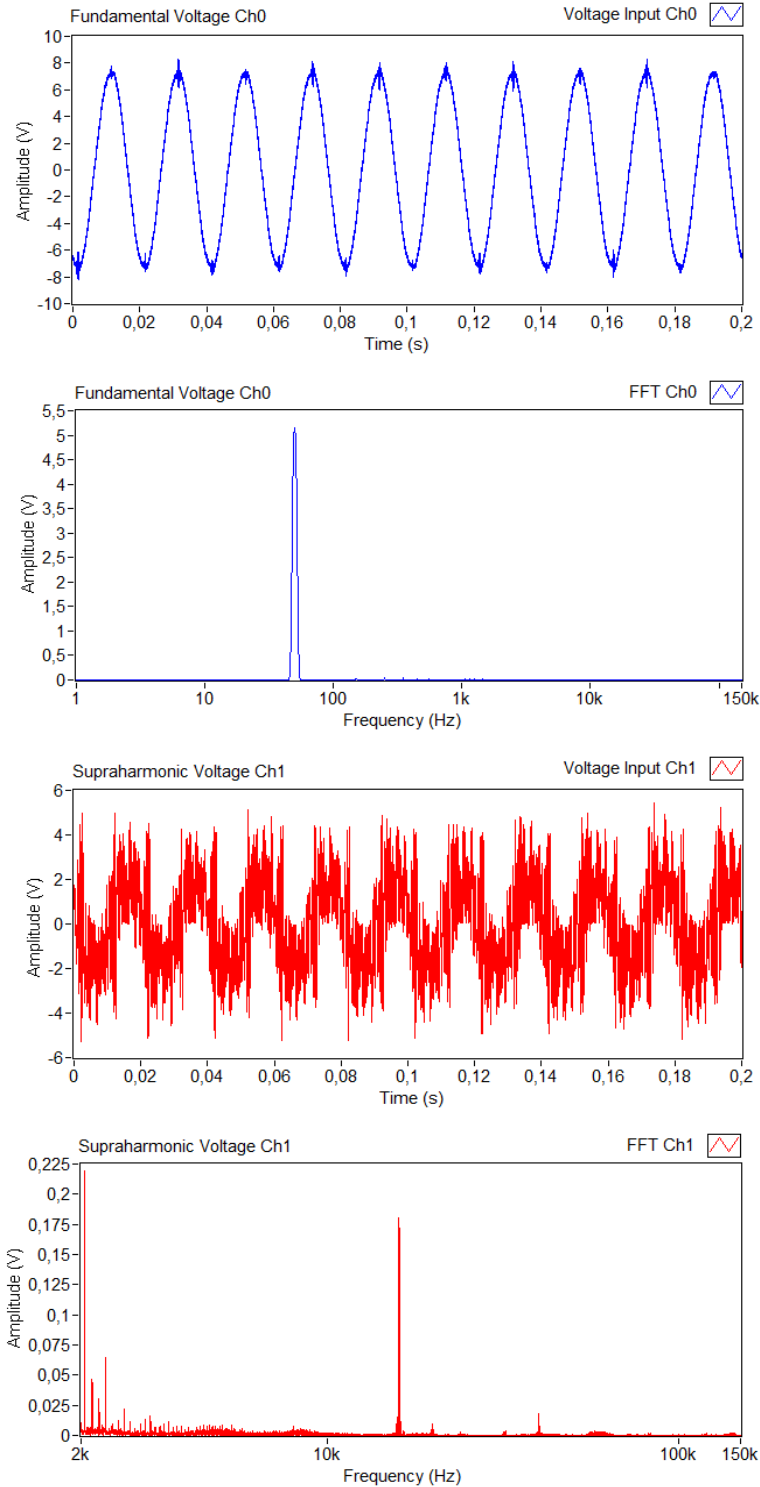
APPENDIX C
MEASUREMENT CAMPAIGN 2
MATHEMATICAL ANALYSIS RESULTS

APPENDIX C

The network characterization measurements with the PVI_I and fast charging EVC with respect to the measurement points are shown here with the acquired and processed sensor output waveforms. The measurement and analysis process is described in section 4.3 and 5.4.

Network Tests with Industrial PV Inverter and EV Charger

Waveforms measured close to Industrial PV inverter



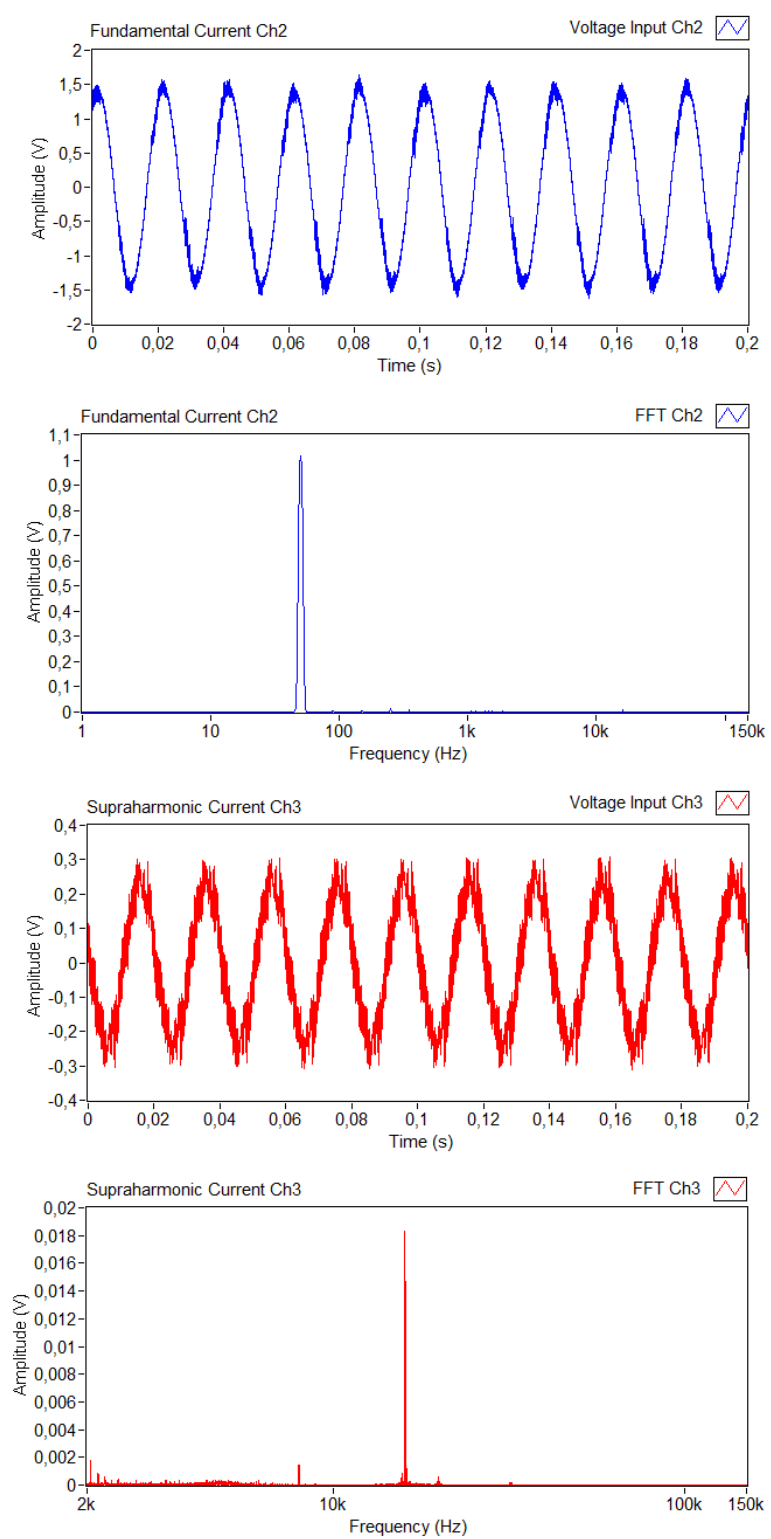
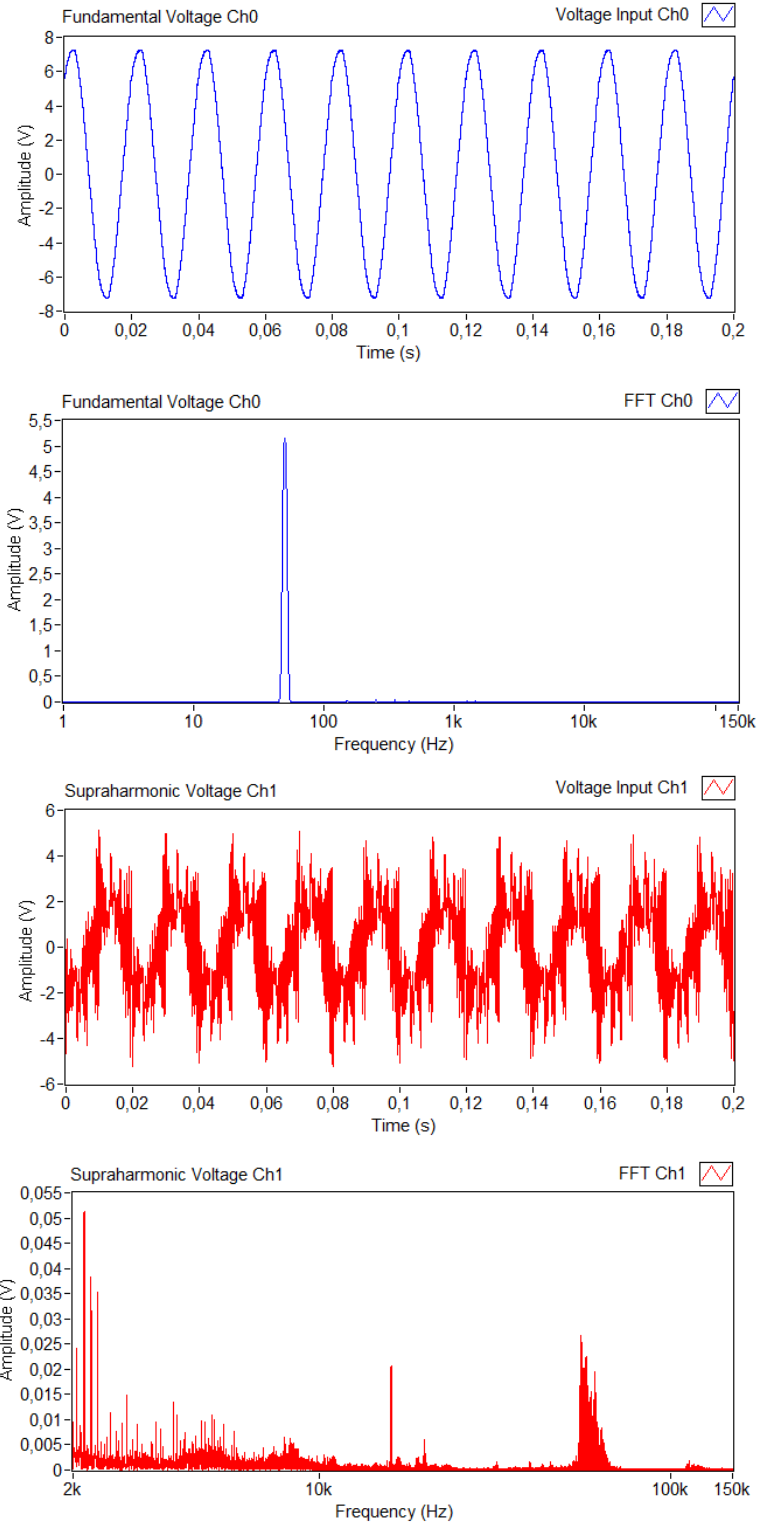


Fig. C.1. Acquired and processed waveforms.

Waveforms measured away from Industrial PV inverter



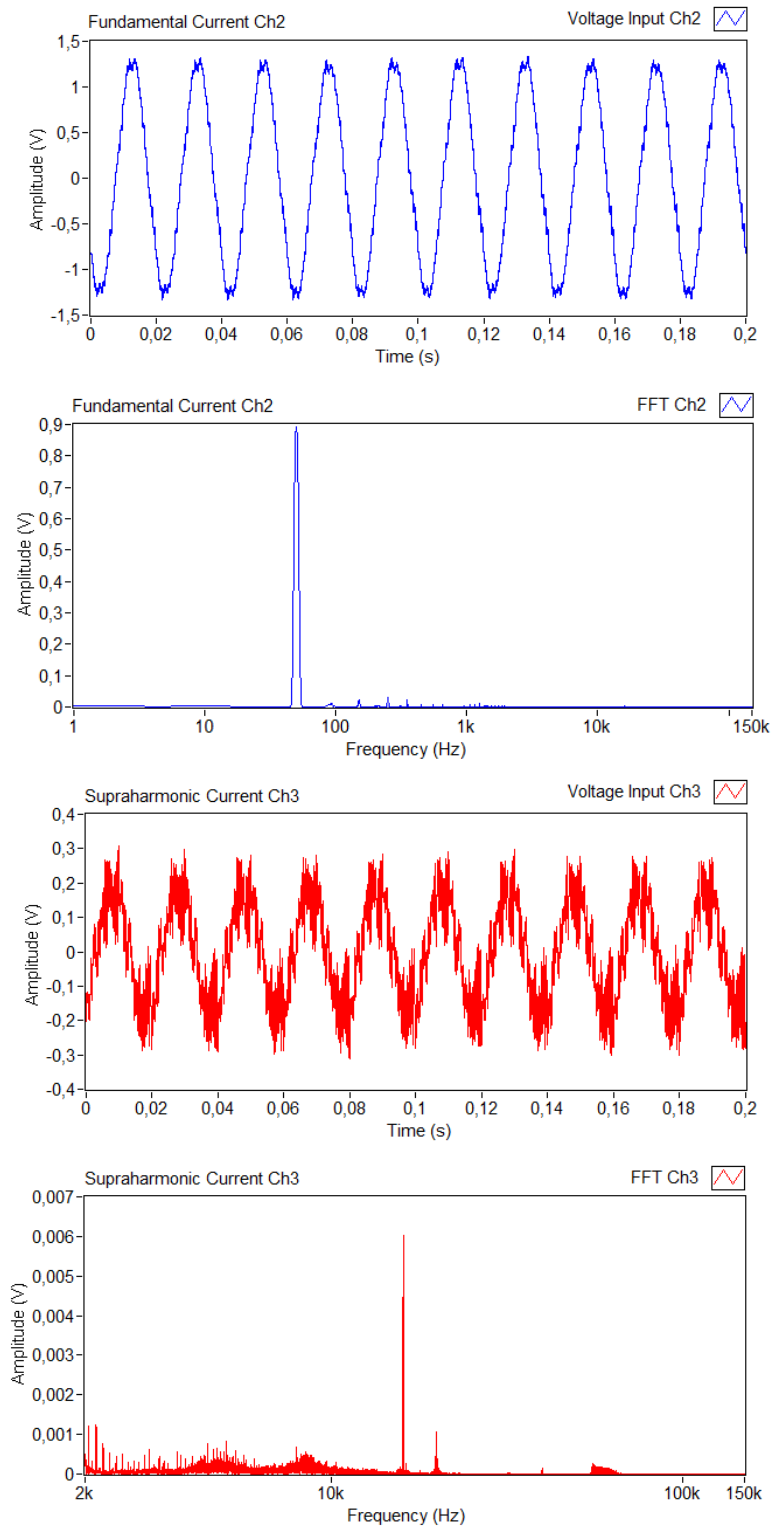
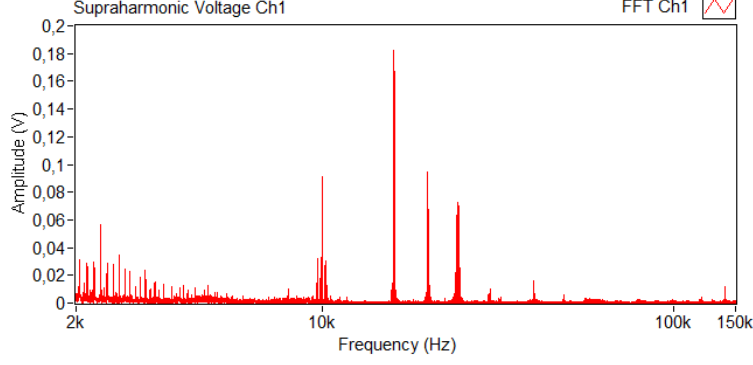
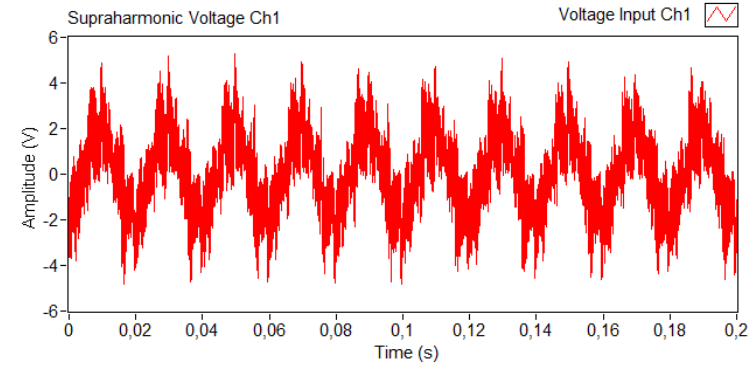
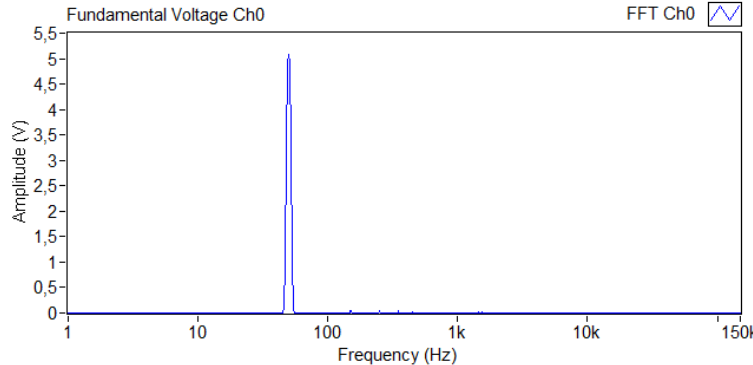
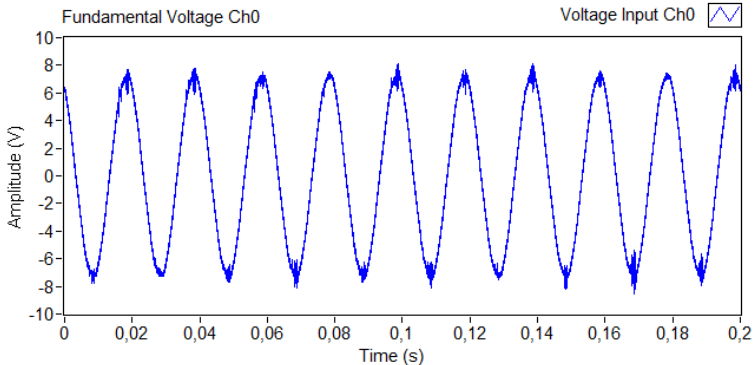


Fig. C.2. Acquired and processed waveforms.

Waveforms measured close to Industrial PV inverter with sudden addition of EV Charger



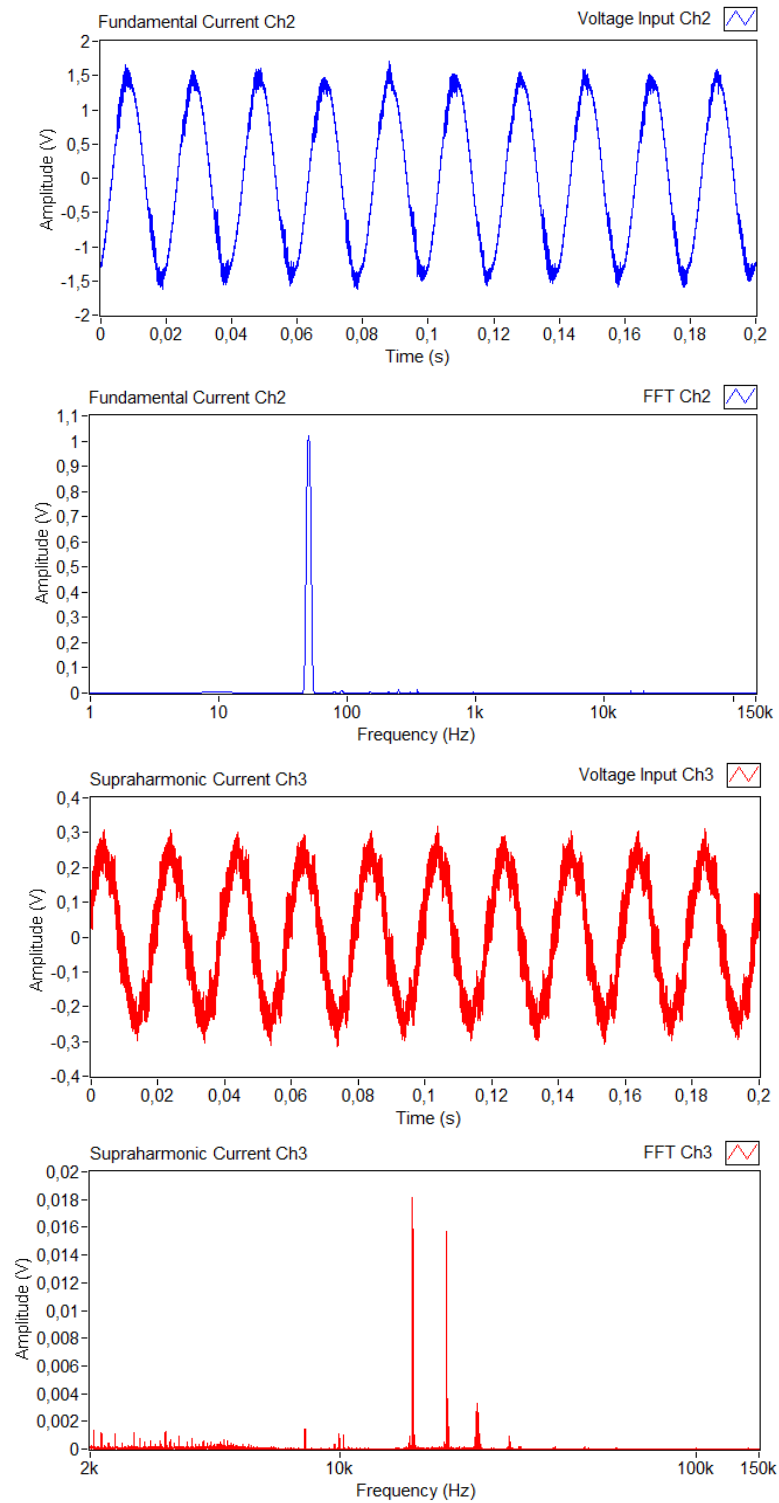
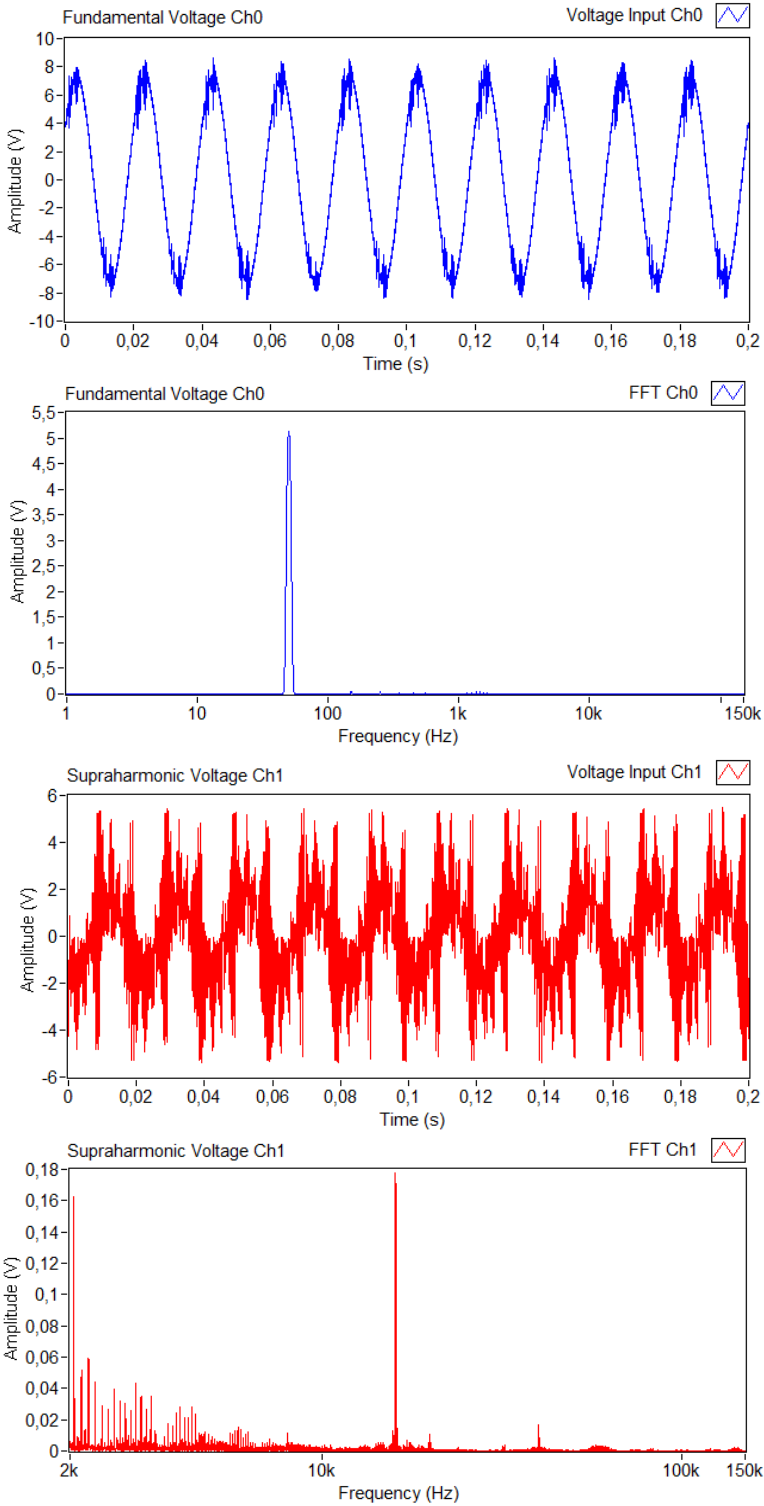


Fig. C.3. Acquired and processed waveforms.

Waveforms measured close to Industrial PV inverter with sudden removal of EV Charger



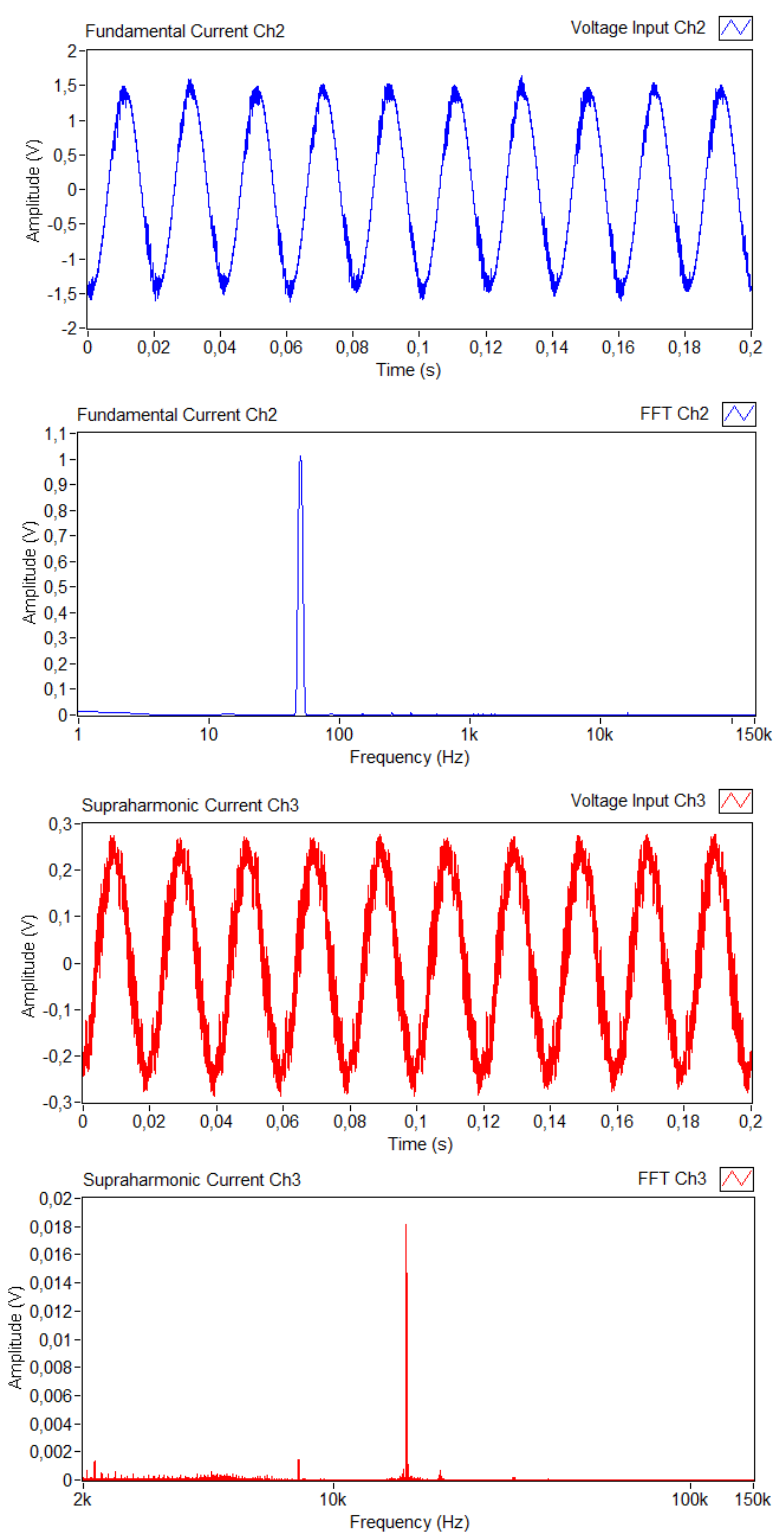
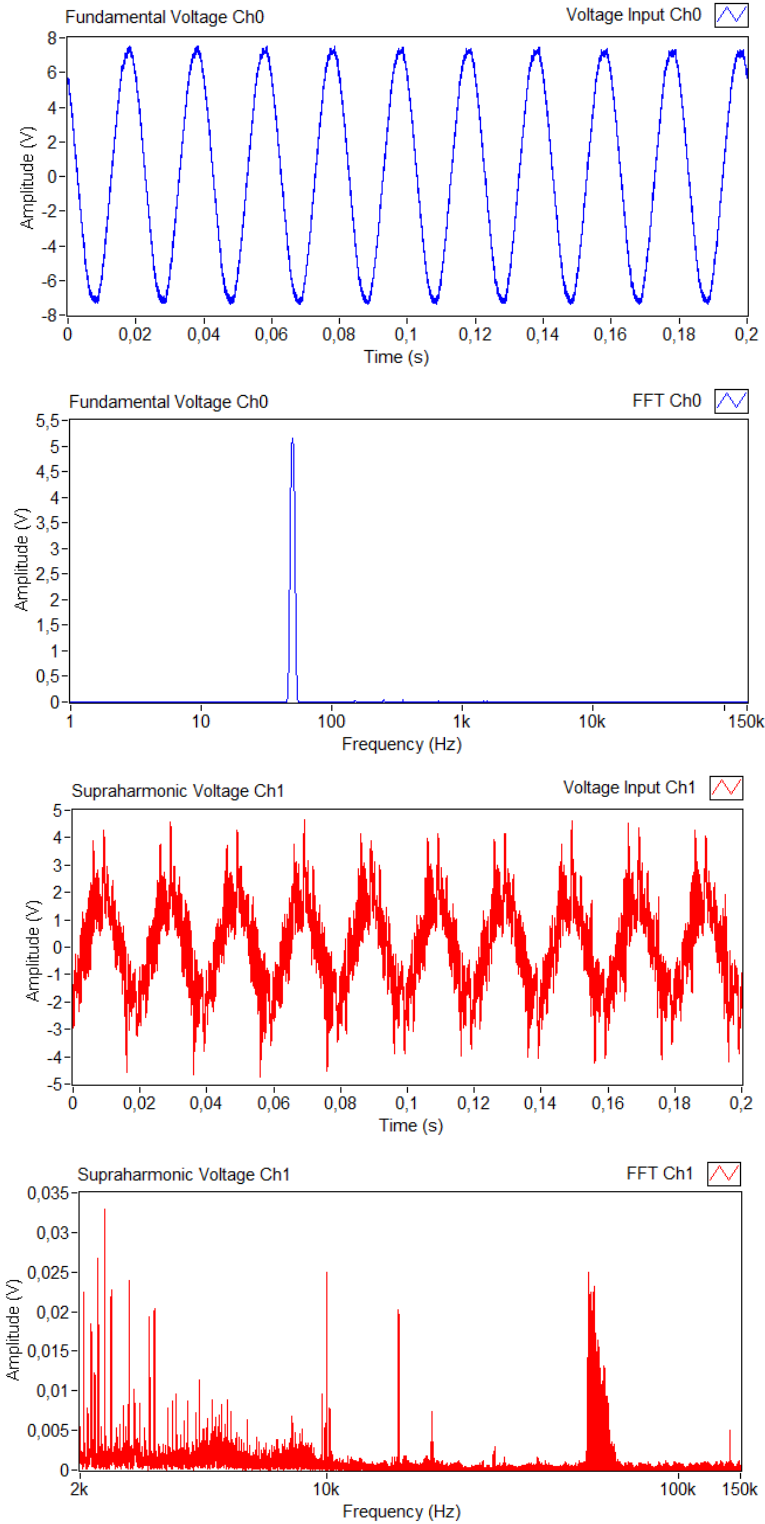


Fig. C.4. Acquired and processed waveforms.

Waveforms measured away from Industrial PV inverter with sudden addition of EV Charger



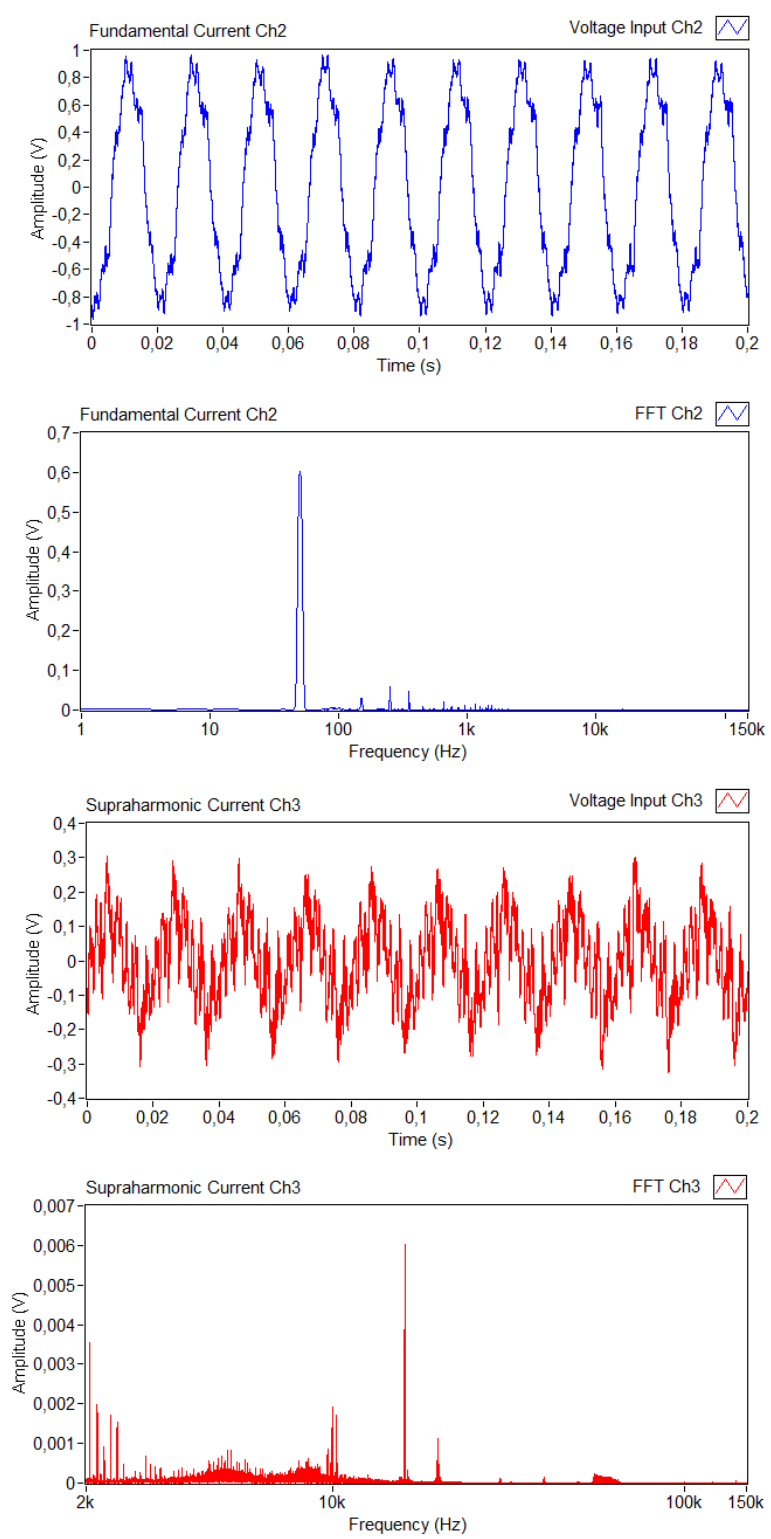
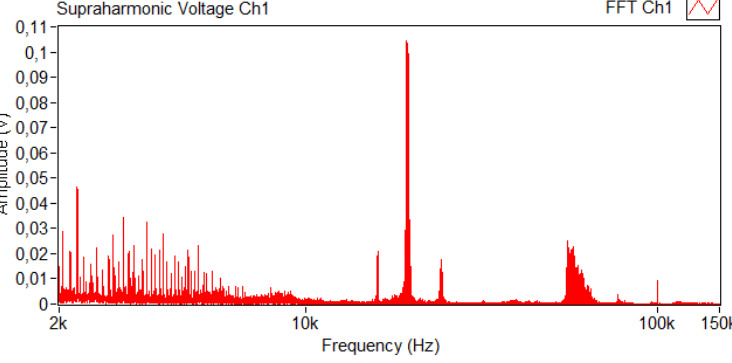
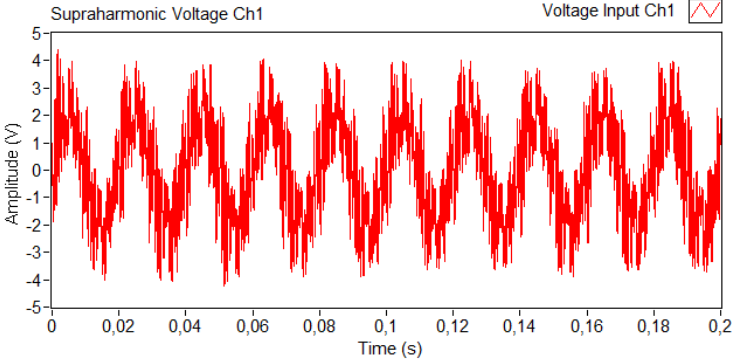
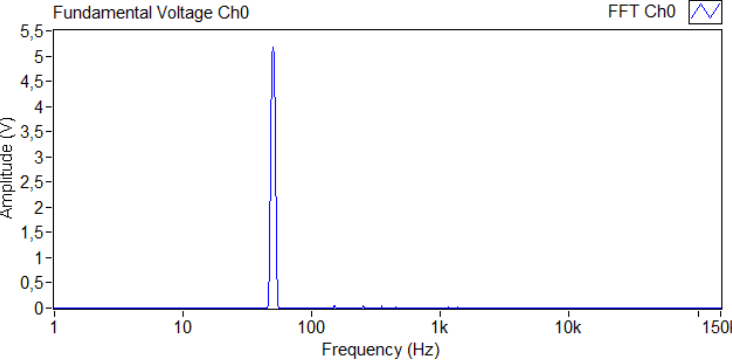
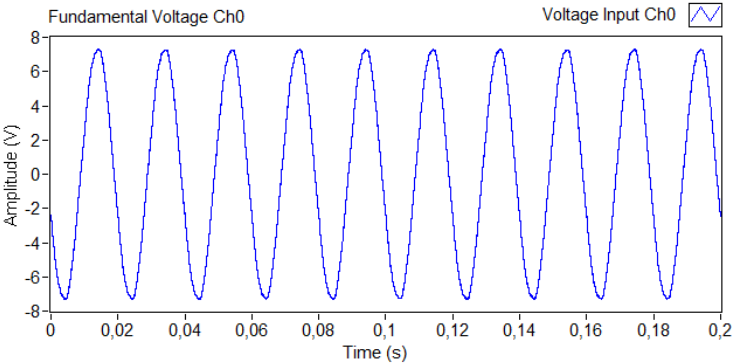


Fig. C.5. Acquired and processed waveforms.

Waveforms measured away from Industrial PV inverter with sudden removal of EV Charger



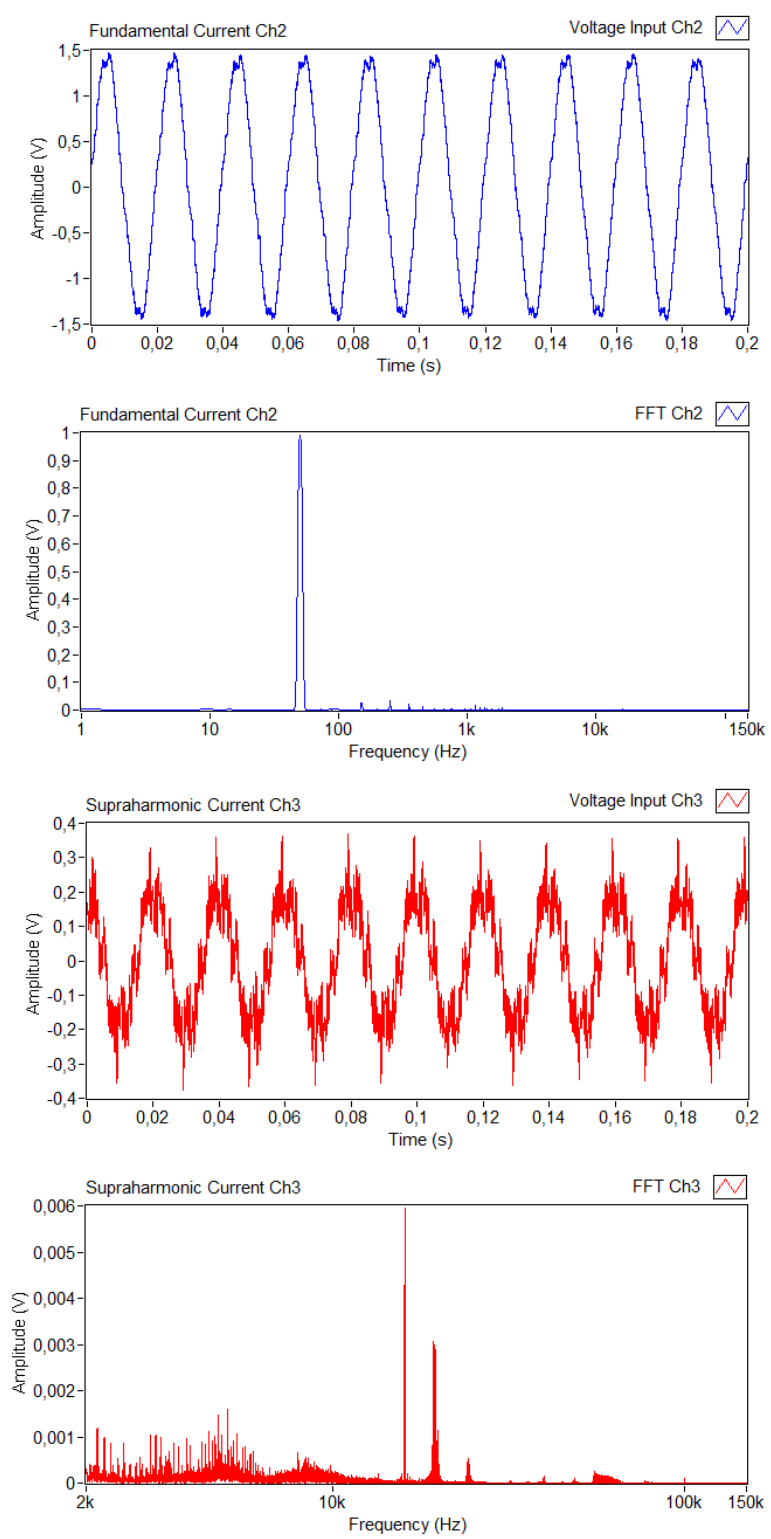
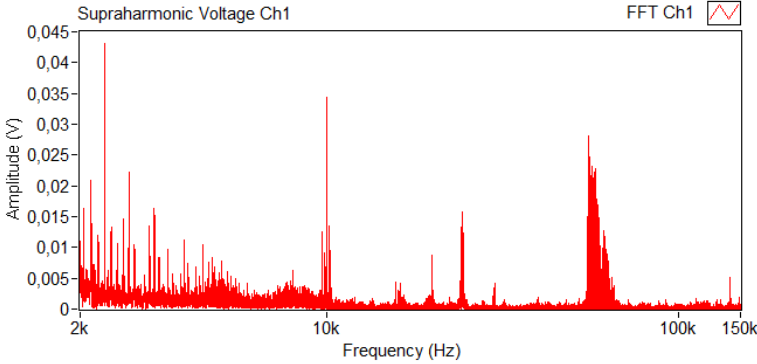
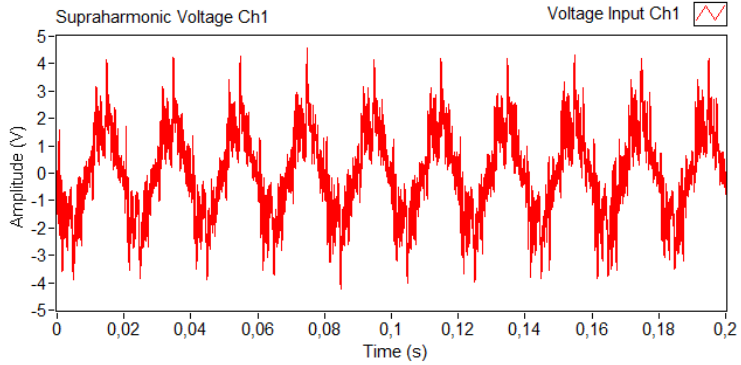
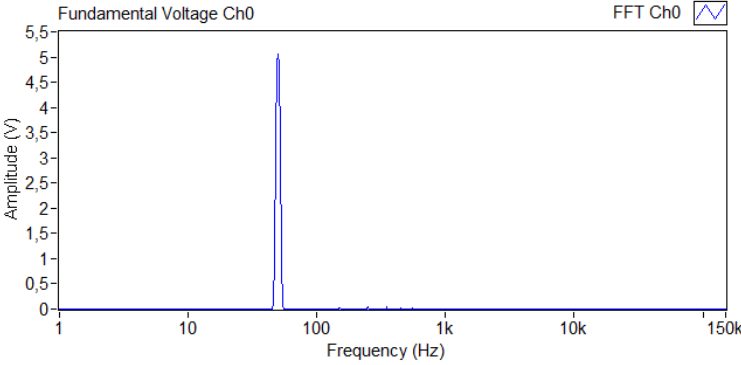
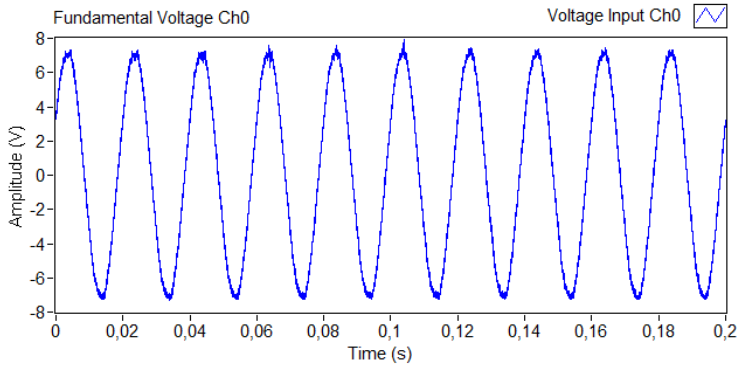


Fig. C.6. Acquired and processed waveforms.

Waveforms measured close to EV Charger



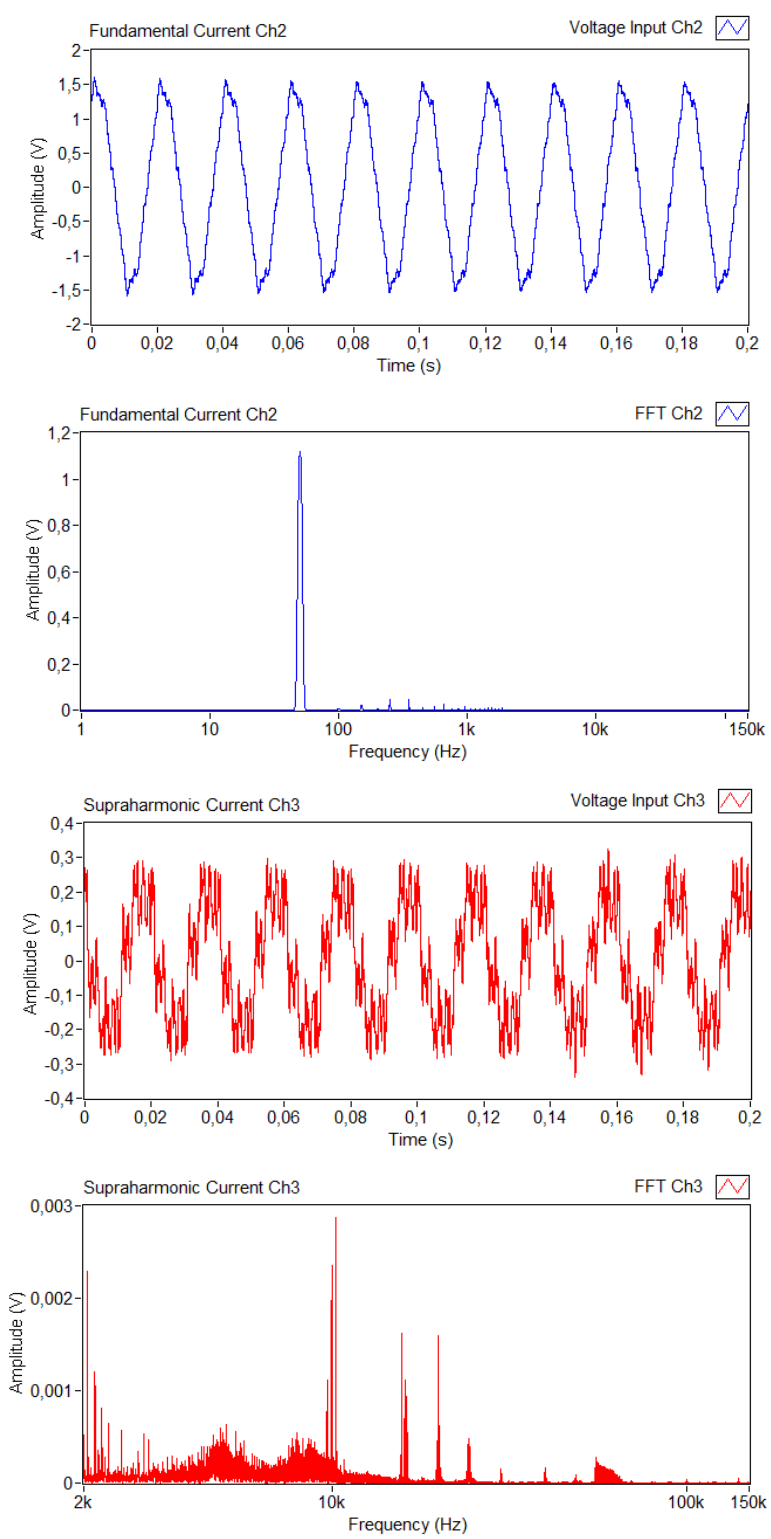
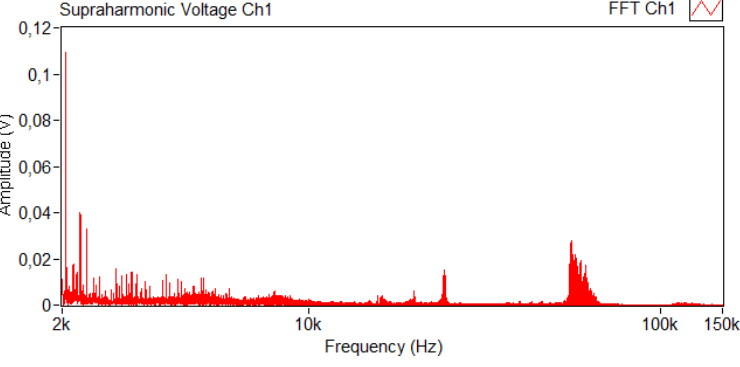
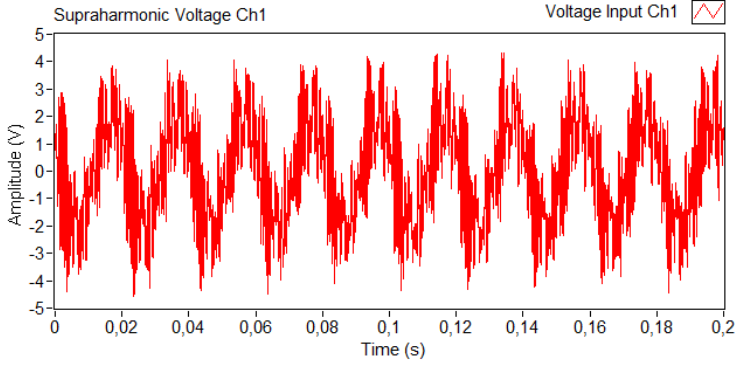
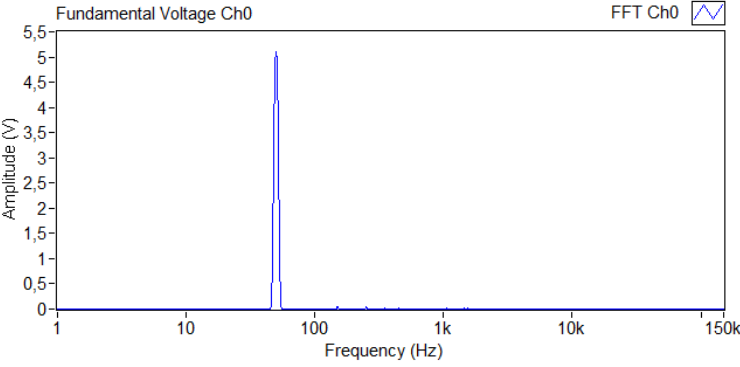
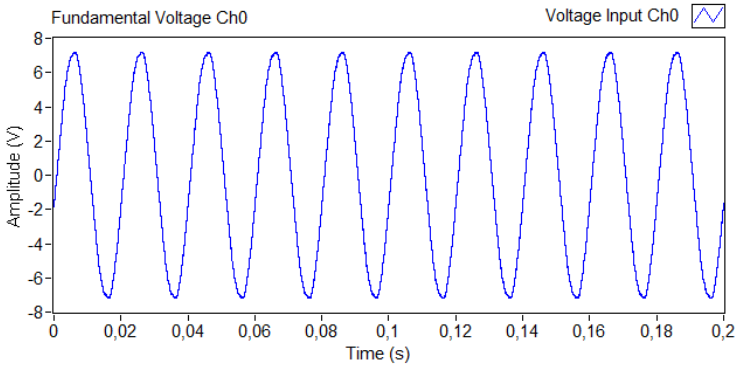


Fig. C.7. Acquired and processed waveforms.

Waveforms measured from Electrical Network after sudden removal of EV Charger



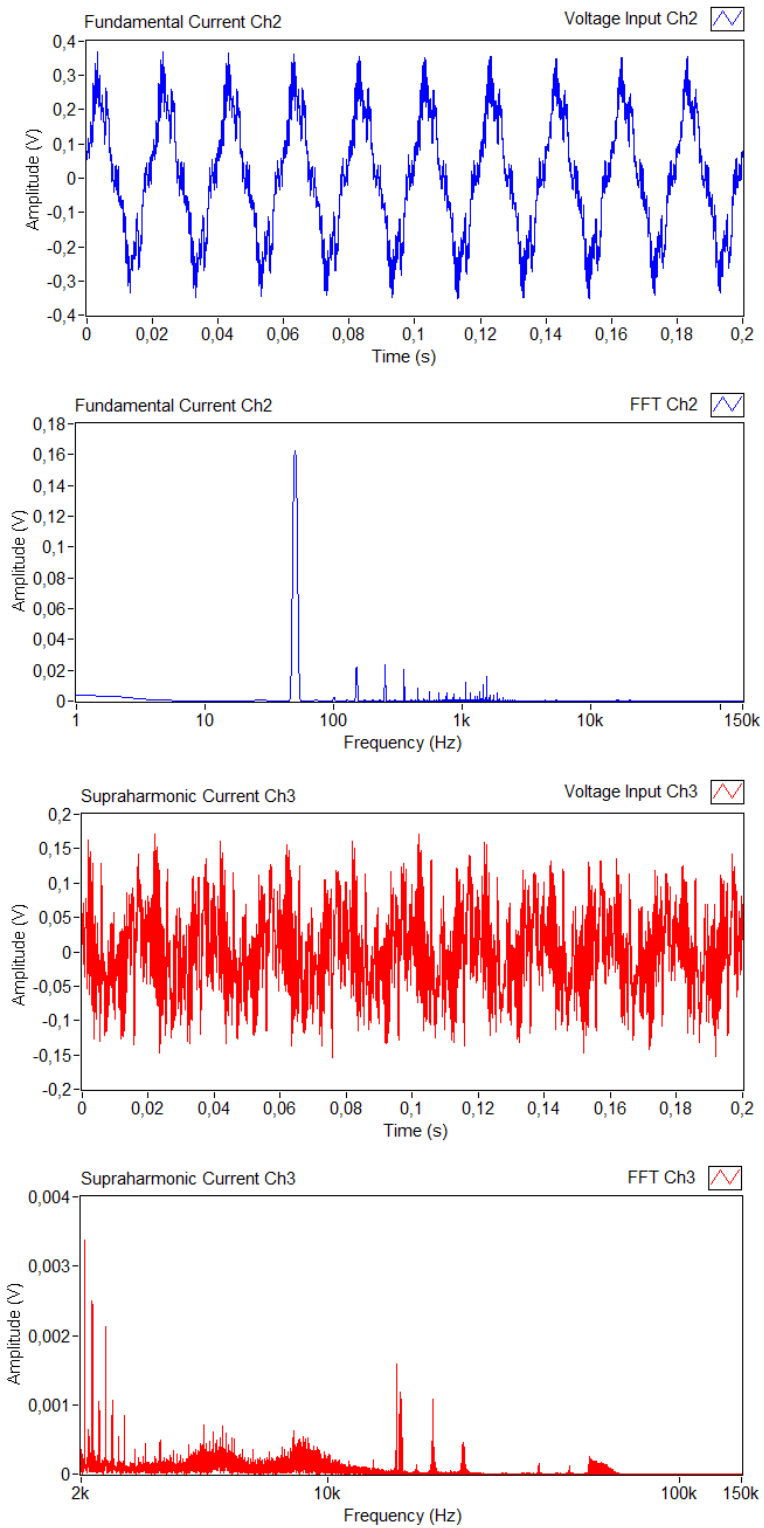


Fig. C.8. Acquired and processed waveforms.

APPENDIX D
MEASUREMENT CAMPAIGN 2
STATISTICAL ANALYSIS RESULTS

APPENDIX D

The statistical analysis results using the ANOVA for the voltage and current waveforms acquired during the measurement campaign 2 are listed here. The analysis process is explained in section 5.4.3.

Voltage Amplitude for Absolute Measurements

Table D.1. ANOVA table for the voltage waveform in the frequency range of 2 to 4 kHz.

Analysis of Variance					
Source	Sum of Squares	df	Mean Square	F Value	p-value Prob > F
Model	0.0026	1	0.0026	6.14	0.0480
D-Measurement Point	0.0026	1	0.0026	6.14	0.0480
Residual	0.0026	6	0.0004		
Cor Total	0.0052	7			

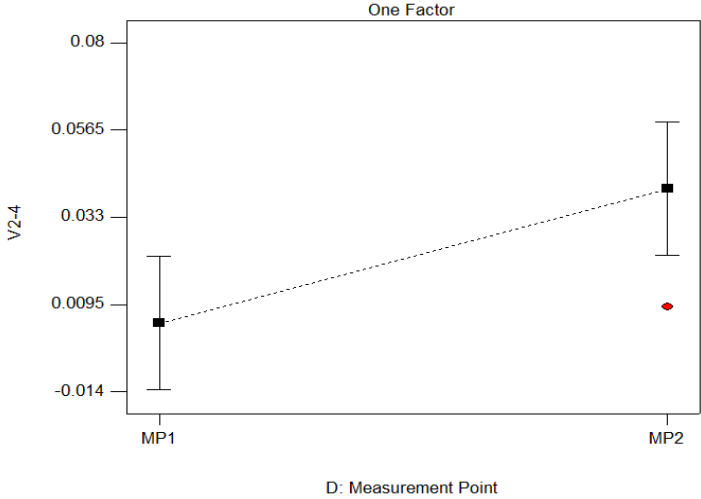


Fig. D.1. Effect of the measurement point on the voltage waveform in the frequency range of 2 to 4 kHz.

Table D.2. ANOVA table for the voltage waveform in the frequency range of 9 to 11 kHz.

Analysis of Variance					
Source	Sum of Squares	df	Mean Square	F Value	p-value Prob > F
Model	0.2090	3	0.0697	77.55	0.0005
C-Load	0.0729	1	0.0729	81.12	0.0008
D-Measurement Point	0.0734	1	0.0734	81.76	0.0008
CD	0.0627	1	0.0627	69.77	0.0011
Residual	0.0036	4	0.0009		
Cor Total	0.2126	7			

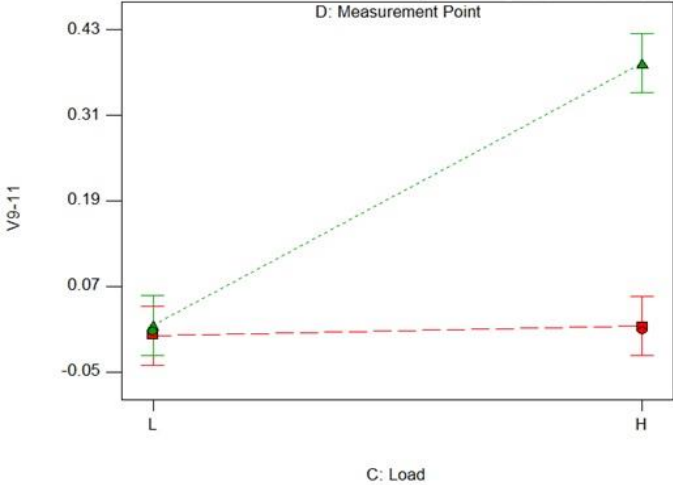


Fig. D.2. Interaction effect between the load and measurement point on the voltage waveform in the frequency range of 9 to 11 kHz.

Table D.3. ANOVA table for the voltage waveform in the frequency range of 19 to 21 kHz.

Analysis of Variance					
Source	Sum of Squares	df	Mean Square	F Value	p-value Prob > F
Model	0.0992	3	0.0331	13.12	0.0154
B-Industrial PV Inverter	0.0403	1	0.0403	16.00	0.0161
D-Measurement Point	0.0422	1	0.0422	16.74	0.0150
BD	0.0167	1	0.0167	6.63	0.0617
Residual	0.0101	4	0.0025		
Cor Total	0.1093	7			

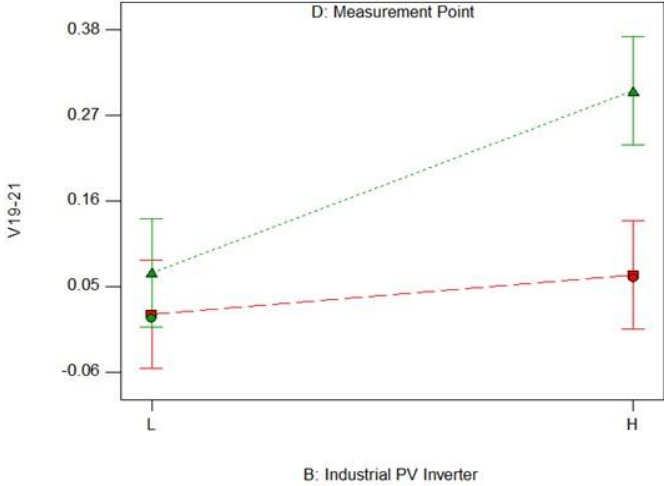


Fig. D.3. Interaction effect between the PVI_I and the measurement point on the voltage waveform in the frequency range of 19 to 21 kHz.

Table D.4. ANOVA table for the voltage waveform in the frequency range of 39 to 41 kHz.

Analysis of Variance					
Source	Sum of Squares	df	Mean Square	F Value	p-value Prob > F
Model	0.0252	1	0.0252	6.59	0.0425
D-Measurement Point	0.0252	1	0.0252	6.59	0.0425
Residual	0.0229	6	0.0038		

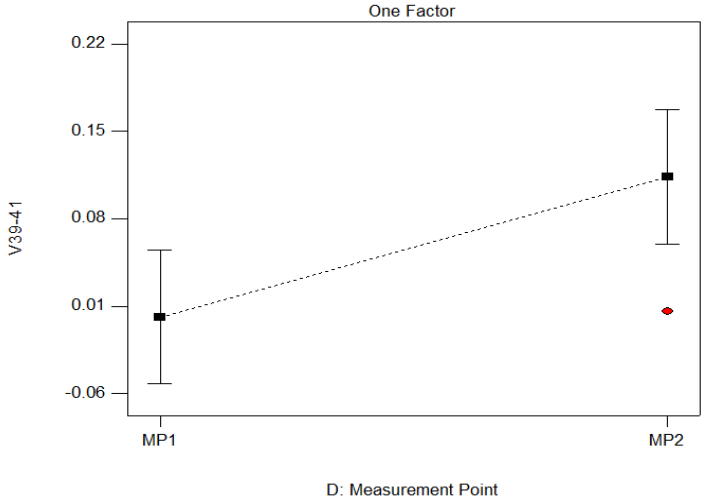


Fig. D.4. Effect of the measurement point on the voltage waveform in the frequency range of 39 to 41 kHz.

Table D.5. ANOVA table for the voltage waveform in the frequency range of 59 to 61 kHz.

Analysis of Variance					
Source	Sum of Squares	df	Mean Square	F Value	p-value Prob > F
Model	0.0058	3	0.0019	10.21	0.0240
B-Industrial PV Inverter	0.0009	1	0.0009	4.94	0.0903
D-Measurement Point	0.0040	1	0.0040	20.90	0.0102
BD	0.0009	1	0.0009	4.78	0.0940
Residual	0.0008	4	0.0002		
Cor Total	0.0066	7			

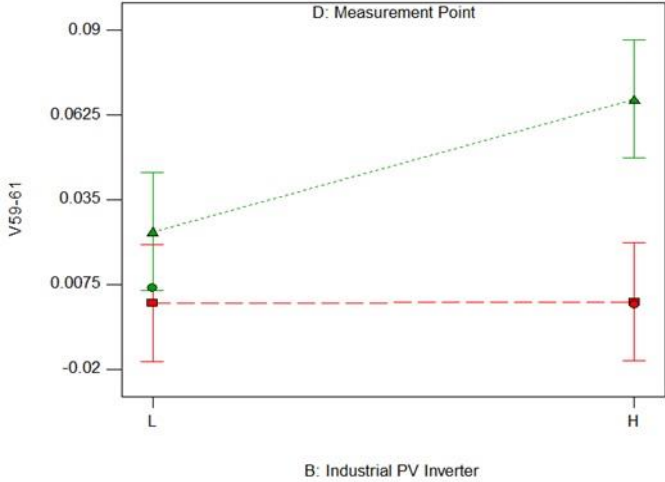


Fig. D.5. Interaction effect between the PVI_I and measurement point on the voltage waveform in the frequency range of 59 to 61 kHz.

Table D.6. ANOVA table for the voltage waveform in the frequency range of 79 to 81 kHz.

Analysis of Variance					
Source	Sum of Squares	df	Mean Square	F Value	p-value Prob > F
Model	0.0210	3	0.0069	17.40	0.0093
C-Load	0.0056	1	0.0056	13.94	0.0202
D-Measurement Point	0.0100	1	0.0100	25.33	0.0073
CD	0.0052	1	0.0052	12.93	0.0229
Residual	0.0016	4	0.0004		
Cor Total	0.0224	7			

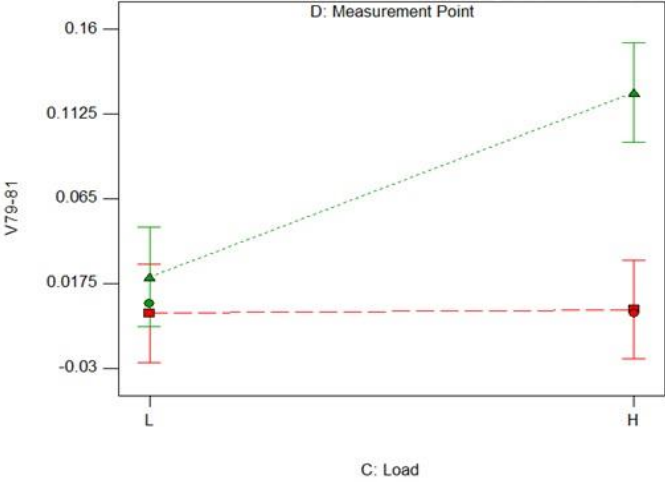


Fig. D.6. Interaction effect between the load and measurement point on the voltage waveform in the frequency range of 79 to 81 kHz.

Table D.7. ANOVA table for the voltage waveform in the frequency range of 99 to 101 kHz.

Analysis of Variance					
Source	Sum of Squares	df	Mean Square	F Value	p-value Prob > F
Model	0.0167	3	0.0056	9.18	0.0288
C-Load	0.0031	1	0.0031	5.04	0.0882
D-Measurement Point	0.0100	1	0.0100	16.48	0.0153
CD	0.0037	1	0.0037	6.02	0.0701
Residual	0.0024	4	0.0006		
Cor Total	0.0191	7			

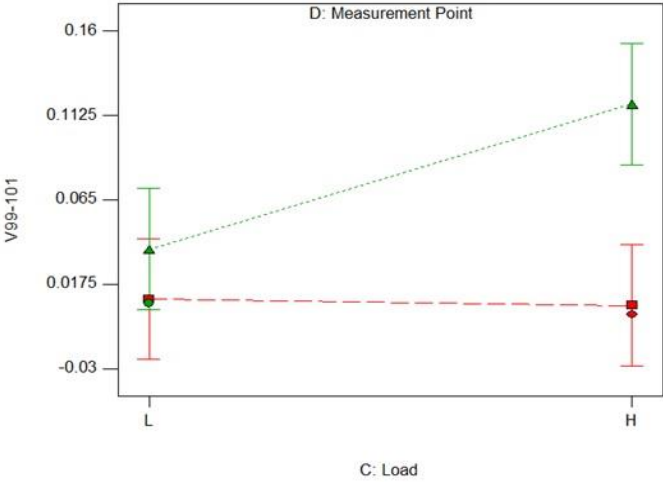


Fig. D.7. Interaction effect between the load and measurement point on the voltage waveform in the frequency range of 99 to 101 kHz.

Table D.8. ANOVA table for the voltage waveform in the frequency range of 119 to 121 kHz.

Analysis of Variance					
Source	Sum of Squares	df	Mean Square	F Value	p-value Prob > F
Model	0.0060	3	0.0020	22.58	0.0057
C-Load	0.0014	1	0.0014	15.21	0.0175
D-Measurement Point	0.0035	1	0.0035	39.57	0.0033
CD	0.0012	1	0.0012	12.97	0.0227
Residual	0.0004	4	0.0001		
Cor Total	0.0064	7			

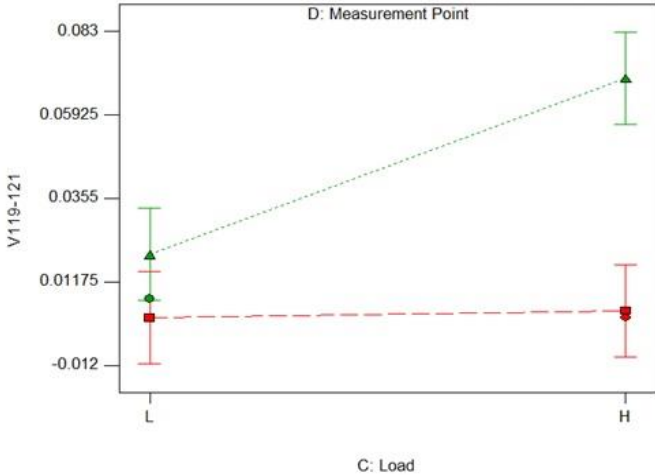


Fig. D.8. Interaction effect between the load and measurement point on the voltage waveform in the frequency range of 119 to 121 kHz.

Table D.9. ANOVA table for the voltage waveform in the frequency range of 139 to 141 kHz.

Analysis of Variance					
Source	Sum of Squares	df	Mean Square	F Value	p-value Prob > F
Model	1.23E-03	3	4.09E-04	15.88	0.0110
C-Load	2.37E-04	1	2.37E-04	9.18	0.0388
D-Measurement Point	8.43E-04	1	8.43E-04	32.69	0.0046
CD	1.49E-04	1	1.49E-04	5.77	0.0742
Residual	1.03E-04	4	2.58E-05		
Cor Total	1.33E-03	7			

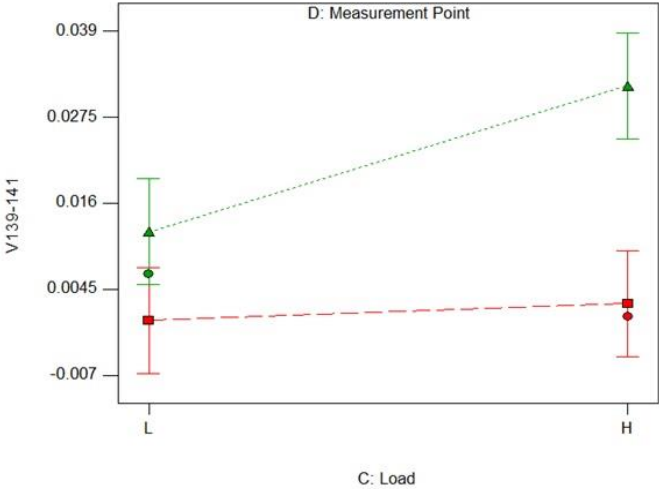


Fig. D.9. Interaction effect between the load and measurement point on the voltage waveform in the frequency range of 139 to 141 kHz.

Current Amplitude for Absolute Measurements

Table D.10. ANOVA table for the current waveform in the frequency range of 2 to 4 kHz.

Analysis of Variance					
Source	Sum of Squares	df	Mean Square	F Value	p-value Prob > F
Model	0.00	1	0.00	9.17	0.0231
D-Measurement Point	0.00	1	0.00	9.17	0.0231
Residual	0.00	6	0.00		
Cor Total	0.00	7			

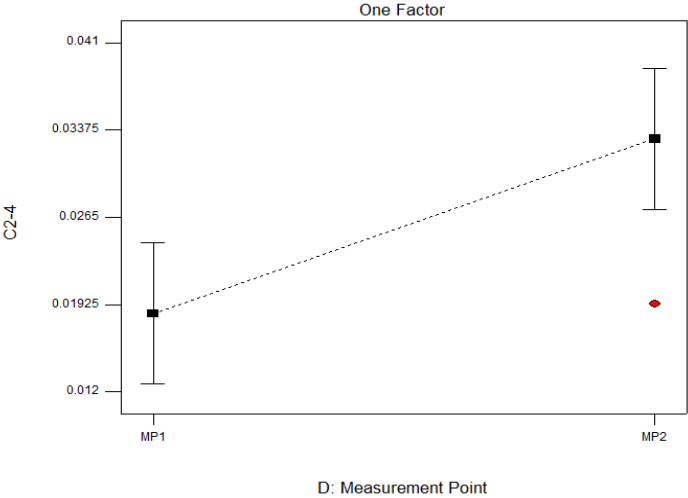


Fig. D.10. Effect of the measurement point on the current waveform in the frequency range of 2 to 4 kHz.

Table D.11. ANOVA table for the current waveform in the frequency range of 9 to 11 kHz.

Analysis of Variance					
Source	Sum of Squares	df	Mean Square	F Value	p-value Prob > F
Model	0.01	1	0.01	5.59	0.0559
C-Load	0.01	1	0.01	5.59	0.0559
Residual	0.01	6	0.00		
Cor Total	0.02	7			

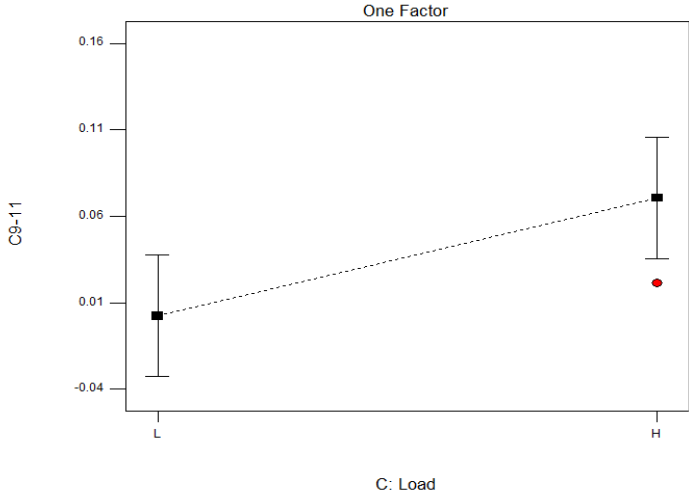


Fig. D.11. Effect of the load on the current waveform in the frequency range of 9 to 11 kHz.

Table D.12. ANOVA table for the current waveform in the frequency range of 19 to 21 kHz.

Analysis of Variance					
Source	Sum of Squares	df	Mean Square	F Value	p-value Prob > F
Model	0.001	1	1.4E-03	3.75	0.1010
D-Measurement Point	0.001	1	1.4E-03	3.75	0.1010
Residual	0.002	6	3.6E-04		
Cor Total	0.004	7			

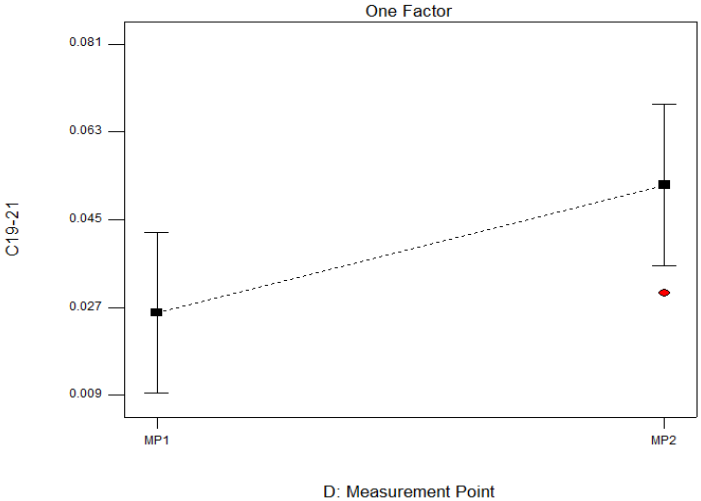


Fig. D.12. Effect of the measurement point on the current waveform in the frequency range of 19 to 21 kHz.

Table D.13. ANOVA table for the current waveform in the frequency range of 39 to 41 kHz.

Analysis of Variance					
Source	Sum of Squares	df	Mean Square	F Value	p-value Prob > F
Model	4.06E-06	1	4.06E-06	28.75	0.0017
D-Measurement Point	4.06E-06	1	4.06E-06	28.75	0.0017
Residual	8.48E-07	6	1.41E-07		
Cor Total	4.91E-06	7			

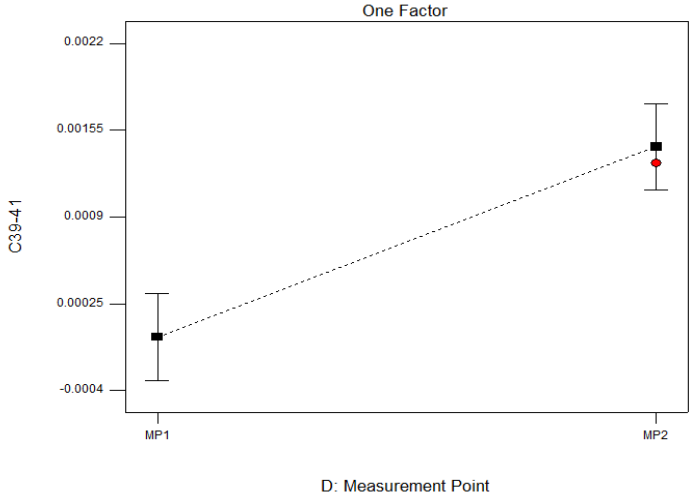


Fig. D.13. Effect of the measurement point on the current waveform in the frequency range of 39 to 41 kHz.

Table D.14. ANOVA table for the current waveform in the frequency range of 99 to 101 kHz.

Analysis of Variance					
Source	Sum of Squares	df	Mean Square	F Value	p-value Prob > F
Model	5.67E-05	1	5.67E-05	68.78	0.0002
D-Measurement Point	5.67E-05	1	5.67E-05	68.78	0.0002
Residual	4.95E-06	6	8.25E-07		
Cor Total	6.17E-05	7			

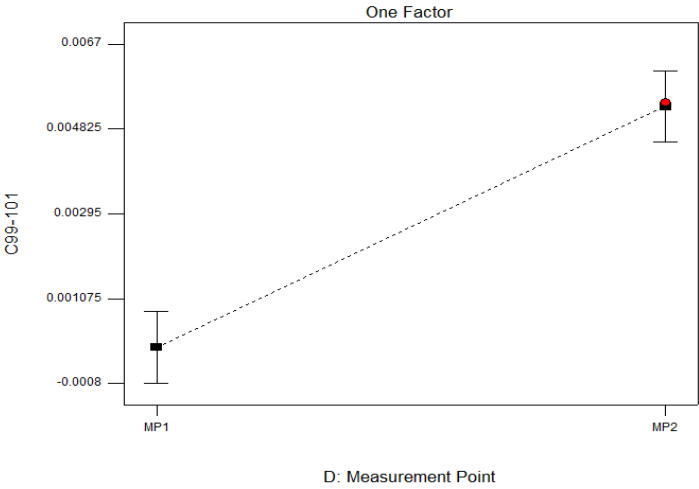


Fig. D.14. Effect of the measurement point on the current waveform in the frequency range of 99 to 101 kHz.

Table D.15. ANOVA table for the current waveform in the frequency range of 119 to 121 kHz.

Analysis of Variance					
Source	Sum of Squares	df	Mean Square	F Value	p-value Prob > F
Model	4.35E-06	1	4.35E-06	12.27	0.0128
D-Measurement Point	4.35E-06	1	4.35E-06	12.27	0.0128
Residual	2.13E-06	6	3.55E-07		
Cor Total	6.48E-06	7			

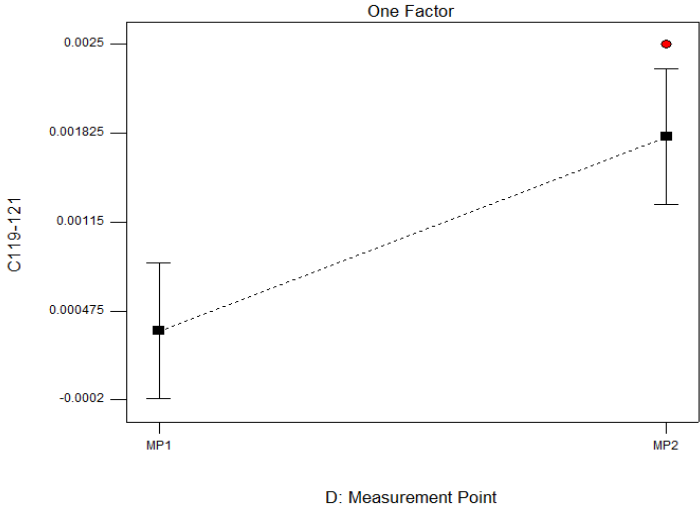


Fig. D.15. Effect of the measurement point on the current waveform in the frequency range of 119 to 121 kHz.

There are no current emissions in the frequency range of 59 to 61 kHz, 79 to 81 kHz, and 139 to 141 kHz. As a result, there are neither any individual effects nor any interactions between the parameters in these frequency ranges.

APPENDIX E
PUBLICATIONS

APPENDIX E

The articles published during the thesis work are given below:

D. Amaripadath et al., “Measurement and Analysis of Supraharmonic Emissions in Smart Grids,” in *54th International Universities Power Engineering Conference (UPEC)*, Bucharest, Romania, 2019, pp 1-6.

D. Amaripadath et al., “Design of Versatile Waveform Platform for Supraharmonic Testing and Calibration,” in *25th International Conference and Exhibition on Electricity Distribution (CIRED)*, Madrid, Spain, 2019, pp 1-4.

D. Amaripadath et al., “Measurement of Supraharmonic Emissions (2 - 150 kHz) in Real Grid Scenarios,” in *Conference on Precision Electromagnetic Measurements (CPEM)*, Paris, France, 2018, pp. 1-2.

D. Amaripadath et al., “Power Quality Disturbances on Smart Grids: Overview and Grid Measurement Configurations,” in *52nd International Universities Power Engineering Conference (UPEC)*, Heraklion, Greece, 2017, pp. 1-6.